Functional Analysis of RIBA, the Introductory Enzyme for Riboflavin Biosynthesis

D I S S E R T A T I O N

zur Erlangung des akademischen Grades

doctor rerum naturalium

(Dr. rer. nat.)

im Fach Biologie

eingereicht an der

Lebenswissenschaftlichen Fakultät

der Humboldt-Universität zu Berlin

von

M. Sc. Hanna-Maija Hiltunen

Präsident der Humboldt-Universität zu Berlin

Prof. Dr. Jan-Hendrik Olbertz

Dekan der Lebenswissenschaftlichen Fakultät

Prof. Dr. Richard Lucius

Gutachter: 1. Prof. Dr. Bernhard Grimm

2. Prof. Thomas Buckhout, Ph.D.

3. Alisdair Fernie, Ph.D.

Tag der mündlichen Prüfung: 27.05.2016

This thesis is dedicated to all people who have fought or still fight for

equal opportunity in education!

Table of Contents

Abstract

Flavin mononucleotide (FMN) and Flavin adenine dinucleotide (FAD) belong to the main redox coenzymes and are involved in central metabolic processes. They derive from riboflavin also referred to as vitamin B_2.

The bifunctional RIBA enzyme, which comprises peptide domains for GTP cyclohydrolase II (GCHII) and 3,4-dihydroxy-2-butanone-4-phosphate synthase (DHBPS) activity, performs the two initial steps of riboflavin biosynthesis in plants. Three genes encode RIBA proteins in *Arabidopsis thaliana* and many other flowering plants. One of the main aims of this study was to elucidate the physiological roles of the three RIBA isoforms. Detailed enzymatic studies were performed with recombinant RIBA proteins *IN VITRO*. It revealed for RIBA2 and RIBA3 the loss of either GCHII or DHBPS activity, respectively. The phosphorylation of RIBA1 as well as the inhibition of its GCHII activity by FMN could be demonstrated.

A knockout of *RIBA1*, encoding the dominant RIBA isoform, led to embryo lethality. The gradual reduction of the RIBA1 protein content in *Arabidopsis* was associated with reduced flavin amounts and a severe bleaching phenotype that was caused by the gradual loss of pigments during leaf development. Flavin deficiency effects caused by RIBA1 depletion were characterised with a constitutive antisense mutant and the virus induced gene silencing method. A comprehensive metabolite profiling, revealed that the loss of almost one third of total flavin content led to a deregulation of several citric acid cycle-associated flavoenzymes. Moreover, a severe reduction of the catabolic capacity of numerous amino acids is seen, while seemingly flavin-dependent processes of the nitrogen assimilation are prioritised.

In summary, this thesis contributes to the extended knowledge about the riboflavin biosynthesis pathway as well as to the understanding about consequences of flavin deficiency in plants. Moreover, the first attempt to increase the vitamin B_2 content in plants is presented.

Zusammenfassung

Flavinmononukleotid (FMN) und Flavin-Adenin-Dinukleotid (FAD) gehören zu den wichtigsten Redox-Coenzymen und sind an zentralen Stoffwechselprozessen aller Organismen beteiligt. Sie entstehen aus Riboflavin (Vitamin B_2).

Das bifunktionale RIBA Enzym, das Peptiddomänen für die GTP Cyclohydrolase II (GCHII) und 3,4-Dihydroxy-2-Butanon-4-Phosphat-Synthase (DHBPS) Aktivität umfasst, führt die beiden ersten Schritte der Riboflavin Biosynthese in Pflanzen durch. Die RIBA Proteine werden durch drei Gene in *Arabidopsis thaliana* und anderen Blütenpflanzen kodiert. Eines der Ziele war es, die physiologischen Rollen der drei RIBA Isoformen aufzuklären. Detaillierte enzymatische Untersuchungen wurden mit rekombinanten RIBA Proteinen *IN VITRO* durchgeführt. Es wurde gezeigt, dass RIBA2 und RIBA3 jeweils die GCHII oder die DHBPS Aktivität verloren haben. Des Weiteren konnte die Phosphorylierung von RIBA1, sowie die Hemmung von dessen GCHII Aktivität durch FMN nachgewiesen werden.

Ein Knockout von RIBA1 führte zu Embryoletalität. Die schrittweise Reduzierung des RIBA1 Proteingehaltes in *Arabidopsis*, welches zu einem verringerten Flavingehalt führte, ergab einen schwerwiegenden Bleichungsphänotyp. Die konstitutive *Antisense*-Mutante, sowie das Verfahren des Virus-induzierten Gen-„Silencing“ wurden verwendet, um den durch RIBA1-Mangel hervorgerufenen Flavin-Defizienz-Effekt zu beschreiben. Eine Metabolomics Analyse ergab, dass die Abnahme des Flavingehaltes zu einer Deregulierung verschiedener Zitronensäurezyklus assoziierten Flavoenzyme und zu einer starken Reduktion der katabolischen Kapazität diverser Aminosäuren führt, während flavinabhängige Stickstoffassimilationsprozesse eher priorisiert wurden.

Diese Arbeit leistet einen Beitrag zur Erweiterung des Kenntnisstands über den pflanzlichen Riboflavin Biosyntheseweg, sowie zum Verständnis über die Folgen von Flavinmangel in Pflanzen. Darüber hinaus wird hier der erste Versuch zu Erhöhung des Vitamin B_2-Gehalt in Pflanzen beschrieben.

List of Abbreviations

Please note that units described in the International System of Units (SI) as well as metric prefixes are not listed here.

ACA	ε-aminocaproic acid/6-aminohexanoic acid
acc.	Acceleration
AGI	*Arabidopsis* Genome Initiative
APS	ammonium persulfate
AS	antisense
AtFMN/FHy	riboflavin kinase/FMN hydrolase
BiFC	bimolecular fluorescence complementation
bp	base pairs
ca.	*CIRCA*, approximately
CaMV	*Cauliflower mosaic virus*
Cat.	category
cDNA	complementary DNA
CDS	coding DNA sequence
CLP	cloning primer
cLSM	confocal laser scanning microscopy
d	days
DAB	3'3-diaminobenzidine
dec.	deceleration
DHBPS	3,4-dihydroxy-2-butanone-4-phosphate synthase
DMRL	6,7-dimethyl-8-ribityllumazine
DMSO	dimethyl sulfoxide
DNA	desoxyribonucleic acid
dNTP	desoxyribonucleoside triphosphate
DTT	dithiothreitol
ECL	enhanced chemiluminescence
EDTA	ethylenediaminetetraacetic acid
e.g.	*EXEMPLI GRATIA*, for example
et al.	*ET ALTERA*
EtBr	ethidium bromide
EtOH	ethanol
etc.	*ET CETERA*
FAA	formalin-acetic acid-alcohol
FAD	flavin adenine dinucleotide
FDR	false discovery rate

FMN	flavin mononucleotide
fw	forward
FW	fresh weight
F6P	fructose-6-phosphate
GABA	γ-aminobutyric acid
GC	gas chromatography
GCHII	GTP cyclohydrolase II
gDNA	genomic DNA
GFP	green fluorescent protein
GSA-At	glutamate-1-semialdehyde-2,1-aminomutase
GTP	guanosine-5'-triphosphate
GUS	β-glucuronidase
G6P	glucose-6-phosphate
HA	human influenza hemagglutinin
HEPES	4-(2-hydroxyethyl)-1-piperazineethanesulfonic acid
HPLC	high-performance liquid chromatography
i.e.	*ID EST*, that is
IgG	immunoglobulin G
IPTG	isopropyl-β-D-thiogalactopyranosid
kDa	kilo Dalton
LB	lysogeny broth
LC	liquid chromatography
LHCB1	light harvesting chlorophyll a/b binding protein 1
$liqN_2$	liquid nitrogen
LS	lumazine synthase
M	molar
MeOH	methanol
MES	2-(N-morpholino)ethanesulfonic acid
METC	mitochondrial electron transport chain
Min	minutes
MOPS	3-(N-morpholino)propanesulfonic acid
MWCO	molecular weight cut-off
MQ	Milli-Q® Water (ultrapure water)
mRNA	messenger RNA
MS	mass spectrometry
n	number of biological replicates
NAD	nicotinamide adenine dinucleotide
NADH	reduced NAD

NADP	nicotinamide adenine dinucleotide phosphate
NBT	nitro blue tetrazolium
NO	nitric oxide
OD	optical density
OE	overexpression
o/n	over night
PS	plastidic signal
P19	suppressor of gene silencing from *TBSV*
PAGE	polyacrylamide gel electrophoresis
PBS	phosphate-buffered saline
PCR	polymerase chain reaction
PEP	phosphoenolpyruvic acid
PYRD	pyrimidine deaminase
PYRP	pyrimidine phosphatase
PYRR	pyrimidine reductase
QPP	qPCR primer
qPCR	quantitative real time PCR
rev	reverse
RF	riboflavin
RIBF1/2	FAD synthase 1/2
RNA	ribonucleic acid
ROS	reactive oxygen species
rpm	rounds per minute
RS	riboflavin synthase
RT	room temperature
SDS	sodium dodecyl sulfate
SDS-PA	SDS-polyacrylamide
SDS-PAGE	SDS-polyacrylamide gel electrophoresis
SNN	Wild type *N. tabacum* cv. Samsun NN
SOC	super optimal broth with catabolite repression
sqPCR	semi-quantitative PCR
TAE	Tris-acetate-EDTA
TB	transformation buffer
TBE	Tris-borate-EDTA
TBS	Tris-buffered saline
TBS-T	Tris-buffered saline incl. Tween
TBSV	*Tomato bushy stunt virus*
TCA	trichloroacetic acid

T-DNA	transferred DNA of the Ti plasmid of *A. tumefaciens*
TE	Tris-EDTA
TEMED	tetramethylethylenediamine
Ti	tumor-inducing
TRV	*Tobacco rattle virus*
TOF	time-of-flight
uidA	gene for β-glucuronidase
UTR	untranslated region
UV	ultra violet
VIGS	virus-induced gene silencing
v/v	volume per volume
w/v	weight per volume
wt	wild type
wt Col-0	*Arabidopsis thaliana* L. HEYNH. Var. Col
wt Ws-0	*Arabidopsis thaliana* L. HEYNH. Var. Was
YEB	yeast extract broth
YFP	yellow fluorescent protein
x *g*	times gravitational force
°C	degrees Celsius
3-PGA	3-phosphoglyceric acid
4-MUG	4-methylumbelliferyl-β-D-glucuronide
35S (CaMV35S)	constitutive promotor of *Cauliflower Mosaic Virus*

List of Figures

List of Tables

List of Publications

Publications:

Hiltunen, H.-M., Illarionov, B., Hedtke, B., Fischer, M. & Grimm, B. (2012) *Arabidopsis* RIBA Proteins: Two out of Three Isoforms Have Lost Their Bifunctional Activity in Riboflavin Biosynthesis. *International Journal of Molecular Sciences*, 13, 14086-14105.

Conference Poster:

Hiltunen, H.-M., Hedtke, B., Illarionov, B., Fischer, M. & Grimm, B. (2011) Role of the RIBA gene family in the riboflavin biosynthesis pathway in *Arabidopsis thaliana*. *Poster* at Botanikertagung 2011, Berlin, GER

Hiltunen, H.-M., Wittrahm, R., Hedtke, B. & Grimm, B. (2014) Characterization of the RIBA Gene Family in *Arabidopsis thaliana*. *Poster* at FESPB/EPSO 2014, Dublin, Ireland.

Master's thesis project:

Trotta, A., Wrzaczek, M., Scharte, J., Tikkanen, M., Konert, G., Rahikainen, M., Holmström, M., Hiltunen, H.-M., Rips, S., Sipari, N., Mulo, P., Weis, E., von Schaewen, A., Aro, E.-M. & Kangasjärvi, S. (2011) Regulatory subunit B'γ of protein phosphatase 2A prevents unnecessary defense reactions under low light in *Arabidopsis*. *Plant physiology*, 156, 1464-1480.

1 Introduction

1.1 Flavins

Flavins are a class of heterocyclic aromatic molecules whose names derive from the latin word *flavus*, referring to their signature colour yellow. Originally extracted from cow milk in 1879 (Blythe, 1879), flavins can be universally found in biological organisms. The most prominent representatives of flavins are **f**lavin **m**ono**n**ucleotide (FMN) and **f**lavin **a**denine **d**inucleotide (FAD), together with their mutual precursor riboflavin, which is commonly referred to as vitamin B_2. FMN and FAD are highly versatile coenzymes, which developed early during evolution. It is hypothesised that ancestral forms already existed during the RNA world and most probably played an important role in the evolution of the modern biotic systems from the prebiotic environment (Kritsky *et al.*, 2010, Nguyen & Burrows, 2012).

Proteins using flavins as coenzymes are called flavoenzymes. Flavoenzymes perform a multitude of enzymatic reactions, including mitochondrial electron transport chain, photosynthesis and fatty acid oxidation (Mansoorabadi *et al.*, 2007), which will be described in detail in chapter 1.1.3. Even though flavins are universally present in all six kingdoms (Animalia, Plantae, Fungi, Protista, Archaea and Bacteria), animals are the only organisms which are incapable of synthesising riboflavin themselves. Therefore, they depend on dietary intake. So far, the flavin biosynthesis pathway has been extensively studied in bacteria, whereas for plants, which are the major sources for dietary riboflavin, our knowledge is mostly limited to the identity of the involved genes. The *status quo* of the plant flavin research will be summarised in chapters 1.3.2 to 1.3.4 and 1.4. The aim of this work is to expand our understanding of the flavin biosynthesis pathway in plants, its regulatory mechanisms and the effects of altered flavin contents due to transgenic manipulation.

1.1.1 Structure of Flavins

Flavins (**Figure 1**) derive from the tricyclic ring system isoalloxazine with two methyl groups linked to positions 7 and 8 and a D-ribitol to position 10, resulting in 7,8-dimethyl-10-(1-D-ribityl) isoalloxazine, also called riboflavin. FMN is formed through the phosphorylation of riboflavin by the riboflavin kinase, whereas covalent attachment of adenine monophosphate (AMP) to the phosphate residue of FMN by the FAD synthase results in FAD (**Figure 1**). The three residues, ribityl, ribityl phosphate, and ribityl adenine diphosphate facilitate the selective binding to the respective flavoenzymes and therefore enable the broad spectrum of biological reactions that flavins are involved in (Müller, 1983). The tricyclic isoalloxazine ring system constitutes the redox active unit (Walsh, 1980).

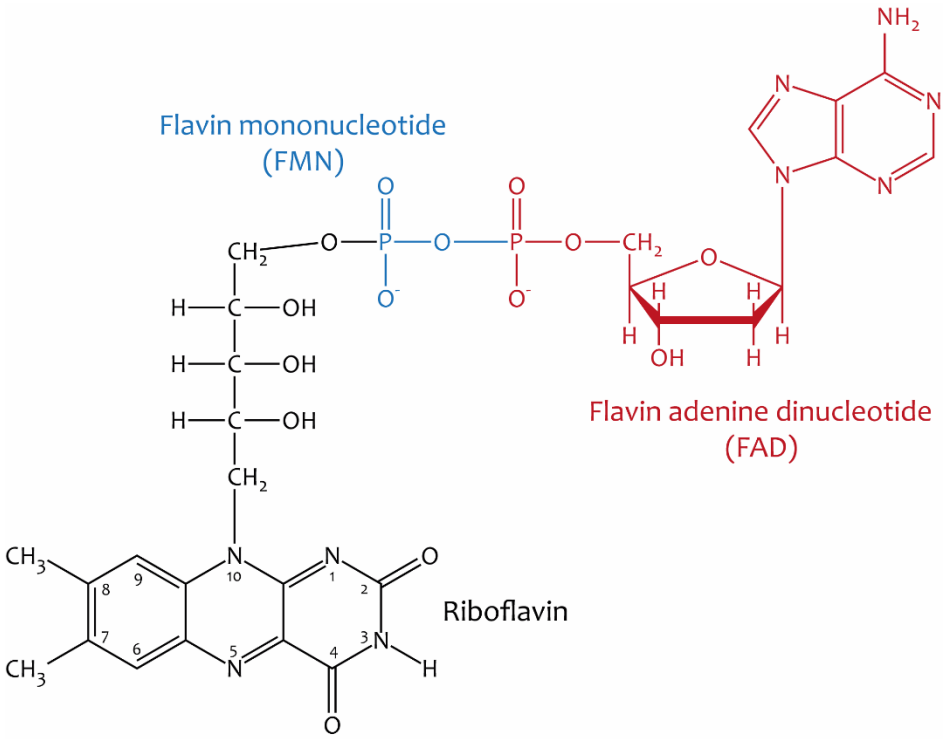

Figure 1: **The molecular formula of flavins.**
Riboflavin (black) with its isoalloxazine ring system with two methyl groups at positions 7 and 8 as well as the D-ribitol residue at position 10. Flavin mononucleotide (FMN) derives from the phosphorylation of riboflavin, whereas the attachment of adenine monophosphate leads to flavin adenine diphosphate (FAD). Adapted from Voet and Voet (1990).

1.1.2 Flavins in Redox Reactions

Redox reactions incorporate the transfer of electrons from a donor to an acceptor molecule. Coenzymes like nicotinamide adenine dinucleotide (NAD) and FAD are common redox partners during electron transfer (Voet & Voet, 1990). The isoalloxazine ring system, also called the flavin group, can be found in three different states: quinone (oxidised), semiquinone (radical) and hydroquinone (reduced) (**Figure 2**).

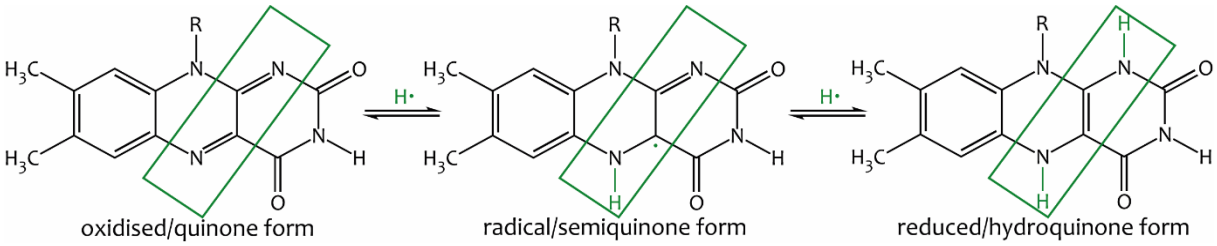

Figure 2: **Redox states of flavins.**
The isoalloxazine ring system allows the stepwise or simultaneous transfer of two electrons. Adapted from Voet and Voet (1990).

These three redox states enable flavins to facilitate one- as well as two-electron transfer reactions, in contrast to most other redox coenzymes which are restricted to transfer either one or two electrons (Walsh, 1980). This special property enables the isoalloxazine moiety to activate molecular oxygen, which for example nicotinamides are inert to do (Massey, 1994).

1.1.3 Flavoenzymes

The first flavoenzyme was isolated from yeast and described by Warburg as the "yellow protein" with oxidising characteristics (Warburg & Christian, 1932). Later, this protein, designated as OLD YELLOW ENZYME (OYE), was characterised as a NADPH dehydrogenase, which binds FMN (Fox & Karplus, 1994, Karplus *et al.*, 1995, Kohli & Massey, 1998). Since then, biochemical and genetic research has uncovered a vast multiplicity of chemical reactions catalysed by flavoenzymes. Besides their function in dehydrogenation, oxidation, monooxygenation, halogenation and reduction reactions (Macheroux *et al.*, 2011), flavins play a crucial role as light and redox sensing molecules within the light-oxygen-voltage (LOV) domains of phototropins in plants (Huala *et al.*, 1997, Christie *et al.*, 1999) as well as their bacterial and eukaryotic counterparts (Losi, 2004). Moreover, flavins function as chromophores in the circadian rhythm and DNA photorepair involved cryptochromes CRY1 /2 (Ahmad & Cashmore, 1993, Jarillo *et al.*, 2001, Sancar, 2003, Hitomi *et al.*, 2009, Yu *et al.*, 2010).

Based on a flavogenomics approach performed by Macheroux *et al.* (2011), the flavoproteomes of humans (Lienhart *et al.*, 2013) and yeast (Gudipati *et al.*, 2014) have recently been published. Conclusively, there are 276 fully and 98 non- or incompletely classified flavoenzymes, of which 75 % use FAD and 25 % FMN as cofactor. The *Arabidopsis thaliana* (*Arabidopsis*) genome contains 230 different genes encoding only 62 distinct flavoproteins (Macheroux *et al.*, 2011).

Important flavoenzymes (**Table 1**) fulfil essential roles in the central energy metabolism, as parts of complex I and II of the mitochondrial electron transport chain (Soole & Menz, 1995, Huang & Millar, 2013) as well as the photosynthetic electron transport chain (Karplus & Daniels, 1991). Moreover, flavoenzymes perform reactions during the citric acid cycle as parts of the pyruvate and α-ketoglutarate dehydrogenase complexes (Lutziger & Oliver, 2001) and the fatty acid oxidation (Bode *et al.*, 1999). Also, the catabolism of many amino acids is performed by diverse flavin-dependent enzymes, e.g. leucine, isoleucine, valine, glycine (Lutziger & Oliver, 2001), lysine (Engqvist *et al.*, 2009, Araújo *et al.*, 2010), as well as proline (Schertl *et al.*, 2014). Beside from their function in the primary metabolism pathways, flavoenzymes also play a role in the tetrapyrrole biosynthesis (Lermontova *et al.*, 1997). Several flavoenzymes act in reactions for protection against photooxidative stress, e.g. the ascorbate biosynthesis pathway (Leferink *et al.*, 2008, Maruta *et al.*, 2010), the glutathione-ascorbate-cycle (Hossain & Asada, 1985, Noctor *et al.*, 1998) and the xanthophyll cycle (Büch *et al.*, 1995). Flavoenzymes are furthermore involved in the hormone metabolism in plants, e.g. abscisic acid biosynthesis (Seo *et al.*, 2000, Barrero *et al.*, 2005) and cytokinin degradation (Hare & Staden, 1994), thereby directly connecting flavins and the hormonal regulation of plant growth and developmental processes.

At present, the involvement of flavins in the *Arabidopsis* assimilatory sulfate reduction by the sulfite reductase (AT5G04590) is questionable (Nakayama *et al.*, 2000, Yarmolinsky *et al.*, 2013) in contrast to its homologue from *Escherichia coli* (Coves *et al.*, 1993). Flavins, however, hold a well-established and important role in the nitrogen metabolism in the flavoenzyme nitrate reductase (Lu *et al.*, 1994).

Table 1: **List of flavoenzymes catalysing metabolic reactions in plants.**

Metabolic Pathway	Flavoenzyme	Reference
Mitochondrial electron transport chain	NADH dehydrogenase and succinate dehydrogenase	Soole and Menz (1995), Huang and Millar (2013)
Photosynthetic electron transport chain	Ferredoxin-$NADP^+$ reductase	Karplus and Daniels (1991)
Citric acid cycle	Succinate dehydrogenase, dihydrolipoamide dehydrogenase	Lutziger and Oliver (2001)
Fatty acid oxidation	Acyl-CoA dehydrogenase	Bode *et al.* (1999)
Branched chain amino acid catabolism	Branched-chain α-ketoacid dehydrogenase complex	Lutziger and Oliver (2001)
Lysine catabolism	D-2-hydroxy acid dehydrogenase	Engqvist *et al.* (2009)
Glycine catabolism	Glycine decarboxylase complex	Lutziger and Oliver (2001)
Proline catabolism	L-proline dehydrogenase	Schertl *et al.* (2014)
Tetrapyrrole biosynthesis	Protoporphyrinogen oxidase	Lermontova *et al.* (1997)
Ascorbate biosynthesis pathway	L-galactono-1,4-lactone dehydrogenase, L-gulono-1,4-lactone oxidase	Leferink *et al.* (2008), Maruta *et al.* (2010)
Glutathione-ascorbate-cycle	Monodehydroascorbate reductase, Glutathione reductase	Hossain and Asada (1985), Noctor *et al.* (1998)
Xanthophyll cycle	Zeaxanthine epoxidase	Büch *et al.* (1995)
Abscisic acid biosynthesis	Zeaxanthine epoxidase, Aldehyde oxidase	Seo *et al.* (2000), Barrero *et al.* (2005)
Cytokinin degradation	Cytokinin oxidase	Hare and Staden (1994)
Nitrogen metabolism	Nitrate reductase	Lu *et al.* (1994)

1.2 Role of Riboflavin in Human Nutrition

Ninety genes encoding for flavin-dependent enzymes have been identified in the human genome (Lienhart *et al.*, 2013). Similar to plants, essential metabolic processes require flavins as coenzymes. In western countries, milk and dairy products mainly cover the riboflavin supply. Populations that consume little meat and dairy products are endemic for riboflavin deficiency (Powers, 2003). In 1997, 12 % of the US population was found to suffer from flavin deficiency, while in undeveloped countries the share was 40 % (Latham, 1997). Even though Ariboflavinosis, the medical condition of riboflavin deficiency, is not assessed as life-threatening, it is connected to many severe disease patterns, e.g. slower recovery from malaria infection (Das *et al.*, 1988), anaemia (Lane & Alfrey, 1965), cancer (Rivlin, 1973), cardiovascular (Mack *et al.*, 1995, Smedts *et al.*, 2008) and neurodegenerative diseases (Sterner & Price, 1973, Leshner *et al.*, 1981). For its bioavailability, the amount of free riboflavin is important. It is especially high in dairy products, meat and dark-green

vegetables (Powers, 2003). Even though many studies on the overproduction of riboflavin exist in fungi and bacteria, such attempts on deliberately increasing the riboflavin content in plants have not been described (Fitzpatrick *et al.*, 2012). Here, the first results of riboflavin biosynthesis overexpression mutants concerning their physiological and metabolic characterisation are presented.

1.3 Biosynthesis of Riboflavin

Riboflavin biosynthesis is highly conserved among biological kingdoms. Interestingly, the eubacterial pathway is very similar to the pathway existing in plants, whereas it seems to be slightly different fungi and Archaea (Fischer & Bacher, 2006). The riboflavin biosynthesis was recently reviewed in great detail by Haase *et al.* (2014) and the postulated pathway in plants is summarised in **Figure 3**.

The first step of riboflavin biosynthesis is executed by the GTP cyclohydrolase II (GCHII, EC 3.5.4.25), using guanosine-5'-triphosphate (GTP) as substrate in the reaction. Pyrophosphate is released after the hydrolytical cleavage of the C(8) of GTP to form 2,5-diamino-6-ribosylamino-4(3*H*)-pyrimidinedione 5'-phosphate. The pyrimidine intermediate is subsequently channelled through three enzymatic reactions: 1.) deamination of the pyrimidine ring to form 5-amino-6-ribosylamino-2,4(1*H*,3*H*)-pyrimidinedione by the pyrimidine deaminase (PYRD), 2.) reduction of the ribosyl side chain to form 5-amino-6-ribitylamino-2,4(1*H*,3*H*)-pyrimidinedione 5'-phosphate by the pyrimidine reductase (PYRR) and 3.) dephosphorylation to 5-amino-6-ribitylamino-2,4(1*H*,3*H*)-pyrimidinedione by the elusive pyrimidine phosphatase (PYRP). The product of the PYRP-catalysed reaction, 5-amino-6-ribitylamino-2,4(1*H*,3*H*)-pyrimidinedione, is condensed with 3,4-dihydro-2-butanone 4-phosphate mediated by the lumazine synthase (LS). The required 3,4-dihydro-2-butanone 4-phosphate molecule is provided by the 3,4-dihydro-2-butanone 4-phosphate synthase (DHBPS, E.C.4.1.99.12) using ribulose-5-phosphate as substrate. Two molecules of 6,7-dimethyl-8-ribityllumazine, the product of LS, are the substrates of the riboflavin synthase (RS), synthesising equimolar amounts of riboflavin and 5-amino-6-ribitylamino-2,4(1*H*,3*H*)-pyrimidinedione via a dismutation reaction incorporating an exchange of a four carbon unit. The second product is fed back into the condensation reaction by the LS.

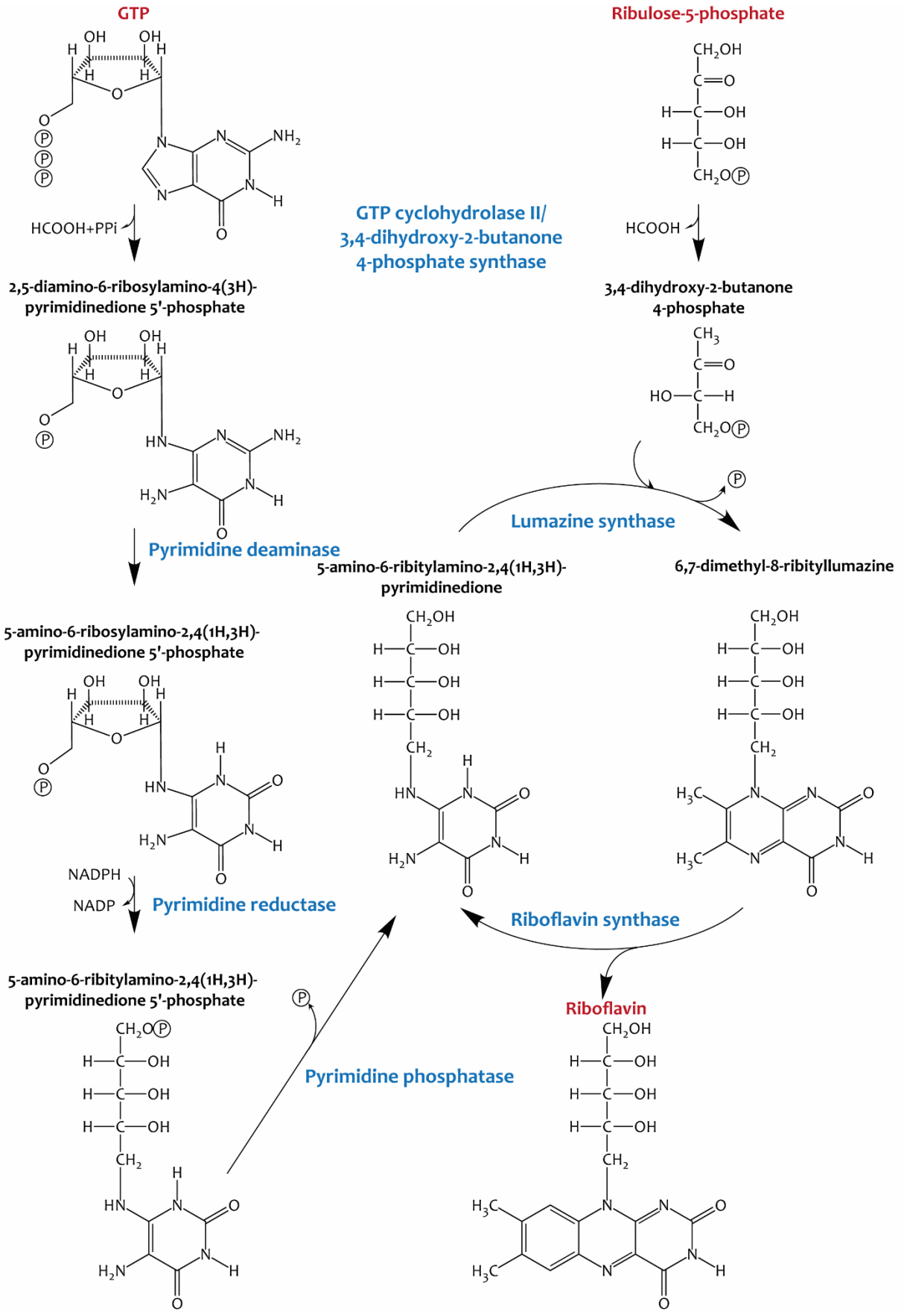

Figure 3: **Riboflavin biosynthesis pathway in plants.**
The enzymes catalysing the reactions are marked in blue and the primary substrates as well as the final product are marked in red. Adapted from Haase *et al.* (2014).

1.3.1 GTP Cyclohydrolase II/3,4-Dihydroxy-2-Butanone-4-Phosphate Synthase

The initial steps of the riboflavin biosynthesis pathway are performed by GCHII and DHBPS, respectively. In fungi, as well as in some bacteria, the proteins performing the GCHII and DHBPS activities are encoded by separate genes like *rib*A (Richter *et al.*, 1993) and *rib*B (Richter *et al.*, 1992) in *E. coli*. In many other microorganisms and plants, however, both enzymatic functions are fulfilled by one protein, e.g. encoded by *RIBA* in plants or *ribBA* in *Bacillus subtilis*. The amino acid sequence of *Arabidopsis* RIBA proteins comprises an N-terminal transit peptide, the central DHBPS domain and GCHII domain at its C-terminus as depicted in **Figure 4**.

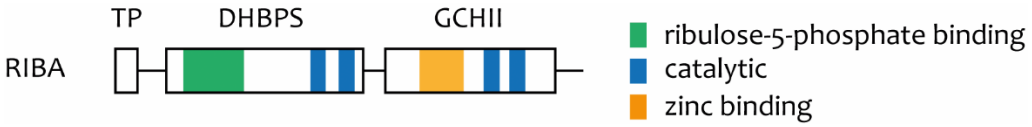

***Figure 4:* Scheme of plant RIBA protein structure.**
Boxes depict the transit peptide (TP) and the functional domains for GTP cyclohydrolase II (GCHII) and 3,4-dihydro-2-butanone 4-phosphate synthase (DHBPS). The colours mark functional residues.

The structure and mechanism of GCHII has been studied in great detail since the 1970s (Foor & Brown, 1975, Ritz *et al.*, 2001, Kaiser *et al.*, 2002, Ren *et al.*, 2005). Crystal structure analysis and *IN VITRO* enzyme assays helped to identify amino acid residues, crucial for the catalytic activity of GCHII (**Figure 5**). The signature for the GCHII domain are one zinc ion coordinated by three cysteine residues (**Figure 4**, orange) and one water molecule (Ren *et al.*, 2005). The zinc and the water molecule at the active site together with the conserved tyrosine of the first catalytic domain (**Figure 4**, blue), have been shown to be essential for the hydrolytic opening of the guanyl ring and the subsequent cleavage of formate (HCOOH) (Kaiser *et al.*, 2002, Ren *et al.*, 2005). The second catalytic domain consists of a conserved arginine (**Figure 5**: E-X-), which acts as the nucleophile for the release of the pyrophosphate (PPi). In addition to the hydrolysis of GTP to 2,5-diamino-6-ribosylamino-4(3*H*)-pyrimidinedione 5'-phosphate, GMP is formed as secondary product in a molar stoichiometry of approximately 1:10 compared to the main product as shown in **Figure 5** (Kaiser *et al.*, 2002).

The enzymatic reaction of the conversion of ribulose-5-phosphate to 3,4-dihydro-2-butanone 4-phosphate (**Figure 6**), catalysed by DHBPS, includes a complex sequence of enolisation-, ketonisation-, dehydratation- and skeleton rearrangement reactions, followed by a final hydrolytic cleavage of formate (Liao *et al.*, 2001). The molecular mechanism of DHBPS was extensively investigated in the 1980s and 1990s (Le Van *et al.*, 1985, Volk & Bacher, 1990, 1991, Richter *et al.*, 1992) and the beginning of the 2000s, when NMR structure (Kelly *et al.*, 2001) and x-ray crystallographic studies (Liao *et al.*, 2001) of the *E. coli* RibB protein provided new insights into the

reaction mechanism. Based on these studies, a set of functional amino acid residues have been identified as pivotal for the DHBPS function.

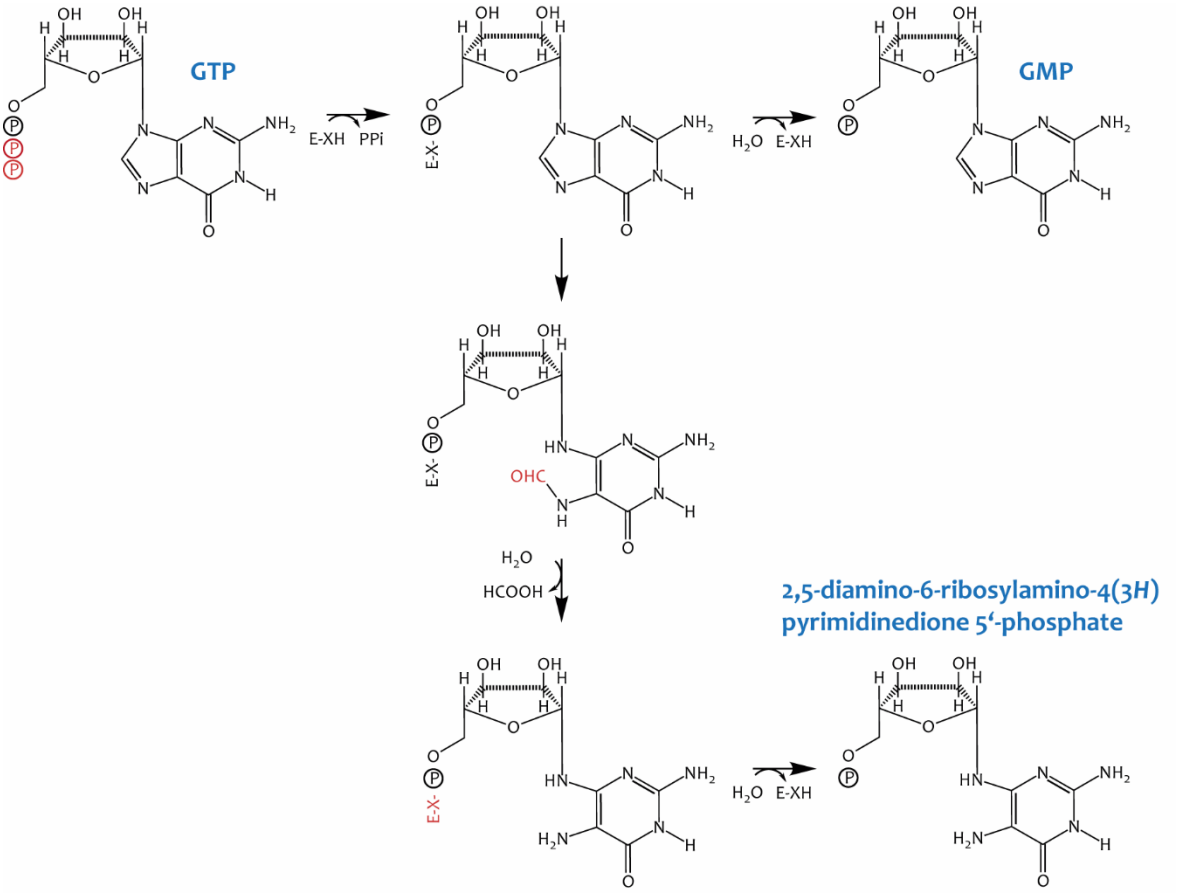

Figure 5: **GTP cyclohydrolase II (GCHII) reaction mechanism.**
The substrate and the two products are marked in blue, while molecules that are changed in the following step are marked red. Adapted from Haase *et al.* (2014).

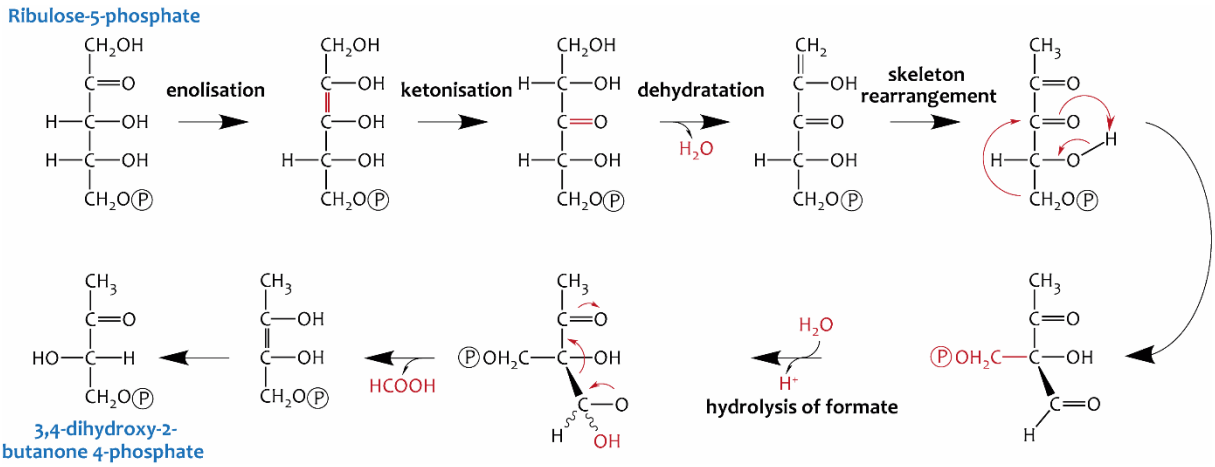

Figure 6: **3,4-dihydroxy-2-butanone 4-phosphate synthase (DHBPS) reaction mechanism.**
Substrate and product are marked in blue. Red indicates the essential result of the labelled reactions. Adapted from Liao *et al.* (2001), Fischer *et al.* (2002b) and Steinbacher *et al.* (2003).

Two aspartates and one arginine in the ribulose-5-binding domain (**Figure 4**) are responsible for substrate recognition and recruitment of the essential cofactor Mg^{2+} (Steinbacher *et al.*, 2003). In

E. coli (Kelly *et al.*, 2001) and *Methanococcus jannaschii* (Fischer *et al.*, 2002b), one histidine and glutamine in the catalytic domains have been demonstrated to be mandatory for DHBPS enzyme activity. Finally, also the formation of DHBPS homodimers seems to have a positive effect for substrate binding and active site formation (Richter *et al.*, 1999).

Singh *et al.* (2013) underpinned these results furthermore by publishing the crystal structure of the bifunctional *Mycobacterium tuberculosis* RIBA2 protein. Mtb-RibA2 is present as a homodimer formed by interaction of the GCHII domains. Singh and co-workers demonstrated that the homodimerisation was beneficial for the DHBPS enzyme activity, but not for GCHII enzyme activity.

1.3.2 *Arabidopsis thaliana* Riboflavin Biosynthesis

After identification of the flavin biosynthesis genes in bacteria and fungi, sequence comparison allowed the determination of homologous genes in plants (**Table 2**). Mitsuda *et al.* (1970a) performed first work on plant proteins, during which they purified and characterised riboflavin synthase from spinach. This work was continued by Bacher *et al.* (2001) and Fischer *et al.* (2005) on *Arabidopsis*, when At2g20690 was identified as the gene encoding riboflavin synthase. Herz *et al.* (2000) characterised the *Arabidopsis* RIBBA protein (At5g64300) with a high homology to the bifunctional *B. subtilis* RibBA, triggering the hypothesis that plants possess a bifunctional RIBA protein, catalysing both initial steps of the riboflavin biosynthesis pathway, as well. This hypothesis was verified by an *IN VITRO* assay demonstrating GCHII as well as DHBPS activity of the *Arabidopsis* RIBA. Herz and co-workers hypothesised a plastidial localisation of the protein due to the N-terminal stretch, not homologous to the bacterial sequence. This hypothesis has been confirmed by studies performed in our group (Hiltunen *et al.*, 2012). Jordan *et al.* (1999) cloned At2g44050, verified the *IN VITRO* LS activity, wherein Peltier *et al.* (2006) demonstrated the stromal localisation of the protein. Fischer *et al.* (2004) introduced At4g20960 as PYRD based on its high degree of homology to the deaminase domain of the bifunctional pyrimidine deaminase/reductase (RibG) from *B. subtilis*. Fischer and co-workers demonstrated deaminase activity *IN VITRO* and hence were able to prove that plants follow a similar route of riboflavin biosynthesis pathway as eubacteria. A gene (At4g20960) that has earlier been found by sequence comparison, encoding a protein with homology to bacterial pyrimidine reductase domain (Chatwell *et al.*, 2006). Hasnain *et al.* (2013) demonstrated *IN VITRO* pyrimidine reductase activity for the gene product of At4g20960. Interestingly, this protein has an N-terminal stretch with high homology to the before mentioned PYRD. However, a sequence analysis revealed exchanges of essential amino acid residues within the functional zinc-binding domain essential for the deaminase activity. Consequently, no PYRD activity could be detected *IN VITRO* (Hasnain *et al.*, 2013). The missing pyrimidine phosphatase has

been elusive until recently, when Haase and co-workers (2013, 2014) identified a member of the haloacid dehalogenase (HAD) superfamily that was able to catalyse the dephosphorylation of 5-amino-6-ribitylamino-2,4(1*H*,3*H*)-pyrimidinedione 5'-phosphate. Rawat *et al.* (2011) introduced a HAD, encoded by At1g79790, as a FMN hydrolase that is active in chloroplasts. Haase and co-workers demonstrated its ability to dephosphorylate 5-amino-6-ribitylamino-2,4(1*H*,3*H*)-pyrimidinedione 5'-phosphate *IN VITRO*.

Table 2: **List of proteins involved in *Arabidopsis thaliana* riboflavin biosynthesis.**
The AGI ID codes (based on TAIR10 annotation) of respective genes, subcellular localisation (Ch=chloroplast), as well as the associated references are stated.

Enzyme	Abbreviation	AGI ID	Localisation	Reference
GTP cyclohydrolase II/3,4-dihydroxy-6-butanone-4-phosphate	GCHII/DHBPS, (RIBA)	At5g64300	Ch	Herz *et al.* (2000)
Pyrimidine deaminase	PYRD	At4g20960	Ch	Fischer *et al.* (2004), Hasnain *et al.* (2013)
Pyrimidine reductase	PYRR (PHS1)	At3g47390	Ch	Hasnain *et al.* (2013)
Pyrimidine phosphatase (elusive)	PYRP	At1g79790 (suggested as a candidate)	Ch	Rawat *et al.* (2011), Haase *et al.* (2013)
Lumazin synthase	LS (COS1)	At2g44050	Ch	Jordan *et al.* (1999)
Riboflavin synthase	RS	At2g20690	Ch	Fischer *et al.* (2005)

1.3.3 Flavin Nucleotide Synthesis and Degradation

Since organisms generally do not utilise free riboflavin, it is mainly further processed by phosphorylation to FMN or adenylation to FAD. These processes have been studied in bacteria (Eberhardt *et al.*, 1996, Krupa *et al.*, 2003, Wang *et al.*, 2005, Frago *et al.*, 2008, Herguedas *et al.*, 2009), fungi (Wu *et al.*, 1995, Santos *et al.*, 2000, Bauer *et al.*, 2003) and naturally also in animals (McCormick *et al.*, 1997, Karthikeyan *et al.*, 2003, Galluccio *et al.*, 2007, Torchetti *et al.*, 2010, Barile *et al.*, 2013, Giancaspero *et al.*, 2015). In contrast to prokaryotes, in which riboflavin kinase and FAD synthase reactions are often combined in one bifunctional protein, eukaryotes host mostly monofunctional enzymes (Yruela *et al.*, 2010).

In *Arabidopsis* eight genes, encoding enzymes involved in the processing of flavin nucleotides, were identified so far (**Table 3**). Among these Sandoval and Roje (2005) identified in a BLAST search an *Arabidopsis* gene (At4g21470), which was shown to possesses a C-terminal stretch homologous to yeast and mammal riboflavin kinases, fused to an N-terminal domain of a HAD superfamily enzyme. Sandoval and Roje measured not only riboflavin kinase, but also FMN-hydrolase activity *IN VITRO* and hence named the protein riboflavin kinase/FMN hydrolase (AtFMN/FHy). Moreover, two chloroplastic FAD synthases, RIBF1 and RIBF2 (Sandoval *et al.*, 2008) and one enzyme catalysing the conversion of FAD to FMN and ADP, the FAD pyrophosphohydrolase (AtNUDX23), were identified

(Ogawa *et al.*, 2008) in *Arabidopsis*. Finally, the potential homologous genes for prokaryotic riboflavin kinases or FAD synthases were added to **Table 3** although the roles of the gene products in *Arabidopsis* remain elusive.

Table 3: Proteins involved in FMN and FAD synthesis/hydrolysis in Arabidopsis thaliana.
The AGI ID codes (based on TAIR10 annotation) of respective genes, subcellular localisation (Cy=cytosol, Ch=chloroplast), as well as the associated references are stated.

Enzyme	Abbreviation	AGI ID	Localisation	Reference
Riboflavin kinase/ FMN hydrolase	AtFMN/FHY	AT4G21470	Cy	Sandoval and Roje (2005)
FAD synthase	RIBF1 RIBF2	At5g23330, At5g08340	Ch	Sandoval *et al.* (2008)
Homologous to yeast Fad1p	FADS	At5g03430	Cy	Sandoval and Roje (2005)
FMN hydrolase	AtcpFHy1	At1g79790	Ch	Rawat et al. (2011)
Homologous to FMN hydrolase		At3g48420	?	Rawat et al. (2011) No *IN VITRO* FMN hydrolase activity
Homologous to FMN hydrolase		At4g11570	?	Rawat et al. (2011) No *IN VITRO* FMN hydrolase activity
FAD pyrophosphohydrolase	AtNUDX23	AT2G42070	Ch	Ogawa *et al.* (2008)

Riboflavin is supposed to be synthesised exclusively within the chloroplast. Consistently, all proteins of the riboflavin biosynthesis pathway, described in chapter 1.3.2, possess plastidial localisation, either verified experimentally or at least predicted from amino acid sequence analysis. Flavins, however, are needed as coenzymes (1.1.3) in all cellular compartments. So far, no flavin exporting transporters have been reported. Therefore, the compartmentalisation of the flavin nucleotide biosynthesis was proposed as already assessed by Mitsuda *et al.* (1970b), who reported riboflavin kinase activity in cytosolic as well as in organellar fractions, containing chloroplasts and mitochondria. The idea was further underpinned when Sandoval *et al.* (2008) measured riboflavin kinase, FMN hydrolase and FAD pyrophosphohydrolase activities in Percoll®-isolated *Pisum sativum* (pea) chloroplasts and mitochondria. On the other hand, FAD synthase activity was only detected in pea chloroplasts, wherein Giancaspero *et al.* (2009) demonstrated riboflavin kinase and FAD synthase activity as well as riboflavin import and FAD export in *Nicotiana tabacum cv.* Bright Yellow 2 suspension-cultured cells (TBY-2).

1.3.4 Flavin Biosynthesis Mutants

Only a few flavin biosynthesis knockdown mutants were described in plants so far. Intriguingly, knockout mutants of flavin biosynthesis genes are often lethal underlining the pivotal role of flavins in plants in general (Borchardt, 2015).

Xiao *et al.* (2004) identified an *Arabidopsis* knockdown mutant of the lumazine synthase (*cos1*) in a screen for suppressors of CORONATINE INSENSITIVE 1 (COI1), a jasmonic acid (JA) receptor (Yan *et*

al., 2009). This LS mutant, which was named *coronatine insensitive 1 suppressor* (*cos1*), was reported to restore the *coi1* mutants' wt-like phenotype of JA-mediated root elongation, gene expression, senescence, and defence responses. Interestingly, the *cos1xcoi1-2* double and the *cos1* single mutants (personal communication D. Xie) show a bleaching phenotype under 16 h light, 8 h darkness period. The authors interpreted these results as de-repressed senescence, due to the decrease in flavin contents that was caused by the incomplete disruption of the flavin biosynthesis pathway by the *cos1* mutation and thereby attenuating negative regulators of JA signalling that require flavins to employ their action.

Tomé and co-workers (unpublished data) as well as previous work performed in our group (Borchardt, 2015) have demonstrated that homozygous LS knockout mutants are embryo-lethal in *Arabidopsis*. Moreover Hasnain *et al.* (2013) failed to generate a knockout mutant of the *Arabidopsis* homologous gene in *Zea mays* encoding the PYRR protein (see chapter 1.3.2). This result agrees with the failed attempts of our group to generate *Arabidopsis* knockout mutants of *PYRR* (Borchardt, 2015). Conclusively, knockout of *LS* or *PYRR* most likely cause an embryo-lethal phenotype.

On the other hand, the knockdown of the PYRR (Ouyang *et al.*, 2010) induces a photo bleaching phenotype at 140 µmol photons $m^{-2}s^{-1}$ light intensity and short-day conditions (10 h light, 14 h darkness) similar to *cos1*. The mutant that was called *photosensitive 1* (*phs1*) showed strongly bleached leaves already at 80 µmol photons $m^{-2}s^{-1}$ light intensity. It was extensively characterised concerning its photooxidative stress features by Ouyang *et al.* (2010). They postulated that the decreased FNR activities, decreased NADPH/$NADP^+$ ratio and slower P700 oxidation and re-reduction rates hinted at electrons being channelled from photosystem I to the Mehler reaction, resulting in formation of superoxide radical (O_2^-), thus causing the chlorosis. Ouyang and co-workers demonstrated elevated O_2^- contents and antioxidant activities at normal (80 µmol photons $m^{-2}s^{-1}$) and high light (140 µmol photons $m^{-2}s^{-1}$) conditions. They also showed that the contents of proteins involved in photosynthesis were reduced.

Finally, Hedtke *et al.* (2012) studied the RIBA1 knockdown mutant *red fluorescent in the dark 1* (*rfd1*). As demonstrated by the authors, elevated protochlorophyllide (Pchlide) levels caused fluorescence of the etiolated *rfd1* seedlings in the dark. Pchlide is a phototoxic precursor of chlorophyll, which does not accumulate in *wt Col-0* plants in darkness due to the repression of the glutamyl-tRNA reductase (GluTR) activity, which performs the initial step of tetrapyrrole bio-synthesis (Brzezowski *et al.*, 2015). In *rfd1*, elevated cytokinin levels, caused by the impaired function of the FAD-dependent cytokinin oxidase (Hare & Staden, 1994), an enzyme responsible for cytokinin

degradation, lead to increased cytokinin levels. Elevated cytokinin content can induce chloroplast development in darkness, including transcriptional activation of *HEMA1*, which encodes GluTR.

1.3.5 Regulation of Flavin Biosynthesis

As flavin biosynthesis is a highly essential pathway, regulatory elements controlling flavin homeostasis are of great importance. A lot of publications dealing with the topic are based on organisms that are used as industrial riboflavin producers like *B. subtilis*. Hümbelin *et al.* (1999) showed that RibBA activity is the rate-limiting step in an industrial riboflavin producing *B. subtilis* strain. Moreover, the introduction of an additional copy of the *ribBA* gene led to improved riboflavin production. Mack *et al.* (1998) reported that FMN negatively regulates riboflavin biosynthesis in *B. subtilis*. Later, the effect was found to be caused by FMN binding to the so called riboswitch element (*RFN*) in the mRNA of the riboflavin operon, entailing folding into a hairpin structure and, thereby, negatively regulating the translation of the riboflavin operon (Gelfand *et al.*, 1999, Mironov *et al.*, 2002). Since then, riboswitches have been recognised as an ancient regulatory mechanism found to adjust diverse metabolic pathways in bacteria (Mandal *et al.*, 2003). The only riboswitch found to date in eukaryotes (Sudarsan *et al.*, 2003) is the TPP riboswitch regulating thiamine biosynthesis by binding thiamine pyrophosphate. It was originally identified in *E. coli* (Winkler *et al.*, 2002) and later also found in plants and algae (Bocobza *et al.*, 2007, Wachter *et al.*, 2007).

Another organism closely studied for regulatory mechanisms of the riboflavin biosynthesis is the naturally riboflavin overproducing (flavogenic) fungus *Ashbya gossypii,* often used as an industrial producer of riboflavin (Kato & Park, 2012). It has been demonstrated that overproduction of riboflavin starts at the transition between growth and stationary phase and hence transcriptional regulation upon growth stress has been postulated (Schlosser *et al.*, 2001, Schlosser *et al.*, 2007). *Pichia guilliermondii,* a representative of flavogenic yeast species, has been elaborated according to its feature to overproduce riboflavin upon iron limitation (Boretsky *et al.*, 2007, Boretsky *et al.*, 2011, Blazhenko, 2014). The underlying reasons and mechanisms behind this phenomenon are not yet known but a transcriptional upregulation of some riboflavin biosynthesis genes at iron limiting conditions has been shown (Boretsky *et al.*, 2005). A similar reaction has been observed in plants and will be further elucidated in chapter 1.4.

Recently, Yadav and Karthikeyan (2015) reported two forms of GCHII in *Heliobacter pyroli* that appeared depending on the redox environment *IN VITRO*. One was a form in which the cysteines of the zinc binding domain (see chapter 1.3.1) were in an oxidised state forming disulphide bridges and therefore not binding zinc, leading to the inactivity of GCHII. This state, however, could be reversed

by incubation with reducing agents like DTT, indicating a redox regulation of GCHII activity in *H. pyroli*.

The FAD pyrophosphohydrolase, as described in chapter 1.3.3, has been further characterised for its involvement in the homeostasis of flavins in plants by Maruta *et al.* (2012). Thereby, AtNUDX23-suppressor and –overexpressor lines were used to explore the effects on flavin levels and transcription of flavin biosynthesis genes. Interestingly, intracellular flavin- as well as the transcript levels of flavin biosynthesis were decreased in both the AtNUDX23-suppressor and the -overexpressor plants. The authors concluded a role of AtNUDX23 in the negative feedback regulation of flavin biosynthesis by the hydrolysis of FAD.

COG3236 was introduced as another regulator of flavin biosynthesis by Frelin *et al.* (2015). The enzyme is fused to the C-terminus of PYRR in plants and RibA in E. coli as well as some other bacteria. It is postulated to be able to cleave the N-glycosidic bond of the first two intermediates of riboflavin biosynthesis, 2,5-diamino-6-ribosylamino-4(3*H*)-pyrimidinedione 5'-phosphate and 5-amino-6-ribosylamino-2,4(1*H*,3*H*)-pyrimidinedione. The authors claim that these two intermediates are potentially harmful to the enzymes of the riboflavin biosynthesis pathway and that by their degradation, COG3236 contributes to the maintenance of a functional flavin biosynthesis.

1.4 Flavins and Plants

As described before for fungi, many plants over-accumulate riboflavin and excrete it from roots to soil as a response to iron deficiency. This has been reported for *N. tabacum* (Wallace *et al.*, 1967), *Beta vulgaris* (Susin *et al.*, 1993) and *Medicago truncatula* (Rodríguez-Celma *et al.*, 2011, Rodriguez-Celma *et al.*, 2011). Vorwieger *et al.* (2007) published two helix-loop-helix transcription factor genes, which were induced under iron starvation. Moreover, it was described that the heterologous overexpression of AtbHLH38 and AtbHLH39 in *N. tabacum* causes the excretion of riboflavin that is independent from iron-deprivation. Rodríguez-Celma *et al.* (2011) described for the accumulation of *RIBA*, *PYRD*, *LS* and *RS* transcripts, as well as RIBA and LS proteins, accompanied by the typical accumulation of riboflavin in iron-deprived *M. truncatula* root tissues.

Another wide area of flavin related research in plants deals with riboflavin enhanced pathogen defence, an effect that was first described by Dong and Beer (2000). They postulated that externally supplied riboflavin can trigger signal transduction pathways leading to systemic acquired resistance and that it requires protein kinase signalling and *NIN1*/*NPR1* expression. This mechanism was later declared as priming (Zhang *et al.*, 2009, Azami-Sardooei *et al.*, 2010, Taheri & Tarighi, 2010). Priming is a reaction of the plant to environmental cues inducing physiological changes, which can

help the plant to faster trigger pathogen defence reactions in case of a pathogen attack (Conrath *et al.*, 2006, Frost *et al.*, 2008).

Another interesting approach for flavin research in plants was first described by Deng *et al.* (2011), who modulated the intracellular flavin content by the expression of a turtle (*Trionyx sinensis japonicus*) gene encoding the riboflavin binding protein (RfBP) in *Arabidopsis*. With this system, the group of Hansong Dong was enabled studies on consequences of riboflavin depletion, which was postulated to account for the induction of H_2O_2 formation, coupled with enhanced pathogen defence (Deng *et al.*, 2011). This effect was later hypothesised to be derived from repressed gene expression for proteins of the mitochondrial electron transport chain (Li *et al.*, 2014). Furthermore, it was reported that the H_2O_2 accumulation promotes the expression of photoperiod genes, entailing an early flowering phenotype (Ji *et al.*, 2014).

Asai *et al.* (2010), however, paint a slightly different picture. They postulated that flavin synthesis is required for nitric oxide (NO) and reactive oxygen species (ROS) formation and thus necessary for disease resistance. This hypothesis was based on virus-induced gene silencing (VIGS) experiments in *Nicotiana benthamiana* decreasing RIBA expression and hence total flavin amounts by approximately 2/3 compared to control. They demonstrated decreased ROS and NO contents, which they linked with the increased susceptibility to infection by *Phytophthora infestans*.

Recently, the role of externally applied riboflavin causing a priming effects, was subject of an investigation on drought stress response in tobacco plants (Deng *et al.*, 2013) and could shed some light on the before presented discrepancy. They reported that the application of low riboflavin concentrations led to better drought tolerance, whereas the application of high riboflavin concentrations resulted in impaired drought tolerance. Deng and co-workers explained this effect by riboflavin entailing ROS accumulation within the plant, as the result of riboflavin's known photosensitising influence (Massey *et al.*, 1969, Huang *et al.*, 2004, Eichler *et al.*, 2005). They hypothesised that riboflavin applied in low concentrations may cause little ROS formation and a simultaneous activation of antioxidant systems, which would enhance drought tolerance. But if riboflavin is applied in high concentrations, it causes high amounts of ROS which then have a toxic effect on the defence system and hence cause low drought tolerance. Deng and co-workers grant riboflavin a rather complicated role in the interplay of ROS metabolism and abiotic/biotic stress signalling, since flavins are needed as cofactors for enzymes, which generate ROS and NO, as well as by enzymes of the antioxidant systems.

1.5 Objectives

As mentioned in chapter 1.3.2, Herz *et al.* (2000) identified and initially characterised the RIBA1 enzyme from *A. thaliana* and *Solanum lycopersicum*, performing the two primary steps of riboflavin biosynthesis. Work done in our group identified two additional members of the *RIBA* gene family (At2g22450/At5g59750), each with a high sequence homology to *RIBA1* (Hedtke *et al.*, 2012). Until now, no data on these additional members has been available neither in *Arabidopsis*, nor in any other plant species. The high degree of conservation of multiple isoforms among angiosperms hints at non-arbitrary roles that remain yet to be identified. As it is dealt here with a protein that performs both initial enzymatic steps of a highly important biosynthesis pathway, it seemed logical that one of the main aims of this thesis was defined as the exploration of the *RIBA* gene family members and their physiological roles. The procedure involved enzymatic characterisation of recombinant enzymes *IN VITRO* and *IN VIVO*, as well as reverse genetics approaches by using deletion and overexpression mutants. Beyond that, a comprehensive metabolomics analysis was performed to learn about metabolic consequences of *RIBA* deletion and overexpression. By that, it was intended to draw conclusions about roles of the RIBA isoforms as well as studying the metabolic effects of deregulated flavin biosynthesis.

Additionally, a protein-protein interaction analysis by co-immunoprecipitation with the aim to find potential interacting proteins was initiated. Moreover, a **Bi**molecular **F**luorescence **C**omplementation assay was performed to study potential dimerisation behaviour of RIBA proteins. The results were evaluated with a special focus to learn more about regulatory mechanisms and the organisation of the flavin biosynthesis pathway and to obtain more hints on possible other roles of RIBA isoforms.

In the introduction, on the one hand the great impact of flavins in a multitude of biological reactions, as well as the complexity of the biosynthetic pathway were demonstrated. On the other hand, the interesting aspects of flavin related research in plants and the necessity for further research especially concerning the deeper understanding of the flavin biosynthetic pathway could be illustrated. The studies performed in this thesis are justified with efforts to make use of improved understanding of regulatory mechanisms on vitamin B_2 biosynthesis, in order to ultimately enhance the natural production of vitamin B_2 in plants. No such attempts have been published up to date. This, however, could be an important aspect given the rising necessity for future meat and dairy alternatives in consequence of world population growth and the negative emission values of industrial livestock farming (Popp *et al.*, 2010).

2 Materials and Methods

2.1 Companies

Table 4: **List of companies**

Company	City, Country
Agilent Technologies	Santa Clara, USA
Agrisera	Vännäs, SWE
Analytic Jena	Jena, DE
AppliChem GmbH	Darmstadt, DE
BANDELIN electronic GmbH & Co. KG	Berlin, DE
Bayer Crop Science	Monheim, DE
Beckman Coulter	Brea, USA
Becton, Dickinson and Company	New Jersey, USA
Biogenes	Berlin, DE
Biometra	Göttingen, DE
Bioline	London, UK
Bio-Rad	Hercules, USA
Biotool.com	Houston, USA
Biozym Scientific GmbH	Hessisch Oldendorf, DE
BISCHOFF Chromatography GmbH	Leonberg, DE
Cambia Labs	Brisbane, AUS
Carl Roth	Karlsruhe, DE
CLF Plant Climatics	Wertingen, DE
Duchefa	Haarlem, NL
E. coli Genetic Stock Center	Yale, USA
Eppendorf	Hamburg, DE
Gebr. Patzer	Sinntal-Jossa, DE
GE Healthcare	Uppsala, SWE
Genscript®	Piscataway, USA
Heidolph Instruments GmbH & Co. KG	Schwabach, DE
Heraeus	Osterode am Harz, DE
Hettich AG	Bäch, CH
IBA GmbH – solutions for life sciences	Göttingen, DE
ibs tecnomara GmbH	Fernwald, DE
INRA (Versailles Stock Centre)	Versailles, FR
Invitrogen	Karlsruhe, DE
Lehle Seeds	Round Rock, USA
LI-COR	Lincoln, USA
Martin Christ Gefriertrocknungsanlagen GmbH	Osterode am Harz, DE
Merck Millipore	Darmstadt, DE
NASC (The European *Arabidopsis* Stock Centre)	Nottingham, UK
neoLab	Heidelberg, DE
New England Biolabs GmbH	Ipswich, USA
Qiagen	Hilden, DE
raytest Isotopenmessgeräte GmbH	Straubenhardt, DE
Retsch GmbH	Haan, DE
Roche Diagnostics	Rotkreuz, CH
Serva	Heidelberg, DE
Sigma-Aldrich	St. Louis, USA
SMB Services in Molecular Biology GmbH	Berlin, DE
Stratec Molecular GmbH	Berlin, DE
Thermo Fischer Scientific	Waltham, USA
UniEquip Laborgerätebau- und Vertriebs GmbH	Planegg, DE
Vacuubrand GmbH	Wertheim, DE
Waters	Milford, USA

2.2 Chemicals

Basic chemicals were generally purchased at Sigma Aldrich, AppliChem, Carl Roth or Serva if not stated otherwise.

Table 5: **List of chemicals and kits**

Chemical/ Kit	Company/ Source
Adonitol (Ribitol; A4337)	AppliChem GmbH
Amino, 5-amino-6-ribitylamino-2,4(1H,3H)-pyrimidinedion, Synthesis as stated in Kis *et al.* (2001)	Hamburg School of Foodscience
Avidin	IBA GmbH
BASTA®, 200 g l^{-1} Glufosinatammoniumn	Bayer, Crop Science AG
Biotool™ 2x SYBR Green qPCR Master Mix	Biotool.com
BSA, Albumin Fraction V (pH 7)	AppliChem GmbH
CloneJET PCR Cloning Kit	Thermo Fischer Scientific
cOmplete, Mini, EDTA-free, Protease Inhibitor Cocktail Tablets	Roche Diagnostics
Coomassie® Brilliant Blue G250	Serva
Coomassie® Brilliant Blue R-250	Serva
CutSmart-Puffer	New England Biolabs GmbH
Difco™ Agar, granulated	Becton, Dickinson and Company
6,7-dimethyl-8-ribityllumazine	Hamburg School of Foodscience
6x DNA loading dye	Thermo Fischer Scientific
DNase I Solution (1 unit/µL), RNase-free + Reaction Buffer with MgCl2 (10X)	Thermo Fischer Scientific
DreamTaq, DNA-Polymerase + DreamTaq 10x buffer, green	Thermo Fischer Scientific
Flavin adenine dinucleotide disodium salt hydrate (F6625)	Sigma Aldrich
GeneJET Plasmid Miniprep Kit	Thermo Fischer Scientific
GeneRulerTM 1 kb and 100 bp DNA Ladder	Thermo Fischer Scientific
HF-5x buffer	New England Biolabs GmbH
HisPur Ni-NTA Resin	Thermo Fisher Scientific
HisTrap HP 1ml	Amersham
Imidazol	AppliChem
innuPREP Plant RNA Kit	Analytik Jena
Invisorb® Spin DNA Extraktion Kit	Stratec Molecular
IPTG	Duchefa
Lumazinsynthase, recombinant Lumazinsynthase from *B. subtilis*	Hamburg School of Foodscience
MSB® Spin PCRapace	Stratec Molecular GmbH
Murashige-Skoog-Medium with Vitamins	Duchefa Biochemie
Percoll(R)	GE Healthcare
Phosphate, 3,4-dihydroxy-2- butanon-4-phosphat, Synthesis as stated in Kis *et al.* (2001)	Hamburg School of Foodscience
Phosphatase, not fully characterized Phosphatase (Haase *et al.*, 2013)	Hamburg School of Foodscience
Phusion-Polymerase	New England Biolabs GmbH
Polypropylene Columns 1 ml	Qiagen
Ponceau S	Sigma Aldrich
PVP-40, Polyvinylpyrrolidon	Sigma Aldrich
RevertAid™ Reverse Transcriptase	Thermo Fischer Scientific
RibA, recombinant DHBP Synthase/ GTP Cyclohydrolase II from *B. subtilis*	Hamburg School of Foodscience
RibG, recombinant bifunctional Desaminase/ Reductase from *B. subtilis*	Hamburg School of Foodscience
(-)-Riboflavin (R9504)	Sigma Aldrich
Riboflavin 5'-monophosphate sodium salt dehydrate (F6750)	Sigma Aldrich
D-Ribulose 5-phosphate disodium salt (83899)	Sigma Aldrich
RNase A	Thermo Fischer Scientific
SensiMix™ SYBR No-ROX One Step Kit	Bioline
Silicon dioxide (Quartz sand; 84878)	Sigma Aldrich
Silwet L-77	Lehle Seeds
Strep-Tactin® MacroPrep® 50 % suspension	IBA GmbH
T4-DNA Ligase & T4 DNA Ligase Reaction Buffer (10x)	New England Biolabs GmbH
Unstained Molecular Weight Marker Prestained Protein Molecular Weight Marker Unstained PAGE Ruler	Thermo Fischer Scientific

2.3 Equipment

Table 6: **List of equipment**

Equipment	Designation, Company
Agarose gel electrophoresis	SUB Cell GT with Powerpac 300, Biorad
Ball mill	MM301, Retsch
CCD-camera for detection of chemiluminescence	stella 3200, raytest Isotopenmessgaräte GmbH
Centrifuges	Biofuge fresco, Thermo Fischer Scientific Centrifuge 5424, Eppendorf Avanti J-26 XP (fixed angle: JA10,JLA16250, JA 30.50, swing-out: JS 24), Beckman Coulter Rotina 35R/38R, Hettich
Clean bench	Lamin Air®, Heraeus Lamina Airflow Workstation, Integra Biosciences
Concentrator	U-Tube™ Concentrator 6-10, Novagen
Dialysis tubing	SnakeSkin™ Pleated Dialysis Tubing (10,000 MWCO), Thermo Fischer Scientific
Growth chamber	MobyLux GroBank (BB-XXL3 / BB-XXL3+, TS-110), CLF Plant Climatics
Electroporator	MicroPulser™ Electroporator, Biorad
FPLC-System	ÄKTA FPLC System with UV/conductivity detector UPC900 and fraction collector Frac920, GE Healthcare
Geldocumentation system	AlphaImager, Biozym
Gel dryer	Unigeldryer 3545 D, UniEquip Laborgerätebau- und Vertriebs GmbH
Heating block	Thermomixer compact, Eppendorf
HPLC-System	System: Agilent-1100 series with fluorescence detector, Agilent; Columns: Novapak C18, particle size: 4µm, 3.9x150 mm, Waters; Prontosil 200-3-C30 particle size: 3 µm, 4.6 x 250 mm, Bischoff Chromatography
Incubator shaker	Innova 4000, New Bruinswick Scientific
Light meter	LI-250, Li-Cor
Mass spectrometre	LTQ-Orbitrap Elite, Thermo Fischer Scientific
Miracloth	Merck Millipore
NanoDrop®2000 Spektrophotometer	Thermo Fischer Scientific
NanoHPLC	NanoAcquity UPLC system, Waters Column: C18, 75 µmx150mm, particle size: 1.8 µm, Material: HSS T3, Waters
Nitrocellulose blotting membrane	Amersham Protran Supported 0.45 NC, GE Healtcare
Open-top thinwall tube	Thinwall Polypropylene tube 38.5 ml and Thinwall Ultra-Clear® tube 38.5 ml, Beckman Coulter
Phosphoimager	Personal Molecular Imager™ (PMI™) System, Biorad
Phyto chamber	PGV 36, Conviron
Real-time PCR	CFX96 Touch™ Real-Time PCR Detection System, Biorad
SDS-PAGE-System	Mini PROTEAN®3, Biorad
Semidry blotter	TransBlot R_SD, Biorad
Shaker	Orbital Shaker 7-0031, neoLab
Sonicator	SONOPLUS HD2070 mit Sonotrode MS73, Bandelin
Spectrophotometer	Ultrospec 3300 pro, GE Healthcare
Speed vac	RVC 2-25 CD plus + CT 02-50 SR, Christ Diaphragm vacuum pump MZ 2C NT, Vacuubrand
Thermocycler	T3 und Tpersonal, Biometra
Vacuum pump	Diaphragm vacuum pump MZ 2C, Vacuubrand

2.4 Media

Table 7: **Frequently used media for bacteria or plant cultivation.**

Medium	Composition
LB	10 g l^{-1} Bacto Tryptone, 5g l^{-1} Yeast extract, 10 g l^{-1} NaCl, pH 7.5 with NaOH (for LB solid add 15 g Bacto Agar)
SOC	5 g l^{-1} Bacto Tryptone, 1 g l^{-1} Yeast extract, pH 7.2 with NaOH → autoclave, 5 g l^{-1} Sucrose, 0,5 g l^{-1} $MgSO_4*7H_2O$
5xM9	42.5 g l^{-1} $Na_2HPO_4*2H_2O$, 15 g l^{-1} KH_2PO_4, 2.5 g l^{-1} NaCl, 5 g l^{-1} NH_4Cl → autoclave and add 2 ml 1 M $MgSo_4$, 0.1 ml 1 M $CaCl_2$, 20 ml 20% Glucose
YEB	5 g l^{-1} Bacto Tryptone, 1 g l^{-1} Yeast extract, pH 7.2 with NaOH → autoclave and add 5 g l^{-1} Sucrose, 0.5 g $MgSO_4*7H_2O$,
¼ MS	1.1 g l^{-1} Murashige & Skoog Medium with Vitamins, 0.5 g l^{-1} MES, pH 5.7 with KOH

Table 8: **List of antibiotics used for the selection of transgenic bacteria and plants.**

Substance	Source	Stock Solution	Solvent	Working Conc.
Ampicillin	AppliChem	100 mg ml^{-1}	Water	100 µg ml^{-1}
Carbenicillin	Carl Roth	50 mg ml^{-1}	Water	50/75 µg ml^{-1}
Chloramphenicol	Duchefa	34 mg ml^{-1}	Ethanol	34 µg ml^{-1}
Gentamycin	Serva	15 mg ml^{-1}	Water	15 µg ml^{-1}
Hygromycin	Carl Roth	50 mg ml^{-1}	Water	35-50 µg ml^{-1}
Kanamycin	Carl Roth	50 mg ml^{-1}	Water	50 µg ml^{-1}
Rifampicin	Duchefa	25 mg ml^{-1}	DMSO	100 mg ml^{-1}

2.5 Biological Material

2.5.1 Plants and Growth Conditions

Plants used in the experiments were *Arabidopsis thaliana* L. HEYNH. Var. Col (wt Col-0), *Arabidopsis thaliana* L. HEYNH. Var. Was (wt Ws-0), *Nicotiana tabacum* L. cv. Samsun NN (SNN) and *Nicotiana benthamiana* Domin.

Standard growth conditions for *A. thaliana* were as follows: seeds were sown on a mixture of three parts soil (Einheitserde Typ GS90, Gebr. Patzer) and one part vermiculite. After two days stratification at 4 °C the pots were moved to a growth chamber with short-day conditions (10 h light, 14 h darkness) at 90 to 100 µmol photons $m^{-2}s^{-1}$ light and a temperature of 23 °C. After 10 to 14 day (in special cases 28 days), seedlings were transplanted to individual pots.

For induction of flowering approximately 8-week-old *Arabidopsis* were moved to long-day conditions (16 h light, 8 h darkness).

Standard growth conditions for *N. tabacum* were long-day conditions (16 h light, 8 h darkness) at 150 µmol photons $m^{-2}s^{-1}$ in the greenhouse. Generally tobacco was grown on soil (Einheitserde Typ-T, Gebr. Patzer), wherein germination and possible selection of seedlings was, if required, performed on 2MS-Agar plates containing sucrose (4.43 g l^{-l} Murashige Skoog with vitamins, 0.5 g l^{-l} MES, 20 g l^{-l} sucrose, pH 5.7 KOH, 10 g l^{-l} Difco™ Agar) and respective selective agent.

2.5.1.1 *Sampling of Plant Material*

In order to prevail standardisation, sampling took place three to four hours after beginning of the light phase. It was taken care that the samples were snap frozen in liq. N_2 to avoid DNase, RNase or protease activity. Plant material was stored at -80 °C before final use.

Samples were generally collected from single plants. For some purposes, pooled samples were generated, originating from seedlings of one transgenic line before transplantation into single pots.

2.5.1.2 *Determination of Embryo Lethality*

For the verification of an embryo lethal phenotype of T-DNA knockout lines, viable and non-viable seeds were counted in siliques of heterozygous progenies of mutant lines. Therefore, green siliques shortly before yellowing were opened longitudinally and fixed on sticky tape. Non-viable seeds, characterised by arrested or clearly delayed state of growth, as well as viable seeds were counted using binocular magnification.

2.5.2 T-DNA Insertion Lines

A. thaliana T-DNA insertion lines that were utilised in the experiments are listed in **Table 9**.

Table 9: **List of T-DNA insertion lines used in the experiments.**

AGI ID	Designation	Genotype	Code	Source
At5g64300	*riba1* GABI	heterozygote	GK-082E03.09	NASC
At5g64300	*riba1* SALK	heterozygote	SALKseq_055177.3	NASC
At5g64300	*riba1* FLAG	heterozygote	FLAG_391E03	INRA
At2g22450	*riba2*	homozygote	SALK_073421	NASC
At5g59750	*riba3*	homozygote	SALK_039631	NASC

2.5.2.1 *Cross fertilization of A. thaliana*

A double mutant carrying T-DNA insertions mutating two different genes was generated by crossing homozygous individuals of two T-DNA insertion lines. Therefore, the single mutants were initially grown under standard short-day growth conditions and flowering was induced by moving plants to long-day conditions. Flower buds of maternal mutant line plants were manually opened and anthers were removed carefully before dehiscence. For mating 2 to 3 days later flowers with dehiscent anthers of the paternal mutant line were brushed against the stigmatic surface of the exposed carpels of the prepared maternal mutant line plants. The F1 seeds were collected and grown as usually and screened for double homozygotes via genotyping as described in 2.7.5.1.

2.5.3 Bacterial Strains and Growth Conditions

The bacterial strains that were employed in the experiments are described in **Table 10.**

Table 10: **Summary of *A. tumefaciens* and *E. coli* strains used in the experiments.**

	Strain	Genotype	Application	Source/Reference
E. coli	CGSC# 6992 (BSV18)	*ribA18::Tn5*	ribA Complementation	*E. coli* Genetic Stock Center
	CGSC# 6991 (BSV11)	*ribB11::Tn5*	ribB Complementation	*E. coli* Genetic Stock Center
	DH5α	F-Φ80*lac*ZΔM15 Δ(*lac*ZYA-*arg*F) U169 *rec*A1 *end*A1 *hsd*R17 (rK-, mK+) *pho*A *sup*E44 λ- *thi*-1 *gyr*A96 *rel*A1	Cloning	Invitrogen
	ArcticExpress ™ (DE3) RIL	*E. coli* B F⁻ *ompT hsdS*(r_B^- m_B^-) *dcm*⁺ Tet^r *gal* λ(DE3) *endA* Hte [*cpn10 cpn60* Gent^r] [*argU ileY leuW* Str^r]	Low temperature protein expression	Agilent Technologies
A. tumefaciens	GV2260	C58, Rif^r, pGV2260 (pTiB6S3 ΔT-DNA), Carb^r	Plant transformation	Hellens *et al.* (2000)
	GV3101 (pMP90RK)	C58, Rif^r, pMP90RK (pTiC58 ΔT-DNA), Gent^r, Kan^r	Plant transformation	Koncz and Schell (1986)
	C58C1	C58, Rif^r, (pCH32 35S:p19), Tet^r, Kan^r	Suppression of silencing through expression of P19 from *TBSV*	Voinnet *et al.* (2003) Witte *et al.* (2004)

2.5.4 Plasmids

The plasmids utilised for subcloning and cloning purposes in the experiments are listed in **Table 11.**

Table 11: **Plasmids used for experiments. P indicates resistance marker for prokaryotic selection and E for eukaryotic selection.**

Plasmid	Resistance	Application	Source/Reference
pJet1.2/blunt	Ampicillin	Cloning of PCR Products	Thermo Fischer Scientific
pUC57-ribA1	Ampicillin	Delivery of synthetized gene insert	Genscript®
pUC57-ribA2	Ampicillin	Delivery of synthetized gene insert	Genscript®
pUC57-ribA3	Ampicillin	Delivery of synthetized gene insert	Genscript®
pET22b(+)	Ampicillin	Protein expression	Merck Millipore
pACYC184	Chloramphenicol	E. coli complementation	NEB
pGL1	Kanamycin (P), BASTA® (E)	Binary vector for plant transformation	Modified pGPTV-bar Becker *et al.* (1992), Hiltunen *et al.* (2012)
pXCS-HA-Strep	Ampicillin (P), BASTA® (E)	Binary vector for plant transformation	Witte *et al.* (2004)
pCambia3301	Kanamycin (P), BASTA® (E)	Binary vector for plant transformation	Cambia Labs
pCambia1305.2	Kanamycin (P), Hygromycin (E)	Binary vector for plant transformation	Cambia Labs
pTRV1	Kanamycin	VIGS	Liu *et al.* (2002)
pTRV2	Kanamycin	VIGS	Liu *et al.* (2002)
pSpyCE	Kanamycin	BiFC	Walter *et al.* (2004)
pSpyNE	Kanamycin	BiFC	Walter *et al.* (2004)

2.6 Transformation Techniques

2.6.1 Preparation and Transformation of Competent *E. coli*

To prevent contaminations and loss of competency, cells and solutions were kept cold and sterile at all times during preparation of competent cells.

2.6.1.1 Chemocompetent E. coli

A liquid culture with 2 ml LB medium was inoculated with a single colony from a fresh plate and incubated at 37 °C, 250 rpm o/n. Subsequently 1 ml of the over-night culture was used to inoculate 500 ml LB medium supplemented with 5 ml 1 M $MgCl_2$ and incubated at 18 °C, 250 rpm until an $OD_{600\,nm}$ of 0.25-0.7 was reached. Thereafter the culture was cooled down on ice for 10 min and the cells were harvested at 4500 rpm, 4 °C for 10 min. The obtained pellet was resuspended in 80 ml ice cold TB buffer (10 mM Pipes, 15 mM $CaCl_2$, 250 mM KCl, pH 6.7 with KOH +55 mM $MnCl_2$) and incubated on ice for 10 min. Aliquots of 100-200 µl were snap frozen in $liqN_2$ and stored at -80 °C. For transformation an aliquot was thawed on ice and ca. 100 ng plasmid DNA or 10 µl ligation mixture (2.7.9.3) was added and mixed by careful tapping of the tube. After 20 min incubation on ice, the cells were quickly transferred to 42 °C and incubated for 90 s. Subsequently the cells were incubated on ice for 5 min and 500 µl SOC medium was added. After 1 h incubation at 37 °C, 220 rpm, different amounts ranging from 50-500 µl of the culture (depending on the construct and on the competency of respective *E. coli* line) was plated on selection media and grown o/n at 37 °C.

2.6.1.2 Electrocompetent E. coli

The preparation of electrocompetent *E. coli* cells was described by Miller and Nickoloff (1995). The procedure was started with the inoculation of 200 ml LB with 2 ml of an o/n LB culture. The culture was grown until an $OD_{600\,nm}$ of ~0.8 was reached and then cooled at 4 °C for 30 min. The cells were pelleted at 4000 x *g*, 4 °C for 15 min. The pellet was resuspended in 1 vol cold MQ and centrifuged as stated before. After the washing step was repeated once more, the pellet was resuspended in 20 ml cold 10%-glycerol and centrifuged again. The final resuspension of the pellet took place in 2 ml cold 10%-glycerol and 40 µl aliquots were snap frozen in $liqN_2$ and stored at -80 °C. For transformation, 10 µl of the competent cells was mixed with approximately 50-100 ng purified plasmid DNA and electroporated in 0.1 cm cuvettes at 1800 V with a time constant of approximately 5 ms. After electroporation, cells were resuspended in 500 µl SOC medium and incubated for 1 h at 37 °C, 230 rpm. Thereafter different amounts of the culture (depending on the construct and on the competency of respective *E. coli* line) were plated on solid LB medium containing respective selection agent in concentrations as stated in **Table 8**.

2.6.2 Preparation and Transformation of Electrocompetent *A. tumefaciens*

A 200 ml YEB culture with respective antibiotics was inoculated with 2 ml fresh o/n culture of *A. tumefaciens* and grown under 30 °C, 250 rpm until an $OD_{600\,nm}$ of 1.5-2 was reached. The cells were pelleted at 4000 x *g*, 4 °C, for 10 min and subsequently resuspended in 200 ml cold MQ. This washing step was repeated four times before the pellet was resuspended in 20 ml cold 10%-glycerol (v/v) and centrifuged again. Finally the pellet was resuspended in 2 ml cold 10%-glycerol (v/v) and the cells snap frozen in 20-40 µl aliquots in $liqN_2$ and stored at -80 °C.

For transformation 10 µl of the competent cells was mixed with 50-100 ng purified plasmid DNA and electroporated in 0.1 cm cuvettes at 2200 V with a time constant of approximately 5 ms. After electroporation cells were resuspended in 500 µl liquid YEB medium and incubated for 2-3 hours at 230 rpm, 28 °C. Subsequently 50 µl of the cells was plated on solid YEB plates with respective selection agent at concentrations stated in **Table 8** and grown for two days at 30 °C.

2.6.2.1 Special Treatment of GV3101

Growth of GV3101 was found to be slightly more difficult than GV2260. As GV3101 were mostly used for the handling of pXCS-HA-Strep which has ampicillin/carbenicillin resistance, a general protocol for growth was as follows:

Selection of transformed GV3101 (containing pXCS-HA-Strep) was performed for 4 days at 30 °C on YEB plates (100 µg ml^{-1} rifampicin, 50 µg ml^{-1} kanamycin, 15 µg ml^{-1} gentamycin and 75 µg ml^{-1} carbenicillin) until colonies appeared. These colonies were picked and immediately streaked on fresh plates. After 2 days liquid YEB cultures (100 µg ml^{-1} rifampicin, 50 µg ml^{-1} kanamycin, 15 µg ml^{-1} gentamycin and 50 µg ml^{-1} carbenicillin) were inoculated with two inoculation loops full of cell material. Next day cryo storage cultures were established as described in 2.6.3. Liquid cultures for plant transformations were inoculated from plates streaked freshly each time from respective cryo cultures.

2.6.3 Cryo Storage Cultures

In order to obtain cryo storage cultures, 870 µl of fresh o/n liquid culture was mixed with 130 µl sterile 87 % glycerol (v/v) and 200 µl aliquots were snap frozen in $liqN_2$. The cultures were stored at -80 °C until further use.

2.6.4 Stable Transformation of *A. thaliana*

The described method for stable transformation of *Arabidopsis* is a modification of the "floral dip" method described by Clough and Bent (1998).

Bolting was started in approximately 8-week-old plants. The primary bolt was clipped to initiate the growth of secondary bolts. *A. tumefaciens* o/n culture (4 ml YEB + antibiotics) was inoculated with a single colony from a selection plate. Cells were pelleted at 4000 x *g*,12 °C for 20 min and resuspended in 4 ml inoculation medium (0.5 x Murashige-Skoog-Medium with Vitamins, 0.05 % MES (w/v), 5 % sucrose (w/v), 0.05 % Silwet L77 (v/v), pH 5.7) and $OD_{600\ nm}$ was adjusted to 0.8-1. Three to five days after clipping *A. tumefaciens* culture carrying the desired binary vector was applied directly on the buds. After treatment with the Agrobacteria, the plants were covered with dark plastic bags for 1.5-2 days. The procedure was repeated two to three times at an interval of three to four days for the newly emerging buds.

2.6.4.1 *Selection of T1 Generation after Transformation*

2.6.4.1.1 With BASTA

Plants transformed with constructs carrying the bialaphos resistance gene (bar) as selection marker (White *et al.*, 1990) were treated with a 0.05 % BASTA® (v/v) solution. Therefore, 1-1.5 ml T2 seeds were sown on trays and grown under standard short-day conditions. After 14 days, BASTA® treatment was started and repeated two to three times at an interval of four to five days until selection was completed.

2.6.4.1.2 Selection on Sand

For plants transformed with constructs carrying the hygromycin phosphotransferase II (hptII/ *aph*IV) gene as selection marker (Waldron *et al.*, 1985) the selection method described by Davis *et al.* (2009) was used. Quartz sand soaked with ¼ MS Medium served as substrate. Hygromycin concentrations between 35-50 µg ml^{-1} were used. Seedlings surviving the treatment were transplanted to soil filled pots 14-20 days after sowing.

2.6.5 Transient Transformation of *Nicotiana benthamiana*

For transient expression of proteins in *N. benthamiana*, leaves of 3- to 4-week-old plants were infiltrated from the abaxial side with a mixture of desired transgenic *A. tumefaciens*. Therefore, fresh liquid cultures of agrobacteria carrying the respective constructs (2.6.2) were pelleted, resuspended in infiltration medium (10 mM $MgCl_2$, 10 mM MES, pH 5.7, 100 µM acetosyringon) and $OD_{600\ nm}$ adjusted to 0.2-0.6. Before infiltration, the cultures were incubated at RT for 2-3 hours.

2.7 DNA Techniques

2.7.1 Isolation of Genomic DNA from *A. thaliana*

For the isolation of pure and RNA free genomic DNA from *A. thaliana,* 1-2 young leaves were collected and homogenised in 500 µl DNA ex-buffer (0.1 M Tris, 0.05 M EDTA, 0.5 M NaCl, 1 % PVP-40 (v/v)) with the ball mill (25 Hz, 1 min). The sample was supplemented with 66 µl 10% SDS and mixed by vortexing before incubation at RT for 10 min. Debris of cell lysis was removed by centrifugation at 13,000 rpm, RT for 10 min. The supernatant was collected and mixed thoroughly with 166 µl 5 M KOAc (3 M potassium acetate, 2 M acetic acid, pH ~5.8). The sample was centrifuged again at 13,000 rpm, RT for 15 min. To precipitate DNA, the supernantant was supplemented with 500 µl isopropanol and mixed by gentle agitation. After 20 min incubation on ice, DNA was spun down by centrifugation at 16,000 rpm, 4 °C for 20 min. The pellet was washed twice with 500 µl 70% EtOH, followed by centrifugation at 16,000 rpm, 4 °C for 5 min. Finally, the pellet was dried at RT for 10 min and resuspended in 100 µl RNase A-solution (40 µg μl^{-1} in TE-buffer (10 mM Tris-HCl, pH 8, 1 mM EDTA)). RNase treatment was applied for 1.5 h at RT. The DNA was then used for amplification of genomic fragments for cloning or genotyping purposes and otherwise stored at -20 °C.

2.7.2 Quick Isolation of Genomic DNA from *A. thaliana*

A small piece of a preferably young *Arabidopsis* leaf was homogenised in 95 µl extraction buffer w/o SDS (200 mM Tris-HCl, pH 8, 150 mM NaCl, 25 mM EDTA) with the ball mill (25 Hz, 1 min). After a short centrifugation to spin the leaf material to the bottom of the tube, 5 µl 10 % SDS was added and mixed by vortexing. Cell debris was removed from the sample by centrifugation for 3 min at 13,000 rpm and the supernatant transferred to a new tube containing 100 µl isopropanol. DNA was pelleted at 16,000 rpm, 4 °C for 15 min and washed twice in 500 µl 70 % EtOH. The pellet was dried at RT and resuspended in 25 µl MQ. The DNA was used for genotyping purposes only and stored short-term at 4 °C.

2.7.3 Isolation of Genomic DNA from *N. tabacum*

Three leaf discs (Ø 9 mm) were homogenised in the ball mill (25 Hz, 1 min) and resuspended in 600 µl of prewarmed DNA extraction solution mixture (65 °C), consisting of 1 part extraction buffer (350 mM sorbitol, 100 mM Tris-HCl, pH 8, 5 mM EDTA), 1 part of lysis buffer (200 mM Tris-HCl, pH 8, 50 mM EDTA, 2 M NaCl, 2 % CTAB (w/v)) and 0.4 parts of sarcosyl buffer (5 % n-lauroylsarcosine (w/v), 0.38 % sodiumbisulfite (w/v), 1 % PVP-40 (w/v)). The mixture was incubated at 65 °C for 20 min. Afterwards 600 µl CHCl3:Isoamylalcohol (24:1) was added and the sample vortexed. During the subsequent centrifugation at 10,000 rpm for 10 min, phase separation took place. The upper

aqueous phase, containing the nucleic acids was collected, supplied with 20 µl RNase A (10 mg ml^{-1}) and incubated at 37 °C for 15 min. DNA was precipitated by adding 500 µl isopropanol and pelleted at 13,000 rpm, 4 °C for 10 min. The DNA pellet was washed twice with 1 ml of 75 % EtOH, dried at RT and resuspended in 50-80 µl MQ.

2.7.4 Isolation of Plasmids from *E. coli*

2.7.4.1 Alkaline Lysis

Standard procedure for plasmid isolation from 2 ml o/n *E. coli* cultures was the so called alkaline lysis method. Therefore, 2 ml o/n culture was pelleted at 13,000 rpm for 3 min and resuspended in 250 µl resuspension buffer (50 mM Tris-HCl pH 8, 10 mM EDTA, 100 µg ml^{-1} RNase A) and incubated at RT for 5 min. For cell lysis 250 µl lysis buffer (200 mM NaOH, 1 % SDS (w/v)) was added and the sample was inverted 6-8 times and incubated for 5 min at RT. Then 250 µl neutralization buffer (3 M potassiumacetate, pH 5.5) was added and the mixture inverted again 6-8 times and incubated for 10 min on ice. Precipitated proteins were pelleted at 13,000 rpm, 4 °C for 10 min. The DNA was precipitated from the supernatant by addition to 600 µl isopropanol and incubation at RT for 10 min. After centrifugation at 13,000 rpm, 4 °C for 10 min the obtained DNA pellet was washed twice with 70 % EtOH. Finally, the DNA pellet was dried at RT and resuspended in 40 µl MQ.

2.7.4.2 Plasmid Miniprep Kit

To gain highly pure plasmid DNA, plasmid isolation from 2-5 ml o/n cultures was performed with GeneJET Plasmid Miniprep Kit according to manufacturer's recommendations.

2.7.5 Polymerase Chain Reaction for Amplification of DNA Fragments

The polymerase chain reaction (PCR) (Mullis *et al.*, 1986) was used to amplify desired fragments of DNA employing primers complementary to the target sequence and marking the beginning "forward" (fw) and the end "reverse" (rev) of each fragment to be amplified.

2.7.5.1 Detection of Plasmid DNA (Colony PCR)/T-DNA (Plant Genotyping)

Via the detection of specific sequences by PCR, genotyping of transgenic bacteria or plants can be performed. Therefore, primers were used that anneal in a vector specific region to identify "positive" bacteria after transformation. For plant, genotyping construct specific primers were used for newly generated transgenic lines. For purchased T-DNA lines, where the site of the insertion (mutagenized gene) is known, primers flanking the insertion were chosen to be able to differentiate between three possible genotypes: 1.) homozygous mutants, in which only combination of T-DNA specific and genome specific primer results in a PCR product;

2.) homozygous individuals for the wt allele, in which only combination of the two flanking genome specific primers yield a PCR product; 3.) heterozygous mutants, in which both primer combinations yield a product due to two different alleles within the genome. A standard PCR reaction mix as described in **Table 12** was used. Thermocycling conditions used for DreamTaq® PCRs are shown in **Table 13.**

Table 12: **Reaction mix for custom 10 µl DreamTaq® PCR**

10 µl DreamTaq® PCR Mix	
Template*	0.5 µl
10xDreamTaq® Green Buffer	1 µl
dNTP mix (10 mM each)	0.2 µl
Primer fw (10 µM)	0.25 µl
Primer rev (10 µM)	0.25 µl
DreamTaq® (5U/µl)	0.05 µl
MQ	Final volume 10 µl

*plant genotyping: genomic DNA described in 2.7.2
E. coli: a colony from selection plate is resuspended in 20 µl MQ
A. tumefaciens: 100 µl of o/n culture is pelleted and resuspended in 100 µl MQ, incubated at 98 °C for 10 min

Table 13: **Thermocycling conditions for standard DreamTaq® PCR.**

Step	**Temperature**	**Time**
1.) Initial Denaturation	94 °C	2 min
2.) Denaturation	94 °C	30 s
3.) Annealing	X °C*	30 s
4.) Elongation	72 °C	60 s/kb
Cycle	→to 2.) 39 times	
5.) Final Elongation	72 °C	5 min
	12 °C	∞

*Depends on the specific melting temperature of the primers used.

2.7.5.2 Amplification of DNA Fragments for Cloning

If DNA fragments gained by PCR were used for cloning, Phusion® Polymerase High-Fidelity Polymerases with proof-reading function was employed to decrease sequence errors in the fragments. Phusion® possesses additionally to its 5'→3' polymerase function also a 3'→5' exonuclease function which enables low error rates. The inclusion of restriction sites as overhangs of the primers used for amplification of the fragment, allows the ligation of the fragment into given restrictions sites within a chosen vector. Standard Phusion® PCR reaction mixture as described in **Table 14** and the thermocycling conditions as described in **Table 15** were followed for the amplification of DNA fragments for cloning. As template, either *wt Col-0* genomic DNA prepared as described in 2.7.1 or *wt Col-0* cDNA prepared as described in 2.8.4 were used as templates.

Table 14: **Standard Phusion® PCR reaction mixture for amplification of DNA fragments for cloning.**

20 µl Phusion® PCR Mix	
Template	1 µl
5xHF-buffer	4 µl
dNTP mix (10 mM each)	0.4 µl
Primer fw (10 µM)	0.4 µl
Primer rev (10 µM)	0.4 µl
Phusion® (2U/µl)	0.15 µl
MQ	Final volume 20 µl

Table 15: **Thermocycling conditions for standard Phusion® PCR.**

Step	Temperature	Time
1.) Initial Denaturation	98 °C	30 s
2.) Denaturation	98 °C	10 s
3.) Annealing	X °C*	10 s
4.) Elongation	72 °C	30 s/kb
Cycle	→to 2.) 39 times	
5.) Final Elongation	72 °C	10 min
	4 °C	∞

*Temperature is determined by the melting temperatures of the used primers as shown in **Table S3** and were calculated by NEB Tm Calculator.

2.7.5.3 Overhang-Extension PCR

For the linkage of two or three PCR fragments the overhang-extension PCR method was used (Shevchuk *et al.*, 2004).

First, the single fragments were separately prepared. Amplification was performed using genomic *wt Col-0* DNA prepared as described in 2.7.1 following the usual protocol as described in 2.7.5.2. The fragments were purified as described in 0 and the concentration determined as described in 2.7.7. The feature enabling the fusion of the fragments in following steps consisted of primer overhangs, which were complementary to the fragment to which they were linked to. This procedure is depicted in **Figure 7** on the example of the genomic complementation constructs described in 0.

In the next step, the linkage of the single fragments took place in the overhang-extension PCR. Whereas the first phase contained no primers and was conducted so that the overhangs aligned with the complementary sequences within the other fragments. In the second phase 0.75 µl of the reaction product of phase 1 was used as template, for a second PCR whereas the fw primer of the first and the rev primer of the last fragment were used to amplify the full-length triple fusion product.

The PCR reaction mixtures and Thermocycling conditions used in the overhang-extension PCR are described in **Table 16** and **Table 17,** respectively.

Table 16: **Phusion® overhang-extension PCR reaction mixtures used in the experiments.**

Phase 1: 25 µl Overhang-Extension PCR Mix	
Fragment 1	25 ng
Fragment 2	5 ng
Fragment 3	25 ng
5xHF-buffer	5 µl
dNTP mix (10 mM each)	0.5 µl
Phusion® (2U/µl)	0.25 µl
MQ	Final volume 25 µl
Phase 2: 25 µl Overhang-Extension PCR Mix	
Phase 1 Product	0.75 µl
5xHF-buffer	5 µl
dNTP mix (10 mM each)	0.5 µl
Primer fw (10 µM)	0.625 µl
Primer rev (10 µM)	0.625 µl
Phusion® (2U/µl)	0.25 µl
MQ	Final volume 25 µl

Table 17: **Thermocycling conditions for overhang-extension PCR.**

Phase 1		
Step	**Temperature**	**Time**
1.) Initial Denaturation	98 °C	30 s
2.) Denaturation	98 °C	7 s
3.) Annealing	56 °C	20 s
4.) Elongation	72 °C	75 s
Cycle	→to 2.) 9 times	
	4 °C	∞
Phase 2		
1.) Initial Denaturation	98 °C	30 s
2.) Denaturation	98 °C	7 s
3.) Annealing	68 °C	20 s
4.) Elongation	72 °C	100 s
Cycle	→to 2.) 34 times	
5.) Final Elongation	72 °C	7 min
	4 °C	∞

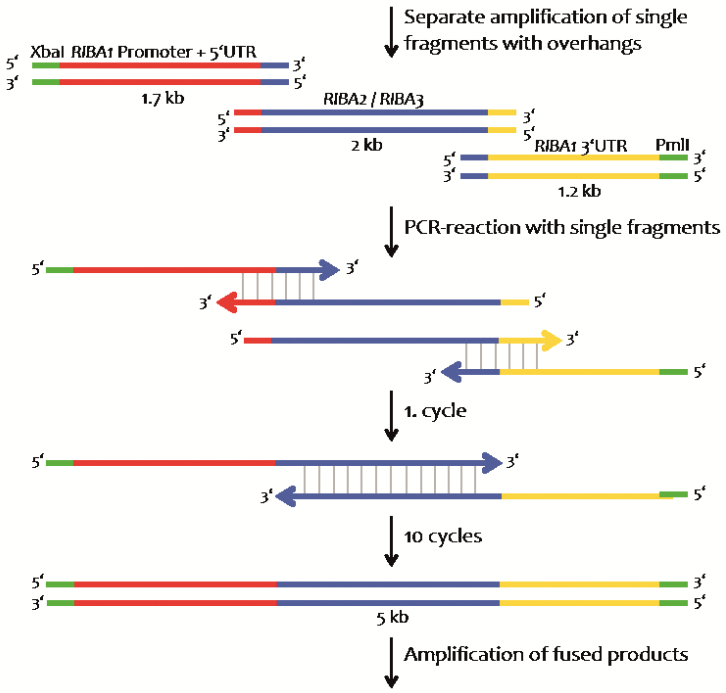

Figure 7: **Triple overlap PCR.**
Here the scheme of the triple overlap PCR, as used for the fusion of RIBA1 promoter and UTRs with the genomic sequence of RIBA2 or RIBA3, respectively (modified from Wittrahm (2014)).

2.7.5.4 *Adapter Ligation*

For the insertion of small fragments into vectors, e.g. an extension of the multiple cloning site of the pCambia1305.2 plasmid, the adapter ligation method was used. Therefore, primers were designed including the restriction sites HpaI, PmeI and SwaI as well as overhangs serving as sticky ends for a subsequent ligation into the HindIII and NcoI sites of pCambia1305.2 (**Figure 8**).

Figure 8: **Scheme of adapter ligation.**
Here primers used for the adapter ligation for the insertion of *PmeI*, *HpaI* and *SwaI* into the multiple cloning site of pCambia1305.2 are depicted.

Both primers were mixed in a total volume of 50 µl. The concentration of each primer was 2 µg/50 µl. The tube was placed in a beaker with 500 ml water, preheated to 80 °C, which then was left to cool down to RT for several hours. This procedure causes the annealing of the complementary sequences of the fw and rev primers so that small double stranded fragments were formed. These were subsequently ligated into the pCambia1305.2 vector which had been cleaved with HindIII and NcoI, removing the *CaMV*-35S promoter. Further steps of cloning of the pCambia105.2-MCS were performed as described in 2.7.9.3.

2.7.6 Purification of DNA Fragments

2.7.6.1 PCR Purification

The purification of PCR fragments, as well as plasmids after alkaline lysis mini prep (2.7.4.1), was performed with MSB® Spin PCRapace Kit according to manufacturer's recommendations.

2.7.6.2 Gel extraction

For the extraction of DNA fragments after separation via gel electrophoresis Invisorb® Spin DNA Extraktion Kit according to manufacturer's recommendations was used.

2.7.7 Determination of DNA/RNA Concentrations

If the purity of the nucleic acid sample was pure enough photometric determination of the concentration took place with the NanoDrop® Spectrophotometer. Additionally, for samples with high salt or DNA/RNA contaminations, concentrations were determined using known amounts of λ-Phage-DNA on agarose gel (2.7.8).

2.7.8 Agarose Gel Electrophoresis of DNA

Visualization of DNA fragments mixed with 6x DNA Loading Dye was performed by agarose gel electrophoresis. Therefore, according to the size of the fragment, 0.8-1.2 % (w/v) agarose was solved by boiling in 1x TAE-buffer (40 mM Tris, 20 mM acetate, 1 mM EDTA). For visualisation of nucleic acids within the gel in UV-light, 0.3 µg ml^{-1} EtBr was supplemented. Separation of the DNA fragments took place in electrophoresis chambers submerged with 1xTAE-buffer at 2-4 V/cm chamber length. As markers for PCR fragment length GeneRuler™ 1 kb and 100 bp DNA Ladder were used.

2.7.9 Cloning Procedure

2.7.9.1 Cloning of PCR Fragments into pJet1.2 Vectors (Pre-Clone)

The CloneJET PCR Cloning Kit was used for ligation of blunt-end PCR products from 2.7.5.2 in to the pJet1.2 vector, which, as a high-copy plasmid, enables good yield in plasmid mini prep as described in 0. At this stage, sequencing of the pre-clone took place before further steps were executed.

2.7.9.2 Preparation of Insert/Vector DNA via Restriction Enzyme Cleavage

Restriction enzyme digestion and the resulting blunt or sticky ends enable the later linkage of the insert and vector, the so called ligation. Restriction enzymes and corresponding buffers were purchased from New England Biolabs or Thermo Fischer Scientific. Cleavage reactions were mostly carried out o/n at the given temperature. The result was checked via gel electrophoresis.

2.7.9.3 Creation of Recombinant DNA with DNA Ligase

Sticky as well as blunt end ligations took place at 16 °C o/n in a 10 µl reaction containing 1 µl 10x ligase buffer, 0.5 µl T4 ligase and given amount of vector and insert. Mostly 20 ng vector was used and according to a molar ratio of 1:5 (vector:insert) the amount of insert was calculated due to fragment length with the help of the Ligation Calculator.

2.7.10 DNA Sequencing

For routine Sanger (Sanger *et al.*, 1977) sequencing of purified plasmid DNA or PCR products, samples were prepared according to the rule: size of plasmid or fragment divided by 12 yields the amount of DNA needed in ng, supplied with 0.5 µM of the respective sequencing primer, in a total volume of 8 µl. Further processing of the sample, including the cycling with the fluorescence dyed nucleotides, as well as the chromatographic analysis took place at the sequencing service company (SMB Services in Molecular Biology GmbH).

2.8 RNA Techniques

2.8.1 Isolation of RNA from Plant Material

2.8.1.1 TRIsure®

For extraction of total RNA 20-30 mg leaf material was harvested. The samples were immediately frozen in $liqN_2$ and kept frozen during homogenisation with the ball mill. Homogenised samples were mixed with 250 ml TRIsure® and incubated at RT for 5 min. Before 50 µl chloroform was added, plant material was shortly spun down to the bottom of the tube. After chloroform addition, the sample was vortexed and incubated for another 5 min on ice. Phase separation was facilitated by centrifugation at 4 °C, 16,000 x *g* for 10 min. Thereafter 90 µl of the aqueous supernatant containing the nucleic acid was carefully transferred to a fresh tube and 125 µl cold isopropanol was added, the sample mixed thoroughly and incubated at RT for 10 min. RNA was pelleted by centrifugation at 4 °C, 16,000 x *g* for 10 min. The pellet was washed twice with 1 ml 75% EtOH and subsequently dried at RT for 10-15 min. RNA was resuspended in 30 µl MQ.

2.8.1.2 Isolation with Na-Citrate/Citric acid

This phenol-free RNA isolation method was conducted according to Onate-Sanchez and Vicente-Carbajosa (2008). Therefore, 20-30 mg plant material was ground with the ball mill (25 Hz, 1 min), mixed with 300 µl cell lysis solution (2 % (w/v) SDS, 68 mM sodium citrate, 132 mM citric acid, 1 mM EDTA) and incubated at RT for 5 min. Subsequently, 100 µl protein-DNA precipitation solution (4M NaCl, 16 mM sodium citrate, 32 mM citric acid) was added and the sample mixed by gentle inversion.

After 10 min incubation on ice the samples were centrifuged at 4 °C and 16,000 x g for 10 min to remove cell debris and precipitated DNA and proteins. Next, 250 µl of the supernatant was centrifuged once more in a fresh tube as described before, precipitated in 300 µl isopropanol and finally pelleted at 13,000 rpm, RT for 4 min. The RNA pellet was washed twice with 900 µl 70 % EtOH and air dried for 10 min. RNA was dissolved in 25 µl MQ.

2.8.2 Solving of RNA Pellet

In order to completely resolve the RNA pellet after addition of MQ and resuspension via pipetting, the samples were frozen. After thawing, they were incubated at 65 °C for 10 min. To assure accurate quantification, RNA samples were centrifuged at 4 °C, max speed for 3 min, to pellet remaining undissolved RNA. RNA was stored at -80 °C.

2.8.3 Agarose Gel Electrophoresis of RNA

Quality- and quantity control of isolated RNA took place in gels containing 1.2 % agarose (w/v) in 0.5x TBE buffer (45 mM Tris, 45 mM borate, 1 mM EDTA) and 0.3 µg ml^{-1} EtBr. One µg RNA mixed with 6x DNA Loading Dye was run at 4 V/cm chamber length for 20-30 min.

2.8.4 cDNA Synthesis

For cDNA synthesis genomic DNA had to be removed by DNase treatment. Therefore, a concentration of 1 µg RNA per 4 µl were adjusted and together with 0.5 µl DNase buffer and 0.5 µl DNase I incubated for 30 min at 37 °C. DNase I was inactivated by adding 0.5 µl 25 mM EDTA, followed by an incubation at 65 °C for 10 min. For reverse transcription reaction, mixture as described in **Table 18** was prepared and incubated for 1 h at 42 °C. Reverse transcriptase was subsequently inactivated at 70 °C for 10 min. For use in sqPCR or qPCR cDNA was diluted 1:5 with MQ. To account for differences of RNA concentrations, unravelled by gel electrophoresis, the dilution of the obtained cDNA was adjusted to ensure similarity across samples.

Table 18: **Reverse transcription reaction mixture used for cDNA synthesis from DNase I-treated RNA samples.**

10 µl Reverse Transcription Reaction Mixture	
DNase I-treated RNA (0.5 µg)	5.5 µl
Oligo-dT Primer (100 µM)	0.5 µl
5x RT Buffer	2.0 µl
MQ	0.25 µl
dNTP mix (10 mM each)	1.0 µl
Ribo Lock RNase-Inhibitor	0.25 µl
Reverse Transkriptase RevertAid	0.5 µl

2.8.5 Quantification of Gene Expression

2.8.5.1 *Semi-quantitative PCR (sqPCR)*

For quality control, the synthesised cDNA was subjected to a semi-quantitative PCR. Hence, a PCR with a reaction mixture as described in 2.7.5.1 using the diluted cDNA as template was conducted basically as described in **Table 13** with an annealing temperature of 60 °C, an elongation time of 30 s and in total 20 cycles. Thereby the primers for the housekeeping gene *TUBULIN ALPHA-5* (QPP20) were used as reference (**Table S 2**) to allow the comparison across the samples.

2.8.5.2 *Quantitative Real Time PCR (qPCR)*

For quantitative real time PCR (qPCR) cDNA was amplified with SensiMix SYBR No-ROX kit (Bioline) using reaction mixtures as described in **Table 19**. The qPCR was performed on a CFX96 Real-Time System using the oligonucleotides listed in **Table S 2** and the thermocycling conditions as shown in **Table 20**. Expression rates were calculated either relative to the housekeeping gene SAND according to the $2^{-\Delta CT}$ method or relative to *wt Col-0* expression according to the $2^{-\Delta\Delta CT}$ method (Livak & Schmittgen, 2001).

Table 19: **Standard 6 µl qPCR reaction mixture for SensiMix SYBR No-ROX kit.**

Standard 6 µl qPCR Reaction Mixture for SensiMix SYBR No-ROX kit	
cDNA Template	0.6 µl
2x Sensi Mix	3 µl
Primer Mix (3 µM each)	1 µl
MQ	2.4 µl

Table 20: **Thermocycling conditions used for qPCR**

Step	Temperature	Time
1.) Initial Denaturation	95 °C	10 min
2.) Denaturation	95 °C	15 s
3.) Annealing	60 °C	30 s
4.) Elongation	72 °C	15 s
Cycle:	→to 2.) 40 times	
Melting Curve:	→Gradient from 65 °C to 95 °C in 0.5 °C increments (10 s each)	

2.8.5.2.1 Determination of qPCR-Amplification Efficiencies

For the determination of amplification efficiencies of primers *wt Col-0* cDNA dilution series as shown in **Table 21** was set up and used as the template in a qPCR standard curve for each primer pair tested. The C(t) values were then plotted against the log of dilution values and a linear trendline was added. From the slope of the trendline the primer efficiency value (E) and % Efficiency (%E) were calculated according to Biorad software Application guide using the following equations:

$$E = 10^{\frac{-1}{Slope}} \qquad \%E = E - 1 \cdot 100$$

Table 21: **cDNA dilution series for determination of primer amplification efficiencies per qPCR.**

Step	Dilution with MQ	Dilution value
1	1:10,000	$1*10^{-4}$
2	1:4	$2.5*10^{-5}$
3	1:4	$6.25*10^{-6}$
4	1:4	$1.56*10^{-6}$
5	1:4	$3.91*10^{-7}$
6	1:4	$9.77*10^{-8}$

2.9 Protein Techniques

2.9.1 Isolation of Total Protein from Plant Tissue

Total proteins were extracted from plant tissues in 2x Laemmli buffer wherein 10 µl was used per mg FW plant tissue (100 mM Tris-HCl pH 6.8, 4 % SDS (w/v), 20 % glycerol (v/v), 200 mM DTT, 0.15 % Bromphenol blue (w/v)). After homogenisation with the ball mill (25 Hz, 1 min) , the frozen plant material was thoroughly mixed with Laemmli buffer and then incubated at 96 °C for 5 min. Plant tissue debris was removed by centrifugation at 13,000 rpm, RT for 3 min. 10-15 µl of the supernatant was used for the SDS-PAGE (2.9.2).

2.9.2 SDS-Polyacrylamide Gel Electrophoresis (SDS-PAGE)

SDS-PAGE was used for separation of proteins according to their electrophoretic mobility under denaturing conditions. Due to the denaturation by the anionic detergent SDS, the proteins are negatively charged and can be separated due to their size in an electrical field. Tris-glycine running buffer (25 mM Tris, 192 mM glycine, 0.1 % (w/v) SDS) was used according to Laemmli (1970). The concentration of applied polyacrylamide in the separating gel varied according to the molecular weight of the proteins to be examined. In the case of RIBA proteins, separating gel concentrations of 10 or 12 % polyacrylamide were used. The composition of SDS polyacrylamide gels is described in Table 22. Electrophoresis was carried out at 100 V during stacking and 130 V during separation. As standards for determination of the protein size Unstained Molecular Weight Marker, Prestained Protein Molecular Weight Marker and Unstained PAGE Ruler were used.

Gels were stained with Coomassie® Brilliant Blue R-250 with Coomassie staining solution (40 % (v/v) methanol, 10 % (v/v) acetic acid, 0.25 % (w/v) Coomassie® Brilliant Blue R-250) wherein destaining was conducted with Coomassie destain solution (40 % (v/v) methanol, 10% (v/v) acetic acid).

Table 22: **Composition of SDS polyacrylamide gel**

For 1 Gel	Stacking Gel 5 %	Separating Gel 10 %	Separating Gel 12 %
30 % Acryl-Bisacrylamide 29:1 (Applichem)	0.3 ml	1.3 ml	1.6 ml
0.5 M Tris-HCl, pH 6.8 (Sta) 1.5 M Tris-HCl, pH 8.8 (Sep)	0.25 ml -	- 1 ml	- 1 ml
10 % SDS (w/v)	20 µl	40 µl	40 µl
10 % APS (w/v)	20 µl	40 µl	40 µl
TEMED	2 µl	1.6 µl	1.6 µl
MQ	Final volume 2 ml	Final volume 4 ml	Final volume 4ml

2.9.3 Western Blot, Immunohistochemical Detection and Imaging

Transfer of proteins from SDS-polyacrylamide (SDS-PA) gels to nitrocellulose membrane was conducted with semi-dry blotting method. Transfer was carried out for 1 h at a constant current density of 1.2 mA/cm^2 with Western transfer buffer (25 mM Tris, 200 mM glycine, 20 % methanol (v/v)). Subsequently, the transfer result was controlled via staining with Ponceau solution (5 % (v/v) acetic acid, 0.1 % Ponceau S), wherein staining solution was applied for 1 min and the membrane subsequently destained with $_{dest}H_2O$. After Ponceau stain, membranes were blocked with with 2 % lowfat powdered milk (w/v) in TBS-T (50 mM Tris, 150 mM NaCl, 0.1 % (v/v) Tween-20) either 1 h at RT or o/n at 4 °C. After blocking, the membrane was washed once for 10 min with TBS-T and twice for 10 min with TBS (50 mM Tris, 150 mM NaCl) before the primary antibody in the indicated (**Table 23**) dilution in 1 % lowfat powdered milk (w/v) in TBS was applied. Incubations with the primary antibody was performed either for 2 h at RT or o/n at 4 °C. Washing steps, as mentioned before, were executed before and after incubation with the peroxidase-conjugated secondary antibody. Incubation with the secondary antibody took place for 1 h at RT or o/n at 4 °C. A homemade ECL system (SolA: 100 mM Tris, 0.025 % (w/v) Luminol, pH 8.6; Sol B: 0.11 % (w/v) p-coumaric acid in DMSO; 35 % H_2O_2) provided the substrate for HRP-dependent chemiluminescence. Solutions A and B were mixed in a 10:1 ratio and per ml solution A 0.3 µl 35 % H_2O_2 was added and the mixture poured on the membranes. Images were immediately taken with a CCD-camera.

Table 23: **Antibodies used in the Western blot experiments**

Antibody	Description	Dilution	Source/Reference
α-RIBA	Rabbit-IgG, against *Arabidopsis* RIBA1	1:500	Hiltunen *et al.* (2012)
α-HA	Rabbit-IgG, against HA peptide	1:1,000	Agrisera
α-LHCB	Rabbit-IgG, against *Arabidopsis* LHCB1	1:5,000	Agrisera
α-GSA-At	Rabbit-IgG, against *Arabidopsis* GSA-At	1:2,000	Grimm *et al.* (1989)
α-rabbit	Horseraddish peroxidase	1:10,000	Agrisera

2.9.4 Recombinant Protein Expression in *E. coli*

For recombinant overexpression coding sequence of desired gene was inserted into pET22b(+) expression vector as described in 2.7.9. The construct was transformed into chemocompetent ArcticExpress™ (DE3) RIL cells (2.6.1.1). Subsequently a 15 ml culture was inoculated with a single colony from a selection plate and incubated at 37 °C and 260 rpm o/n. Thereafter 750 ml LB expression culture w/o antibiotics was inoculated with the o/n culture and grown in baffled flasks at 30 °C and 260 rpm until $OD_{600\ nm}$ of 0.5-0.7. The culture was cooled in ice water for 30 min and the expression was induced by adding 1 mM IPTG (final concentration). After induction, the culture was incubated at 13 °C, 250 rpm for 24 h for protein expression. Subsequently the cells were pelleted at 2000 x *g*, 4 °C for 15 min. For cell lysis, the pellet was resuspended in 2 ml lysis buffer (50 mM NaH_2PO_4, 300 mM NaCl, 10 mM imidazole, pH 8 with NaOH) per g FW plant material. After addition of 1 mg ml^{-1} lysozyme and subsequent incubation on ice for 30 min the cells were sonicated 6 times for 10 s at 100 % amplitude, with a 10 s pause each time. After the cell debris was pelleted at 10,000 x *g*, 4 °C for 25 min, the supernatant was collected and used immediately for protein purification.

2.9.5 Native Purification of Recombinant RIBAs from *E. coli*

The suitable purification method was chosen depending on the desired degree of purity and requirements for following application. Antibody production requires a high purity that can be achieved with the Fast Protein Liquid Chromatography (FPLC).

2.9.5.1.1 Purification via FPLC

His-tagged RIBA proteins were purified from *E. coli* cell lysate, obtained as described in 0, via FPLC using HisTrap HP columns as stationary phase and running buffer (20 mM NaH_2PO_4, pH 7.4, 500 mM NaCl) with rising imidazole concentration as mobile phase. While during binding a concentration of 10 mM imidazole was used, it was step-wise increased during the elution phase from 50 till 250 mM and finally to 500 mM in the washing phase as shown in **Figure 9**. Buffer flow was set to 1 ml min^{-1}. After the lysate was loaded on the column, binding step was run for 40 min, each elution gradient step was run for 5 min, whereas washing phase was run for 10 min. Protein concentration of the eluate was monitored via absorbance at 280 nm wavelength with an UV detector. Eluates with highest protein concentrations were directly subjected to dialysis to remove imidazole (2.9.5.1.3).

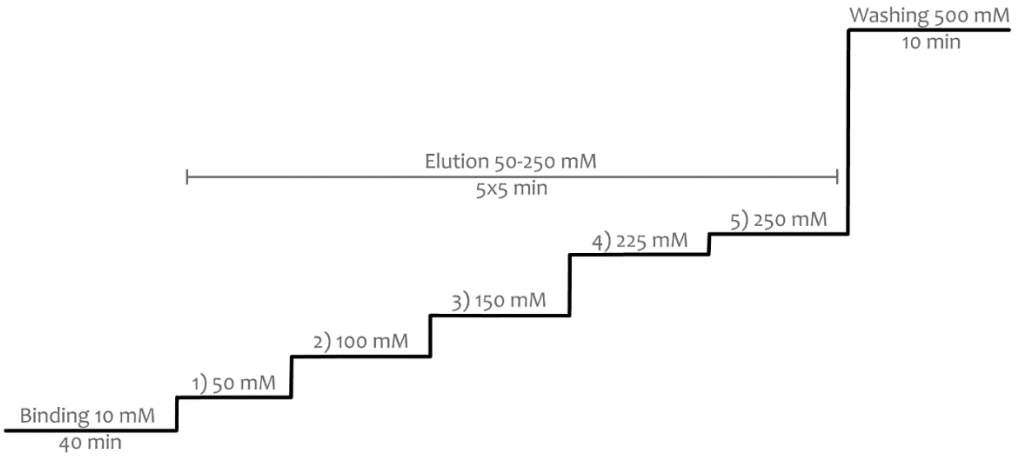

***Figure 9: FPLC* gradient used for the purification of His-tagged recombinant proteins.**
HiTrap HP column were used as the stationary and running buffer (20 mM NaH_2PO_4, pH 7.4, 500 mM NaCl) with rising imidazole concentration as the mobile phase.

2.9.5.1.2 Batch Purification

Batch purification was performed at 4 °C and was started by equilibration of 87.5 µl Ni-NTA-Agarose suspension per ml cell lysate with double volume of lysis buffer. The lysate was diluted with lysis buffer up to 10 ml total volume containing one cOmplete™-Mini-EDTA-free protease inhibitor cocktail tablet per 10 ml buffer and incubated under agitation for 1 h. The suspension was transferred to 10 ml filter columns and remained for 20 min until the beads had settled to the bottom of the column. Subsequently the cap of the column was opened and after drainage of the lysis buffer, the beads were washed four times with 5 ml washing buffer (50 mM NaH_2PO_4, 300 mM NaCl, 20 mM imidazole, pH 8 with NaOH). Finally, elution was performed 5 times with 100 µl elution buffer (50 mM NaH_2PO_4, 300 mM NaCl, 250 mM imidazole, pH 8 with NaOH). Elution fractions with the highest concentration were pooled. Concentrations were determined with a quick Ponceau test, whereas 1 µl of the eluate was spotted on nitrocellulose membrane which then was dried and dyed with Ponceau as described in 2.9.3.

2.9.5.1.3 Dialysis

In order to remove imidazole, the extracts were loaded into SnakeSkin™ Pleated Dialysis Tubing (10,000 MWCO) and incubated 1h, o/n and 2h at 4 °C (each time fresh) in 500 ml of an optimized dialysis buffer containing 20 mM Tris-HCl, 200 mM NaCl, 5% (v/v) glycerol, pH 8.4. In beforehand it was tested, that the buffer is suitable to maintain the enzyme's activity and does not have adverse effects on activity under assay conditions.

2.9.6 Determination of Protein Concentration

Protein concentrations were determined according to Bradford (1976), wherein bovine serum albumin (BSA) was used as standard.

2.9.7 Generation of the RIBA-Antibody

FPLC purified RIBA1 protein (as described in 2.9.5.1.1) was denatured by the addition of 1 M Urea and sent to BioGenes GmbH, where the immunization of a rabbit was performed according to BioGenes GmbH standard immunisation protocol.

2.9.7.1 Purification of the RIBA-Antibody

Serum that was provided by BioGenes GmbH after the immunisation was purified as follows. Small pieces of Nitrocellulose blotting membrane were loaded with antigen, whereas the membrane was moistened with drops of recombinant RIBA1. The membranes were dried at RT for 10 minutes before they were washed five times for 5 min with 1% lowfat powdered milk in TBS. For affinity purification of the antibody from the serum, the membranes were incubated for 2 days at 4 °C in 40 ml of 1:10 diluted serum (in 1% lowfat powdered milk in TBS). Subsequently the membranes were washed three times for 5 min with 1% lowfat powdered milk in TBS. The elution of the antibody was achieved by incubating the membranes in 500 µl glycinbuffer (0.2 M Glycin-HCl, 0.5 M NaCl, 1 mg ml^{-1} BSA, pH 2.77) for 1 minute. Thereafter the eluate was immediately neutralised with 100 µl 1 M Tris-HCl, pH 8.

2.9.8 Expression and Purification of HA Strep-Tagged Proteins

For expression of HA Strep-tagged proteins in plants, the desired coding sequences were inserted into the pXCS-HA-Strep vector as described in 2.7.9. The subsequent transformation into *A. thaliana* or *N. benthamiana* was conducted with the *A. tumefaciens* strain GV3101.

2.9.8.1 Transient Expression in N. benthamiana

In order to verify the absence of frame shifts, pXCS-HA constructs were transiently expressed in *N. benthamiana* leaves as described in 2.6.5. Therefore, o/n cultures, as described in 2.6.2.1, were grown, cells pelleted at 4,000 x *g*, 12 °C for 20 min, resuspended in inoculation medium (10 mM $MgCl_2$, 10 mM MES, 100 µM Acetosyringone pH 5.7) and $OD_{600\ nm}$ was adjusted to 0.8-1. The culture was incubated at RT for 2 h and then mixed 1:1 with C58C1 strain (**Table 10**), which was adjusted to $OD_{600\ nm}$ of 0.2. Both strains were co-infiltrated into *N. benthamiana* leaves as described in 2.6.5. After 3-4 days at standard long-day light conditions, 6 mm leaf discs were sampled and analysed via SDS-PAGE as described in 2.9.2 and 2.9.3 using the HA-antibody.

2.9.8.2 Constitutive Expression in A. thaliana

For constitutive expression of HA-Strep tagged proteins in *Arabidopsis*, pXCS-HA-Strep constructs were transformed into *A. thaliana* as described in 2.6.4. The BASTA® resistant progenies, acquired as described in 2.6.4.1.1, were self-pollinated to produce T2 seeds. Progeny lines were tested

regarding their expression of the respective HA-Strep-tagged protein with SDS-PAGE and immunological detection with the HA-antibody. One to two ml T2 seeds were sown on trays and grown for 4 weeks at standard short-day conditions.

2.9.8.3 Purification from A. thaliana Extracts

Described in 2.18.1.2.

2.10 Organelle Isolation

2.10.1 Isolation of Chloroplasts from *A. thaliana*

2.10.1.1 Crude Chloroplast Isolation

For crude chloroplast isolation, leaf material of four to five 3- to 4-week-old *wt Col-0* plants were harvested and homogenised in 50 ml homogenisation buffer (50 mM HEPES/KOH pH 7.6, 330 mM Sorbitol, 5 mM $MgCl_2$, 10 mM KCl) in a Waring® blender (2-3 pulses, each 4 s) at 4 °C. Plant material was filtrated through single layer of Miracloth into a 50 ml Falcon tube and centrifuged at 2000 x *g*, 4 °C for 5 min to pellet chloroplasts. The supernatant was discarded and the pellet was resuspended in 1-2 ml of the respective buffer suitable for following experiments.

2.10.1.2 Chloroplast Isolation via Percoll® Gradient

For chloroplast isolation via Percoll® gradient 1-2 ml *A. thaliana* seeds was sown on trays and 4-week-old half to whole tray of seedlings were harvested. Plants were kept dark for 12 hours before harvest to avoid starch accumulation. The plant material was homogenised in a Waring® blender (2x4 s puls low) with 250 ml homogenisation buffer (0.45 M sorbitol, 20 mM tricine-KOH pH 8.4, 10 mM EDTA, 10 mM $NaHCO_3$, 0.1 % BSA (w/v)). The extract was filtrated through a single layer of Miracloth, collected in a 500 ml polypropylene centrifugation bottle and immediately centrifuged at 500 x *g*, 4 °C for 8 min (acc max/dec max). The pellet was gently resuspended in 1 ml resuspension buffer (0.3 M sorbitol, 20 mM tricine-KOH pH 8.4, 2.5 mM EDTA, 5 mM $MgCl_2$) and transferred with a cut 1 ml tip on a Percoll® gradient (5 ml 40 %-Percoll® / 13 ml 80 %-Percoll® in resuspension buffer) in open-top polypropylene tubes. Isolation of intact chloroplasts was performed via centrifugation with a swing out rotor at 6,500 x *g*, 4 °C for 30 min (acc slow/dec off). Chloroplasts were carefully transferred to 20 ml resuspension buffer in 50 ml falcon tubes and pelleted in fixed angle rotor at 3,800 x *g*, 4 °C for 6 min. The pellet was resuspended, depending on size, in 500-1,000 µl of the respective buffer suitable for the subsequent experiments.

2.10.1.2.1 Chloroplast Fractionation

Fractionation of chloroplasts into thylakoid and stroma fraction was performed via osmolysis and mechanical treatment. In this case, either protein extraction buffer or Strep-ex buffer were used to solve the chloroplast pellet. By pipetting up and down 10-15 times and subsequent incubation for 10 min proper lysis was ensured. The stroma protein extract was obtained by centrifugation at 16,000 x *g*, 4 °C for 10 min, wherein this step was repeated as many times as required to yield a clear supernatant (green colour means contamination with thylakoid membrane). In order to gain pure thylakoid membrane, the green pellet that was acquired after the soluble supernatant was collected, was washed several times by resuspending the pellet thoroughly in the buffer and following centrifugation step. The purity of both fractions was controlled via SDS-PAGE and subsequent Western blotting. The LHCB1-antibody was used as a marker for thylakoid proteins and the GSA-At-antibody for stroma proteins.

2.10.2 Isolation of Mitochondria from *N. tabacum*

Isolation of mitochondria from *N. tabacum* leaves was performed according to a modified protocol from Sabar *et al.* (2000). One hundred g leaf material was homogenised in a Waring® blender (2x 8 s at high speed) in 400 ml grinding buffer (0.6 M sorbitol, 0.4 % BSA, 5 mM EDTA, 50 mM MOPS, 0.5 % PVP-40, pH 7.5 (KOH), 8 mM cysteine (added directly before use)). The homogenate was filtrated through a double layer of Miracloth and a single layer of nylon mesh directly into 250 ml centrifuge tubes and centrifuged immediately at 900 x *g*, 4 °C, for 10 min to pellet the debris. The supernatant containing mitochondria was transferred to 8 open-top Ultra-Clear® tubes and filled up to 30 ml with wash buffer (0.6 M sorbitol, 10 mM MOPS, pH 7.2 with KOH). The mitochondria were pelleted at 10,000 x *g*, 4 °C, for 20 min and the supernatant was discarded. The pellet was carefully resuspended in 2 ml wash buffer, pooled to one aliquot and homogenised with a potter (15 to 20 times). Homogenised mitochondria were then transferred to two open-top Ultra-Clear® tubes, filled up to 30 ml with wash buffer and centrifuged for 10 min at 900 x *g*, 4 °C. The resulting supernatant was transferred into two open-top Ultra-Clear® tubes and mitochondria pelleted at 10,000 x *g*, 4 °C for 20 min. Supernatant was discarded and pellets were resuspended in 1 ml wash buffer, pooled and homogenised with the potter (3-5 times). The mitochondria were then loaded on a Percoll® gradient (2.5 ml 18% Percoll® /12.5 ml 25 % Percoll®/2,5 ml 50% Percoll® in washbuffer) and centrifuged at 45,000 x *g*, 4 °C, for 45 min (acc slow). The mitochondria were carefully transferred to an open-top Ultra-Clear® tube and filled up to 30 ml with wash buffer and subsequently pelleted at 20,000 x *g*, 4 °C for 10 min. The supernatant was discarded and the mitochondria resuspended and filled up with wash buffer and centrifuged as mentioned before. These washing steps were repeated as long as the pellet appeared solid. Finally, pellet was

resuspended in wash buffer and the protein concentration was determined by Bradford (2.9.6) and set to a concentration of 5 µg µl^{-1} by centrifugation and resuspension in desired amount of wash buffer. The mitochondria were stored at -80 °C.

2.10.3 Blue Native PAGE of Organelle Extracts

For the native separation of protein complexes from isolated mitochondria, Blue Native PAGE was performed. Therefore, a native gradient gel was cast into Biorad Protean® II cast system with the help of a gradient mixer as stated in **Table 24**.

Table 24: **Composition of a Blue Native polyacrylamide gel for the Biorad Protean® II XL cell system.**

For 1 Gel	Stacking Gel	Separating Gel	
	3.5 %	4.5 %	16 %
6x Gel Buffer (1.5 M ACA, 150 mM Bis-Tris, pH 7 with HCl)	1.25 ml	2.5 ml	2.5 ml
Acrylamide 4K (40 %)	0.75 ml	1.7 ml	6 ml
50 % Glycerol	-	-	5.7 ml
MQ	Add 8.5 ml	Add 15 ml	Add 15 ml
10 % APS	65 µl	70 µl	70 µl
TEMED	6.5 µl	7 µl	7 µl

Sample preparation took place as follows. Per well 20 µl isolated mitochondria with a protein concentration of 5 µg µl^{-1} was loaded. Therefore, the mitochondria were pelleted at 20,000 x *g*, 4 °C for 10 min and the supernatant was discarded, the pellet resuspended carefully in 10 µl digitonin extraction buffer (30 mM HEPES, 150 mM potassium acetate, 10 % Glycerol, 50 mg ml^{-1} digitonin, pH 7.4 with HCl) and incubated for 10-15 min on ice. The mitochondria debris was pelleted at 20,000 x g, 4 °C, for 10 min and the supernatant mixed with 1 µl 5 % Serva Blue G (750 mM ACA, 50 mM Bis-Tris, 0.5 mM EDTA, 5 % Coomassie G250, pH 7 with HCl). For empty wells blanks were prepared with 10 µl digitonin extraction buffer and 1 µl 5 % Serva Blue G. Gel was run o/n at 4 °C with kathode buffer (50 mM tricine, 15 mM Bis-Tris, 0.1 % Coomassie G250, pH 7 with HCl) and anode buffer (50 mM Bis Tris, pH 7 with HCl). For the first 45 minutes, the electrophoresis was performed at 100 V (currency limited to max. 6 mA) and after that at 300 V (currency limited to max. 110 mA).

2.10.3.1 In-gel Complex I Activity Assay

The obtained blue native PAGE gel was directly used for an in-gel complex I activity assay as described by Meyer *et al.* (2009). Therefore, the gel was initially washed three times for 5 min with distilled water and then incubated in the reaction buffer (0.14 mM NADH, 1.22 mM NBT, 0.1 M Tris-HCl, pH 7.4) until the desired strength of staining developed. The reaction was stopped by transferring the gel to 40 % MeOH/10 % acetic acid (v/v).

2.11 Enzymatic Characterization of Recombinant RIBAs

2.11.1 RIBA Enzyme Activity Assay

For the quantification of RIBA activity, the enzyme assay was modified according to a protocol received from Dr. Illarionov (Hamburg School for Food Science). The components as stated in **Table 25** were mixed and the reaction started by addition of the substrate GTP or ribulose-5-phosphate for GCHII or DHBPS, respectively. The RIBA-assay buffer consisted of 100 mM Tris, 30 mM KCl, 10 mM $MgCl_2$ and 5 mM DTT. Reactions were stopped after 1 h at 37 °C by the addition of 6.3 µl 10 % TCA. The samples were centrifuged at 13,000 x *g*, 4 °C for 10 min, the supernatant collected and neutralised with 0.625 µl 5 M KOH. Before the samples were transferred into the HPLC vials they were centrifuged again at 13,000 x *g*, 4 °C for 30 min. 6,7-dimethyl-8-ribityllumazine, the product of both enzyme assays was quantified via HPLC. A Novapak C_{18}-column (150 mm; 3.9 mm diameter; 4 µm particle size) was used for separation. Elution was performed isocratically with 3% MeOH and 30 mM formic acid in H_2O at 18 °C. 6,7-dimethyl-8-ribityllumazine was detected fluorometrically (λ_{ex} 408 nm, λ_{em} 490 nm) and quantified according to known amounts of synthetic 6,7-dimethyl-8-ribityllumazine standard.

Table 25: **Assay composition for RIBA enzyme activity measurements.**

GCHII-Assay		DHBPS-Assay	
RIBA-Assay Buffer	Add to 25 µl	RIBA-Assay Buffer	Add to 25 µl
RIBA	1 µg	RIBA	1 µg
200 mM NADPH	0.125 µl	Amino	0.1 µl
RIBG (10 mg ml^{-1})	0.375 µl	Lumazinsynthase (24 mg ml^{-1})	2.5 µl
Phosphatase	0.125 µl	Phosphoribosiomerase (0.8 U μl^{-1})	0.25 µl
Phosphate	0.125 µl	***200 mM Ribose-5-phosphate***	***0.125***
Lumazinsynthase (24 mg ml^{-1})	0.625 µl		
20 mM GTP	***0.25 µl***		

2.11.1.1.1 Enzyme Kinetics Measurements

For the measurement of the enzyme kinetics of GCHII and DHBPS, enzymatic activity was determined after 30 min reaction time at GTP concentrations from 10 to 3200 µM and ribulose-5-phosphate concentrations from 1 µM to 12 mM, respectively (**Table 26**).

Table 26: **Assay composition for RIBA enzyme kinetics measurements.**

GCHII-Assay		DHBPS-Assay	
RIBA-Assay Buffer	Add to 25 µl	RIBA-Assay Buffer	Add to 25 µl
RIBA	1 µg	RIBA	1 µg
100 mM NADPH	0.5 µl	Amino	0.1 µl
RIBG (10 mg ml^{-1})	0.75 µl	Lumazinsynthase (24 mg ml^{-1})	2.5 µl
Phosphatase	0.25 µl	Ribulose-5-phosphate	variable
Phosphate	0.25 µl		
Lumazinsynthase (24 mg ml^{-1})	1.25 µl		
20 mM GTP	variable		

By plotting the reaction rate (velocity) against the substrate concentration Michaelis-Menten saturation curves were determined. V_{max} (maximal enzyme activity rate) and K_m (Michaelis constant) were determined, according to the method described in "HOW TO: Calculate Km and Vmax with Excel" (**Table 31**). Hence, the data was subjected to a fitting by Microsoft Excel 2013 Solver add-in, using nonlinear regression analysis by the simple Michaelis-Menten equation (**Equation 1**).

Equation 1: **Michaelis-Menten equation, wherein V stands for Velocity, [S] for substrate concentration, K_m for the Michaelis constant and V_{max} for maximum velocity.**

$$V = \frac{V_{max}[S]}{[S] + K_m}$$

2.11.1.1.2 FMN Inhibition

Influence of added FMN concentrations between 0.9 and 9 µM was tested on RIBA enzyme activity in GCHII and DHBPS enzyme assays as stated in **Table 25**. In order to test whether FMN was inhibiting RIBA specifically, the reaction was started only with RIBA1 and GTP in order to form 2,5-diamino-6-ribosylamino-4(3H)-pyrimidinone. For this purpose, a 500 µl reaction mixture was supplied with 40 µg RIBA1 and 2 µmol GTP. After 1 h incubation time RIBA1 was filtered out of the reaction mixture with a concentrator (10,000 MWCO). The supernatant containing 2,5-diamino-6-ribosylamino-4(3H)-pyrimidinone was used as substrate for the further assay. FMN, RIBG, phosphatase, phosphate and lumazinsynthase were added and the enzyme assay was further conducted as stated in 2.11.1. To examine FMN inhibition, enzyme kinetics for the RIBA1 GCHII reaction were determined as described before in 2.11.1.1.1 with different FMN concentrations (0.9, 1.8, 3.5 µM) supplemented to the reaction.

2.11.2 Phosphorylation Assay

The protocol used here was adapted from Bellafiore *et al.* (2005) to assay phosphorylation of recombinant proteins by A. Richter (unpublished). The assay was performed with crude plastid extracts acquired as described in 2.10.1.1. The chloroplast pellet was resuspended in phosphoassay buffer (50 mM HEPES/KOH pH 7.5, 0.4 mM ATP (add fresh), 100 mM sorbitol, 5 mM $MgCl_2$, 5 mM NaCl, protease inhibitor cocktail). Chlorophyll concentration was determined as described in 2.16 and a volume corresponding 10 µg chlorophyll was used for assay mixture as stated in **Table 27**.

Table 27: **Reaction mixture for phosphorylation assay of recombinant RIBAs.**

100 µl Phosphorylation Assay Mix	
Crude CP extract (10 µg Chl)	X µl
RIBA Protein (1 µg)	X µl
γ-^{32}P-ATP (10µCi µl^{-1})	1 µl
Assay buffer with ATP	Final volume 100 µl

The reaction was started by adding radioactive ATP and incubation at 23-25 °C for 30 min. Thereafter the thylakoid membranes were pelleted by centrifugation at 16,000 x *g* for 5 min and 80 µl of the supernatant and the remaining pellet were mixed with 5x Laemmli-buffer, respectively. Subsequently, 15-20 µl (corresponding 0.5-1 µg protein) was loaded in each slot of the SDS-PA gel, which then was subjected to electrophoresis and finally Coomassie stained as stated in 2.9.2. Thereafter the gel was destained, dried and exposed to a phosphor screen. After o/n exposure radioactivity, marking phosphorylated proteins was detected with a phosphoimager.

2.12 *IN VIVO* Complementation of *E. coli* Mutants

For the *IN VIVO* complementation assay of *E. coli* ribA and ribB knockout mutants, *RIBA* coding sequences were inserted into pACYC184 as described in 2.7.9.3. Constructs were transformed into *E. coli* knockout strains BSV18 and BSV11 defective in RibA (GCHII) and RibB (DHBPS), respectively (Bandrin *et al.*, 1983). These mutants are only able to grow in media supplemented with 0.4 g l^{-1} riboflavin. For the growth assay, LB medium with 0.4 g l^{-1} riboflavin was inoculated with a fresh o/n culture and grown under 37 °C, 250 rpm to an $OD_{600\ nm}$ of 0.6. The cells were pelleted and washed three times in M9 minimal medium (Sambrook & Russell, 2001). M9 culture containing antibiotics was inoculated with washed cells to give an initial $OD_{600\ nm}$ of 0.1 and grown under 37 °C, 250 rpm. Growth was assayed by determination of $OD_{600\ nm}$ for 26 h every 2 h, wherein the measurements were started 8 h after inoculation of the assay culture.

2.13 Metabolite Profiling of Mutants

The sample preparation, derivatisation and GC-TOF-MS analysis was performed following the protocol as described in Fernie *et al.* (2004) and Lisec *et al.* (2006).

2.13.1 Sample Preparation

For the preparation of samples for metabolite profiling by GC-TOF-MS, 20 mg above ground plant material was collected and homogenised with a ball mill (25 Hz, 1 min). Immediately after homogenisation 280 µl cold methanol was added to the still frozen plant material and mixed thoroughly. Subsequently, 12 µl ribitol (0.2 mg ml^{-1} stock solution in water) was added to serve as

internal standard for the analysis, and the samples mixed again and incubated at 70 °C and 550 rpm shaking. After 10 min centrifugation at 4,000 rpm at 25 °C, the supernatant was transferred into 2 ml tubes, 150 µl $CHCl_3$ and 300 µl MQ was added and each of the samples was vortexed carefully for 15 s. After 15 min centrifugation at 4,000 rpm at 25 °C, 150 µl of the upper polar phase was transferred into fresh 2 ml tubes and dried in the speedvac o/n without heating. Next day, tubes were filled with gaseous N_2 and stored at -80 °C until derivatisation.

2.13.2 Derivatisation and GC-TOF-MS Analysis

Derivatisation and GC-TOF-MS analysis was performed at Max-Planck-Institute of Molecular Plant Physiology (Potsdam-Golm, Germany), in cooperation with the research group of Dr. A. Fernie.

2.14 Determination of Pigment Contents

2.14.1 Extraction of Pigments from Leaf Material

For the extraction of pigments from *Arabidopsis*, approximately 50 mg frozen leaf material were homogenised with the ball mill (25 Hz, 1 min) and 500 µl cold (-20°C) pigment extraction solution (acetone/0.1 M NH_4OH (9:1, v/v)) was added and the sample vortexed well. After centrifugation at 16,000 x *g*, 4 °C for 10 min the supernatant was collected and the extraction repeated 3 times with 300 µl pigment extraction solution until the pellet was fully decoloured. The supernatants were mixed and 50 µl of the mixture was used for further analysis as described in 2.14.2.

2.14.2 Quantification of Pigments via HPLC

Before the samples were transferred into HPLC vials, they were centrifuged at 16,000 x *g*, 4 °C, for 30 min to pellet possible non-solvent floating particles. The analysis of the pigment extracts was performed on HPLC system 1100 (Agilent) using a Prontosil 200-3-C30 column (250 mm; 4.6 mm diameter; 3 µm particle size) with a run scheme as described in **Table 28** with solvent A: 90 % acetonitrile (v/v), 0.1 % trimethylamine (v/v) and solvent B: 100 % ethyl acetate.

Table 28: **HPLC run scheme for separation of pigments.**
Solvent A: 90 % acetonitrile (v/v), 0.1 % trimethylamine (v/v) and solvent B: 100 % ethyl acetate.

Time [min]	Solvent A [%]	Solvent B [%]	Step
0	100	0	**Elution**
3	70	30	
20	0	100	**Washing**
24	0	100	
21.1	100	0	**Equilibration**
28	100	0	

Chlorophyll and carotenoids were detected by diode-array detection (λ_{Abs} 440 nm) and quantified using authentic standards (Frontier Scientific, Logan, USA).

2.15 Determination of Total Flavin Amounts

2.15.1 Extraction from Recombinant Protein

Three µg of recombinant protein were diluted to a total volume of 20 µl in dialysis buffer. For extraction of flavins, 80 µl of methanol/methylene chloride (9:10, v/v) was added, mixed thoroughly by vortexing and incubated for 30 min at 4 °C under gentle agitation. Thereafter the samples were centrifuged at 16,000 x *g*, 4 °C for 15 min and the supernatant collected and analysed as described in 2.15.3.

2.15.2 Extraction from Plant Material

For extraction of total flavins, 50 mg plant material was homogenised with the ball mill (25 Hz, 1 min) and 250 µl methanol/methylene chloride (9:10) was added and the sample vortexed well. Thereafter the samples were incubated at 4 °C under gentle agitation for 1 h. Phase separation was facilitated by centrifugation at 16,000 x *g*, 4 °C for 15 min and 100 µl of the upper phase was collected. The rest of the sample was mixed thoroughly with 250µl 10mM NaH_2PO_4 + 10% acetonitrile and incubated again at 4 °C under agitation for 1h. After centrifugation at 16,000 x *g*, 4 °C for 15 min, 100 µl of the supernatant was collected and mixed with the supernatant of the first extraction step. Both samples were pooled and analysed as described in 2.15.3.

2.15.3 Quantification of Flavins via HPLC

Before samples were transferred into HPLC vials, they were centrifuged at 16,000 x *g*, 4 °C, for 30 min to pellet possible non-solvent floating particles. Analysis was performed on HPLC system 1100 (Agilent) using a NovaPak C18 column (150 mm; 3.9 mm diameter; 4 µm particle size) with a run scheme as described in **Table 29** with solvent A (10 mM NaH_2PO_4, pH 5.5) and solvent B 100 % methanol. Riboflavin, FMN and FAD were detected by fluorescence (λ_{ex} 265 nm, λ_{em} 530 nm) and quantified using authentic standards as listed in **Table 30**.

Table 29: **HPLC run scheme for separation of flavins.**
Solvent A: 10mM NaH_2PO_4, pH 5.5 and solvent B: 100 % methanol.

Time [min]	Solvent A [%]	Solvent B [%]	Step
0	90	10	**Elution**
11	60	40	
11.1	0	100	**Washing**
15	0	100	
15.1	90	10	**Equilibration**

Table 30: **Authentic Standards used for quantification of flavins after separation with HPLC.**

	FAD	FMN	Riboflavin
Concentration [ng µl^{-1}]	3	1	0.1
Injection volume [µl]	5	3	1
Retention time [min]	~ 6.9	~ 8.6	~10.9

2.16 Photometric Determination of Chlorophyll Concentration

Chloroplast or plant extracts were mixed with 80 % acetone and absorption (A) was measured at 645 nm and 663 nm wavelength in a glass cuvette. Chlorophyll concentration was calculated according to Porra *et al.* (1989) with **Equation 2**.

Equation 2: **Equation used for the calculation of total chlorophyll content according to Porra et al. (1989).**

$$[Chl\ a + b] = 20.21 \cdot A_{(645\ nm)} + 8.02 \cdot A_{(663\ nm)}\ in\ \mu g\ ml^{-1}$$

2.17 Detection of H_2O_2 in *A. thaliana* Leaves by DAB Staining

Whole rosettes of *A. thaliana* were DAB stained according to protocol from Daudi and O'Brien (2012) by submersion with DAB staining solution (1 mg ml^{-1} DAB, 10 mM NaH_2PO_4, 0.05 % Tween 20 (v/v), wherein DAB was first solved in MQ at pH 3.0 with HCl and then Tween and NaP buffer were added) and gentle vacuum for 5 min to foster uptake of the solution. After 4 hours incubation at gentle agitation and RT the plants were bleached with 3:1:3 EtOH:acetic acid:glycerol.

2.18 Analysis of Interacting Proteins

2.18.1 Affinity Purification and LC-MS Analysis

2.18.1.1 Pull-down from Chloroplast Extract with Recombinant Protein

In advance, 300 µl of 50 % Ni-NTA Agarose suspension was pre-incubated with 2 ml PBS (20 mM Na_2HPO_4/NaH_2PO_4, 150 mM NaCl, pH 7.4 + protease inhibitor cocktail) at 4 °C for 10-20 min. For pull-down analysis, 450 µg recombinant His-tagged RIBA1 protein, purified as stated in 2.9.5, was immobilised on Ni-NTA-Agarose beads by loading the respective amount of protein to the suspension and subsequent incubation at 4 °C under gentle agitation for 1h. Thereafter, either total chloroplast extract (2.10.1.2) or stroma fraction (2.10.1.2.1) was added to the suspension and incubated at 4 °C under gentle agitation for 1 h. The suspension was subsequently loaded on 1 ml polypropylene columns and left to settle for 15 min. The beads were washed twice with 4 ml washing buffer (50 mM NaH_2PO_4, 300 mM NaCl, 20 mM imidazole, pH 8 with NaOH) and bound proteins were eluted twice with 150 µl elution buffer (50 mM NaH_2PO_4, 300 mM NaCl, 250 mM imidazole, pH 8 with NaOH). Both fractions were pooled, 300 µl 2xLaemmli were added and the sample incubated at 96 °C for 5 min. For LC-MS analysis, 25 µl of the sample were loaded on SDS PA gels and run shortly into the separating gel, cut out and sent for analysis (2.18.1.3).

2.18.1.2 StrepII Affinity Purification from A. thaliana Chloroplasts

Chloroplast extracts, isolated as described in 2.10.1.2 from plants acquired as described in 2.9.8.2, were used for the StrepII affinity purification. The chloroplast pellet was resuspended in 500 µl

Strep-ex buffer (100 mM HEPES, pH 8, 100 mM NaCl, 15 mM DTT, 5 mM EDTA, 100 µg ml^{-1} avidin, 0.5 % Triton™ X-100). In order to gain a stroma protein extract, an fractionation step was performed, wherein the chloroplast pellet was thoroughly resuspended in Strep-ex buffer by pipetting up and down 10-15 times, incubated on ice for 10 min and centrifuged at 16,000 x g, 4 °C for 10 min. In order to remove as much thylakoids as possible, the centrifugation step was repeated and the supernatant was carefully pipetted into a fresh tube. This was repeated until the supernatant was clear and could be used as purified stroma protein extract. 50 % Strep-Tactin® Macroprep® solution was equilibrated before it was added to the chloroplast/stroma protein extract. Therefore, 200 µl of the solution was transferred into a 1.5 ml tube and shortly centrifuged at 700 x g, 4 °C and the supernatant, containing the buffer the resin was stored in, was discarded. Subsequently, 500 µl Strep-ex buffer was added to the resin followed by an incubation at 4 °C on rotating mixer for 30 min. The Strep-ex buffer was removed by centrifugation at 700 x g, 4 °C, before the chloroplast/stroma extract was added to the resin. Incubation of the resin with the chloroplast/stroma extract took place for 2 h at 4 °C under gentle agitation on a rotating mixer. After incubation, the slurry was loaded on 1 ml polypropylene columns and left to settle for 5 min. The resin was washed with 5 ml Strep-wash buffer (100 mM HEPES pH 8, 100 mM NaCl, 2 mM DTT, 0.5 mM EDTA, 0.005 % Triton™ X-100) and subsequently eluted in four steps, each time with 100 µl Strep-elution buffer (10 mM Hepes pH 8, 100 mM NaCl, 2 mM DTT, 0.5 mM EDTA, 0.005% Triton™ X-100, 10 mM biotin). The four elution fractions were tested on SDS-PAGE and the two fractions with the highest protein amount were chosen. Selected fractions were mixed 5:1 with 5x Laemmli and incubated at 96 °C for 5 min.

2.18.1.3 LC-MS

Sample preparation for LC-MS was performed as follows. The protein samples containing Laemmli buffer were loaded on 1.5 mm 12 % SDS PA gels and run at 100 V. In order to have two technical replicates per sample, each elution fraction was loaded twice and measured twice. The gel electrophoresis was stopped before the samples entered the separating gel and the gel was Coomassie stained as described before (2.9.2). The protein band was cut out of the gel and sent for LC-MS analysis that was performed in cooperation with Dr. Sascha Rexroth (Plant Biochemistry – Ruhr University Bochum). Peptides were acquired with an in-gel digestion and analysed with a mass spectrometer "in-line" with an upstream nanoHPLC, wherein the peptides were eluted in a gradient of increasing amount of solution B (0.1 % formic acid in acetonitrile (v/v)) in solution A (0.1 % formic acid in MQ (v/v)). Protein database search was performed with Proteome Discoverer 1.3 (Thermo Fischer Scientific) with the SEQUEST-algorithm. Peptide result validation was conducted with a false discovery rate (FDR) of 5 %.

2.18.2 BiFC

For **B**imolecular **F**luorescence **C**omplementation **A**ssay according to Walter *et al.* (2004) full or partial coding sequences of desired genes were inserted into pSpyCE-35S and pSpyNE-35S, in order to express the examined protein/peptide as a fusion to the C- or N-terminal part of YFP, respectively. These constructs were transformed into GV2260 *Agrobacteria* as described in 2.6.2. Subsequently N. *benthamiana* leaves were infiltrated with a GV2260 suspension that had been prepared as described in 2.6.2. Infiltrations were carried out as co-infiltrations of a combination of C- and N-terminal fusion constructs, wherein an $OD_{600\ nm}$ of 0.2 per culture was set for mild expression or an $OD_{600\ nm}$ of 0.6 per culture for strong expression. After infiltration plants were kept in darkness for 2 to 3 days, until leaf discs were analysed via confocal laser scanning microscopy (excitation at 514 nm, emission 530-555 nm for YFP- und 600-700 nm for chlorophyll autofluorescence).

2.19 Tissue Specific Localisation of Promotor Activities (GUS)

The tissue specific localisation of promoter activities was investigated by the detection of the expression of the reporter gene β-glucuronidase (GUS) in plant tissues carrying fusion gene constructs of the promoter region of the examined gene and the coding region of GUS. The expression of GUS can be quantified either via fluorometric assay or qualitatively for tissue specific localisation via histochemical staining of GUS in plant material.

2.19.1 Fluorimetric Quantification of GUS activity

Fluorometric GUS assay was used for the selection of the T2 progeny lines carrying the respective constructs. The goal was to choose lines carrying only one T-DNA insertion after transformation, since this was shown to have an effect on the stability of the GUS expression in the transgenic plants. A negative correlation has been demonstrated for high copy numbers and *uidA* expression/GUS activity (Hobbs *et al.*, 1993).

Therefore, 100 mg plant material from 2-week-old seedlings was homogenised in a ball mill (25 Hz, 1 min) and resuspended in 100 µl GUS ex-buffer (50 mM $NaPO_4$, pH 7.0, 10 mM DTT, 1 mM EDTA, 0.1 % sodium lauryl sarcosine, 0.1 % Triton^{TM} X-100). Samples were centrifuged at 16,000 x *g*, 4 °C for 5 min and the supernatant was collected. Simultaneously, 500 µl aliquots of GUS assay buffer (1 mM 4-MUG in GUS ex buffer) were pre-warmed to 37 °C and 50 µl of the GUS extract was added (a null control with 50 µl GUS ex-buffer was included) and the reaction was conducted at 37 °C either for 1-4 h or o/n, depending on the individual strength of the promoter examined. After the incubation time 100 µl aliquots were collected and immediately mixed thoroughly with 900 µl GUS stop-buffer

(0.2 M Na_2CO_3). 4-MU, which is the product of the hydrolysis of 4-MUG by GUS, was detected by fluorescence (λ_{ex} 365 nm, λ_{em} 455 nm). Values were normalized to FW.

2.19.2 Histochemical GUS staining

For histochemical staining of β-glucuronidase activity, 4-week-old plants or inflorescences of 8-week-old plants were fixed in 90 % acetone at RT for 20 min. Acetone was removed and the plant material was washed with staining solution (50 mM $NaPO_4$, 2mM $K_4Fe(CN)_6$, 2 mM $K_3Fe(CN)_6$, 0.2 % Triton^{TM} X-100, pH 7.2). Thereafter the solution was replaced by staining solution containing 1 mM x-gluc and the plant material was infiltrated by gentle vacuum for 15-20 min. After incubation at 37 °C for 3 h or o/n, the plant samples were bleached via several steps of EtOH washings with increasing EtOH concentrations (from 20 to 50 %) and thereafter fixed in FAA solution (50 % Ethanol, 5 % Formaldehyde, 10 % acetic acid). Fixed plant material was stored in 70 % EtOH at 4 °C until documentation.

2.20 VIGS

For **V**irus-**I**nduced **G**ene **S**ilencing a method described by Liu *et al.* (2002) was employed. A cDNA fragment of the gene to be silenced (between 300-1500 bp in length) was inserted into pTRV2. pTRV2 construct containing the sequences for the desired cDNA and the viral coat protein, as well as pTRV1, carrying sequences for the viral replication and movement proteins (Velásquez *et al.*, 2009) were each transformed into GV2260. Three ml YEB o/n cultures, containing 100 µg ml^{-1} rifampicin, 50 µg ml^{-1} kanamycin and 100 µg ml^{-1} ampicillin, were grown from a single colony. Next day 4 ml VIGS cultures (LB + 10 mM MES, 20 µM acetosyringon, 100 µg ml^{-1} rifampicin, 50 µg ml^{-1} kanamycin, 100 µg ml^{-1} ampicillin) were inoculated with 40 µl of the previous culture and grown o/n at 28 °C. The cells were pelleted at 4,000 x *g*, 12 °C for 20 min and resuspended in infiltration medium (10 mM $MgCl_2$, 10 mM MES, 200 µM acetosyringon). $OD_{600\ nm}$ was adjusted to 1.5 and the cultures were incubated at RT for 4 h. Subsequently pTRV2 and pTRV1 cultures were mixed 1:1 and co-infiltrated into 2-week-old (four leaf stage) *wt Col-0* plants, which were grown under 16 h day, 8 h night, 20 °C, 120 µmol photons $m^{-2}s^{-1}$. Plants were well watered and covered with a lid for 2-3 days. After 10-12 days, first phenotypic changes were noticeable. The samples were collected after 14 d.

2.21 Statistical Analyses

Statistical significance was determined with an unpaired two-tailed Student's t-test, assuming a similar variance of the data sets. Statistical significance is indicated for p-values <0.05.

2.22 Websites/Web Services

Table 31: **List of websites and web services used in the experiments.**

Application	Website	Usage	Reference	Date
The *Arabidopsis* Information Resource	www.*Arabidopsis*.org	*Arabidopsis* gene information and sequence data	Lamesch *et al.* (2012)	18.1.16
Phytozome v.9.0	www.phytozome.net	Sequence data for chlorobiont RIBA sequences	Goodstein *et al.* (2012)	26.4.15
Pfam 28.0	http://pfam.xfam.org	Sequence data for other RIBA sequences	Finn *et al.* (2014)	26.4.15
TargetP 1.1	http://www.cbs.dtu.dk/services/TargetP/	Subcellular Localisation Study	Emanuelsson *et al.* (2000)	9.8.15
Unioprot Retrieve/ID Mapping	http://www.uniprot.org/uploadlists/	Convertion of Accession number to Agi	Consortium (2015)	22.615
Phylogeny.fr	http://www.phylogeny.fr/simple_phylogeny.cgi (one-click mode)	Phylogenetic Tree	Barion *et al.* (2007)	13.7.15
NCBI BlastN	http://blast.ncbi.nlm.nih.gov/blast/Blast.cgi?PROGRAM=blastn&PAGE_TYPE=BlastSearch&BLAST_SPEC=&LINK_LOC=blasttab&LAST_PAGE=blastn	Alignment of nucleotide sequences	Zhang *et al.* (2000), Morgulis *et al.* (2008)	9.7.15
NCBI BlastP	http://blast.ncbi.nlm.nih.gov/blast/Blast.cgi?PROGRAM=blastp&PAGE_TYPE=BlastSearch&LINK_LOC=blasthome	Alignment of protein sequences	Altschul *et al.* (1997), Altschul *et al.* (2005)	9.7.15
Dendrome tBlastPN	http://dendrome.ucdavis.edu/resources/blast/	Pinus Sequence Blast	Wegrzyn *et al.* (2008)	8.5.15
EMBOSS Needle	http://www.ebi.ac.uk/Tools/psa/emboss_needle/	Pairwise Sequence Alignment	Rice *et al.* (2000)	7.8.15
Clustal Omega	http://www.ebi.ac.uk/Tools/msa/clustalo/	Multiple Sequence Alignment	Sievers *et al.* (2011), Li *et al.* (2015)	24.12.15
Ligation Calculator	http://www.insilico.uni-duesseldorf.de/Lig_Input.html	Calculation of molar ratios for ligations	-	27.1.15
NEB Tm Calculator v1.8.1	http://tmcalculator.neb.com/#!/	Calculation of primer melting temperatures	-	27.1.15
HOW TO: Calculate Km and Vmax with Excel	http://src.sfasu.edu/~avk/BTC560/HOW%20TO.htm	Determination of Km and Vmax from enzyme kinetic data	-	13.5.15
PhosPhAt 4.0	http://phosphat.uni-hohenheim.de/phosphat.html	Phosphorylation site predictions	Heazlewood *et al.* (2008), Durek *et al.* (2010)	31.12.15
Gene Expression Map of *Arabidopsis* Embryo Development	http://www2.bri.nrc.ca/plantembryo/	RIBA1 expression data during embryo develoment	Xiang *et al.* (2011)	20.10.14
ProtScale	http://web.expasy.org/protscale/	Hydrophobicity scale for proteins according to Kyte and Doolittle (1982)	Gasteiger *et al.* (2005)	23.2.16

3 Results

3.1 RIBA Proteins in *Arabidopsis thaliana*

The initial steps of riboflavin biosynthesis are performed by DHBPS and GCHII. Throughout the riboflavin producing taxa, the two enzymatic functions are often combined on one bifunctional protein encoded by so called *ribBA* or *RIBA* genes. These fusion proteins consist of an N-terminal DHBPS domain and a C-terminal GCHII domain. In *A. thaliana* a bifunctional RIBA protein, annotated RIBA1 (At5g64300), was described by Herz *et al.* (2000). *RIBA1* belongs to a three member gene family, together with RIBA2 (At2g22450) and RIBA3 (At5g59750).

3.1.1 Alignment of *Arabidopsis* RIBA Protein Sequences Reveals Amino Acid Exchanges in Functional Domains

In order to closer analyse the *Arabidopsis* RIBA proteins, a protein sequence alignment (ClustalOmega, **Table 31**) as shown in **Figure 10** was performed. The bifunctional *B. subtilis* RibBA sequence was included in this alignment to demonstrate the high degree of evolutionary conservation of the functional domains.

Despite the high overall sequence identity of 59 % between RIBA1 and RIBA2, 54 % between RIBA1 and RIBA3, and 46 % between RIBA2 and RIBA3 (according to pairwise sequence alignment with EMBOSS Needle, **Table 31**), some amino acid exchanges were striking. RIBA3 amino acid sequence shows the following exchanges within the functional domains of DHBPS:

1.) at position 125 a glycine instead of the central arginine and

2.) at position 130 an asparagine instead of the second aspartic acid of the ribulose-5-phosphate binding domain.

3.) RIBA3 sequence displays an alanine instead of the glutamic acid at position 264 of the second catalytic domain.

RIBA2 is characterised by several exchanges and deletions between the conserved glycine residues at positions 369 and 374 within the zinc binding domain of GCHII, including the deletion of the second cysteine and an exchange of the third cysteine to glutamine. Kaiser *et al.* (2002) demonstrated that the deletion of these cysteine residues, which are essential for the zinc binding, leads to the loss of GCHII activity. Hence, it is hypothesised that: two of the three RIBA isoforms in *Arabidopsis* have lost their bifunctional activity in riboflavin biosynthesis due to the exchange of important amino acids in the functional domains of the proteins.

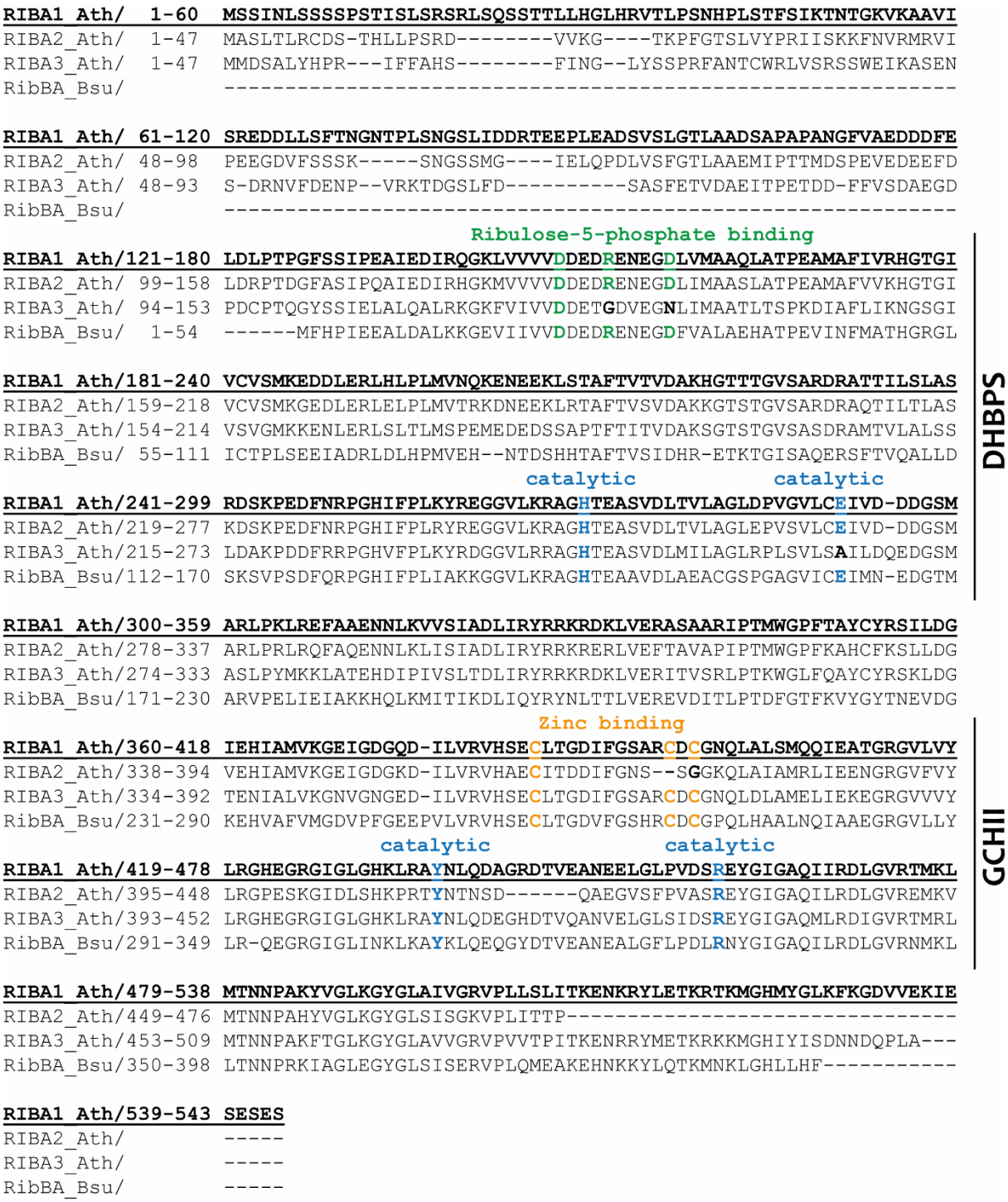

Figure 10: **Protein sequence alignment of *Arabidopsis* RIBA isoforms and *B. subtilis* RibBA.**
Functional amino acid residues of the respective enzymatic domains are marked, whereas the ribulose-5-phosphate binding residues are marked green, the catalytic residues are marked blue and the zinc binding residues are marked orange.

3.1.2 Amino Acid Exchanges in GCHII Domain of RIBA2 and in DHBPS Domain of RIBA3 Cause the Loss of the Respective Enzymatic Function

In order to examine the hypothesis formulated in chapter 3.1.1, *Arabidopsis* RIBA1, RIBA2 and RIBA3 were heterologously expressed in *E. coli*. Therefore, the sequences were adapted to *E. coli* codon usage and an *N*-terminal hexa-histidin-tags (His-tags) was integrated in place of the transit peptides

(**Data S 1**). DNA sequences were synthesised and provided as pUC57 subclones by GenScript®. The *RIBA* fragments were digested with *Nde*I/*Hind*III and cloned into pET22b(+), as described in chapter 2.7.9.3. Subsequently, the RIBA-pET22b(+) constructs were transformed into ArcticExpress™ (DE3) RIL cells and the expression carried out as described in chapter 2.9.5. The recombinant RIBA proteins were purified via FPLC and His-trap columns as described in chapter 2.9.5.1.1.

A SDS-PA gel picture of the purified recombinant proteins is shown in **Figure 11** (panel A). The proteins were subjected to *IN VITRO* DHBPS and GCHII activity assays as described in chapter 2.11.1. The results are presented in **Figure 11** (panel B). An extract of *E. coli* carrying the empty expression vector was used as negative control and treated in the same way as the recombinant RIBA proteins. The background activity, measured with the extract of the negative control, was subtracted from all values. The protein purification and enzyme assays were performed by R. Wittrahm in her Bachelor's thesis (Wittrahm, 2014).

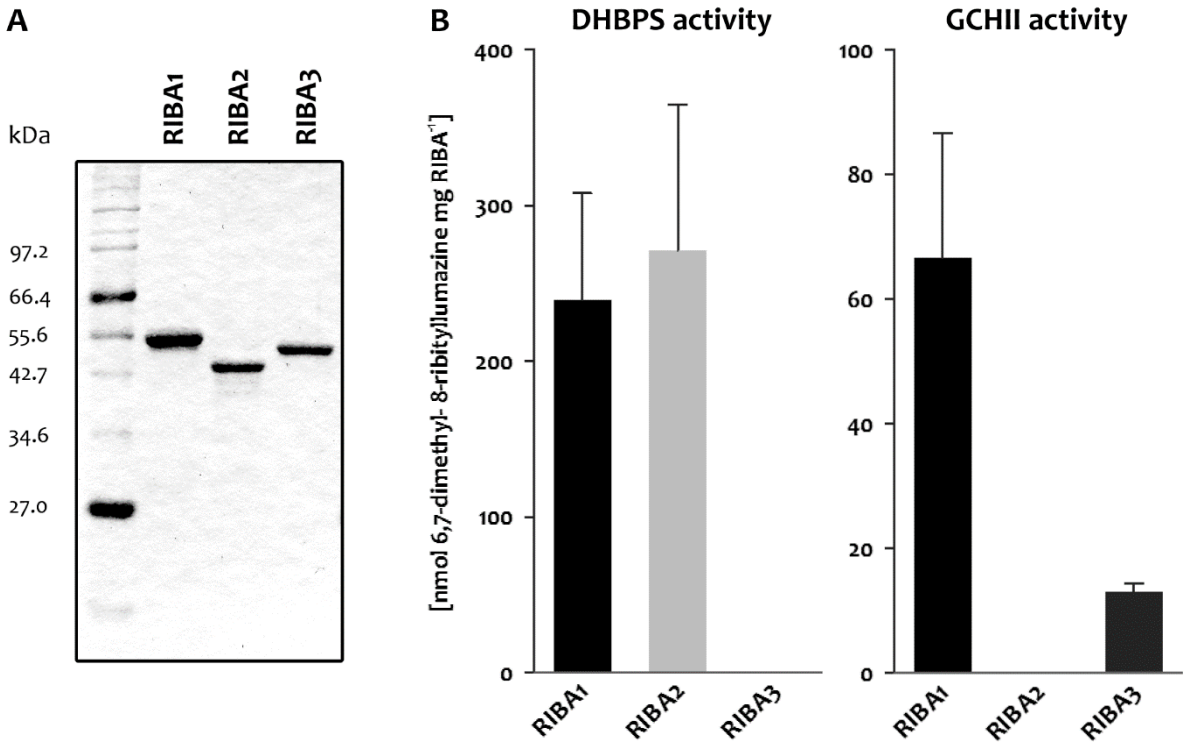

***Figure 11: IN VITRO* activities of *Arabidopsis* RIBA proteins.**
Panel A: SDS-PA gel of the recombinant proteins, which were used for the enzyme assay of DHBPS and GCHII activity. Panel B: The results of the assay of RIBA1 (black), RIBA2 (light grey) and RIBA3 (dark grey) in DHBPS and GCHII assay, shown as nmol 6,7-dimethyl-8-ribityllumazine per mg RIBA protein. Negative control was subtracted from values, n=3, error bars represent standard errors of the mean.

RIBA1 and RIBA2 showed approximately the same DHBPS activity, whereas GCHII activity of RIBA1 was approximately 6 times higher as opposed to RIBA3. No GCHII or DHBPS activity was detectable for RIBA2 or RIBA3, respectively. This is in agreement with the assumption made based on the amino acid sequence comparison (**Figure 10**).

3.2 Enzymatic Characterisation of Recombinant RIBA Proteins

The regulatory mechanisms behind the first steps of riboflavin biosynthesis and their possible role in the maintenance of the general pathway homeostasis have not been extensively investigated in plants so far. The initial characterization of *Arabidopsis* RIBA isoforms was performed on recombinant proteins expressed and purified as described in chapters 2.9.4 and 2.9.5.

3.2.1 RIBA Enzyme Kinetics

In order to unravel the enzymatic properties, all three recombinant RIBA proteins were used in steady state kinetic analyses. Therefore, enzyme activities were determined in a coupled assay (chapter 3.1.2), measuring 6,7-dimethyl-8-ribityllumazine, the product of the lumazine synthase. Here, different substrate concentrations and a reaction time of 30 min were applied. Beforehand, test assays were conducted, determining the accurate reaction time, confirming that the time-point of measurement laid within the linear phase of the product accumulation progress curve.

3.2.1.1 GCHII

The analysis of the GCHII steady state enzyme kinetics for RIBA1 and RIBA3 was conducted at GTP concentrations from 10 to 3,200 µM (**Figure 12**). Since RIBA2 is not able to perform GCHII activity, it was not included in the analysis.

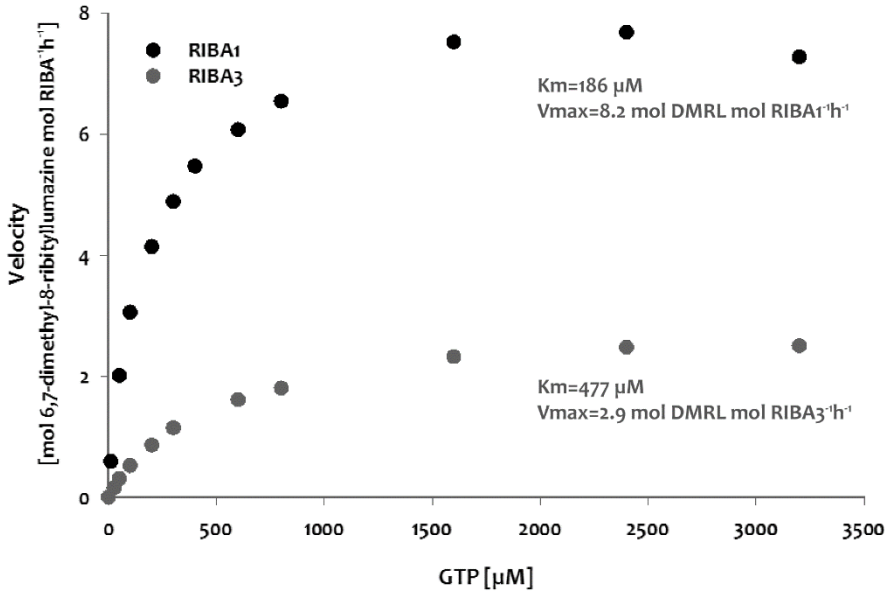

Figure 12: **Enzyme kinetics of GCHII reaction for RIBA1 and RIBA3.**
GCHII activity was determined at GTP concentrations from 10 to 3,200 µM after 30 min at 37 °C. Values are given in mol 6,7-dimethyl-8-ribityllumazine (DMRL) per mol RIBA protein and h. K_m and V_{max} were determined from fitted (Excel Solver) enzyme activity curves according to Michaelis Menten (Michaelis & Menten, 1913).

The presented curves show Michaelis-Menten typical saturation behaviour. The enzyme activity (velocity, v) increases with rising substrate concentration [S], approaching asymptotically the maximal enzyme activity rate (v_{max}). Using nonlinear regression analysis by the simple Michaelis-

Menten equation (**Equation 1**) v_{max} and Michaelis constant (K_m) could be determined. Both, v_{max} and K_m of RIBA1 and RIBA3 were clearly different. While v_{max} of RIBA1 was calculated to be 8.2 mol DMRL mol^{-1} $RIBA1^{-1}$ h^{-1}, RIBA3 reached 2.9 mol DMRL mol^{-1} $RIBA3^{-1}$ h^{-1}. The K_m value of RIBA1 and RIBA3 were determined at 186 µM and 477 µM GTP, respectively, representing the concentration of substrate needed for half v_{max}.

3.2.1.2 *DHBPS*

In **Figure 13**, the DHBPS enzyme kinetics for RIBA1 and RIBA2 were determined at ribulose-5-phosphate concentrations from 1 to 800 µM. Since RIBA3 is not able to perform DHBPS activity, it was not included in the analysis. The presented values show Michaelis-Menten typical saturation behaviour, so that K_m and v_{max} values could be determined as described before (chapter 3.2.1.1). v_{max} of RIBA2, which lied at 41 mol DMRL mol^{-1} $RIBA2^{-1}$ h^{-1}, was slightly higher than v_{max} of RIBA1 at 36 mol DMRL mol^{-1} $RIBA1^{-1}$ h^{-1}. The K_m values of RIBA1 and RIBA2 were at 27 µM and 35 µM ribulose-5-phosphate, respectively.

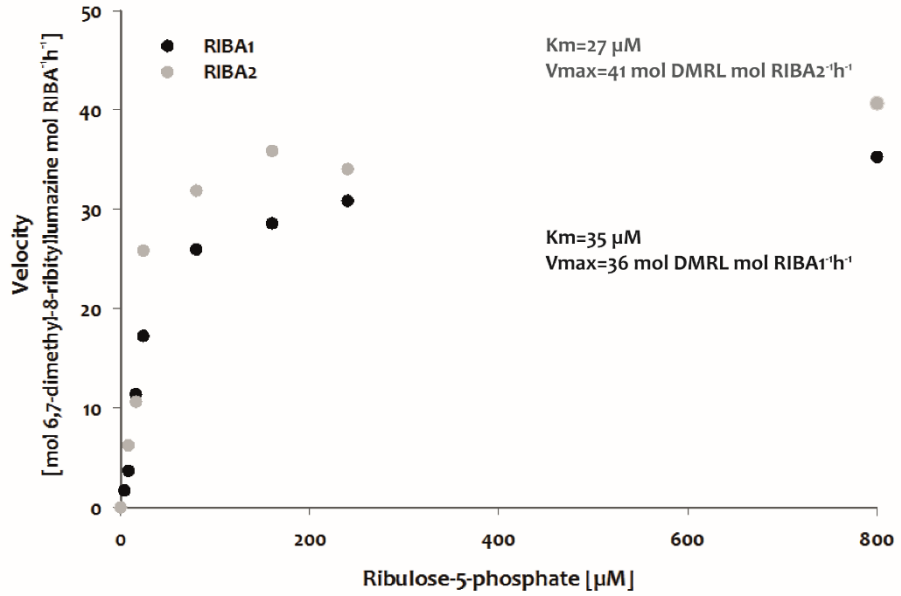

Figure 13: **Enzyme kinetics of DHBPS reaction for RIBA1 and RIBA2.**
DHBPS activity was determined at ribulose-5-phosphate concentrations from 1 to 800 µM after 30 min at 37 °C. Values are given in mol 6,7-dimethyl-8-ribityllumazine (DMRL) per mol RIBA protein and h. K_m and V_{max} were determined from fitted (Excel Solver) enzyme activity curves according to Michaelis Menten.

3.2.2 RIBA Enzyme Activities *IN VIVO*

In order to test the enzymatic functionalities IN VIVO, the RIBA fragments used for the recombinant expression in E. coli were utilised. The RIBA1 and RIBA3 fragments were cloned via their Ecl136II/HincII (RIBA1) or Ecl136II/SmaI (RIBA3) sites into pACYC184. For RIBA2, primers CLP7/8 (**Table S 3**) were employed using RIBA2-pUC57 as template and the resulting product was also cloned via the inserted PsiI sites into pACYC184. pACYC184 was chosen for the *E. coli* complementation due to its low copy characteristics, which allows suitable transgene expression.

The constructs, as well as an empty pACYC184 were transformed into *E. coli* knockout strains BSV18 and BSV11 defective in RibA (GCHII) and RibB (DHBPS), respectively, leading to riboflavin auxotrophy (Bandrin et al., 1983). Beforehand, the expression of the three proteins in the E. coli strains was confirmed by Western blot (data not shown). Growth assay was performed as stated in chapter 2.12.

Figure 14 and **Figure 15** show the growth curves of the *E. coli ribA* and *ribB* mutants carrying the above mentioned constructs. In both cases, negative controls showed initial growth, reaching the stationary phase at approximately an $OD_{600\,nm}$ of 0.2, despite lack of riboflavin. This growth is likely to be enabled by remaining intracellular flavin.

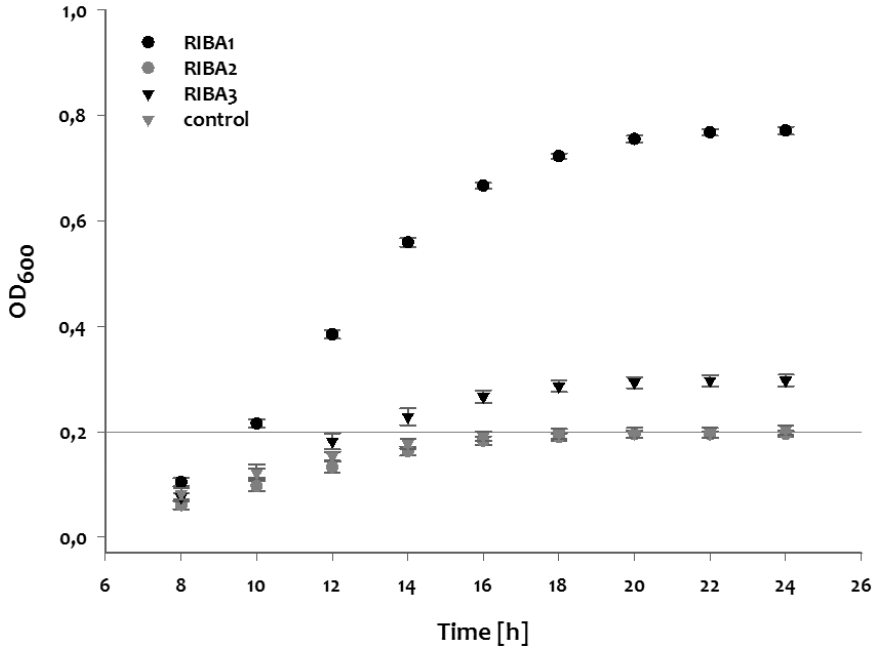

***Figure 14*: Growth assay of *E. coli ribA* mutants expressing *Arabidopsis* RIBA proteins.**
The bacteria carry empty pACYC184 as negative control (grey triangle), pACYC184 expressing *A. thaliana* RIBA1 (black circle), RIBA2 (grey circle) or RIBA3 (black triangle). Growth of the M9 minimal medium liquid cultures were monitored for 24 h. Initial OD of each culture was subtracted, n=3, error bars represent standard errors of the mean.

The growth behaviour of *ribA* expressing RIBA2 did not differ from the negative control. The growth of *ribA* expressing RIBA1 or RIBA3 was 4 and 1.5 times increased compared to control, respectively, and reached an $OD_{600\,nm}$ of 0.8 and 0.3 after 24 h (**Figure 14**).

In the case of the *ribB* mutant, expression of RIBA3 did not enhance the mutant's growth compared to the negative control. *ribB* mutant expressing RIBA2 or RIBA1, however, showed slightly, namely, 0.3 and 0.2 fold increased growth, respectively (**Figure 15**).

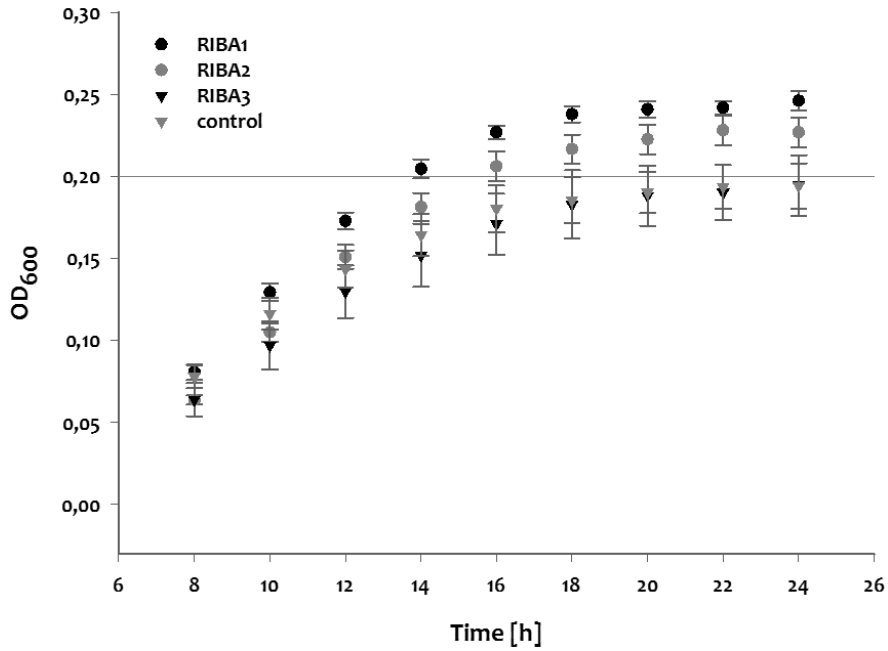

***Figure 15*: Growth assay of *E. coli ribB* mutants expressing *Arabidopsis* RIBA proteins.**
The bacteria carry empty pACYC184 as negative control (grey triangle), pACYC184 expressing *A. thaliana* RIBA1 (black circle), RIBA2 (grey circle) or RIBA3 (black triangle). Growth of the M9 minimal medium liquid cultures were monitored for 24 h. Initial OD of each culture was subtracted, n=3, error bars represent standard errors of the mean.

3.2.3 Recombinant RIBA1 Binds FMN

It was noticed that purified recombinant RIBA1 protein (chapter 2.9.5) was characterised by bright yellow colouration. In order to identify the origin of the pigment, aliquots of all three recombinant RIBA proteins with equal protein amounts were subjected to flavin extraction (chapter 2.15.1). The HPLC analysis, performed as described in chapter 2.15.3, revealed one distinct peak in the chromatogram at 9.9 min for RIBA1 and RIBA3, which coincided with the main peak of the FMN standard at 9.9 min (**Figure 16**). The result of the quantification (chapter 2.15.3) is depicted in **Figure 16**. RIBA1 bound 13.7 ng FMN per µg recombinant protein, which corresponds to a 1:1 molar ratio. RIBA3 bound approximately 1.1 ng FMN per µg recombinant protein. FMN was not detectable in extracts of RIBA2.

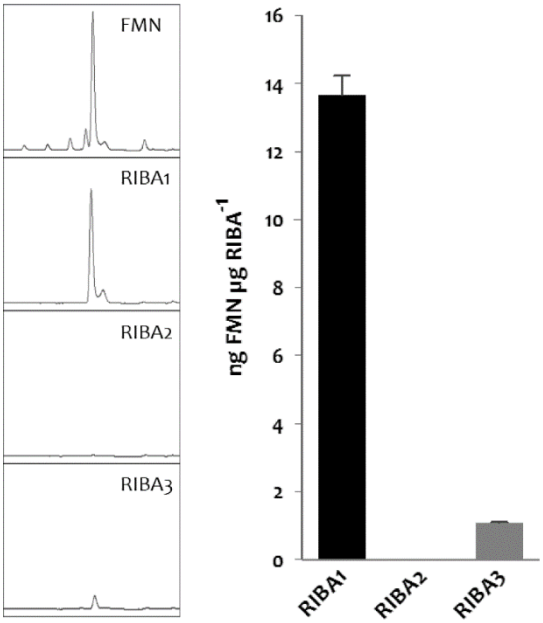

Figure 16: **HPLC analysis of flavin compounds bound to recombinant RIBA proteins.**
The same amounts of each recombinant protein were used for the extraction. In the left panel, chromatogram of the analysis is presented. The compounds were identified using authentic standards. Values of the bar diagram are given as ng FMN per µg recombinant protein, n=3, error bars represent standard errors of the mean.

3.2.4 GCHII Activity Is Inhibited upon FMN Addition *IN VITRO*

In order to analyse the effect of the before detected FMN binding (**Figure 16**), GCHII and DHBPS enzyme assays were performed with RIBA1 and RIBA3, respectively, at rising FMN concentrations. Thereby FMN concentrations between 0.9 and 9 µM, corresponding to molar ratios of RIBA protein to FMN of 1:1 and 1:10, respectively, were used (**Figure 17**). As depicted in **Figure 17**, FMN had no effect on DHBPS activity of RIBA1, whereas GCHII activity of RIBA1 decreased approximately by 15 % at 0.9 µM FMN and finally by 90 % at 9 µM FMN. For RIBA3 a decrease of GCHII activity by 35 % at 9 µM FMN could be measured. Since the measurement of GCHII enzyme activity is coupled and premises the activity of three additional enzymes RIBG, pyrimidine phosphatase and lumazine synthase, the effect of FMN on these enzymes was tested as well. Therefore, the reaction to 2,5-diamino-6-ribosylamino-4(3H)-pyrimidinone was performed first, with merely RIBA1 and its substrate GTP (w/o added FMN). Thereafter, RIBA1 was removed by filtration and the supernatant containing 2,5-diamino-6-ribosylamino-4(3H)-pyrimidinone used as substrate for the subsequent reaction. At this point, FMN and the other required enzymes were added. As shown in **Figure 17**, FMN did not affect the activity of the other enzymes involved in the GCHII enzyme activity assay.

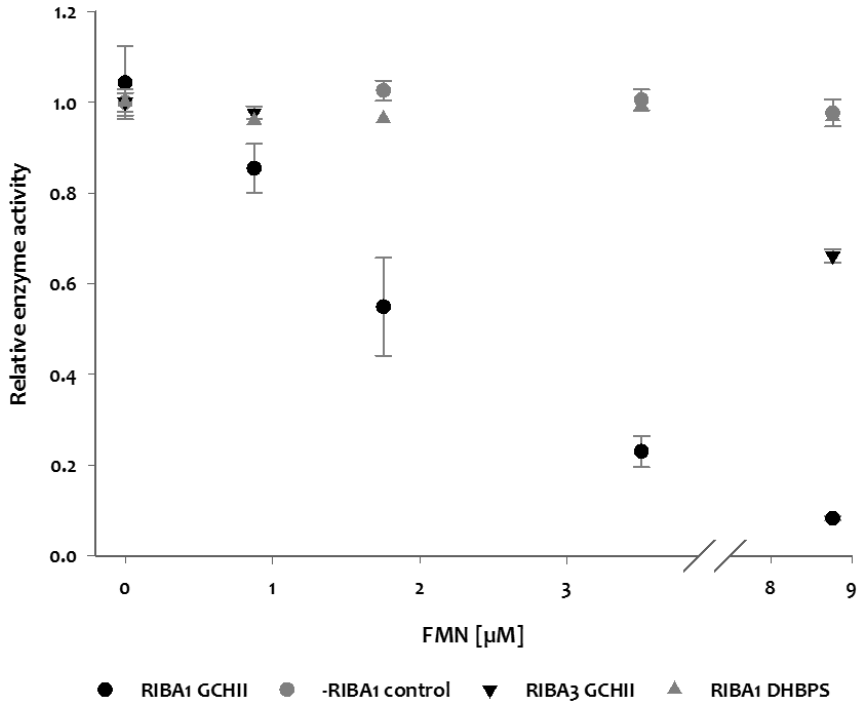

***Figure 17:* Effects of FMN on GCHII and DHBPS activity.**
Relative enzyme activities were determined for RIBA1 GCHII reaction (black circle), control GCHII reaction, where RIBA1 was filtrated from the reaction mixture before addition of FMN (grey circle), RIBA3 GCHII reaction (black triangle), RIBA1 DHBPS reaction (grey triangle) at supplemented FMN concentrations between 0.9 and 9 µM and normalised to activity w/o supplemented FMN.

Additionally, the question arose if all flavins had an inhibitory effect on GCHII activity. Therefore, the RIBA1 GCHII activity was measured at different FAD and riboflavin concentrations as shown in **Figure 18**.

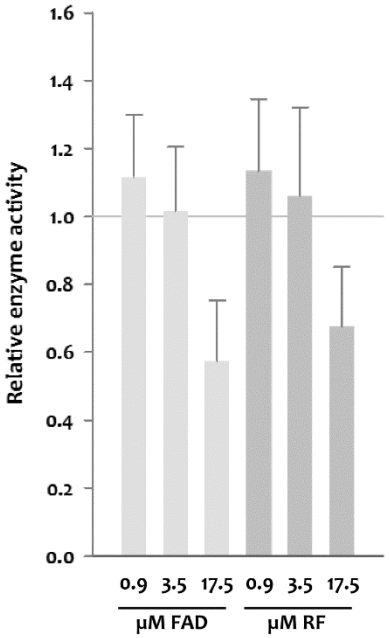

***Figure 18:* Effect of supplemented FAD and riboflavin on RIBA1 GCHII activity.**
Relative enzyme activities were determined for RIBA1 GCHII reaction at supplemented FAD and riboflavin concentrations of 0.9, 3.5 and 17.5 µM corresponding to molar ratios of RIBA1 protein to flavin of 1:1, 1:4 and 1:20. The data is presented as relative enzyme activity normalised to GCHII activity w/o supplemented FAD or RF.

For the determination of possible inhibitory effects, FAD and riboflavin concentrations of 0.9, 3.5 and 17.5 µM corresponding to molar ratios of RIBA1 protein to flavin of 1:1, 1:4 and 1:20 were used. As seen in **Figure 18**, FAD as well as riboflavin only had an inhibitory effect on RIBA1 GCHII activity at the highest tested concentrations, corresponding to the molar protein to flavin ratio of 1:20. In both cases, the inhibitory effect accounted for a 40 % decrease of GCHII activity compared to control, without flavin supplementation. A molar protein to FMN ratio of 1:2 already achieved this degree of inhibition.

For the determination of the type of FMN inhibition, RIBA1 GCHII enzyme kinetics were measured with 0, 0.9, 1.8 and 3.5 µM FMN (**Figure 19**) as described in chapter 2.11.1.1.2. This measurement showed that increasing FMN concentrations caused the decrease of the maximal reaction rate (v_{max}), while the ability to utilise GTP, indicated by increasing K_m values, decreased as well.

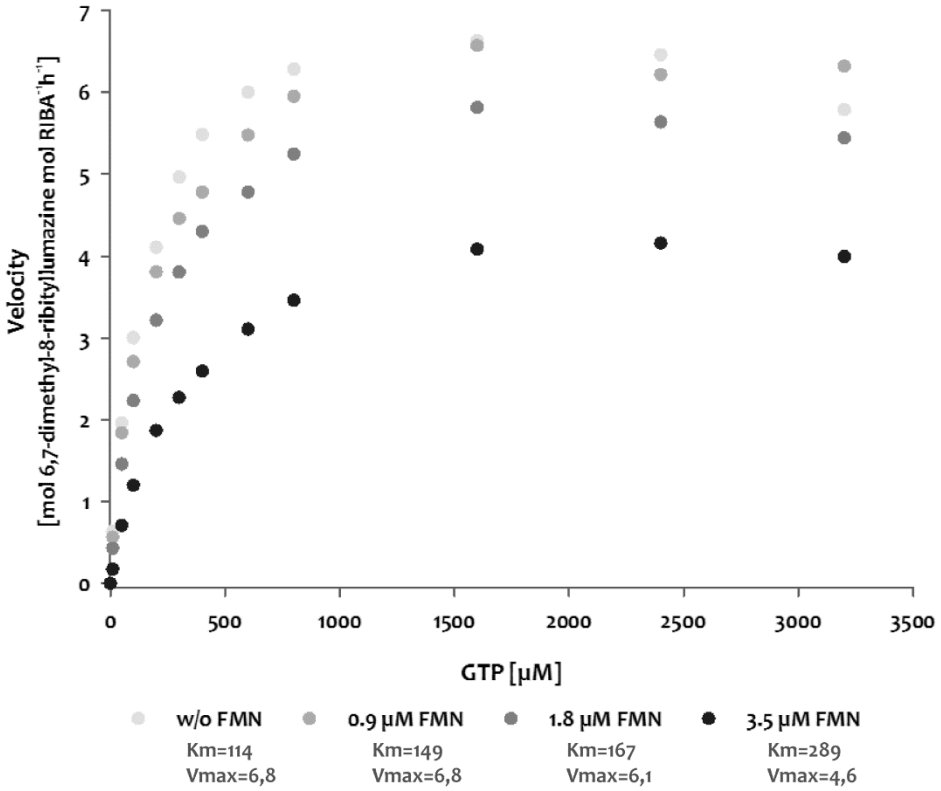

Figure 19: **Inhibition effect of supplemented FMN on RIBA1 GCHII activity.**
GCHII enzyme kinetics for RIBA1 were measurement at GTP concentrations from 10 to 3,200 µM after 30 min at 37 °C and FMN concentrations of 0, 0.9, 1.8 and 3.5 µM. Values are given in mol 6,7-dimethyl-8-ribityllumazine (DMRL) per mol RIBA protein and h. K_m and v_{max} were determined from fitted (Excel Solver) enzyme activity curves according to Michaelis Menten.

3.2.5 RIBA1 is Phosphorylated *IN VITRO*

A large scale phosphoproteome analysis of the *A. thaliana* chloroplast as described by Reiland *et al.* (2009) revealed a peptide originating from the C-terminus of RIBA1 as a potential target for phosphorylation. **Figure 20** shows the alignment of the above mentioned peptide with the

C-terminal region of RIBA2 and RIBA3. The alignment reveals that this peptide is missing in RIBA2 as well as RIBA3, even though the C-terminus is highly conserved. It was proposed that only RIBA1 is subject to phosphorylation. This hypothesis was examined in a phosphorylation assay as described in chapter 2.11.2.

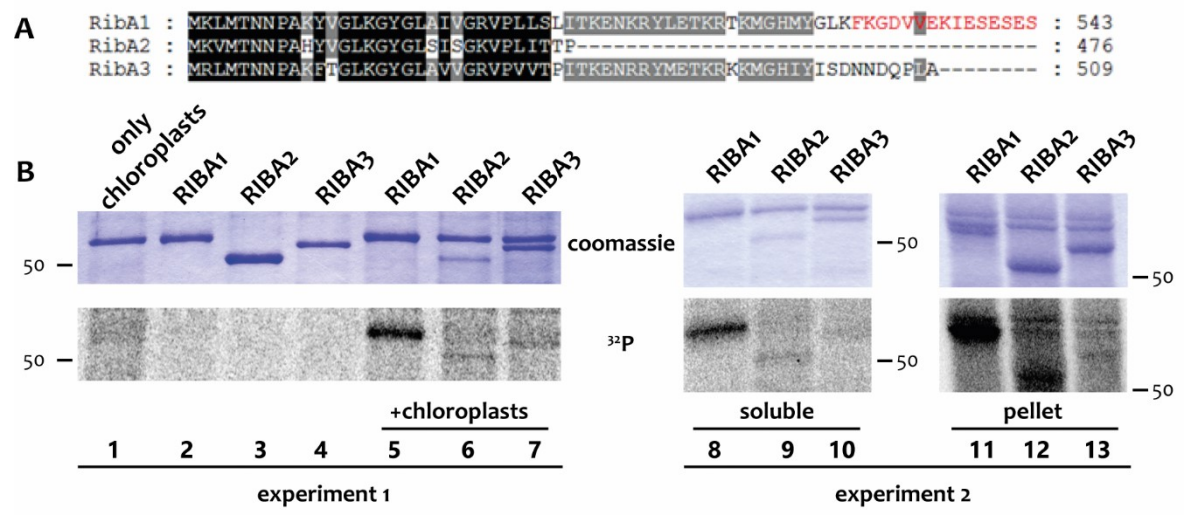

Figure 20: **Phosphorylation of RIBA proteins.**
Panel A depicts an alignment of the C-termini of *Arabidopsis* RIBA proteins. Predicted phosphopeptide, which was published by Reiland *et al.* (2009) is marked red, high degree of homology is marked black and close homology grey. Panel B shows on top the Coomassie stained SDS-PA gels and below the radiogram of ^{32}P detection, of experiment 1 and 2. For experiment 1 soluble extracts of the phosphorylation assay were loaded: 1. lane chloroplast crude extract without RIBA used as control to demonstrate that there are no background signals emitted by proteins from the chloroplast extract, lanes 2-4 contain RIBA autophosphorylation controls, whereas here recombinant RIBA proteins were not treated with chloroplast extracts (mock), lanes 5-7 RIBAs treated with chloroplast crude extracts. For experiment 2 the soluble (lanes 8-10) and pellet (lanes 11-13) extracts after phosphorylation assay with respective RIBAs treated with chloroplast crude extract were loaded.

In **Figure 20** results of two phosphorylation assays are depicted. In both experiments, crude chloroplast extracts were used as the source for the kinase and the assay was started by the addition of γ-^{32}P-ATP. After the assay was stopped, the reaction mixture was fractioned into the soluble and pellet fraction. In experiment 1, only the soluble fraction was separated by SDS-PAGE.

The picture of the Coomassie stained gel of experiment 1 shows a band in lane 1, which represents Rubisco large subunit. In the radiogram, no signal at this size is present. Lanes 2-4 show that in absence of chloroplast extracts, RIBA proteins were not autophosphorylated. If chloroplast crude extracts were added to the assay mixture (lanes 5-7) RIBA1 was clearly phosphorylated, while signals emitted by RIBA2 and RIBA3 were very weak. Moreover, the Coomassie stained gels reveal a decrease of protein amount when mock treated (lanes 2 and 3) and chloroplast treated RIBA1 and RIBA2 (lanes 5 and 6) are compared.

Experiment 2 was conducted in a similar way, wherein the soluble as well as the pellet fraction were separated by SDS-PAGE. In the Coomassie stained gel, containing the soluble fractions (lanes 8-10),

bands representing the recombinant proteins appeared weak, whereas same protein bands appeared approximately three times stronger in the gel containing the pellet fraction (lanes 11-13). Apparently, the majority of the proteins that were used in the assay had precipitated upon addition of the chloroplast extract. The radiogram shows a strong signal originating from RIBA1, and a weak signal from RIBA2 and RIBA3 in the soluble fraction, respectively. The signals obtained from the gel containing the pellet fractions were stronger, especially for RIBA1. Even though the protein bands of RIBA2 and RIBA3 were much stronger, the signal emitted was still very weak. These findings support the hypothesis that RIBA1 was phosphorylated. The weak signals detected from RIBA2 and RIBA3 can be interpreted as the result of unspecific phosphorylation events due to *IN VITRO* conditions. This hypothesis is reinforced by the phosphorylation site prediction analysis (PhosPhAt 4.0, **Table 31**), which results no phosphopeptide for RIBA3 and only one phosphopeptide for RIBA2, lying within the predicted transit peptide region ($G_pTKPFGT_pSLVYPR$).

3.3 Phylogenetic Analysis of RIBA Gene Family

3.3.1 Evolution of Plant RIBA Proteins

A phylogenetic tree (**Figure 21**) with RIBA protein sequences of representatives of the main Chlorobionta divisions was constructed to analyse the evolution of plant RIBA isoforms. Two representatives of the division of Chlorophyta, namely *Chlamydomonas reinhardii* (Chlorophycaea) and *Ostreococcus trauri* (Prasinophyceae) were included in the set. These early Chlorobionta possess only one bifunctional RibBA isoform and are located on a clade formed by the split of Chlorophyta and Streptophyta, also evident here in the evolution of RIBA proteins. Among the Embryophyta, *Physcomitrella patens,* as the representative of the early division of Bryophytes, shows a gene duplication event that, in the case of RIBA, caused the appearance of the second isoform. According to their amino acid sequences, it is assumed that both are bifunctional. Initial monofunctional RIBA proteins occured before the split of lycophytes and spermatophytes. *Selaginella moellendorfii*, the representative of Lycopodiophyta, has one RIBA form, showing several exchanges in the important amino acid residues of the DHBPS domain. Due to its homology to the *Arabidopsis* RIBA3 protein it was also denominated RIBA3 even though there are only two annotated RIBA isoforms in Selaginella. The same annotation was applied to *Pinus taeda*, as a representative of Gymnospermae, and *Amborella trichopoda*, as a representative of the early Angiospermae, which also have two annotated RIBA isoforms, wherein one of the sequences shows alterations in the amino acid residues of the DHBPS domain (RIBA3).

The evolution of the RIBA isoforms was further analysed in representatives of flowering plants (Angiospermae/Magnoliopsida): *Amborella trichopoda* as the base of the lineage, *Oryza sativa* and

Sorghum bicolor as representatives of monocotyledons. For dicotyledons *Nicotiana sylvestris* (Solanaceae), *Vitis vinifera* (Vitaceae), *Arabidopsis thaliana* (Brassicaceae), *Tarenaya hassleria* (Cleomaceae), *Citrus sinesis* (Malvaceae) and *Medicago truncatula* (Facaceae) were chosen as species of the main orders. All of the mentioned species, except Amborella, possess three RIBA isoforms. The annotation of these proteins was undertaken according to the degree of homology with the *Arabidopsis* RIBA isoforms.

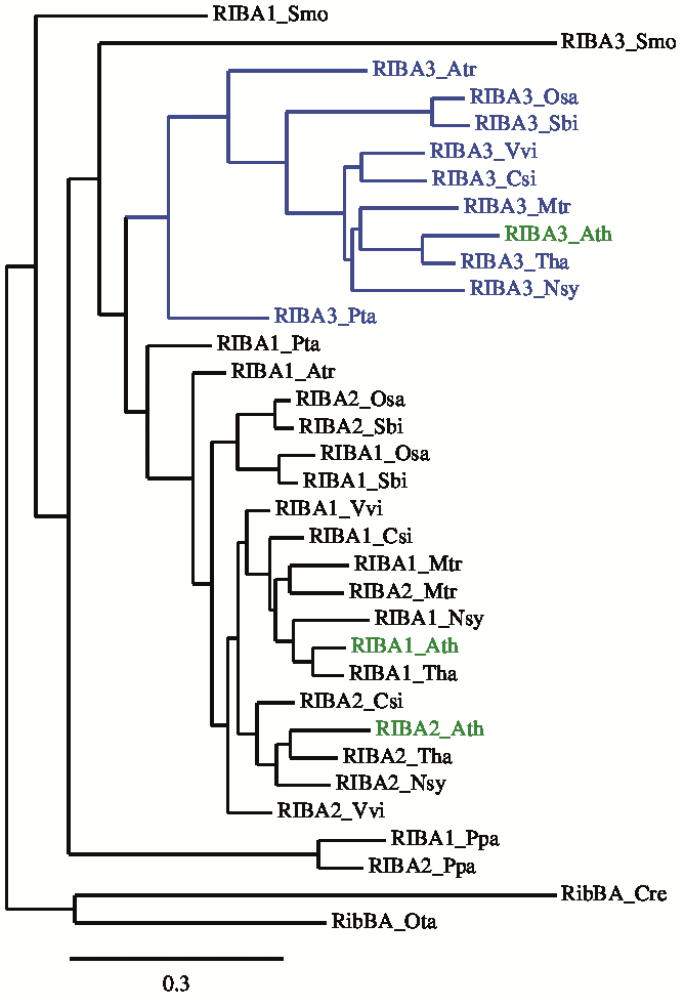

Figure 21: **Phylogenetic tree of RIBA sequences of selected Chlorobionta.**
Chlorophyta: Cre: *Chlamydomonas reinhardii* (Chlorophycaea), Ota: *Ostreococcus trauri* (Prasinophyceae), Bryophyta: Ppa: *Physcomitrella patens*, Lycopodiophyta: Smo: *Selaginella moellendorfii*, Gymnospermae: Pta: *Pinus taeda*, Angiospermae/Magnoliopsida: Atr: *Amborella trichopoda* (Amborellales), Monocotyledons: Osa: *Oryza sativa*, Sbi: *Sorghum bicolor* (Poaceae), Dicotyledons: Nsy: *Nicotiana sylvestris* (Solanaceae), Vvi: *Vitis vinifera* (Vitaceae), Ath: *Arabidopsis thaliana* (Brassicaceae), Tha: Tarenaya hassleria (Cleomaceae), Csi: Citrus sinesis (Malvaceae), Mtr: *Medicago truncatula* (Fabaceae). The phylogenetic tree was constructed with an algorithm service provided by Phylogeny.fr. The scale represents a branch length value of 0.3. RIBA isoforms from *Arabidopsis* thaliana are highlighted in green, while the clade of RIBA3 proteins is highlighted in blue.

The phylogenetic tree shows a distinct clade accommodating spermatophyte RIBA3 proteins and a more heterogeneous clade that accommodates spermatophyte RIBA1 and RIBA2 proteins.

To closer analyse the development of the RIBA isoforms and the respective enzymatic properties, the three *RIBA* gene family members of *Arabidopsis thaliana* and 37 other tracheophyte species were examined via amino acid sequence alignment. A summary of the result is shown in **Figure 22**. Attention was paid on amino acid residues known to perform specific enzymatic functions for the DHBPS and GCHII domains. The analysis of RIBA sequences revealed a group of RIBA proteins with altered DHBPS domains, showing high homology to *Arabidopsis* RIBA3. Closer analysis of the RIBA3 sequences of the 38 tracheophyte species revealed in 32 cases exchanges at least in the central arginine and the second aspartic acid of the ribulose-5-phosphate binding domain, as well as an exchange of the glutamic acid residue of the second catalytic DHBPS domain, as already shown in **Figure 10**. In these cases, it can certainly be assumed that the DHBPS function is as severely disturbed as in *Arabidopsis* RIBA3 (**Figure 11**). Some RIBA3 protein sequences showed an altered exchange pattern, whereas the first aspartic acid of the ribulose-5-phosphate domain was never affected and the tyrosine, belonging to the first catalytic domain, was only affected in *Selaginella moellendorfii*. This particular RIBA3 sequence was exceptional showing exchanges in four of five functional residues. The RIBA3 sequence of *Pinus taeda* revealed only an exchange of the glutamic acid of the second catalytic residue. In *Amborella trichopoda* as well as *Sorghum bicolor* RIBA3 sequences, exchanges of the arginine of the ribulose-5-phosphate binding domain, as well as the aspartic acid (ribulose-5-phosphate binding) or the glutamic acid of the second catalytic domain, were found. In these three cases, when less exchanges were seen than in the *Arabidopsis* RIBA3 sequence, the consequences on the DHBPS activity needs to be tested *IN VITRO* to verify the assumption of their monofunctionality.

The analysis also revealed a second group of RIBA proteins with high homology to *Arabidopsis* RIBA2. Eleven out of 38 species that were studied showed like *Arabidopsis* RIBA2 altered amino acid residues in the GCHII functional domains. Exchanges of two of three cysteine residues of the zinc binding domain, like were described earlier for *Arabidopsis* RIBA2 (3.1.1), was also present in other analysed Brassicaceae species, including *Arabidopsis lyrata*, *Capsella rubella*, *Brassica rapa* and *Thellungiella halophila*. Moreover, the mutation present in the Brassicaceae family, as shown in **Figure 22**, was caused by a single deletion event as demonstrated in a cDNA sequence alignment shown in **Figure 23**. The studied sequences of the Caricaceae (*Carica papaya*) and Cleomaceae (in **Figure 21** *Tarenaya hassleria*) species, which like Brassicaceae belong to the order of Brassicales, did not show the above mentioned deletion.

***Figure 22*: Alignments of DHBPS and GCHII domains of RIBA isoforms from several plant species.**
Ath: *Arabidopsis thaliana*, Smo: *Selaginella moellendorfii*, Ppa: *Physcomitrella patens*, Pta: *Pinus taeda*, Atr: *Amborella trichopoda*, Osa: *Oryza sativa*, Nsy: *Nicotiana sylvestris*, Bra: *Brassica rapa*, Cru: *Capsella rubella*, Mtr: *Medicago truncatula*. Functional amino acid residues are colour coded: green: ribulose-5-phosphate binding, blue: catalytic, orange: zinc binding. Amino acid exchanges and mutations within the functional amino acid residues are marked in red.

```
Cru_RIBA2   CGGATGATATATTCGG------AAACAGCTCTGGTGGAAAACAATTAGCGATTGCAATGA 1384
Ath_RIBA2   CAGATGATATATTCGG------AAATAGCTCTGGTGGAAAACAGTTAGCGATTGCAATGA 1251
Bra_RIBA2   CAGATGATATATTTGG------AAACGGCTCTGGTGGGAAGCAATTAGCAATCGCTATGA 1237
Ath_RIBA1   CAGGGGACATATTTGGGTCTGCAAGGTGTGATTGCGGGAACCAGCTAGCACTCTCGATGC 1271
              D  D  I  F  G                          Q  L  A
```

***Figure 23*: Alignment of Brassicaceae RIBA2 and *Arabidopsis* RIBA1 cDNA sequences demonstrating the deletion causing monofunctionality of RIBA2.**
cDNA stretches from Cru: *Capsella rubella*, Ath: *Arabidopsis thaliana* and Bra: *Brassica rapa* were aligned using multiple sequence alignment tool ClustalW2.

Furthermore, *Phaseolus vulgaris* and *Linum usitatissimum* RIBA2 sequences showed exchanges of the tyrosine and arginine residues of the catalytic domains. Single amino acid exchanges were discovered in RIBA2 sequences of *Manihot esculenta*, *Ricinus communis*, *Glycine max* and *Zea mays*. Whereas the amino acid exchanges as described for *Arabidopsis* RIBA2 cause the loss of the GCHII

enzyme function (3.1.2), the consequence of the other described exchanges have to be tested in an *IN VITRO* assay.

3.3.2 Evolution of Bacterial RibBA Proteins

Additionally to the plant RIBA sequences, the evolution of bacterial RibBA proteins was analysed. It was intended to learn whether RIBA proteins were originally mono- or bifunctional.

In **Figure 24** some prokaryotic and protist RibBA proteins were comprised in a phylogenetic tree. Representatives from different phyla were chosen for the analysis to draw a picture of the development of bifunctional RibBA proteins from early bacteria until Choanoflagellatae as close ancestors of Metazoa and therefore, probably last taxon in that lineage able to produce riboflavin.

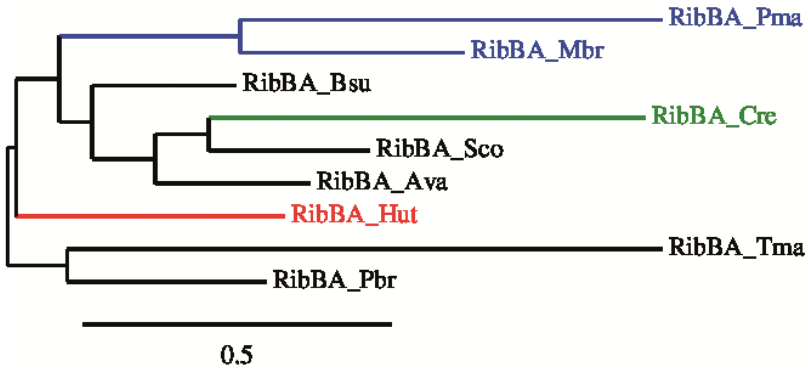

Figure 24: **Phylogenetic tree of RibBA proteins from selected prokaryote and protist phyla.**
The domain of Bacteria (black) contains Pbr: *Planctomyces brasiliensis* (Planctomycetes), Tma: *Thermotoga maritime* (Thermotogae), Bsu: *Bacillus subtilis* (Firmicutes), Ava: *Anabaena variabilis* (Cyanobacteria), Sco: *Streptomyces coelicolor* (Actinobacteria). The representative of the domain of Archea (red) includes Hut: *Halorhabdus utahensis* (Euryarchaeota). The domain Eukaryota (blue) is represented by, Pma: *Perkinsus marinus* (Perkinsozoa, Superphylum Alveolata), Mbr: *Monosiga brevicollis* and Cre: *Chlamydomonas reinhardtii* (Chlorophyte). The phylogenetic tree was constructed with an algorithm service provided by Phylogeny.fr. The scale represents a branch length value of 0.5.

Representatives of the phyla, which have been postulated to be the common ancestors of bacteria, were also included. Those are, according to Brochier and Philippe (2002), the phylum of planctomycetes, whereas this hypothesis was opposed by Barion *et al.* (2007) postulating the hyperthermophilic Thermotogales and Aquificales being the common ancestors. The analysis revealed that the sequecens of the three above mentioned phylae contained amino acid stretches that were highly homologous to the DHBPS and the GCHII domain of modern bacteria. This result allows the conclusion that these early RibBA proteins were most likely bifunctional enzymes like still found today e.g. in *B. subtilis* and plants.

The phylogenetic tree (**Figure 24**) shows an early development of RibBA proteins of the ancient bacterial ancestors *Thermotoga maritima* and *Planctomyces brasiliensis* sharing an early clade. Second node in this tree is represented by the domain of Archae and a clade which then divides

into the protist clade and the bacterial clade, from which, as depicted by the elongated branch, *Chlamydomonas reinhardtii* as an early chlorophyte further develops.

3.4 Analysis of *RIBA* Expression

Work done in our group has demonstrated before (Hiltunen *et al.*, 2012) that *Arabidopsis* RIBA proteins do not differ in their subcellular occurrence. Targeting properties were predicted with several online prediction services (TargetP, Predotar) and examined in a localisation experiment. The N-terminus of each RIBA isoform was fused to green fluorescent protein (GFP), transiently expressed in *A. tumefaciens*-infiltrated *N. benthamiana* leaves and visualised via confocal laser scanning microscopy (cLSM). As predicted, all three proteins were localised in the chloroplast. Therefore, it was interesting to investigate whether there are differences in the expression of RIBA proteins concerning different tissues or developmental stages. Hence, the spatiotemporal transcript expression was explored by means of quantitative expression analysis by qPCR and *RIBA* promoter-driven GUS constructs.

3.4.1 Organ Specific Expression of *RIBA* Transcription

In order to gain reliable information on the relative amounts of certain transcripts, the amplification efficiencies of the qPCR primers *RIBA1* (QPP1), *RIBA2* (QPP2) and *RIBA3* (QPP3) (**Table S 3**) were determined. As seen in **Table 32** the amplification efficiencies of the *RIBA1*, *RIBA2* and *RIBA3* primers expressed by the percent efficiency (% E) and determined as described in 2.8.5.2.1, were similar.

Table 32: **Amplification efficiencies for *RIBA* qPCR Primers.**
Primer efficiency value (E) and % Efficiency (%E) were calculated according to Biorad software Application guide. R^2: correlation coefficient.

Primer pair	Slope	R^2	E	% E
QPP1	-3.75	1	1.85	84.9
QPP2	-3.67	1	1.87	87.2
QPP3	-3.74	1	1.85	85.2

Figure 25 describes the relative expression of *RIBA* transcripts in different *Arabidopsis* organs as fold change relative to the expression of the housekeeper *SAND* (At2g28390).

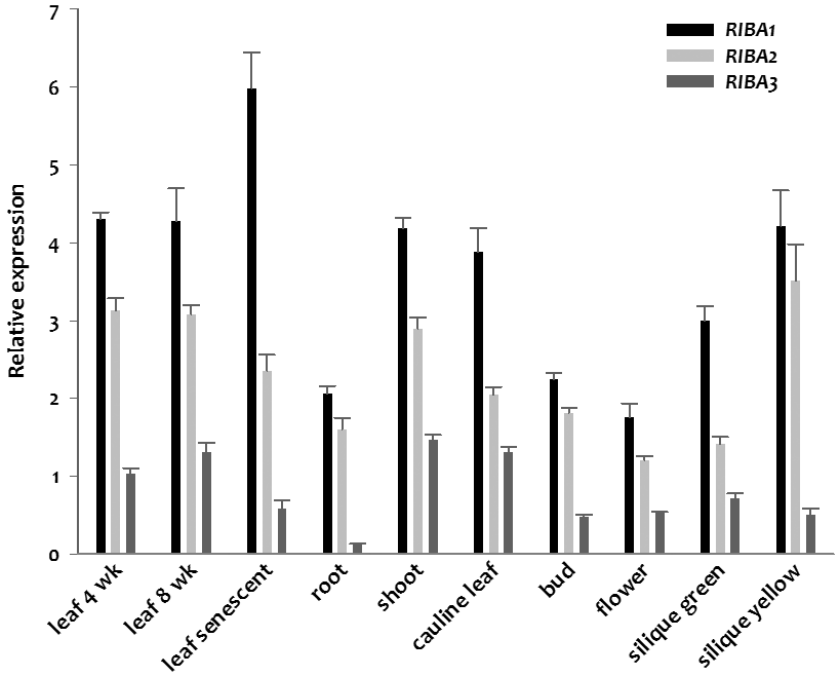

Figure 25: **Expression profile of *RIBA* transcripts in *A. thaliana* organs and developmental stages.**
The data is described as fold change ($2^{-\Delta Ct}$) relative to expression of housekeeper *SAND* (At2g28390). n=3; Error bars represent standard error of the mean.

In general, *RIBA1* showed the highest expression, followed by *RIBA2* and *RIBA3*. When considering the overall expression level of the RIBA transcript in the different organs, it can be stated that *RIBA-genes* were equally expressed in all tested tissues. The exceptions were senescent leaves, in which higher levels of *RIBA1*, than *RIBA2* or *RIBA3* mRNAs were detectable. In roots, buds and flowers *RIBA*-genes were generally less expressed.

All in all, the presented data do not support conclusions about differential organ specific expression and function of the three *RIBA* encoded proteins.

3.4.2 *RIBA* Promoter Analysis Using GUS

The tissue specific *RIBA* promoter activities were assessed by the detection of the expression of the reporter gene β-glucuronidase (GUS) in plant tissues carrying fusion gene constructs of the promoter region of *RIBA1*, *RIBA2* or *RIBA3*, respectively and the coding region of GUS. The expression of GUS can be detected by histochemical staining or can be quantified by means of fluorimetric assay. For these experiments, the *RIBA1* (CLP31/32), *RIBA2* (CLP33/34) and *RIBA3* (CLP35/36) promoter regions were amplified using primers listed in **Table S 3** and cloned into pCambia1305.2. The constructs were designated p*RIBA1*-pCambia1305.2, p*RIBA2*-pCambia1305.2 and p*RIBA3*-pCambia1305.2 and transformed into *wt Col-0* plants, as described in chapter 2.6.4. The following plasmids were included in the GUS analyses as controls: 1.) MCS-pCambia1305.2 (empty),

cloned as described in 2.7.5.4 was used as negative control, as well as 2.) pCambia1305.2, in which GUS is driven by the constitutively active CaMV-35S promoter, was used as positive control.

At least ten transgenic lines were generated per construct (except negative control) and analysed concerning their expression strength in a fluorimetric GUS assay as described in 2.19.1. For each construct, four independent lines, showing the highest GUS activity, were chose for histochemical GUS staining (2.19.2).

In **Figure 26** representative pictures of 4-week-old whole plants stained with x-gluc are presented. The staining of plants carrying *pRIBA1*-GUS and *35S*-GUS control plants was similar, both in strength and in patterning. Both promoters seemed to be more or less evenly active in all tissues, including younger and older leaves and roots. In contrast to the high activity of the *RIBA1* promoter, the strengths of *RIBA2* and *RIBA3* promoter elements were barely above the level of the negative control. *RIBA2*, *RIBA3* and empty control showed faint staining especially of younger leaves, the meristem, and roots.

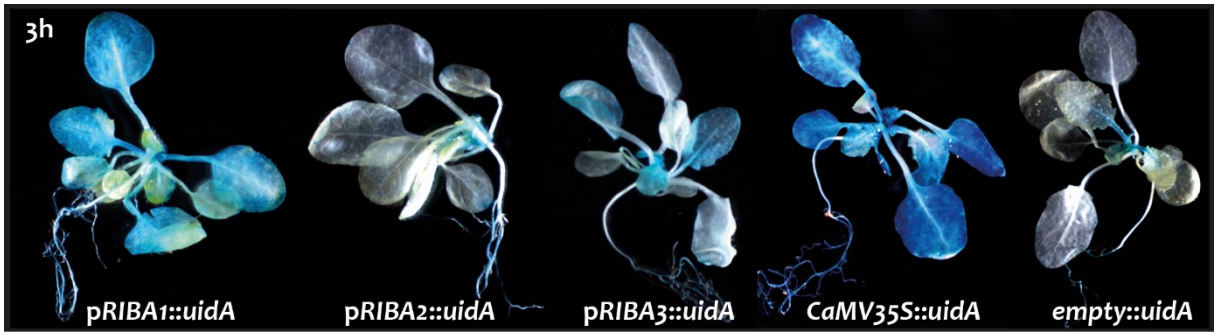

Figure 26: **Histochemical stain of *RIBA* GUS plants.**
4-week-old transgenic plants carrying constructs carrying GUS constructs with RIBA promoter-driven *uidA*, encoding GUS, as well as the positive control CaMV35S::*uidA* and the negative control empty::*uidA* (without promoter) were histochemically stained. The blue colour indicates the product of GUS hydrolysing its substrate x-gluc. Reaction was stopped after 3 h incubation in staining solution.

Staining of inflorescences of approximately 8-week-old GUS lines is shown in **Figure 27**. Like in **Figure 26**, *RIBA2* and *RIBA3* promoters showed a generally weaker activity compared to *RIBA1*. The main difference in the *RIBA* promoter activities, aside from the strength, was found in the lack of staining in sepals and anthers of *RIBA2* and *RIBA3* GUS plants. *RIBA1* promoter activity was very strong in the stem, sepals and anthers, comparable to the *CaMV35S* activity.

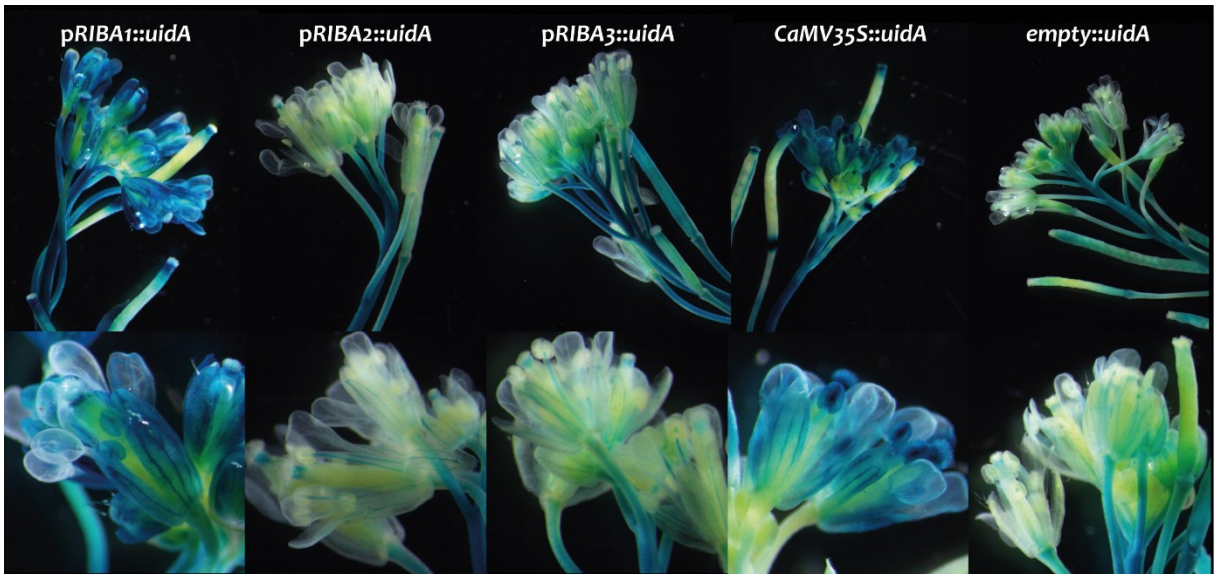

Figure 27: **Histochemical stain of *RIBA* GUS plant inflorescences.**
8-week-old transgenic plants carrying GUS constructs with RIBA promoter-driven *uidA*, encoding GUS, as well as the positive control CaMV35S::*uidA* and the negative control empty::*uidA* (without promoter) were histochemically stained. The blue colour indicates the product of GUS hydrolysing its substrate x-gluc. Reaction was stopped after 16 h incubation in staining solution.

The results gained by *RIBA* promoter analysis agree with the organ specific qPCR data 3.4.1. In general, the *RIBA1* promoter activity was more prominent than the activity of the *RIBA2* and the *RIBA3* promoter. However, according to the data obtained by the organ specific qPCR analysis all three *RIBA* promoters should showed generally less activity in the flowers and buds than in shoot and siliques, whereas here it seems that RIBA1 activity was in all tissues as strong as *CaMV35S* while *RIBA2* and *RIBA3* activity in the flowers was as low as expected.

3.5 Consequences of Modified RIBA Expression in Plants

3.5.1 The RIBA Antibody

For the analysis of the RIBA proteins in plants, the generation of an antibody was of utmost importance. The antibody used in the following immunoblot experiments was raised against recombinant RIBA1 as described in chapter 2.9.7. It was tested to recognise recombinant RIBA1, RIBA2 and RIBA3 (**Figure 28**). Surprisingly the molecular weights of the bands gained by SDS-PAGE differed significantly from the theoretical size of the recombinant proteins. All three recombinant proteins seemed to run approximately 5 kDa higher than their calculated molecular weights, which are 52 kDa for RIBA1, 47 kDa for RIBA2 and 51 kDa for RIBA3. In order to determine the reason for the abnormal in gel running behaviour, the recombinant proteins were analysed via LC-MS, which confirmed the theoretical protein sizes. The immunodetection with the RIBA antibody from *wt Col-0* total leaf extracts revealed three specific bands of approximately 65 (**1**), 61 (**2**) and 55 kDa (**3**), as shown in a representative anti-RIBA immunoblot in **Figure 28**. The theoretical sizes of RIBA

proteins are indicated in the table below. As in the case of the recombinant proteins, also here the theoretical sizes did not agree with indicated protein sizes in the gel. The analysis of whole leaf extracts of *riba2* knockout mutant line (which will be examined later in this chapter, see chapter 3.5.3) revealed the 55 kDa band (**3**) to be specific for RIBA2, since it is absent in this extract as seen in **Figure 28**. None of the remaining two bands could be identified to be corresponding to RIBA3 protein, since there were no changes in the immunoblot pattern between *wt Col-0* and *riba3* mutant extracts (compare **Figure 56**). Hence, the upper two bands (**1** and **2**) were assigned to RIBA1. This finding was supported by the Western blot of antisense *RIBA1#2* plants (**Figure 34**), which showed that the upper two bands were evenly decreased in the antisense extracts compared to *wt Col-0*.

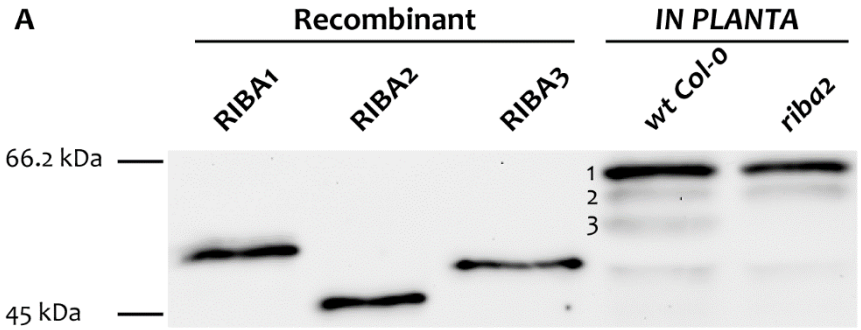

B

	Calculated protein weight [kDa]	
	Recombinant	*IN PLANTA* (+TP)
RIBA1	47	53 (+6)
RIBA2	42	46 (+6)
RIBA3	46	51 (+5)

Figure 28: **Western blot pattern of RIBA antibody.**
Panel A depicts the immunoblot analysis of recombinant RIBA proteins as well as *Arabidopsis wt Col-0* and *riba2* mutant whole leaf extracts using RIBA antibody. In panel B the calculated protein weights, derived from the coding sequences of recombinant proteins and of mature RIBA polypeptides (the size of a predicted transit peptide is indicated in brackets), are listed. Numbers 1-3 mark the bands that represent RIBA1 (1-2) and RIBA2 (3). Weak band below is interpreted as RIBA proteins that are pushed down by the RUBISCO large subunit running at 55 kDa.

3.5.2 RIBA1 Depletion Leads to Severe Effects That Are Not Compensated By RIBA2 and RIBA3

3.5.2.1 Embryo Lethality of Three Independent riba1 Mutants

Three independent *riba1* T-DNA insertion mutant lines were analysed on DNA level. The genotyping PCR, as depicted in **Figure 29**, verified the presence of the T-DNA insertions within the *RIBA1* sequence. Sequencing of the PCR products revealed localisation of the T-DNA insertions in all three lines within the exons: the FLAG insertion in exon two, the T-DNA insertion of the SALK mutant in exon three and the GABI mutant having the insertion in exon seven (**Figure 30**). For all three lines, it was not possible to identify homozygous individuals, leading to the hypothesis that a *RIBA1* knockout causes embryo lethality. Heterozygous individuals were phenotypically, as well as according their RIBA protein amount and flavin levels wt like (data not shown).

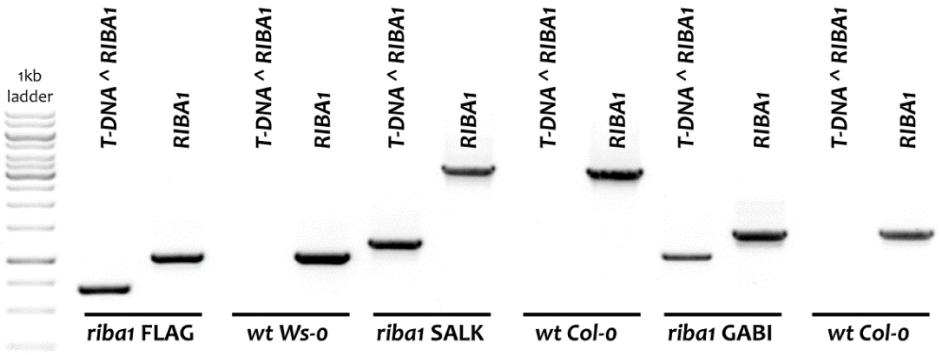

Figure 29: Genotyping of riba1 T-DNA mutant lines.
Agarose gel depicting genotyping PCR products of *riba1* FLAG, *riba1* SALK and *riba1* GABI and the respective wt controls, for *RIBA1* mutant allele (T-DNA^*RIBA1*) and the endogenous *RIBA1* wt gene (*RIBA1*). All plants analysed were heterozygous for the mutant allele.

For the analysis of the possible embryo lethality of homozygous *riba1* mutants, siliques of heterozygous mutants, as well as *wt Col-0* or *wt Ws-0* plants were analysed. All examined plants were grown in parallel, the siliques collected and opened, so that vital and aborted seeds could be counted (**Figure 30**). The amount of aborted seeds in all three heterozygous *riba1* lines was approximately 25 % more than the usual seed abortion rate in respective wt siliques. These figures agreed well with the expected number of homozygous (*riba1*/*riba1*) individuals obtained from heterozygous parents, according to Mendel's law of segregation (first law, Mendel (1866)).

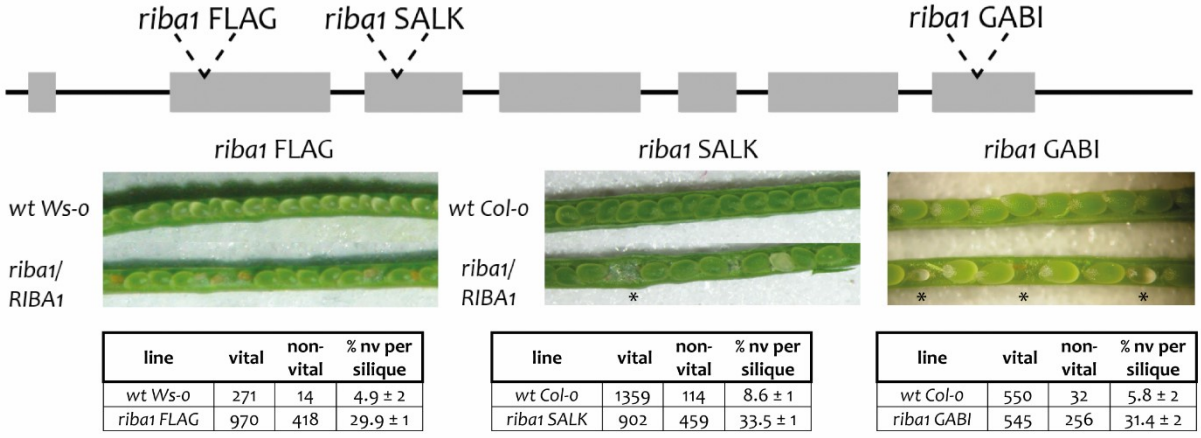

line	vital	non-vital	% nv per silique
wt Ws-0	271	14	4.9 ± 2
riba1 FLAG	970	418	29.9 ± 1

line	vital	non-vital	% nv per silique
wt Col-0	1359	114	8.6 ± 1
riba1 SALK	902	459	33.5 ± 1

line	vital	non-vital	% nv per silique
wt Col-0	550	32	5.8 ± 2
riba1 GABI	545	256	31.4 ± 2

***Figure 30: riba1* T-DNA mutants.**
RIBA1 gene structure with T-DNA insertion sites of the three mutants *riba1* FLAG, *riba1* SALK and *riba1* GABI marked with triangles (grey boxes depict exons). Below respective embryo lethal phenotypes of heterozygous progenies (*riba1*/*RIBA1*) and tables with result of respective seed count of 5-10 individual plants with vital and aborted seeds and the mean value of percentage of aborted seeds per silique (with standard error of the mean indicated). Examples of seeds aborted at different developmental stages and counted such as are marked with asterisks.

3.5.2.2 *Analysis of RIBA1 Antisense and Overexpression Effects on Phenotype, Flavin Contents and Flavin Biosynthesis Gene Expression*

Due to the embryo lethal phenotype of homozygous *riba1* knockout mutants, the effects of reduced or increased RIBA1 contents on plant phenotype and flavin biosynthesis were further studied using antisense *RIBA1* (Hiltunen *et al.*, 2012) and overexpression lines. The *Arabidopsis RIBA1*

coding sequence was cloned in sense (OE) and antisense (AS) orientation downstream of the constitutively active *CaMV35S* promoter.

The antisense fragment was amplified using primers CLP9/10 (**Table S 3**) and cloned in antisense orientation into the pGL1 vector (Hiltunen *et al.*, 2012). The transformation of the antisense construct in *wt Col-0* plants resulted in 11 T1 transgenic lines. The antisense *RIBA1* phenotype was characterised by strong bleaching and a stunted longitudinal growth of the leaves. The bleaching started at the tip or in the middle of the leaf and then spread across the whole leaf and ultimately the whole plant and finally lead to a developmental arrest of the plant. Three of the T1 transformants showed a mild bleaching phenotype already 14 days after germination. In the T2 generation, in one of these three lines the bleaching phenotype developed more quickly, while in two it appeared later in the adult plant and proceeded more slowly. These two kinds of transgenic lines were categorised as strong and weak bleaching phenotypic lines.

Antisense *RIBA1* line #2 (AS*RIBA1*#2) representing the strong phenotypic line was further examined in the following experiments. After 20 days of growth at short-day conditions 1/3 of the T3 generation seedlings were white and 2/3 with a mild or none phenotype and, with the exception of few individuals, developed the bleaching phenotype later.

White and green areas of adult antisense *RIBA1*#2 plants displaying an advanced degree of bleaching phenotype were analysed according to their pigment and flavin contents (**Figure 31**). It could be shown that the apparent loss of chlorophylls in the white areas was characterised by a 70 % decrease of both chlorophylls, whereas the chlorophyll a to b ratio was approximately 20 % decreased in green and white areas of antisense *RIBA1*#2 leaves compared to *wt Col-0*. Moreover, a 60 % decrease of all carotenoids, except antheraxanthine and zeaxanthine was measured in the white leaf areas. The latter was only detectable in the white areas. In the green areas, however, chlorophyll and carotenoid contents were comparable to wt-levels. The total flavin amount was decreased by 30 % in the white and by 15 % in the green leaf areas.

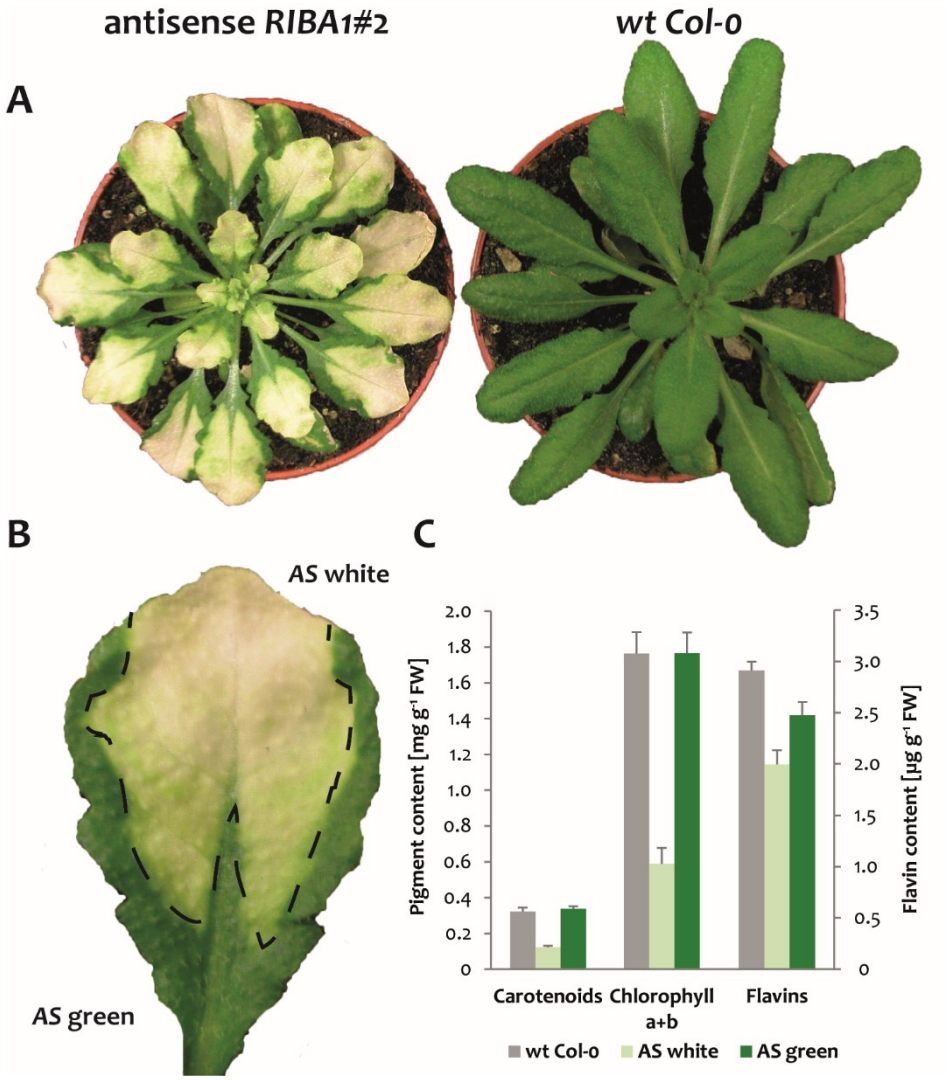

Figure 31: **Adult antisense *RIBA1#2* plant displaying advanced degree of bleaching phenotype.**
Panel A depicts an 8-week-old antisense *RIBA1#2* and *wt Col-0* plant grown under short-day conditions (100 µmol photons $m^{-2}s^{-1}$). Panel B shows the close-up of a bleached leaf of an antisense *RIBA1#2* plant with indicated sectors used for pigment and flavin analysis presented in panel C, n=3, error bars indicate standard errors of the mean.

Because of the non-homogenous appearance of the antisense *RIBA1* plants, a routine was developed by which larger amounts of plants with similar phenotypes could be obtained reproducibly. This routine implied a longer than usual period of growth in a single pot before the transplantation into individual pots. This time period amounted 2.5 or 3.5 weeks, after which plants with either no or mild mutant phenotype were chosen, transplanted into their own pots and grown under short-day conditions. Approximately 10 days after transplantation an even distribution of the phenotype among the plants could be observed and the sampling took place. In **Figure 32** 4- and 6-week-old *wt Col-0* and antisense *RIBA1#2* plants, which were sampled for the following experiments are depicted. The 4-week-old antisense plants were added to the set of samples because it was intended to cover an early as well as an advanced stage of phenotypic changes to retrieve a picture of early and late effects of RIBA1 depletion.

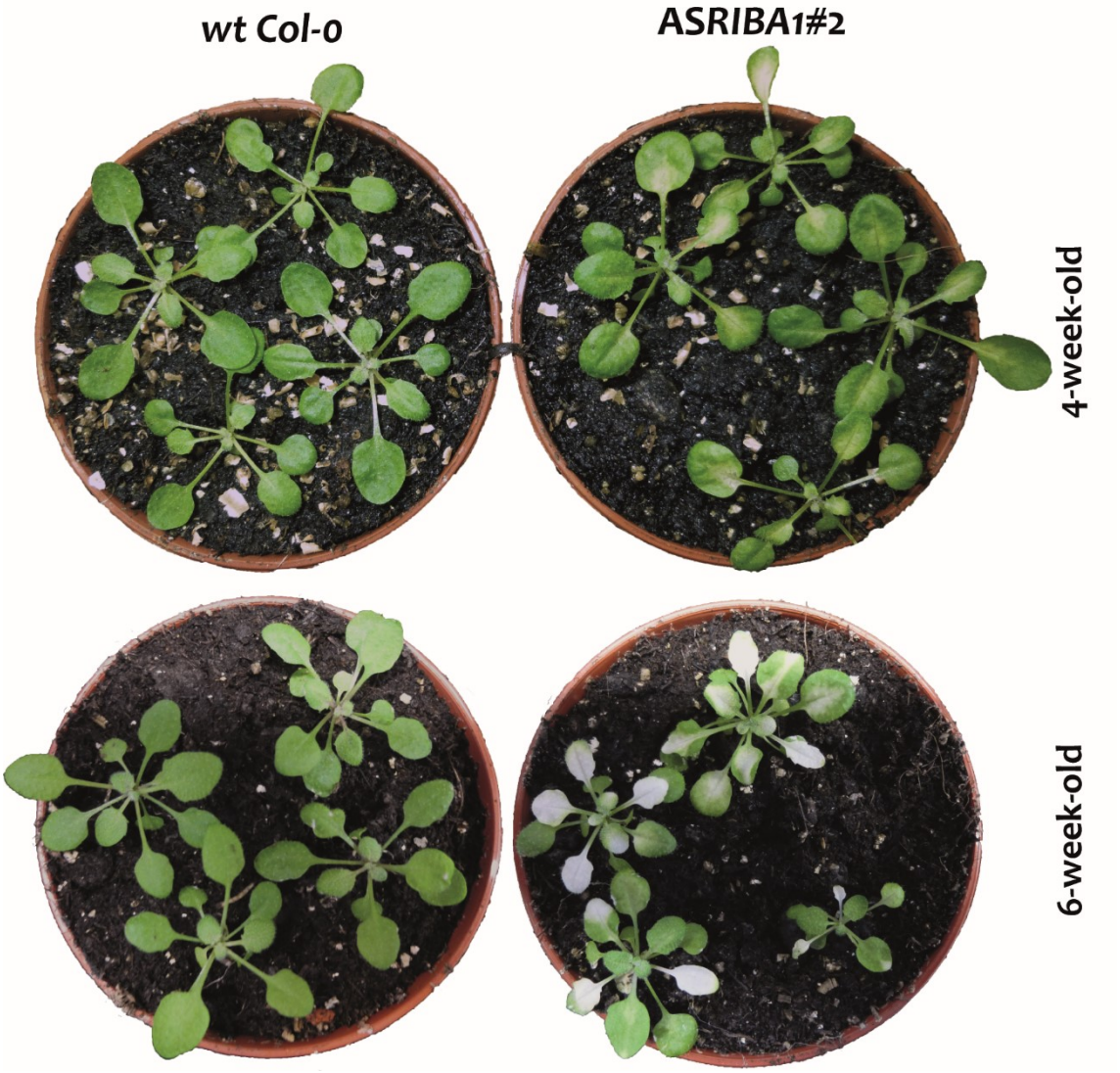

Figure 32: **4- and 6-week old antisense *RIBA1#2* mutant plants.**
Four- and six-week-old *wt Col-0*, *antisense RIBA1#2* (ASRIBA1#2) plants grown under short-day conditions (100 µmol photons $m^{-2}s^{-1}$), showing an early and late stage of the bleached leaf phenotype.

The extent of silencing on mRNA level caused by the *RIBA1* antisense construct was measured in a qPCR analysis. **Figure 37** shows the relative expression of *RIBA1*, *RIBA2* and *RIBA3* as fold change compared to *wt Col-0* in 4- and 6-week-old antisense *RIBA1#2* plants. In 4- as well as 6-week-old antisense *RIBA1#2* plants, the effect of *RIBA1* down regulation was comparable, as at both phenotypic stages the *RIBA1* transcript levels were 70 % lower compared to *wt Col-0*. While *RIBA3* expression was affected neither in 4- nor in 6-week-old antisense plants, *RIBA2* expression was 60 % higher in 6-week-old antisense plants.

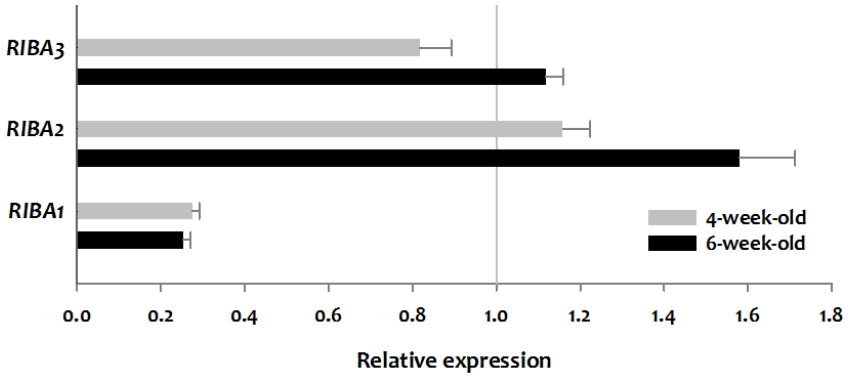

Figure 33: **Relative transcript accumulation of *RIBA* genes in antisense *RIBA1#2* plants**
Relative expression of *RIBA* transcripts in 4- (grey) and 6-week-old antisense *RIBA1#2* (black) plants was determined compared to *wt Col-0*.The plants were grown under short-day conditions (100 µmol photons $m^{-2}s^{-1}$ light intensity). The data is presented as fold change ($2^{-\Delta\Delta Ct}$) compared to *wt Col-0*, n=4, single plants of each line were sampled, error bars indicate standard errors of the mean.

In order to quantitatively evaluate the extent of the silencing on protein level, different amounts of whole plant protein extracts (above ground tissue) of 6-week-old antisense *RIBA1#2* plants and *wt Col-0* were separated via SDS-PAGE and analysed via Western blot using the RIBA antibody. In **Figure 34**, different amounts of *wt Col-0* and antisense *RIBA1#2* extracts were loaded. Thereby a 75 % reduction of RIBA1 protein abundance in antisense *RIBA1#2* compared to *wt Col-0* could be demonstrated. RIBA2 amount was not altered compared to *wt Col-0* extract. Interestingly, the immunoblot analysis of 4-week-old antisense *RIBA1#2* plants (not shown) revealed that the degree of RIBA1 depletion was similar to that observed in 6-week-old antisense plants, even though the bleaching phenotype was far less advanced.

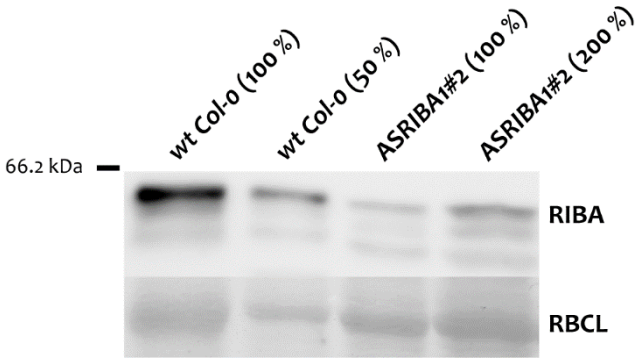

Figure 34: **RIBA protein abundance in 6-week-old *RIBA1* antisense plants.**
Whole plant protein extracts of 6-week-old *wt Col-0* and antisense *RIBA1#2* (AS*RIBA1#2*) plants grown under short-day conditions (100 µmol photons $m^{-2}s^{-1}$ light intensity) were analysed by Western blot using RIBA antibody (upper panel). In the lower panel the Ponceau-stain of the same blot is shown, depicting Rubisco large subunit (RBCL) to illustrate equal loading of the gel (note: less Rubisco in *RIBA1 AS* lane due to bleached tissue). Upper two bands of the immunoblot represent RIBA1, while the lowest band represents RIBA2 protein.

The transformation of the sense constructs (*35S*::cAt*RIBA1*) was performed in the context of the complementation experiments described later (chapter 3.5.4). The lines, that are hereafter called overexpression lines, are the result of the transformation of the *35S*::cAt*RIBA1* construct (**Table 37**) into the heterozygous *riba1 GABI* mutant described in chapter 3.5.2.1. The BASTA selection resulted

in 41 T1 transformants, of which 25 were demonstrated to be heterozygous for mutant allele (*riba1*/*RIBA1*) and 16 homozygous for wt allele (*RIBA1*/*RIBA1*). Eight of the 16 T1 transformants were further studied in the T2 generation, wherein samples of several 2-week-old seedlings of each line were collected and used for immunoblot analysis. The immunodetection with the RIBA antibody revealed 6 of 8 lines overexpressing RIBA1, of which 4 lines were overexpressing RIBA1 strongly (**Figure 35**). Lines #3, #20 and #21 were chosen for further analysis. All three lines did not show any visible phenotypic alterations compared to *wt Col-0* (**Figure 36**) when grown under short- or at long-day (100 µmol photons $m^{-2}s^{-1}$) or at low-light (30 µmol photons $m^{-2}s^{-1}$), or higher-light (300 µmol photons $m^{-2}s^{-1}$) conditions.

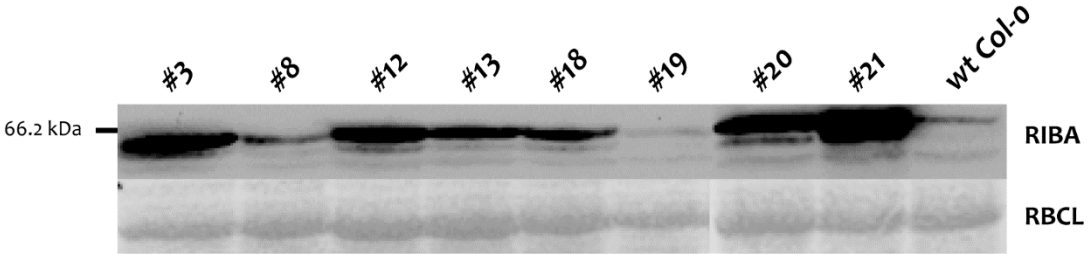

***Figure 35:* RIBA protein abundance in T2 generation *RIBA1* overexpression lines.**
Whole plant protein extracts of 2-week-old *wt Col-0* and *RIBA1* overexpression lines (pooled sample of many seedlings) grown under short-day conditions (100 µmol photons $m^{-2}s^{-1}$ light intensity) were analysed by Western blot using RIBA antibody (upper panel). In the lower panel the Ponceau-stain of the same blot is shown, depicting Rubisco large subunit (RBCL) to illustrate equal loading of the gel. Upper two bands of the immunoblot represent RIBA1, while the lowest band represents RIBA2 protein.

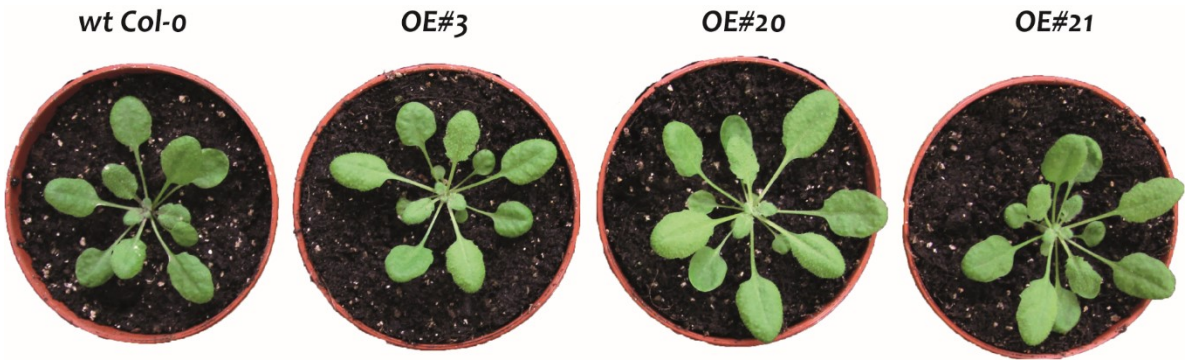

***Figure 36:* RIBA1 overexpression lines.**
Six-week-old *wt Col-0* and RIBA1 overexpression plants grown under short-day (100 µmol photons $m^{-2}s^{-1}$ light intensity) conditions. Representative plants of overexpression lines #3, #20 and #21 are depicted.

The effect of RIBA1 overexpression was studied on *RIBA* mRNA accumulation in a qPCR analysis. **Figure 33** shows the relative expression of *RIBA1*, *RIBA2* and *RIBA3* as fold change compared to *wt Col-0* in RIBA1 overexpression lines OE#3, OE#20 and OE#21.

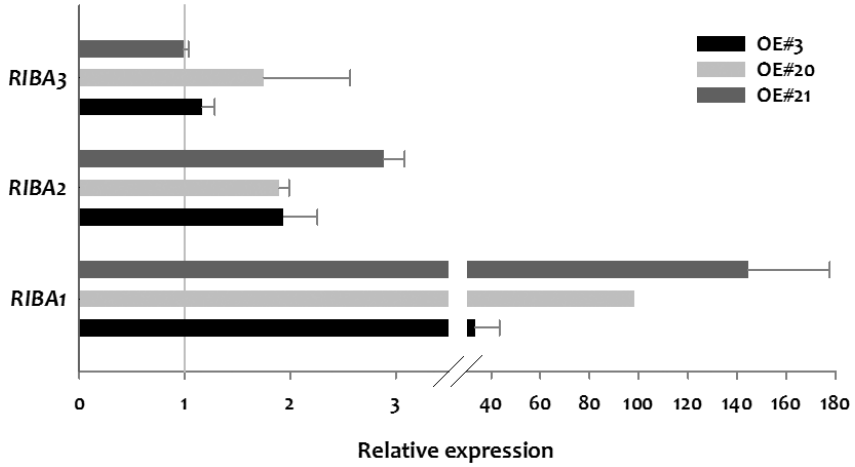

Figure 37: **Relative transcript accumulation of *RIBA* genes in RIBA1 overexpression lines.**
Relative expression of *RIBA* transcripts in 6-week-old RIBA1 OE line #3 (black), #20 (grey) and #21 (dark grey) plants was determined compared to *wt Col-0*. The plants were grown under short-day conditions (100 µmol photons $m^{-2}s^{-1}$ light intensity). The data is presented as fold change ($2^{-\Delta\Delta Ct}$) compared to *wt Col-0*, n=4, single plants of each line were sampled, error bars indicate standard errors of the mean (not available for RIBA1 value of OE 20 because of n=2).

RIBA1 overexpression lines show different degrees of increased RIBA1 transcript accumulation compared to *wt Col-0*, namely 30-, 100- and 140-fold in line OE#3, OE#20 and OE#21, respectively. Whereas *RIBA3* transcripts were not clearly affected by the *RIBA1* transcript accumulation, *RIBA2* expression was almost 2-fold increased in lines OE#3 and OE#20 and even 3-fold in line OE#21. Line OE#21, displaying the strongest *RIBA1* overexpression, was chosen for further analysis and is from now on referred to as *RIBA1* overexpressor (*RIBA1* OE#21).

The strength of the *RIBA1* overexpression was elaborated in an immunoblot analysis with the RIBA antibody. Again, different amounts of the protein extracts were loaded to quantitatively analyse the RIBA accumulation. **Figure 38** shows an immunoblot with different amounts of the whole leaf extracts of RIBA1 overexpressor line compared to *wt Col-0*. The upper band, representing RIBA1, of the lane with the *wt Col-0* extract, is as strong as the upper band in the lane in which 1/8 amount of the overexpressor line extract were loaded. This suggests an eight times higher protein accumulation of RIBA1 in the overexpressor line compared to *wt Col-0*. The intensity of the lowest band, representing RIBA2, in the *wt Col-0* extract is comparable with that of the lane, in which half amount of the overexpression line extract were loaded. This means that a two times higher expression of RIBA2 is accompanying the overexpression of RIBA1.

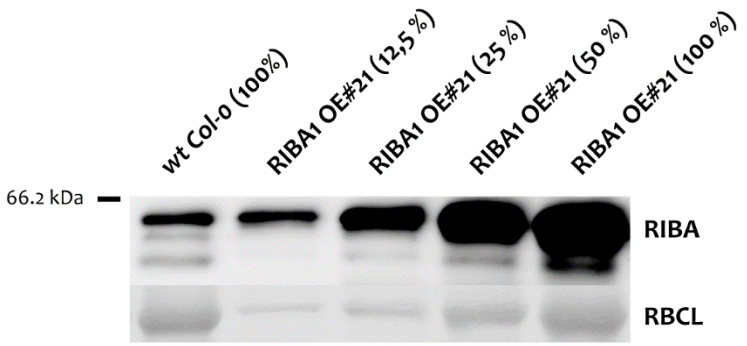

***Figure 38:* RIBA protein abundance in 6-week-old RIBA1 overexpression #21 plants.**
Whole plant protein extracts of 6-week-old *wt Col-0* and RIBA1 overexpression #21 (OE) plants grown under short-day conditions (100 µmol photons $m^{-2}s^{-1}$ light intensity) were analysed by Western blot using RIBA antibody (upper panel). In the lower panel the Ponceau-stain of the same blot is shown, depicting Rubisco large subunit (RBCL) to illustrate equal loading of the gel. Upper two bands of the immunoblot represent RIBA1, while the lowest band represents RIBA2 protein.

Consequently, the impact of reduced or increased RIBA1 protein abundance was studied on flavin biosynthesis end products riboflavin, FMN and FAD. Flavin extraction and quantification was performed as described in chapter 2.15.3, using whole plant (above ground tissue) extracts of 6-week-old plants of *wt Col-0*, antisense *RIBA1#2* and RIBA1 overexpression line #21, as well as 4-week-old *wt Col-0* and antisense *RIBA1#2* plants, grown under short-day conditions. The results are listed in **Table 33**. In general, it can be stated, that in *wt Col-0* FAD was the predominant product (~70 %) of flavin biosynthesis with approximately 3-4 ng mg^{-1} FW. The amount of FMN accounted for ~25 %, while riboflavin (RF) represented less than 10 % of total flavin content. **Table 33** shows a clear effect in both, *RIBA1* antisense as well as overexpression lines on levels of end products of flavin biosynthesis.

***Table 33:* Flavin contents of 6-week-old *wt Col-0*, antisense *RIBA1#2* and RIBA1 overexpression #21, as well as 4-week-old *wt Col-0* and antisense *RIBA1#2* plants.**
All tested plants were grown under short-day conditions. Flavins were determined via HPLC using authentic standards. For total flavin amount single values for FAD, FMN and riboflavin were summed up, n=5. Standard errors of the mean as well as percentage in-/decrease compared to respective *wt Col-0* are indicated.

	FAD [ng mg^{-1} FW]		**FMN** [ng mg^{-1} FW]		**RF** [pg mg^{-1} FW]		**total** [ng mg^{-1} FW]	
wt Col-0 (6 wk)	2.91 ± 0.15	± 0 %	1.11 ± 0.07	± 0 %	328.6 ± 39.1	± 0 %	4.35 ± 0.17	± 0 %
ASRIBA1#2 (6 wk)	2.30 ± 0.11	-21 %	0.75 ± 0.04	-33 %	159.4 ± 22	-51 %	3.21 ± 0.12	-26 %
RIBA1 OE#21 (6 wk)	3.20 ± 0.22	+10 %	1.43 ± 0.04	+29 %	501.6 ± 36.2	+53 %	5.13 ± 0.23	+18 %
wt Col-0 (4 wk)	4.02 ± 0.08	± 0 %	1.28 ± 0.05	± 0 %	308.1 ± 22.6	± 0 %	5.6 ± 0.1	± 0 %
ASRIBA1#2 (4 wk)	2.93 ± 0.39	-27 %	1.02 ± 0.09	-21 %	172.1 ± 44.9	-44 %	4.1 ± 0.4	-27 %

6-week-old as well as 4-week-old plants, displaying stronger and weaker bleaching phenotype, respectively, were investigated in the case of the antisense *RIBA1#2* line. The total flavin amount of 4-week-old *wt Col-0* was 29 % higher than 6-week-old *wt Col-0* (38 % more FAD and 15 % more FMN). In 6- as well as 4-week-old antisense *RIBA1#2* plants total flavin amount were 26 % and 27 % decreased compared to respective *wt Col-0*. For the RIBA1 overexpression line #21 an 18 % increase of total flavin amount was observed.

The 6-week-old antisense and overexpression lines showed the least differences in FAD contents. While the content was 21 % decreased in the antisense, it was 10 % increased in the overexpression line compared to *wt Col-0*. The strongest effect in FMN contents could be seen in 6-week-old antisense plants, where it was 32 % decreased, whereas in the overexpression line it was 29 % increased. Riboflavin content was 51 % decreased in 6-week-old antisense and 53 % increased in the overexpression line.

Even though the decrease of total flavin amount was identical in 4- and 6-week-old antisense *RIBA1#2* plants, the distribution of the individual flavins was slightly different. Compared to *wt Col-0* the riboflavin content was 44 % decreased in the 4-week-old antisense plants, accompanied by a 27 % and a 20 % decrease of FAD and FMN content, respectively.

In a next step, the possible effects of the deregulated flavin contents on gene expression within the flavin biosynthesis pathway were evaluated. Therefore, qPCR primers for a selection of known flavin biosynthetic genes were designed and used in a qPCR analysis. Relative amounts of transcripts encoding pyrimidine deaminase (*PYRD*), pyrimidine reductase (*PYRR*), lumazine synthase (*LS*), riboflavin synthase (*RS*), riboflavin kinase/FMN hydrolase (*FMN*/*FHY*) and two FAD synthases (*RIBF1* and *RIBF2*) examined. For the 6-week-old antisense *RIBA1#2* and overexpression lines, as well as the 4-week-old antisense *RIBA1#2* line the relative fold changes compared to *wt Col-0* are depicted in **Figure 39**.

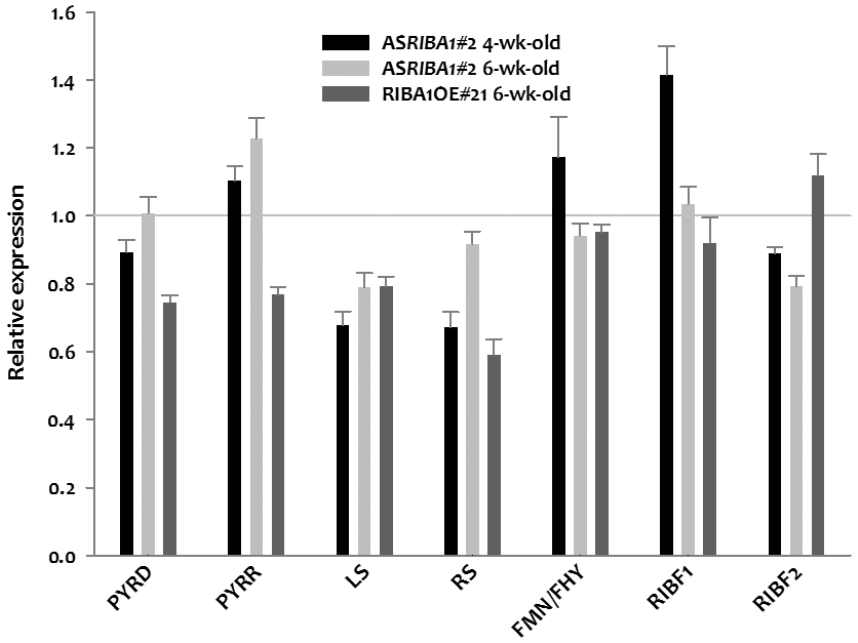

Figure 39: **Expression profile of flavin biosynthesis genes in 4- and 6-week-old antisense *RIBA1#2* *and* RIBA1 overexpression line #21 plants.**
Whole plant (above ground tissue) samples of plants grown under short-day conditions (100 µmol photons $m^{-2}s^{-1}$ light intensity) were analysed. Values are given as fold change ($2^{-\Delta\Delta Ct}$) compared to *wt Col-0*, n=4, error bars indicate standard error of the mean.

Apart from minor variations (up- and downwards), the transcript contents of the flavin biosynthesis genes did not differ drastically from *wt Col-0*. It seems that transcriptional regulation of flavin biosynthesis genes was not affected by altered RIBA1 protein abundance or overexpression and the resulting modifications in flavin contents.

3.5.2.3 Effect of RIBA1 Depletion on Expression of METC, Flavin-dependent PPOX Genes and OxStress Marker Genes

Reduced *RIBA1* expression in antisense *RIBA1#2* plants lead to 26 % reduction of total flavin content that was accompanied by a severe bleaching phenotype (**Figure 32**). It was expected that the flavin deficiency would have an impact on the expression and networking of flavin-dependent proteins. In order to correlate the flavin deprivation phenotype with a deregulation of flavoenzymes or of flavin-associated enzymes, a qPCR analysis was conveyed. For the survey of possible flavin depletion effects, the transcript abundances of genes from three different areas were assessed (**Figure 40**): 1.) The genes of four proteins that are involved in the mitochondrial electron transport chain (METC) and were recently described by Li *et al.* (2014) to be responsive to an induced decrease of riboflavin content. 2.) Two FAD-dependent protoporphyrinogen oxidase isoforms (PPOXI – At4g01690 and PPOXII – At5g14220), performing the oxidation of protoporphyrinogen IX to protoporphyrin IX within the tetrapyrrole biosynthesis pathway (Narita *et al.*, 1996, Lermontova *et al.*, 1997). 3.) Moreover four marker genes for photo-oxidative stress were included (Schlicke *et al.*, 2014) because Deng *et al.* (2011) demonstrated that the down-regulation of riboflavin leads to the accumulation of H_2O_2. Hence four ROS associated marker genes were studied: the $^1O_2$-responsive gene *BONZAI1-ASSOCIATED PROTEIN 1* (*BAP1*) (op den Camp *et al.*, 2003), *ZAT12* encoding a H_2O_2-responsive zinc finger protein (Rizhsky *et al.*, 2004) and the two ROS scavenging enzymes *FE-SUPEROXIDE DISMUTASE 1* (*FSD1*) (Pulido *et al.*, 2010) and *GLUTATHIONE PEROXIDASE 7* (*GPX7*) (Mullineaux *et al.*, 2000).

While METC#1 (NADH-ubiquinone oxidoreductase-like) was only slightly down-regulated (10 %) METC#3 (NADH-ubiquinone oxidoreductase B18 subunit), METC#11 (ATP synthase G subunit) and METC#13 (ATP synthase ε-chain) showed a 40 % reduction compared to *wt Col-0*. Also, both genes for the PPOX isoforms were 40 % decreased. For the surveyed photo-oxidative stress marker genes, the following results emerged: *BAP1*, *ZAT12* and *GPX7* reacted very strongly with a 4- to 11-fold up-regulation compared to *wt Col-0*, *FSD1* expression was 80 % down-regulated compared to *wt Col-0*.

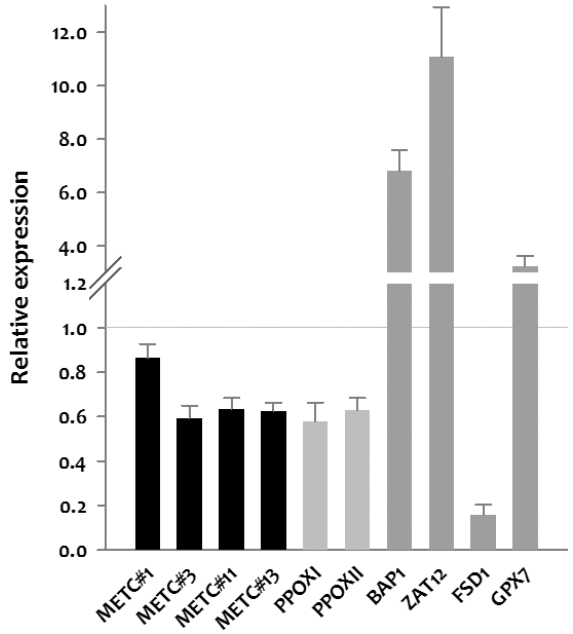

Figure 40: **Expression profile of genes potentially affected by antisense *RIBA1* triggered flavin depletion in plants.** Transcript accumulation of genes associated with the mitochondrial electron transport chain (METC), FAD-dependent protoporphyrinogen oxidase isoforms (PPOXI/II) and four marker genes for photo-oxidative stress *BAP1:* $^1O_2$-responsive *gene BONZAI1-ASSOCIATED PROTEIN 1,* ZAT12: a H_2O_2-responsive zinc finger protein and the two ROS scavenging enzymes *FSD1:* FE-*SUPEROXIDE DISMUTASE 1 and GPX7: GLUTATHIONE PEROXIDASE 7.* Analysis was performed on 6-week-old antisense *RIBA1#2* plants grown under short-day conditions (100 µmol photons $m^{-2}s^{-1}$ light intensity). Data is given as fold change ($2^{-\Delta\Delta Ct}$) compared to wt Col-0, n=4, error bars indicate standard error of the mean.

In summary, these results support the data obtained by Li *et al.* (2014), who described a down-regulation of the tested METC transcripts by more than 50 % caused by a ~64 % decrease of total free flavins through the induced expression of the turtle riboflavin-binding protein (RfBP). The results also suggest a slight down-regulation of the transcripts encoding the FAD-dependent PPOX isoforms. The analysis of the oxidative-stress marker genes allows the conclusion that the decrease of flavins, resulting from the RIBA1 depletion, causes oxidative stress. In order to detect possible H_2O_2 accumulation in antisense plants, DAB staining (2.17) was conducted but did not reveal differences in H_2O_2 amounts compared to *wt Col-0* (data not shown).

3.5.2.4 Shift of Bleached RIBA1 Antisense Plants from Short-day to Continuous Light Conditions Leads to Re-greening

Moving of 6-week-old, strongly bleached antisense *RIBA1#2* plants, grown under short-day conditions (100 µmol photons $m^{-2}s^{-1}$), to continuous light (100 µmol photons $m^{-2}s^{-1}$) lead to a nearly complete re-greening of the plants. **Figure 41** depicts antisense *RIBA1#2* and *wt Col-0* plants that were grown under short-day conditions for 6 weeks and then either shifted to continuous light or further grown under short-day conditions for another 2 weeks. The re-greened antisense *RIBA1#2* plants were characterised by nearly wt-like phenotype and flowering behaviour, except for bleached stems at later stages of flowering.

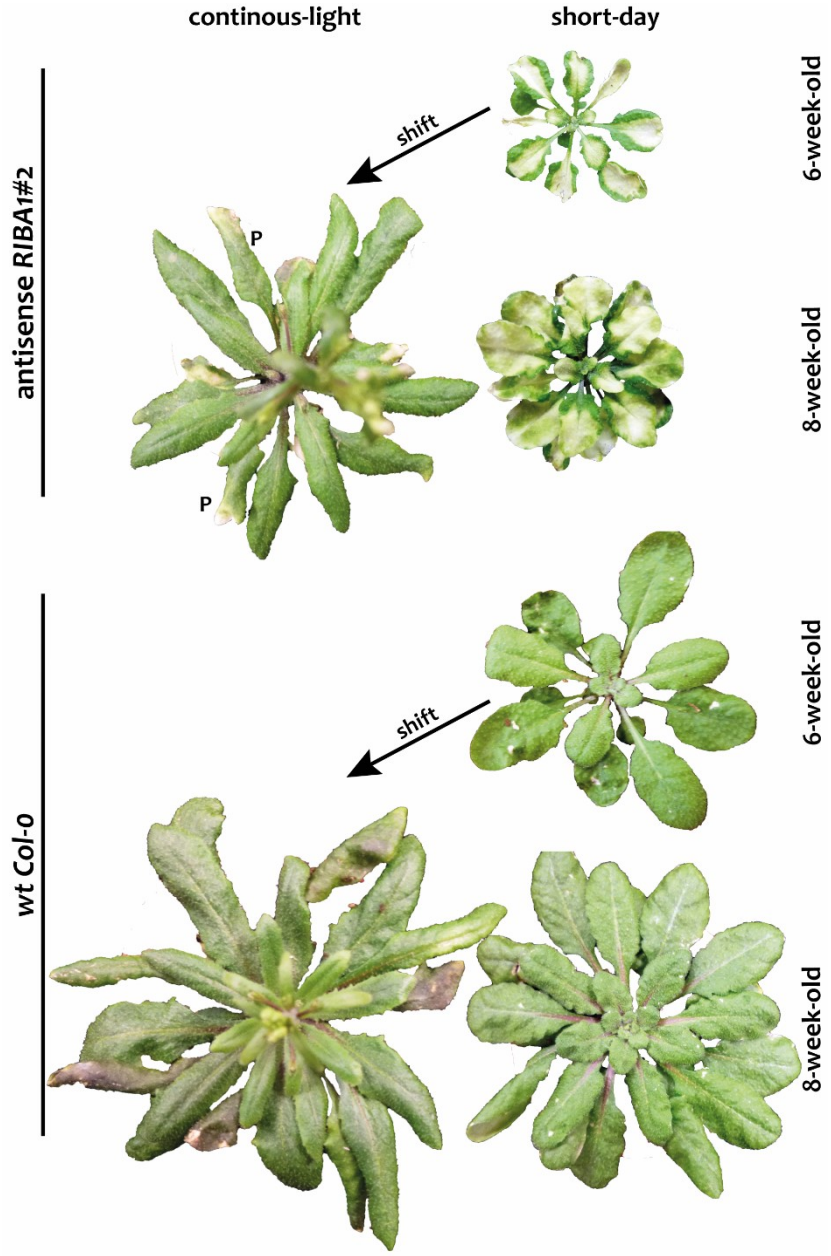

Figure 41: **Re-greening effect of bleached antisense *RIBA1#2* by shift to continuous light.**
Plants were grown under short-day conditions (normal light) for 6 weeks and were then either further grown under short-day or shifted to continuous light (short-day) for 6 weeks. Figure depicts plants before the shift (6 weeks) and 2 weeks after the shift to continuous light (8 weeks). P marks still phenotypic leaves in otherwise re-greened continuous light-grown antisense *RIBA1#2* plants.

The effect of re-greening was studied at the protein level. It was interesting to figure out, whether an altered RIBA1 protein abundance would coincide with the macroscopic changes in continuous light. In **Figure 42** whole leaf extracts of antisense *RIBA1#2* and *wt Col-0*, which were grown in parallel under short-day conditions (SD) and of *RIBA1* antisense and *wt Col-0* plants grown under continuous light (CL), were loaded. In the case of antisense *RIBA1 #2* plants grown under continuous light, also older leaves still showing bleaching phenotype were sampled (P).

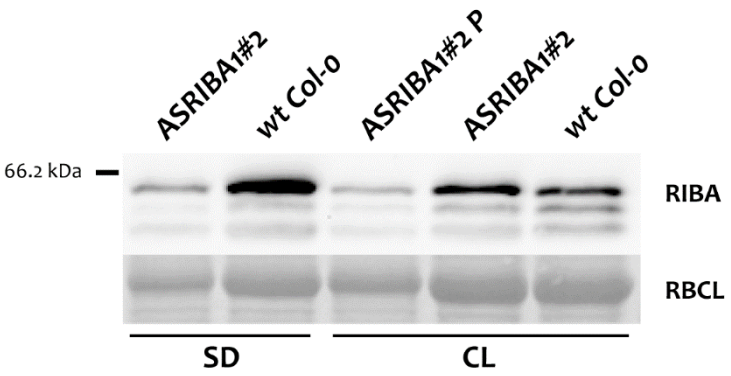

Figure 42: **RIBA protein abundance short-day and continuous-light grown antisense *RIBA1#2* plants.**
Whole leaf protein extracts of 8-week-old *wt Col-0* and antisense *RIBA1#2* plants grown under short-day conditions (SD; 100 µmol photons $m^{-2}s^{-1}$ light intensity) or continuous light (CL; 100 µmol photons $m^{-2}s^{-1}$ light intensity) were analysed by Western blot using RIBA antibody (upper panel). In the lower panel the Ponceau-stain of the same blot, depicting Rubisco large subunit (RBCL) to illustrate equal loading of the samples (note: less Rubisco in AS*RIBA1#2* SD and CL P due to bleached tissue). P marks bleached leaves in otherwise re-greened continuous light-grown *RIBA1* antisense plants. Upper two bands of the immunoblot represent RIBA1, while the lowest band represents RIBA2 protein.

An approximately 4-fold lower RIBA1 abundance of short-day-grown antisense *RIBA1#2* compared to short-day-grown *wt Col-0* can be seen. The extracts from plants adapted to continuous-light showed a clear decrease of RIBA1 protein in bleached antisense *RIBA1#2* leaves, but not in the re-greened leaves when compared to *wt Col-0* plants grown under similar conditions.

Subsequently, flavin levels were examined comparatively in continuous-light- and short-day-grown plants (**Figure 43**).

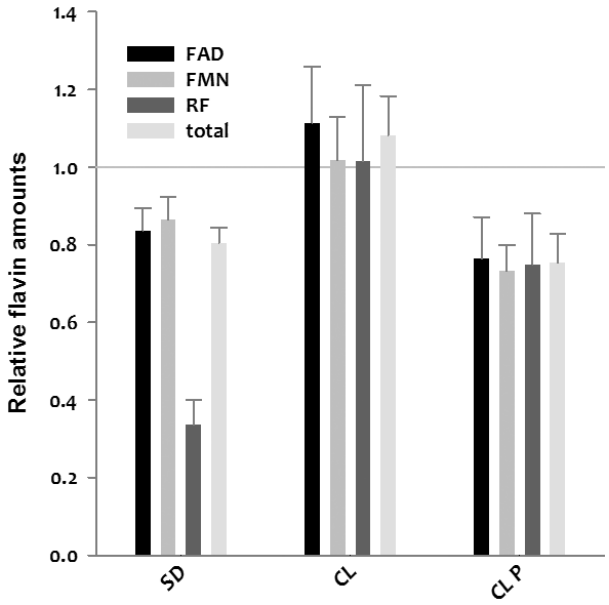

Figure 43: **Relative flavin amounts of antisense *RIBA1#2* plants.**
The plants were grown under short-day (SD; 100 µmol photons $m^{-2}s^{-1}$ light intensity) and at continuous-light (CL; 100 µmol photons $m^{-2}s^{-1}$ light intensity) conditions. The data is given as fold change compared to respective *wt Col-0* control grown under identical conditions. P marks leaves showing bleaching in otherwise re-greened continuous-light-grown antisense *RIBA1#2* plants.

Extracts from short-day-grown antisense *RIBA1#2* plants and continuous light-grown phenotypic (P) antisense *RIBA1#2* leaves, contained approximately 20 % less flavins compared to respective *wt Col-0*. The flavin levels of the re-greened continuous light-grown *RIBA1* antisense plants were comparable to wt Col-0 plants grown under same conditions. These results mirror the observations made on protein levels (**Figure 42**). In general, the total flavin content was slightly (~10 %) higher in continuous light-grown *wt Col-0* plants compared to short-day-grown *wt Col-0* plants (not shown).

3.5.2.5 RNAi Effect via VIGS Confirms the Antisense RIBA1 Phenotype

In order to study the time-course of the flavin decrease through RIBA1 depletion, an inducible RIBA1 knockout system, based on RNA interference (RNAi), was utilised. RNAi is a plant innate defence mechanism, which is used in the *Tobacco rattle virus* (TRV)-based virus-induced gene silencing (VIGS) system (Liu *et al.*, 2002). While plants usually target RNAi mechanism against the attacking viral genome, this system enables the targeting of endogenous transcripts through the insertion of plant specific (in this case *RIBA1* cDNA) sequences into the vector genome of modified viruses (2.20).

Therefore, an 800 bp fragment from *RIBA1* was amplified using the primers CLP37/38 (**Table S 3**) and *wt Col-0* cDNA as template. The PCR product was subcloned into pJet1.2 and clones with plus/minus orientation were chosen via PCR, verified by sequencing and the insert excised with *Bgl*II and *Xho*I. Ligation into the pTRV2 vector was conducted as described in chapter 2.7.9.3. A pTRV2 vector that contained the cDNA sequence of the GFP gene (Liu *et al.*, 2002) served as negative control. VIGS procedure was performed as described in 2.20.

The RIBA1-VIGS phenotype, a severe bleaching emerging from the middle of the leave (**Figure 44**), started to appear approximately ten days after induction and resembled the phenotype seen in the *RIBA1* antisense lines (chapter 3.5.2.2). The bleaching was first visible in the youngest leaves of the rosette and spread from there, either gradually or in patches, and finally appeared in older leaves as well. The phenotype was not observed in all plants at the same time and with the same intensity. Therefore, two stages were defined as shown in **Figure 44**. The control, a pTRV construct carrying GFP cDNA (Liu *et al.*, 2002), did not generate any phenotypic changes when applied in an identical way.

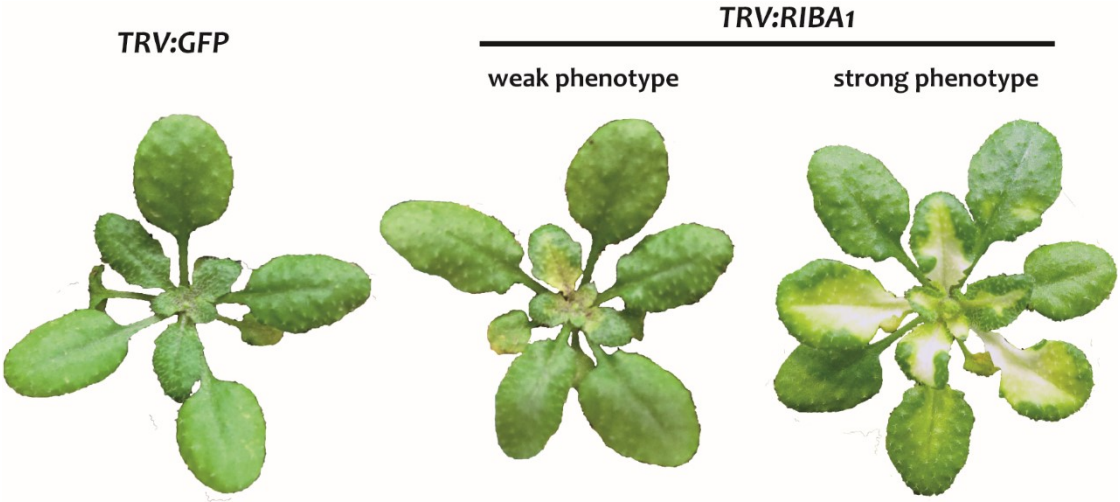

Figure 44: **Phenotype of RIBA1 RNAi plants generated by *Tobacco rattle virus*-based virus-induced gene silencing system 14 d after VIGS treatment.**
Two stages of the bleached phenotype were defined (weak, strong). Representative plants are shown as well as control plant treated with *TRV* carrying GFP cDNA not exhibiting any phenotype. Plants were grown under 16 h light/8 h night, 20 °C and 120 µmol photons $m^{-2}s^{-1}$ light intensity.

In order to quantify the silencing effect of RIBA1 expression, *RIBA* transcript accumulation and RIBA protein abundance were studied in RIBA1-VIGS plants 14 days after induction of VIGS. Four to five individual plants of each phenotypic stage (weak, strong) were chosen and whole plant (above ground tissue) RNA and protein extracts were generated. Result of qPCR and immunoblot analysis are shown in **Figure 45** and **Figure 46**, respectively.

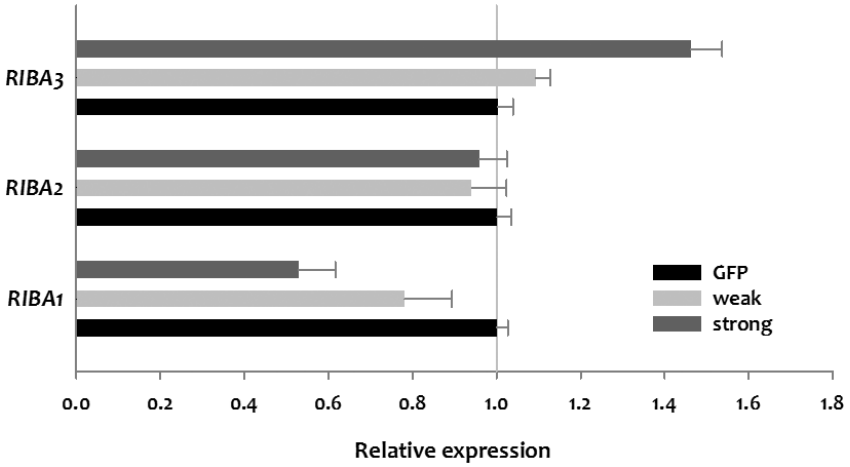

Figure 45: **Relative transcript accumulation of *RIBA* genes in *TRV:RIBA1* plants.**
Representative plants displaying weak and strong phenotypic stage 14 d after VIGS induction were chosen. The plants were grown under 16 h light/8 h night (20°C, 120 µmol photons $m^{-2}s^{-1}$ light intensity). The data is presented as fold change ($2^{-\Delta\Delta Ct}$) compared to *TRV:GFP* plants, n=4 single plants of one phenotypic stage, error bars indicate standard errors of the mean.

The degree of RIBA1 expression reflects well the differences in protein expression as visualised in **Figure 46**. In the "weak phenotype" group *RIBA1* mRNA content is 20 % and in the "strong phenotype" group 50 % decreased compared to GFP control. *RIBA2* expression is not altered at all, whereas *RIBA3* is almost 50 % up-regulated in the "strong phenotype" group.

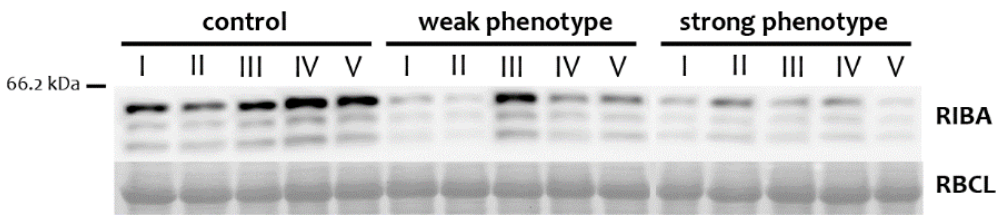

***Figure 46:* Immunoblot analysis of RIBA protein abundance visualising VIGS effect 14 d after induction.**
The Ponceau stain of the Rubisco large subunit (RBCL) protein of the nitrocellulose membrane is depicted to illustrate equal loading of the gel (lower panel). Whole plant protein extracts of five individuals (I-V) of each experimental group are shown: *TRV:GFP* (control) plants as well as plants displaying a weak and strong *TRV:RIBA1-VIGS* phenotype, respectively. Upper two bands of the immunoblot are assigned to RIBA1, while the lowest band represents RIBA2 protein.

Figure 46 clearly reveals differences in the degree of RIBA1 silencing between plants that show macroscopically similar effects, e.g. "weak phenotype" plant II and III. The comparison between the "weak phenotype" and "strong phenotype" groups demonstrates a more even pattern of RIBA1 decrease in the tested plants of the latter and as expected on average less RIBA1 protein, meaning a higher degree of silencing.

The correlation of reduced RIBA1 content and reduced flavin contents as it was already described for antisense *RIBA1#2* plants above (chapter 3.5.2.2), was also studied for the VIGS treated plants 14 days after induction (**Table 34**).

***Table 34:* Flavin contents of whole plant extracts of *TRV:GFP* plants and weak and strong phenotypic stage *TRV:RIBA1* plants 14 d after VIGS induction.**
Flavins were determined via HPLC with authentic standards, for total flavin amount single values for FAD, FMN and riboflavin were summed up, n=5. Standard errors of the mean as well as percentage decrease compared to *TRV:GFP* control.

		FAD [ng mg^{-1} FW]		**FMN** [ng mg^{-1} FW]		**RF** [pg mg^{-1} FW]		**total** [ng mg^{-1} FW]	
TRV:GFP		5.36 ± 0.24	± 0 %	1.43 ± 0.03	± 0 %	327.3± 28	± 0 %	7.15 ± 0.25	± 0 %
TRV: RIBA1	*weak*	4.69 ± 0.09	-12 %	1.21 ± 0.03	-15 %	331.5 ± 14.8	-11 %	6.23 ± 0.12	-13 %
	strong	4.06 ± 0.09	-24 %	1.00 ± 0.03	-30 %	312.8 ± 23.6	-16 %	5.6 ± 0.1	-25 %

The total flavin amount was 14 % decreased in the "weak phenotype" and 25 % decreased in the "strong phenotype" group compared to GFP-control. Latter decrease corresponds to the 27 % decrease seen in the 4- and 6-week-old *RIBA1* antisense plants. Whereas in both groups riboflavin is only decreased by 11 and 16 % compared to GFP-control, the stronger phenotype seems to be particularly accompanied by higher decreases of FAD and FMN levels. When comparing the flavin values of *TRV:GFP* and *wt Col-0* plants (**Table 33**) it is evident that FMN and FAD contents are much higher in the TRV:GFP plants (FAD ~50 % and FMN ~20 %).

To unravel the consequences of the changes on protein as well as flavin contents in the *RIBA1*-VIGS treated plants qPCR analysis exploring flavin biosynthesis gene expression was performed. **Figure 47** shows the relative expression of the two phenotypic stages (weak and strong phenotype) compared to GFP control. The trend is that all transcripts are slightly up-regulated in the strong-phenotypic group. Expression profile in the "weak phenotype" group was not considerably altered

compared to GFP control. Disregarding the slight up-regulation in the case of the strong phenotype, otherwise the expression of flavin biosynthesis genes was not altered due to RIBA1 depletion. This agrees with the result described for *RIBA1* antisense plants in chapter 3.5.2.2.

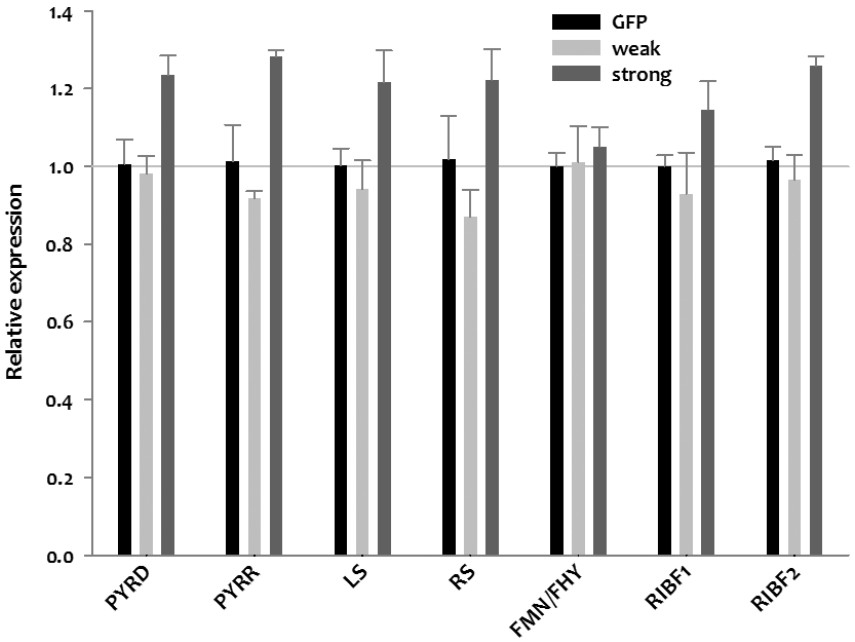

Figure 47: **Expression profile of flavin biosynthesis genes in *TRV:RIBA1* plants showing weak and strong phenotypic stage 14 d after VIGS induction.**
Whole plant (above ground tissue) samples of VIGS plants of weak and strong phenotypic stage (as defined above) were sampled. Values are presented as fold change ($2^{-\Delta\Delta Ct}$) compared to *TRV::GFP*; n=4 single plants of each phenotypic stage, error bars indicate standard error of the mean.

3.5.2.6 Overexpression of Arabidopsis RIBA1 in N. tabacum leads to Co-suppression

All experiments in this chapter were performed by B. Eichstädt under my supervision and results were presented in her Bacherlor's thesis (Eichstädt, 2014).

For an across species study, *Arabidopsis* RIBA1 was over-expressed in *N. tabacum* with the same *CaMV-35S*-driven sense *RIBA1* construct as described before in chapter 3.5.2.2. After BASTA®-selection, two kind of T1 lines were observed. As depicted in **Figure 48** representatives of the first group did not show an altered phenotypic appearance (non-phenotypic) compared to the *N. tabacum* wild type L. cv. Samsun NN (*SNN*) and the second showing more or less bleached leaves in different patterns (phenotypic, **Figure 48**B). The bleaching appeared already either early or late in the development. An immunodetection with the RIBA antibody was conducted on leaf extracts of green and bleached tissue of the phenotypic transgenic lines, and according leaf areas of *SNN* and non-phenotypic transgenic lines (**Figure 49**). It was demonstrated that the non-phenotypic lines over-express RIBA1 approximately 10-fold compared to endogenous RIBA amount in SNN. In contrast, the phenotypic lines did not show additional protein expression but instead a decrease of endogenous RIBA amount compared to *SNN* in the bleached leaf areas. Hence, these two kinds of lines were designated At*RIBA1* overexpressor and co-suppressor.

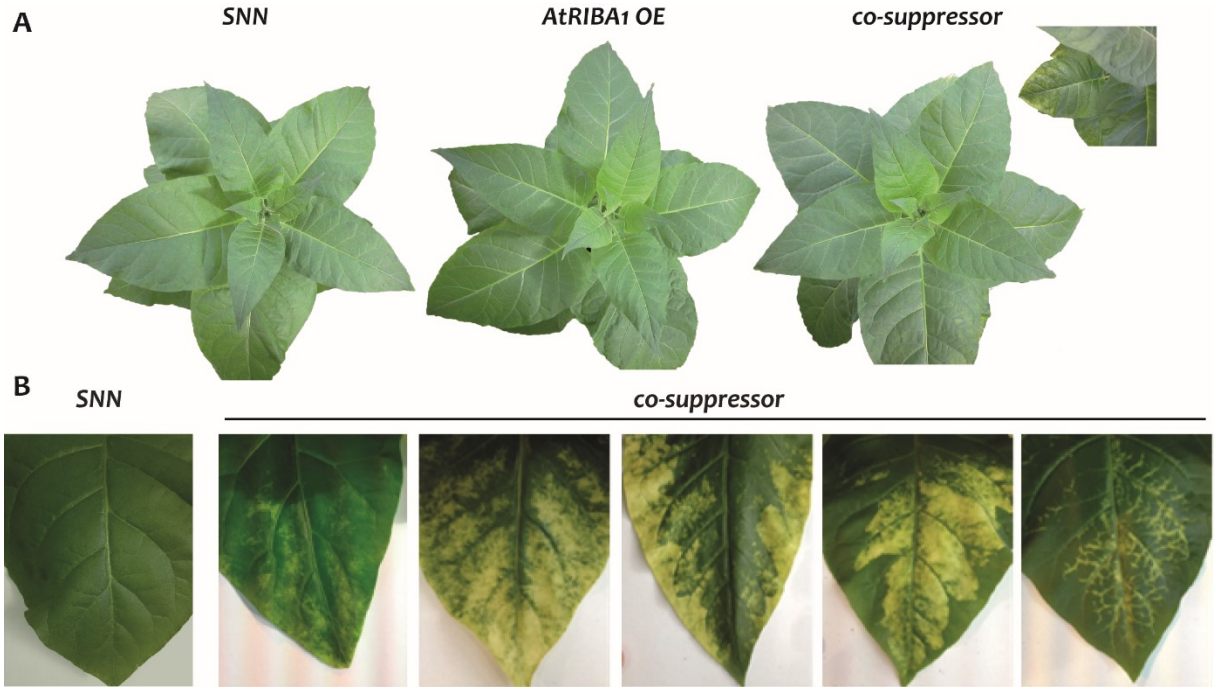

***Figure 48: N. tabacum lines overexpressing* AtRIBA1.**
Panel A depicts representative individuals of 10-week-old *N. tabacum* At*RIBA1* overexpressor or co-suppressor lines showing either wt-like or bleached phenotype. Panel B shows the different appearances of the bleached phenotype in *N. tabacum* co-suppressor line plants.

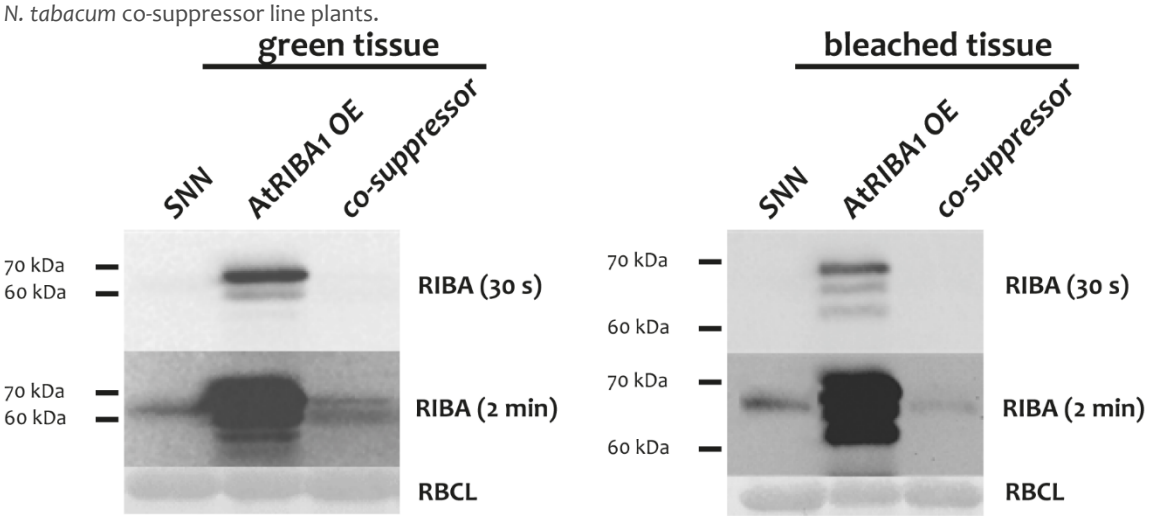

***Figure 49:* RIBA protein abundance in *N. tabacum* lines expressing AtRIBA1**
Protein extracts of either green or bleached leaves of 9-week-old co-suppressor plants and equivalent leaves of SNN and At*RIBA1* OE plants, grown under long-day conditions (150 µmol photons $m^{-2}s^{-1}$ light intensity, greenhouse) were analysed by Western blot using RIBA antibody (upper panels). Shorter (30 s) and longer (2 min) exposure time blot pictures are depicted in order to visualize weak endogenous RIBA bands. In the lower panel the Ponceau-stain of the same blot is shown, depicting Rubisco large subunit (RBCL) to illustrate equal loading of the gel. Extracts represent an equal ratio mixture of three biological replicates.

The At*RIBA1* overexpression and co-suppression line were subjected to a *RIBA* gene expression and flavin quantification study, wherein leaf gradient samples of 11-week-old plants were surveyed. For the leaf gradient every second leaf, starting from leaf#1, designated as the youngest leaf with a minimum length of 12 cm (this size was chosen for technical reasons, so that enough leaf material could be sampled for parallel protein, RNA and flavin extraction) until the lightly senescent leaf#9,

was analysed. **Figure 50** depicts the *RIBA* gene expression as fold change relative to expression of the housekeeper Nt*EF*.

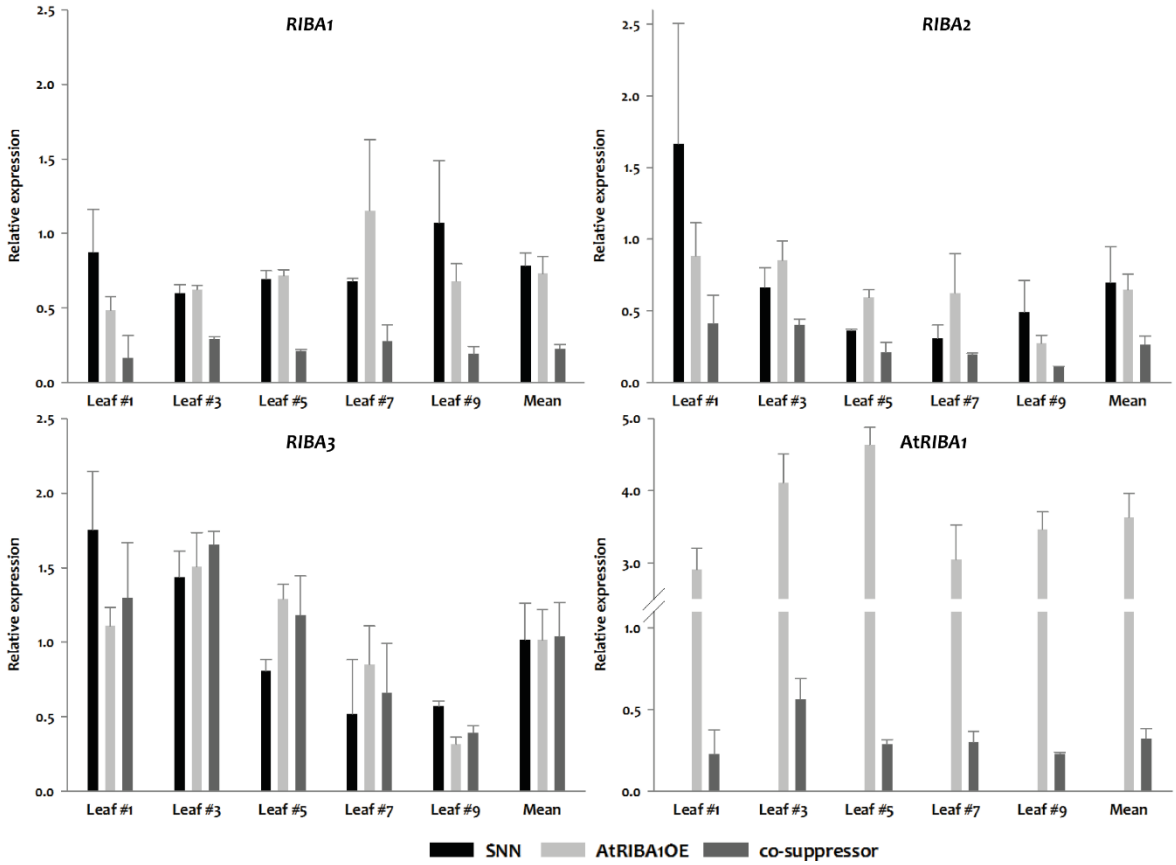

Figure 50: **RIBA expression (RIBA1-3 endogenous and AtRIBA1 transgene) of leaf gradient samples.**
For the leaf gradient every second leaf from the top to bottom was sampled from 11-week-old SNN (black), AtRIBA1 overexpression line (light grey) and co-suppression line (dark grey) plants grown under long-day conditions in (150 µmol photons $m^{-2}s^{-1}$ light intensity, greenhouse), wherein leaf #1 was defined as youngest leaf of minimum 12 cm length. Mean describes the average value over all tested leaves. Data is presented as fold change ($2^{-\Delta Ct}$) relative to expression of housekeeper *NtEF*. n=3, Error bars represent standard error of the mean.

In *SNN* and the At*RIBA1* overexpression line the level of endogenous *RIBA1* and *RIBA2* expression was similar. While *RIBA1* was more or less evenly expressed in all tested leaves, *RIBA2* expression decreased gradually from young towards old leaves. The mean values over all leaves reveal a 50 % decrease of endogenous *RIBA1* and *RIBA2* expression in the co-suppressor line compared to *SNN* and At*RIBA1* overexpression line. *RIBA3* transcript accumulation showed an even stronger gradual decrease from old towards young leaves, than was demonstrated for *RIBA2*. The *RIBA3* content was, however, not altered in the co-suppressor line compared to *SNN*. In all leaves of the At*RIBA1* overexpression line the accumulation of At*RIBA1* was evenly high, whereas in the co-suppression line it was approximately 10-fold lower than in the At*RIBA1* overexpression line. Compared to the endogenous *RIBA1* in *SNN* the transgene was expressed approximately 4 to 6 times more in the At*RIBA1* overexpression line and approximately 50 % less in the co-suppression line. According to EMBOSS Needle, mRNA sequence identity of the transgene At*RIBA1* is 69 % for endogenous

Nt*RIBA1*, 68 % for Nt*RIBA2* and 57 % for Nt*RIBA3*. It can be assumed that due to their high homology (~70 %) endogenous *RIBA1* and *RIBA2* accumulation was influenced by post-transcriptional silencing originating from the heterologous overexpression. This kind of gene silencing of homologous endogenous genes has been described before by Elkind *et al.* (1990) for *N. tabacum* heterologously expressing the bean phenylalanine ammonia-lyase (*PAL*) gene.

The approximately 10-fold overexpression of AtRIBA1 protein as detected by immunoblot analysis (**Figure 38**) was caused by clearly elevated At*RIBA1* transcript levels, which were between 3-5-fold upregulated compared to endogenous *RIBA1* expression. Interestingly, a 3-5 fold increased AtRIBA1 expression led to an approximately 10-fold overexpression of the protein, whereas the same construct transformed into *A. thaliana* causes a 140-fold higher transcript abundance only leading to an approximately 8-fold protein overexpression.

The results of the flavin content analysis on the leaf gradient samples are presented in **Figure 51**.

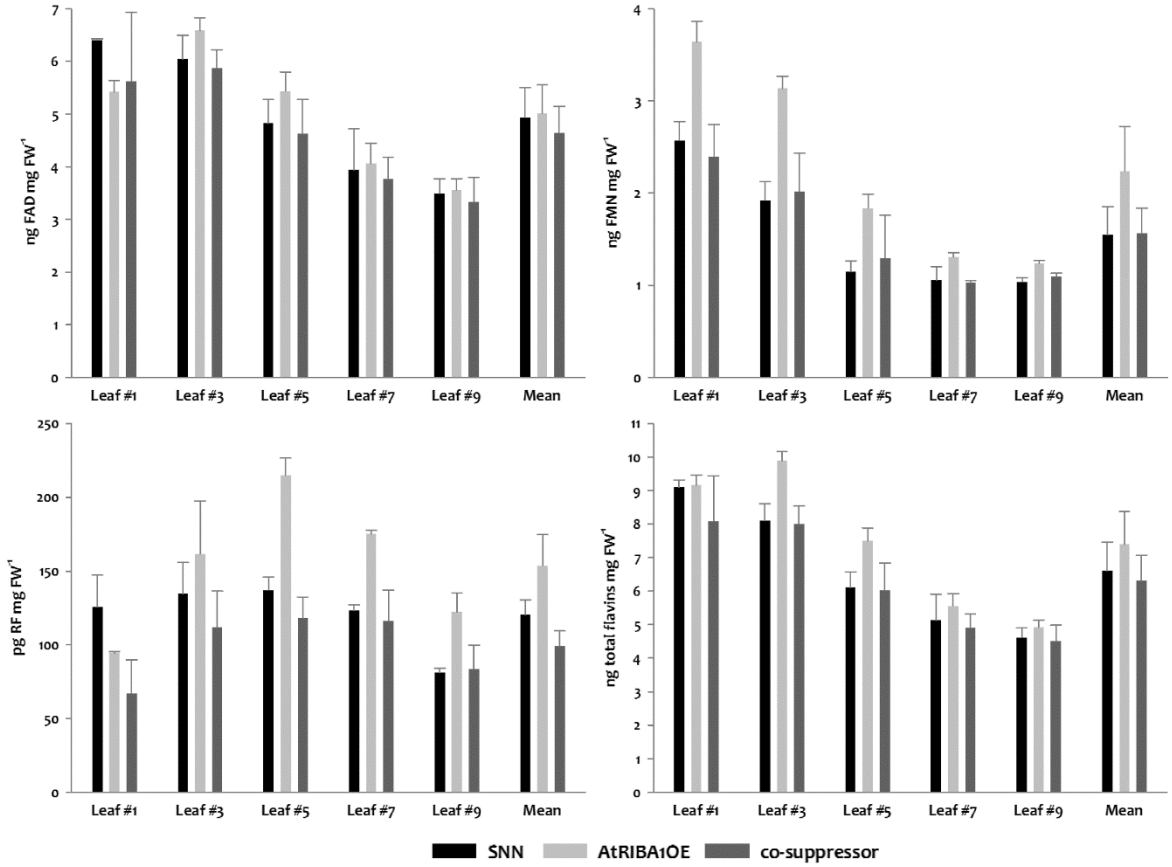

Figure 51: **Flavin contents of leaf gradient samples.**
For the leaf gradient every second leaf from the top to bottom was sampled from 11-week-old SNN (black), AtRIBA1 overexpression line (light grey) and co-suppression line (dark grey) plants grown under long-day conditions in (150 µmol photons $m^{-2}s^{-1}$ light intensity, greenhouse), wherein leaf #1 was defined as youngest leaf of minimum 12 cm length. Mean describes the average value over all tested leaves. Flavins were determined via HPLC with authentic standards, for total flavin amount single values for FAD, FMN and riboflavin were summed up, n=3. Error bars indicate standard errors of the mean.

Generally, it can be stated that in SNN and both transgenic lines FAD and FMN exhibited a gradual decrease of flavins from young to old leaves, whereas riboflavin content did not show any age dependent behaviour. While FAD content was not affected by At*RIBA1* overexpression, especially young leaves accumulated approximately 40 to 65 % more FMN compared to *SNN* and middle old leaves 40 to 60 % more riboflavin. The effect of co-suppression was only slightly visible on flavin content in these samples (almost 20 % decrease of riboflavin), as these represent the intersection over the whole leaf that was sampled. In order to overcome this problem, only bleached leaf areas of the co-supressor line and corresponding leaf areas of SNN and AtRIBA1 overexpression line were sampled and flavin contents were determined. The results are listed in **Table 35**. As shown there, the bleached leaf areas show a decrease of total flavin content by 40 %. In these leaves, also At*RIBA1* overexpression line showed a slight decrease in flavin amounts, whereas it is very small compared to co-suppressor.

***Table 35:* Flavin contents of leaf extracts of bleached areas of 9 week-old plants of co-suppressor line and corresponding areas of *SNN* and At*RIBA1* overexpressor lines.**
The plants grown under custom growth conditions in (150 µmol photons $m^{-2}s^{-1}$ light intensity, long-day, greenhouse), wherein leaf #1 was defined as youngest leaf of minimum 12 cm length. Samples were taken from leaf#5 (±1 leaf). Flavins were determined via HPLC with authentic standards, for total flavin amount single values for FAD, FMN and riboflavin were summed up, n=3, wherein each biological sample was pooled, containing same FW amount of three different plants. Standard errors of the mean as well as percentage decrease compared to *SNN* are indicated.

	FAD [ng/mg FW]		**FMN** [ng/mg FW]		**RF** [pg/mg FW]		**total** [ng/mg FW]	
SNN	4.68 ± 0.11	± 0 %	1.94 ± 0.01	± 0 %	72.8 ± 6.4	± 0 %	6.69 ± 0.11	± 0 %
At*RIBA1* OE	4.33 ± 0.17	-7 %	1.82 ± 0.03	-6 %	63.2 ± 11.2	-13 %	6.22 ± 0.17	-7 %
co-suppressor	2.92 ± 0.1	-38 %	1.05 ± 0.03	-46 %	58.3 ± 9.7	-20 %	4.03 ± 0.1	-40 %

3.5.3 Analysis of *riba2* and *riba3* T-DNA Mutants

As the physiological roles of RIBA2 and RIBA3 have not been characterised, a reverse genetic approach was chosen using T-DNA knockout lines. Therefore, for both genes T-DNA lines were analysed on DNA level. First, presence of T-DNA insertions in the respective genes (in this case either *RIBA2* or *RIBA3*) was confirmed via PCR with T-DNA and gene specific primers (**Figure 52**, T-DNA^*RIBA2*/*RIBA3*) performed as described in chapter 2.7.5.1.

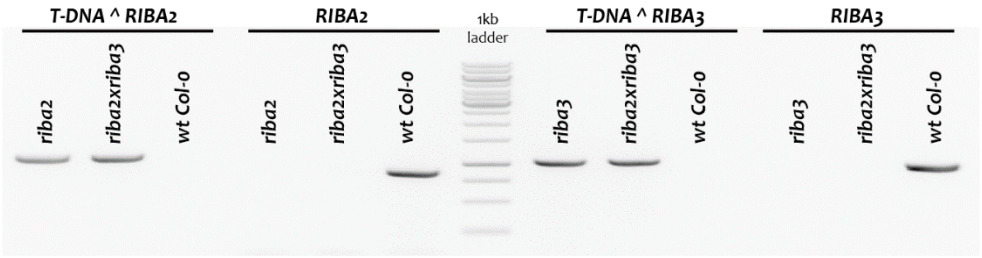

***Figure 52:* Genotyping PCR of homozygous *riba2*, riba3 and *riba2xriba3* T-DNA mutant plants.**
Agarose gel depicting genotyping PCR products of *wt Col-0*, *riba2* and *riba2xriba3* for *RIBA2* mutant allele (lanes 1-3, T-DNA^*RIBA2*) and *RIBA2* wt allele (lanes 4-6, *RIBA2*) as well as of *wt Col-0*, *riba3* and *riba2xriba3* for *RIBA3* mutant allele (lanes 8-10, T-DNA^*RIBA3*) and *RIBA3* wt allele (lanes 11-13, *RIBA3*).

Thereafter, the identification of the exact locus of the respective T-DNA insertions within the gene was performed via sequencing of the mutant allele PCR product (chapter 2.7.10). In this case, the presence of the T-DNA insertions in the second exon in *riba2* and in the first exon in *riba3*, respectively was demonstrated (**Figure 53**). Further genotyping PCR with two gene specific primers spanning the T-DNA insertion, confirmed the absence of an intact wt allele (**Figure 52**, RIBA2/RIBA3) and hence homozygosity of *riba2* and *riba3* mutant lines. A *riba2xriba3* double-mutant (*riba2xriba3*) was generated through crossing of maternal homozygous *riba2* and paternal *riba3* plants (chapter 2.5.2.1). Also here the double knockout could be demonstrated (**Figure 52**).

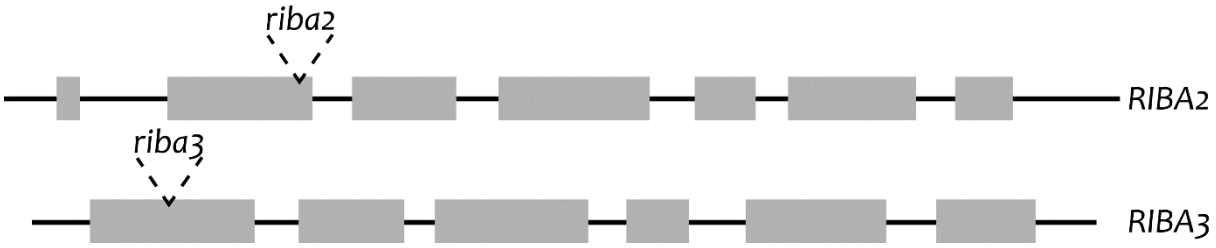

***Figure 53:* Localisation of T-DNA insertion sites in *riba2* and *riba3* T-DNA mutants.**
RIBA2 and RIBA3 gene structure with T-DNA insertion sites of the mutants marked with triangles (grey boxes depict exons).

In order to test the physiological consequences of *RIBA2* and *RIBA3* depletion, *riba2*, *riba3* and *riba2xriba3* were grown under different conditions, e.g. short- and long-day (100 µmol photons $m^{-2}s^{-1}$), at low-light (30 µmol photons $m^{-2}s^{-1}$), and higher-light (300 µmol photons $m^{-2}s^{-1}$). Phenotypically *riba2*, *riba3* and *riba2xriba3* were similar to *wt Col-0* under all tested conditions. In **Figure 54** *riba2*, *riba3* and *riba2xriba3* plants grown under short-day conditions are depicted.

***Figure 54: Six*-week-old *wt Col-0*, *riba2*, *riba3* and *riba2xriba3* mutant plants.**
The depicted plants were grown under short-day conditions (100 µmol photons $m^{-2}s^{-1}$ light intensity).

In order to confirm the knockout in the mutants and to analyse possible effects of the respective knockout, *RIBA* transcripts were studied in whole plant (above ground tissue) extracts of *riba2*, *riba3* and *riba2xriba3* by means of qPCR. In all three lines *RIBA1* mRNA content was slightly decreased. While in the *riba2* mutant the *RIBA1* decrease was not substantial, in *riba3* and *riba2xriba3* mutants it was 20 % reduced compared to *wt Col-0*. *RIBA2* content was, as expected, close to zero in the *riba2* single and the *riba2xriba3* double mutant, whereas it was up to 50 %

increased in the *riba3* single mutant compared to *wt Col-0*. In the same manner, *RIBA3* content was not detectable in the *riba3* single and the *riba2xriba3* double mutant but 20 % higher in the *riba2* single mutant.

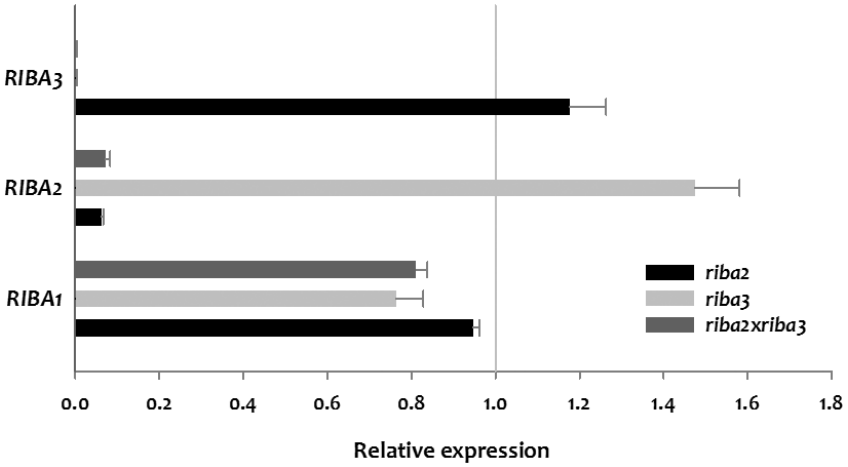

Figure 55: **Relative transcript accumulation of *RIBA* genes in 6-week-old *riba2*, *riba3* and *riba2xriba3* plants compared to *wt Col-0*.**
The plants were grown under short-day conditions (100 µmol photons $m^{-2}s^{-1}$ light intensity). The data is presented as fold change ($2^{-\Delta\Delta Ct}$) compared to *wt Col-0*, n=4, single plants of one line were sampled, error bars indicate standard errors of the mean.

RIBA protein expression in whole leaf extracts of *riba2*, *riba3* and *riba2xriba3* was studied via SDS-PAGE and immunoblot analysis as described in chapters 2.9.2 and 2.9.3. The result of the immunodetection is shown in **Figure 56**. The upper RIBA1 band in this case showed an up to two times higher amount in the *riba2* and *riba2xriba3* mutants, compared to *wt Col-0*. Also the lowest, RIBA2 specific, band showed a faint increase in *riba3* compared to *wt Col-0*.

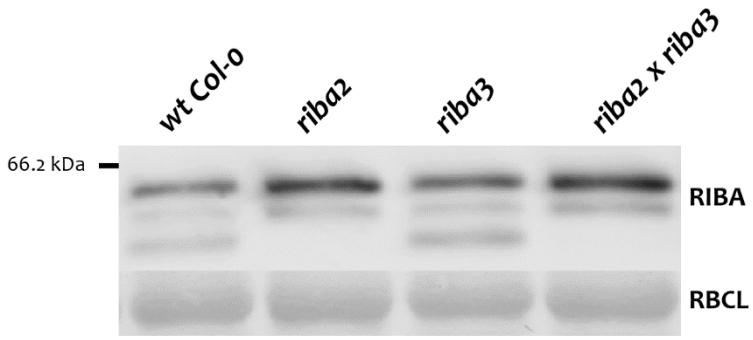

Figure 56: **RIBA protein abundance in 6-week-old *riba2*, *riba3* and *riba2xriba3* mutants.**
Whole plant protein extracts of plants grown under short-day conditions (100 µmol photons $m^{-2}s^{-1}$ light intensity) were analysed by Western blot using RIBA antibody (upper panel). In the lower panel the Ponceau-stain of the same blot is shown, depicting Rubisco large subunit (RBCL) to illustrate equal loading of the gel. Upper two bands of the immunoblot are assigned to RIBA1, while the lowest band represents RIBA2 protein.

A possible effect of RIBA2 and RIBA3 depletion on flavin biosynthesis was studied subsequently. Flavin contents of *riba2*, *riba3* and *riba2xriba3* were determined in whole plant (above ground tissue) extracts of 6-week-old plants grown under short-day conditions. The results are shown in **Table 36**. Only faint differences were observed in the single- and double-mutants compared to

wt Col-0. The main difference concerns FMN concentrations of *riba2* and *riba3*, which was 21 % lower compared to *wt Col-0*. All in all, these differences sum up to a decrease between 4 to 6 % of total flavin biosynthesis end products compared to *wt Col-0*.

***Table 36:* Flavin contents of 6-week-old *wt Col-0*, *riba2*, *riba3* and *riba2xriba3* plants.**
The tested plants were grown under short-day conditions. Flavin contents were determined via HPLC with authentic standards. For total flavin amount the values for FAD, FMN and riboflavin were summed up, n=5. Standard errors of the mean as well as percentage in-/decrease compared to *wt Col-0* are indicated.

	FAD [ng mg^{-1} FW]		**FMN** [ng mg^{-1} FW]		**RF** [pg mg^{-1} FW]		**total** [ng mg^{-1} FW]	
wt Col-0	2.91 ± 0.15	±0 %	1.11 ± 0.07	±0 %	328.6 ± 39.1	±0 %	4.35 ± 0.17	±0 %
riba2	2.95 ± 0.09	+1 %	0.88 ± 0.04	-21 %	307.6 ± 15.1	-6 %	4.14 ± 0.1	-5 %
riba3	2.93 ± 0.07	+0,7 %	0.88 ± 0.07	-21 %	291.5 ± 14.8	-11 %	4.10 ± 0.1	-6 %
riba2xriba3	2.89 ± 0.1	-0,7 %	1.01 ± 0.08	-9 %	282.8 ± 29.3	-14 %	4.19 ± 0.14	-4 %

In 6-week-old *riba2*, *riba3* and *riba2xriba3* mutant plants grown under short-day conditions, possible effects of the RIBA2 and RIBA3 knockout on the gene expression of the flavin biosynthesis genes were studied in a qPCR analysis (**Figure 57**).

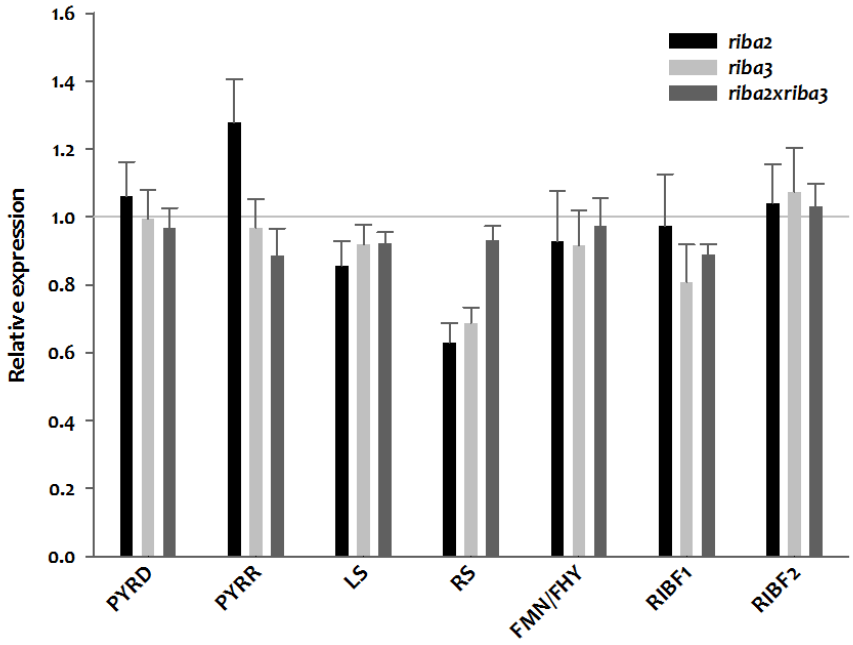

***Figure 57:* Transcript accumulation of flavin biosynthesis genes in 6-week-old *riba2*, *riba3* and *riba2xriba3* plants.**
The tested plants were grown under short-day conditions (100 µmol photons $m^{-2}s^{-1}$ light intensity) as fold change ($2^{-\Delta\Delta Ct}$) compared to *wt Col-0*, n=4, error bars indicate standard error of the mean.

PYRD, *LS*, *FMN/FHY*, *RIBF1* and *RIBF2* contents were not clearly altered, whereas *PYRR* content was up to 30 % increased in *riba2* and *RS* decreased by approximately 40 % in *riba2* and *riba3* compared to *wt Col-0*. It seems that the knockout of neither RIBA2 nor RIBA3 significantly altered the gene expression pattern of the flavin biosynthesis genes.

3.5.4 Complementation of the *riba1* Mutation

In order to learn more about the roles of the RIBA isoforms and the reasons why *RIBA2* and *RIBA3* are not able to complement the knockout of *RIBA1*, a series of complementation constructs with *Arabidopsis* RIBA sequences were generated (**Figure 58**). One construct contained the *RIBA1* cDNA sequence driven by the strong constitutive *CaMV-35S* promoter. Three more constructs contained the genomic sequences of *RIBA1*, *RIBA2* or *RIBA3*, driven by the *RIBA1* promoter (*pRIBA1*) and fused to 5' and 3' UTRs of *RIBA1*. RIBA2 and RIBA3 genomic sequences were fused to RIBA1 promoter and 5'UTR as well as to 3'UTR by the so called triple overhang-extension PCR method, conducted as described in chapter 2.7.5.3, performed by R. Wittrahm under my supervision and presented in her Bacherlor's thesis (Wittrahm, 2014). The in **Table 37** listed constructs were transformed into the heterozygous progenies of the *riba1*-GABI and *riba1*-SALK lines (chapter 3.5.2.1).

***Table 37:* Vectors constructed for complementation of *riba1* mutants.**
The table states name and description of the construct, as well as the promoter, vector and restriction sites included. Primers used for the amplification of the inserts are named here and primer sequences in **Table S3**.

Constructs	Promoter	Description	Vector	Restriction sites	Primers
35S::cAtRIBA1	CaMV 35S	AtRIBA1 cDNA+ 5'UTR	pGL1	SmaI	CLP9/10
pRIBA1::gAtRIBA1	AtRIBA1	Genomic AtRIBA1 +AtRIBA1 5'/3'UTR	pCambia3301	XmaI/PmlI	CLP11/12
pRIBA1::gAtRIBA2	AtRIBA1	Genomic AtRIBA2 +AtRIBA1 5'/3'UTR	pCambia1305.2	XmaI/PmlI	CLP13/14 CLP15/16 CLP17/12
pRIBA1::gAtRIBA3	AtRIBA1	Genomic AtRIBA3 +AtRIBA1 5'/3'UTR	pCambia3301	XmaI/PmlI	CLP13/18 CLP19/20 CLP21/12

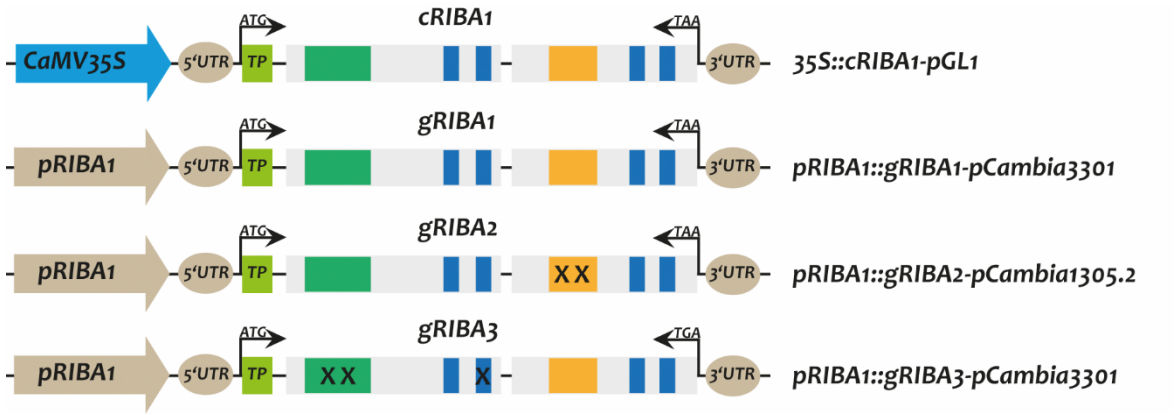

***Figure 58:* Constructs generated for the complementation of *RIBA1* Depletion in riba1 knockout mutants.**
Big arrows indicate promoter regions, the ovals *RIBA1* UTR regions, light green box indicates transit peptide of each RIBA gene. The dark green box indicates the DHBPS ribulose-5-phosphate binding domain, the orange box the GCHII zinc binding domain and the blue boxes the catalytic amino acid residues. **X**s indicate mutated amino acid residues within the functional domains of DHBPS, or GCHII in RIBA3 or RIBA2, respectively.

The transformation of the *35S::cRIBA1*-pGL1 into heterozygous *riba1* GABI plants resulted 41 BASTA-resistantT1 transformants, of which 25 were demonstrated to be heterozygous for *riba1* mutant allele (*riba1*/*RIBA1*) and 16 homozygous for wt allele (*RIBA1*/*RIBA1*). Until date, 332 individual plants

from 26 T2 lines have been analysed of which none could be shown to be homozygous for *riba1* mutant allele. The expression of the transgene was verified for T2 lines by immunodetection with RIBA antibody (not shown). The genotyping work was partly performed by R. Wittrahm under my supervision and the results were presented in her Bachelor's thesis (Wittrahm, 2014).

The results suggest, that it is not possible to complement the RIBA1 mutation by CaMV-35S-driven RIBA1 cDNA construct even though RIBA1 protein expression was demonstrated for the tested lines at the age of 4 weeks.

The constructs p*RIBA1*::*RIBA1*-pCambia3301, p*RIBA1*::*RIBA2*-pCambia1305.2 and p*RIBA1*::*RIBA3*-pCambia3301 were transformed into the *riba1* GABI and SALK mutant lines as described in chapter 2.6.4. Due to time limitation, selection of transformants and subsequent genotyping could not be performed and will be conducted in future.

3.6 Metabolic Profiling of Flavin Mutants

Comprehensive metabolite profiling by gas chromatography-mass spectrometry (GC-MS) (Fernie *et al.*, 2004, Lisec *et al.*, 2006) was used to further pursue the aims of this thesis 1.) deciphering the physiological roles of RIBA2 and RIBA3 and 2.) characterisation of the metabolic and physiological consequences of a deregulated riboflavin biosynthesis. The metabolome analysis was conducted as described in chapter 2.13 for *RIBA1* deficient *Arabidopsis* plants, for tobacco At*RIBA1* overexpressor and co-suppressor lines, as well as for *riba2*, *riba3* and *riba2xriba3* T-DNA knockout mutants. Information provided by KEGG Pathway Database (Kanehisa & Goto, 2000, Kanehisa *et al.*, 2014) was used to generate a metabolic map.

3.6.1 Metabolic Consequences of RIBA1 Deficiency

In the case of antisense *RIBA1#2* and RIBA1-VIGS plants with reduced RIBA1 expression, which have been characterised in chapters 3.5.2.2 and 3.5.2.5, the examination of the effects on the plant metabolism as a result of the disturbances in the flavin homeostasis were of great interest. How does the plant cope with changing flavin contents and possible shortage? Which processes are prioritised and which are shut down under limiting flavin supply? In order to detect primary and pleiotropic effects, plants displaying a different extent of bleaching phenotype due to RIBA1 depletion were sampled. Accordingly, 4- and 6-week-old antisense *RIBA1#2* plants (3.5.2.2), as well as weak and strong phenotypic RIBA1-VIGS plants (3.5.2.5) were used in the analysis. The metabolites differing in antisense *RIBA1#2* plants compared to *wt Col-0* and in RIBA1-VIGS plants compared to GFP-VIGS control plants are listed in **Table 38**. **Figure 59** depicts a metabolic map, showing the metabolites listed in **Table 38** in the context of sugar-, amino acid- and aromatic amino acid metabolism, as well as the arginine/ornithine cycle. In the following paragraph the most eminent effects are summarised.

Aspartate as the precursor of the "aspartate-derived amino acids" lysine, threonine, isoleucine and methionine (Jander & Joshi, 2009) was significantly reduced in the antisense *RIBA1#2* compared to *wt Col-0* plants entailing many changes of amino acid contents. Lysine was significantly increased, while homoserine, which shares the common precursor aspartate semialdehyde, was significantly reduced. Threonine, which directly derives from homoserine and shares the common precursor phosphohomoserine together with methionine, was significantly reduced, while the latter was significantly increased.

Further metabolites in this branch, which are connected to aspartate metabolism and should be mentioned, are β-alanine, uracil, asparagine and nicotinic acid. β-alanine and nicotinic acid contents

were reduced like their precursors aspartate, while uracil and asparagine contents were significantly increased.

Metabolites, which contents are behaving oppositely in antisense and VIGS plants are listed in the fourth column of **Table 38**.

***Table 38:* Result of the metabolome analysis of RIBA1 antisense (AS) and VIGS plants sorted due to the congruent, opposite or mixed behaviour of the metabolite contents.**
Relative strength of metabolite accumulation (+) or reduction (-) is indicated for 4-week-old/6-week-old antisense plants and for weak/strong phenotypic VIGS plants compared to *wt Col-0* or GFP-VIGS control. Colour coding indicates metabolic branch (blue: sugars or sugar derived, orange: amino acid branch, red: aromatic amino acid branch, violet: citric acid cycle, green: arginine/ornithine cycle). Column 1 comprises the metabolites, which contents behave congruently in both lines with defect in flavin synthesis. Column 4 includes the metabolites, which contents behave oppositely in antisense RIBA1#2 plants and RIBA1-VIGS plants. In column 3 metabolites under the category "mixed" are listed, including metabolites, which contents behave differentially in the 4- and 6-antisense RIBA1#2 or weak and strong phenotypic RIBA1-VIGS samples, respectively. Columns 2/3, 5/6 and 8/9 describe the trends of the changes in the metabolite contents, wherein "+" indicates ≤1.4-fold, "++" between >1.4- and ≤2.8-fold, "+++" between >2.8 and 4.2-fold accumulation and "-"≤0.87-fold, "--"between >0.87 and ≤1.74-fold, "---" between >1.74 and 2.6-fold reduction. The slashes mark the trends in the 4-/6-week old antisense and weak/strong phenotypic VIGS plants, respectively.

Congruent			Opposite			Mixed		
	AS	VIGS		AS	VIGS		AS	VIGS
gluconate	+/+	+/+	sucrose	-/-	+/+	raffinose	-/++	+++/+++
glucoheptose	+/+	+/++	glucose	-/---	++/++	galactinol	-/++	+++/+++
rhamnose	+/+	+/+	fructose	-/---	++/+	L-ascorbate	-/-	+/-
maltose	-/-	-/--	trehalose	-/-	+/+	glycerate	-/--	+/-
glycerol	-/o	-/-	fucose	-/-	+/+	erythrose	--/+	---/o
			DHA	-/-	+/+			
			myo-inositol	-/-	+/+			
glycine	---/---	---/---				serine	+/-	+/+
threonine	--/--	o/-				cysteine	+/++	-/+
homoserine	--/---	-/-				alanine	+/--	--/-
methionine	+/+	+/+				aspartate	--/--	-/+
lysine	+/+	+/++				β-alanine	-/o	+/-
uracil	+/+++	+/++				isoleucine	-/+	+/+
asparagine	+/+++	++/+++				valine	--/+	+/+
nicotinate	--/--	-/--						
phenylalanine	+/++	+/++	tyramine	-/-	+/+	tryptophan	-/+	++/+
tyrosine	+/+	+/++						
benzoate	-/-	-/-						
citrate	--/-	--/-	succinate	+/+	-/-	pyruvate	-/--	+/-
			fumarate	-/--	+/+			
			malate	-/--	+/+			
proline	+/+	++/++	glutamate	-/-	+/+	ornithine	--/+	-/+
glutamine	+/+	+/++	putrescine	-/-	+/+	GABA	+/-	+/-
histidine	+/+	+/++				spermidine	+/-	o/-
adenine	+/+	+/+				arginine	-/+	+/+
						pyroglutamate	+/-	+/+

The fourth column of **Table 38** comprises mainly carbohydrates. Especially the strongly opposed contents of glucose and fructose are eye-catching. It must be kept in mind that for the approach of RIBA1-VIGS, *wt Col-0* plants were grown under 16 h light/8 h darkness conditions and *RIBA1* depletion was induced via virus infection. In contrast, antisense *RIBA1#2* plants were grown under

short-day conditions and the *RIBA1* depletion was constitutive. It is proposed that these plant samples were physiologically very different, so that vast differences in the metabolic responses due to RIBA1 depletion were expected. Generally it must be noted, that the before mentioned physiological differences seem to especially affect the sugar metabolism but will not be further discussed.

The metabolites, which contents differ in 6-week-old antisense *RIBA1#2* and strong phenotypic RIBA1-VIGS samples compared to the 4-week-old antisense *RIBA1#2* and weak phenotypic RIBA1-VIGS plants, respectively, are listed under the category "mixed" in column 7 of **Table 38**. These metabolites, which contents change entirely according to the severity of the RIBA1 depletion phenotype can be interpreted to rely on pleiotropic effects. Within this category, there is only one group of metabolites, which contents showed consistent changes in the antisense *RIBA1#2* and RIBA1-VIGS samples, and hence could be interpreted as being specifically caused by flavin deficiency. This group includes three metabolites of the ornithine/arginine cycle, namely ornithine, spermidine and γ-aminobutyric acid (GABA). Spermidine and GABA were reduced in the 4-week-old antisense *RIBA1#2* and weak phenotypic RIBA1-VIGS plants, while they were increased in the 6-week-old antisense *RIBA1#2* and strong phenotypic RIBA1-VIGS plants. The ornithine content however showed the opposite behaviour by being increased in the 4-week-old antisense *RIBA1#2* and weak phenotypic RIBA1-VIGS plants and reduced in the 6-week-old antisense *RIBA1#2* and strong phenotypic RIBA1-VIGS plants.

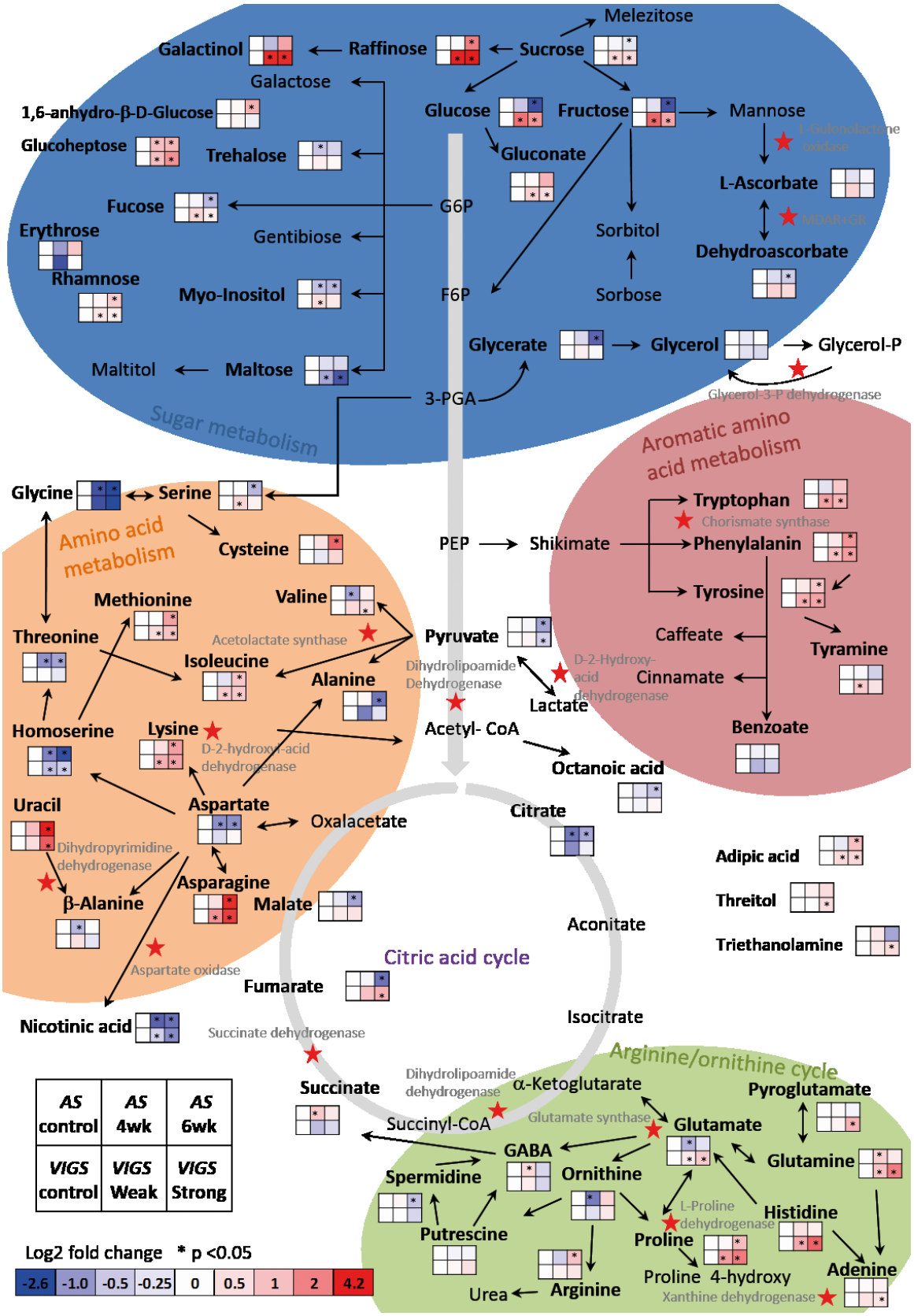

Figure 59: **Metabolome of riba1 depletion mutants.**
Metabolome data presented as fold change compared to control. As samples 4- and 6-week-old *RIBA1* antisense mutant plants grown under short-day conditions (100 µmol photons $m^{-2}s^{-1}$ light intensity) as well as *RIBA1-VIGS* plants, displaying weak and strong phenotype, grown under 16 h day/8 h night light cycle (120 µmol photons $m^{-2}s^{-1}$ light intensity). Red stars mark flavin-dependent enzymes. Values are means of 6-8 biological replicates, asterisks indicate values that were significantly different compared to control ($p<0.05$, calculated with unpaired two-tailed Student's t test).

3.6.2 Metabolic Consequences of RIBA1 Overexpression in *N. tabacum*

The result of the metabolome analysis of *N. tabacum* lines, designated as At*RIBA1* overexpressor and co-suppressor, is presented in **Figure 60**. Leaves equivalent to leaf#5 as described in chapter 3.5.2.6 from 10-week-old plants grown under long-day conditions (150 µmol photons $m^{-2}s^{-1}$, greenhouse) were sampled. It must be noted, that the sampled leaves did not display the bleaching phenotype at the time of sampling. In the case of the co-suppressor line, the plant chosen did, however, show a mild bleaching of older leaves.

Generally, it can be stated that the metabolic *status quo* of the At*RIBA1* overexpressor and the co-suppressor line is very similar. The exceptions are galactonate, rhamnose, tryptophan and α-ketoglutarate, which are slightly reduced in the overexpressor and accumulating in the co-suppressor, as well as idose, which was slightly accumulating in the overexpressor and reduced in the co-suppressor. The metabolic pattern can be described as a general down-regulation of the sugar metabolism and a strong shift towards citric acid cycle and amino acid biosynthesis.

Interestingly, the only major difference between the RIBA1 overexpressor and co-suppressor lines is the content of lactate, which is significantly reduced in the co-suppressor line.

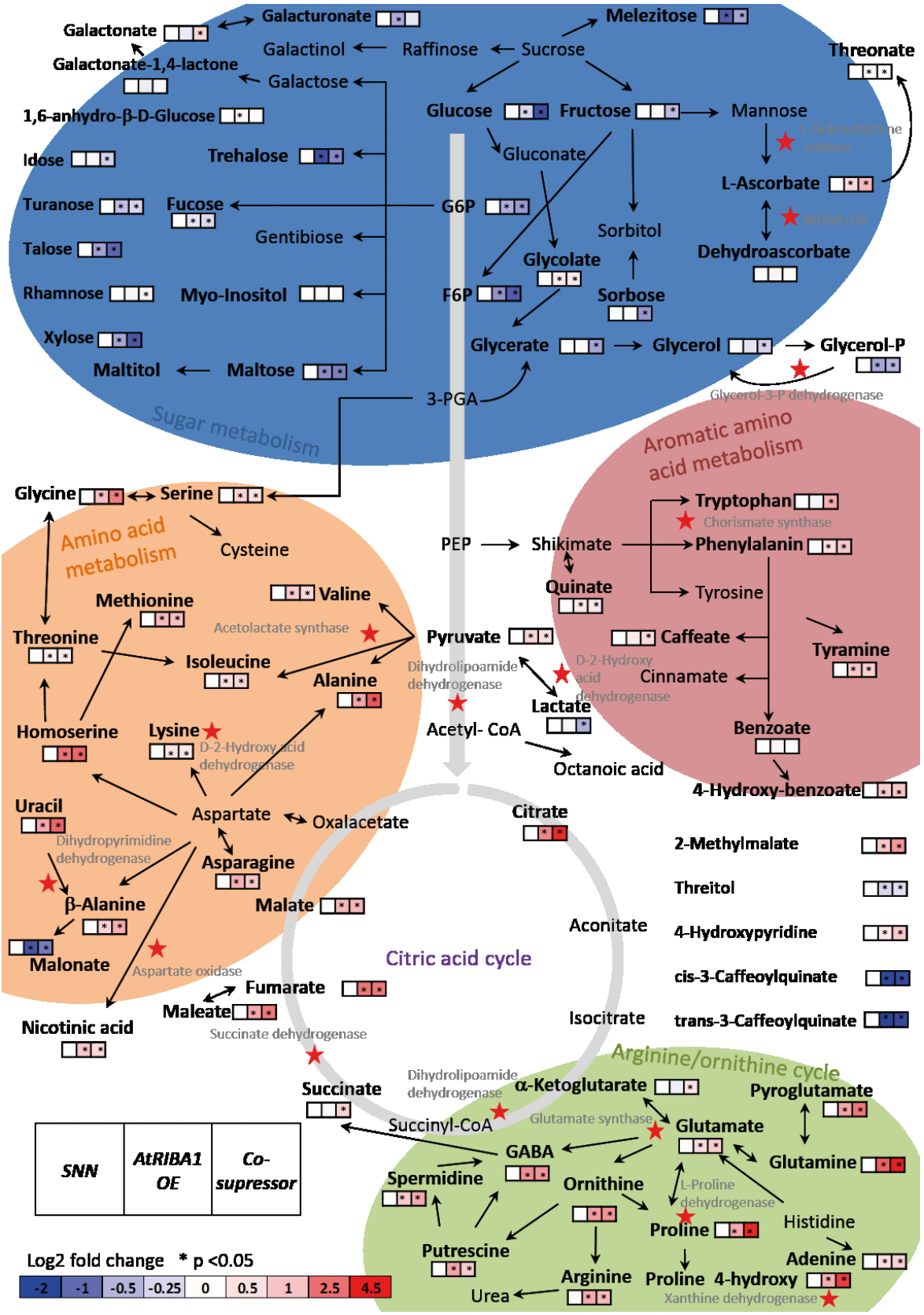

Figure 60: **Metabolome of *N. tabacum* At*RIBA1* overexpressor and co-suppressor lines.**
Metabolome data presented as log2 fold change compared to *SNN* of 10-week-old *N. tabacum AtRIBA1 overexpressor or co-suppressor* grown under long-day conditions (150 µmol photons $m^{-2}s^{-1}$ light intensity, greenhouse). Red stars mark flavin-dependent enzymes. Values are means of 6-8 biological replicates, asterisks indicate values that were significantly different compared to control ($p<0.05$, calculated with unpaired two-tailed Student's t test).

3.6.3 Metabolic Consequences of RIBA2 and/or RIBA3 Depletions

In order to further identify potential physiological roles of RIBA2 and RIBA3, metabolomics analysis was conducted on 8-week-old *riba2* and *riba3* single as well as *riba2*x*riba3* double knockout mutants. The metabolites differing in *riba2*, *riba3* single mutant and *riba2*x*riba3* double mutant plants compared to *wt Col-0* are listed in **Table 39**. **Figure 61** shows the metabolites in the context of sugar, amino acid and aromatic amino acid metabolism, as well as the arginine/ornithine cycle.

As shown in **Table 39**, a big proportion of metabolites behaved in the same manner in *riba2*, *riba3* single mutant and riba2xriba3 double mutant plants. However, the majority of measured metabolite contents levels were different when comparing the single mutants versus the double mutant. As seen in **Table 39**, metabolite contents, which were only altered in the double mutant, were mainly sugars and sugar derived-, aromatic amino acid branch- and arginine/ornithine cycle metabolites.

The comparison of the metabolic data of the antisense *RIBA1#2* plants and the *riba2*, *riba3* single mutants was performed to find metabolic effects evoked by the depletion of each of the RIBA isoforms. Thereby trehalose, dehydroascorbate, threonine and β-alanine and were found to be reduced and succinate, asparagine, methionine and phenylalanine to be accumulating in all compared samples.

Table 39: **Result of the metabolome analysis of *riba2*, *riba3* single mutant as well as *riba2xriba3* double mutant plants sorted due to the congruent, different single vs. double mutant or mixed behaviour of the metabolite contents.**
Relative strength of metabolite accumulation (+) or reduction (-) is indicated for *riba2* and *riba3* single as well as *riba2xriba3* double mutant compared to *wt Col-0* plants. Colour coding indicates metabolic branch (blue: sugars or sugar derived, orange: amino acid branch, red: aromatic amino acid branch, violet: citric acid cycle, green: arginine/ornithine cycle). Column 1 comprises metabolites, which contents behave congruently in all three mutant lines, column 5 comprises metabolites, which contents behave same in the single mutant, but differently in the double mutant plants and finally column 9 which comprises metabolites which behave differently in single mutant plants. Columns 2-4, 6-8 and 10-12 describe the trends of the changes in the metabolite contents, wherein "+" indicates ≤ 0.74-fold, "++" between >0.74 and ≤1.5-fold, "+++" between >1.5 and 2.25-fold accumulation and "-"≤0.31, "--" between >0.31 and 0.62, as well as "---" between>-0.62 and 0.93-fold reduction.

Congruent				**Different single vs. double**				**Mixed**			
	riba2	***riba3***	***a2xa3***		***riba2***	***riba3***	***a2xa3***		***riba2***	***riba3***	***a2xa3***
raffinose	--	---	-	glucose	+	++	-	myo-inositol	+	0	-
trehalose	--	---	--	fructose	++	++	-	galactinol	-	+	+
levoglucosan	-	--	-	sucrose	+	+	--				
fucose	+	+	+	mannose	+	+	-				
turanose	+	+	+	sorbose	++	++	-				
melezitose	++	+	+	idose	+	+	-				
glycerol	+	+	+	xylose	+	+	0				
glycerate	+	++	+	rhamnose	0	0	+				
DHA	-	-	-	maltose	0	0	++				
				maltotriose	0	0	+				
				maltitol	0	0	+				
				galactose	0	0	--				
				gentibiose	0	0	-				
				G6P	0	0	+				
				glycerol-3-P	0	0	+				
				ascorbate	0	0	-				
				threitol	0	0	-				
				erythritol	0	0	+				
glycine	+	+	+	asparagine	+	+	--	serine	-	+	+
alanine	+	++	+	methionine	+	+	--	isoleucine	+	-	--
aspartate	++	++	+	valine	+	+	-				
lysine	--	--	--	uracil	0	0	+				
threonine	-	-	-	nicotinate	0	0	+				
β-alanine	--	---	--								
				phenylalanine	+	+	-	benzoate	+	-	+
				tyrosine	0	0	--				
				cinnamate	0	0	+				
				caffeate	0	0	-				
				4-hydroxybenzoate	0	0	+				
citrate	+++	+++	+	pyruvate	+	+	-				
succinate	+	+	+	lactate	0	0	-				
fumarate	+	+	+	α-ketoglutarate	0	0	+				
malate	+	+	+								
glutamate	+	+	+	proline	0	0	--	urea	-	+	+
pyroglutamate	+	+	+	glutamine	0	0	--	putrescine	+	-	-
				arginine	0	0	-	GABA	+	-	+
				ornithine	0	0	--				
				spermidine	0	0	--				
				proline 4-hydroxy	0	0	+				

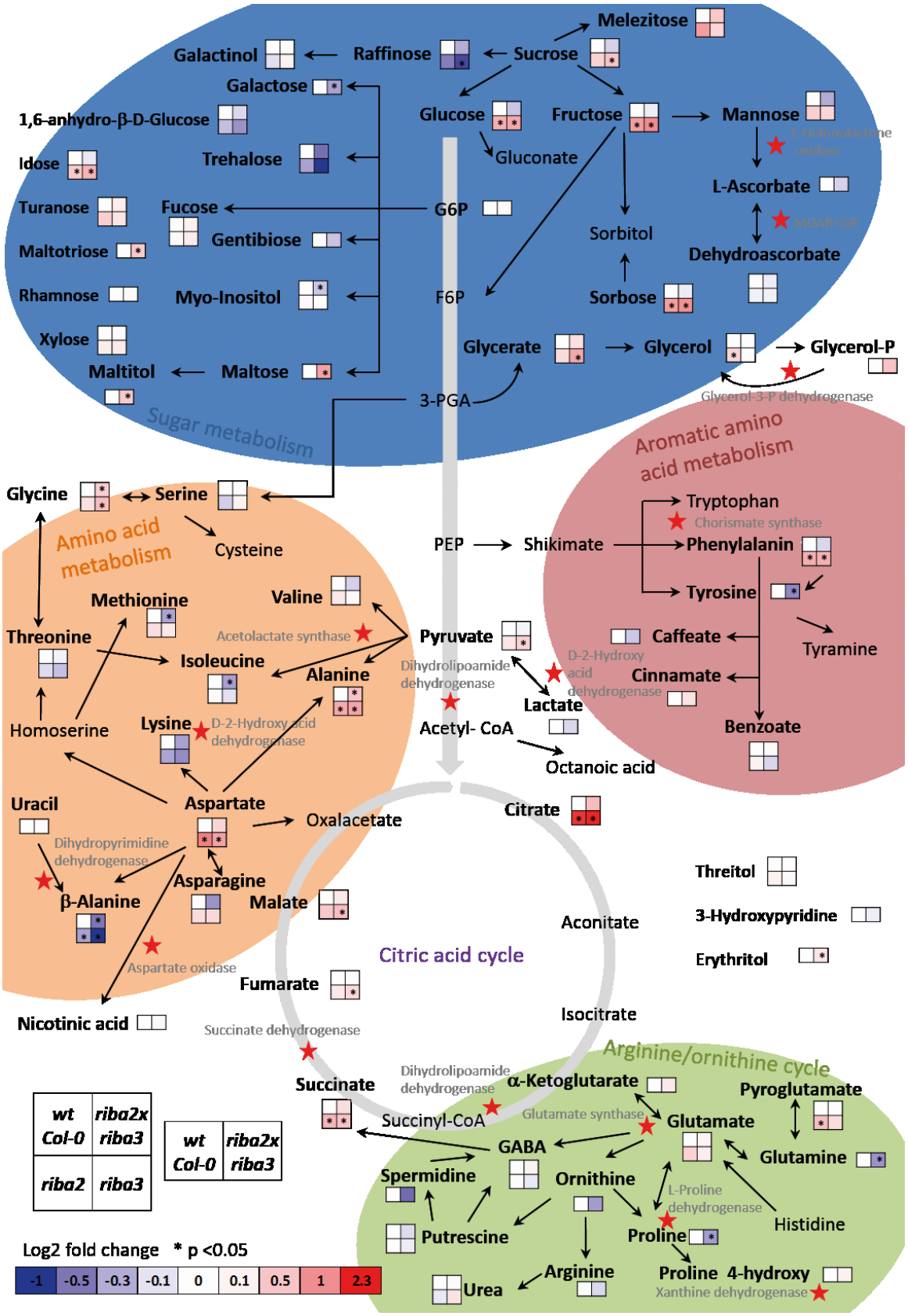

Figure 61: **Metabolome of riba2, riba3 and riba2xriba3 T-DNA mutants.**
Metabolome data presented as fold change compared to *wt Col-0* of 8-week-old *riba2* and *riba3* single and *riba2xriba3* double knockout mutants grown under short-day conditions (100 µmol photons $m^{-2}s^{-1}$ light intensity). Red stars mark flavin-dependent enzymes. Values are means of 6-8 biological replicates, asterisks indicate values that were significantly different compared to control ($p<0.05$, calculated with unpaired two-tailed Student's t test).

3.7 Searching for Interaction Partners

The identification of interaction partners can give valuable insights into the function of a protein within the biological system. It is proposed that integral enzymes of metabolic pathways like RIBA1 are embedded in multienzyme complexes to ensure substrate channeling. Therefore, the search for RIBA1 interacting enzymes of the riboflavin biosynthesis pathway was one of the aims of these studies. For RIBA2 as well as for RIBA3 the search for interacting proteins is of special interest, since the metabolic roles of both proteins are not yet understood and their participation in riboflavin biosynthesis still awaits confirmation.

3.7.1 Pull-down from Chloroplast Extract Using Recombinant RIBA1 Protein

For a first attempt, recombinant RIBA1 was purified as described in 2.9.5 and bound to Ni-NTA resin ("bait") for a pull-down assay, performed as described in 2.18.1. The pull-down was performed with total chloroplast extracts or stroma extracts, since RIBA was shown to reside in the stroma (**Figure 62**).

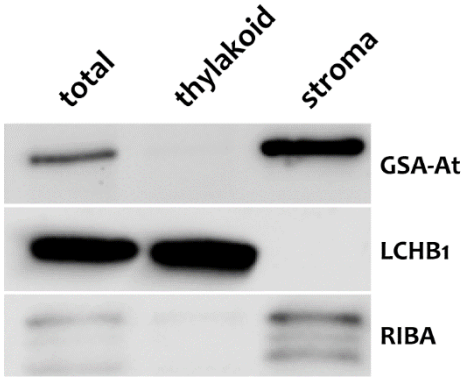

Figure 62: **Subplastidial localisation of RIBA1.**
Western blot analysis of the total chloroplast fraction, the thylakoid fraction and the stroma fraction isolated from 4-week-old *Arabidopsis wt Col-0* plants using GSA-At, LHCB1 and RIBA antibodies, demonstrating the degree of purity of each fractions and the residence of RIBA in the soluble stroma fraction.

The pull-down from total chloroplast extracts was performed twice, wherein each time the eluate was loaded twice on SDS-PA gel and analysed via LC-MS as two technical replicates, resulting in total of four analysed fractions (pull-down 1). For the assay using stromal chloroplast extracts, the eluate of one pull-down experiment was also analysed twice (pull-down 2). In order to distinguish between specifically and unspecifically bound "prey" proteins two controls were used and treated in parallel: 1.) YCF54, which was provided by J. Herbst/A. Girke and the results described in the doctoral thesis of A. Girke (Girke, 2015) and 2.) unbound Ni-NTA resin representing the control without bait. LC-MS analyses of tryptic digests and the subsequent identification of the peptides were performed by Dr. Sascha Rexroth and co-workers (Plant Biochemistry, Ruhr-University Bochum).

The results were arranged due to their "peptide-spectrum matches" (PSMs) value and categorised according to the following criteria:

Set I: The protein is detected in all measured RIBA1 pull-down fractions and in none of the measured control fractions.

Set II: The protein is detected in six of the six measured RIBA1 pull-down fractions. It can also be detected in some of the control fractions, whereas their value of the summarised PSMs is always lower than of the RIBA1 pull-down fractions.

Set III: The protein is detected in five of the six measured RIBA1 pull-down fractions. It can also be detected in some of the control fractions, whereas their value of the summarised PSMs is always lower than of the RIBA1 pull-down fractions.

Set IV: The protein is detected in four of the six measured RIBA1 pull-down fractions. It can also be detected in some of the control fractions, whereas their value of the summarised PSMs is always lower than of the RIBA1 pull-down fractions.

In all cases, plastidic localisation was verified via TAIR and TargetP.

The results of the pull-down analysis are presented in **Table 40**. Thereby an unknown protein (AT1G75335) and the porphobilinogen deaminase HEMC (AT5G08280) were found in set I. ERA-1 (AT5G66470), which has been hypothesised to have RNA-/GTP-binding activity (Suwastika *et al.*, 2014), and RUBISCO large subunit (ATCG00490) were detected and assigned to set II. Interestingly,found RIBA2 in the analysis and was assigned to set III. DIHYDRODIPICOLINATE SYNTHASE 2 (AT2G45440), which has been shown to be involved in lysine biosynthesis (Griffin *et al.*, 2012), is the only representative of set IV.

***Table 40*: Potential RIBA1 interactors, assessed by affinity chromatography on His-tagged recombinant RIBA1 protein.** Incubation was done with chloroplast total or stromal extracts and measured by LC-MS. Criteria for grouping the proteins are described in the text above.

Set	#	Protein	Role	AGI ID	Ø PSMs
I	1	Unknown Protein	Unknown	AT1G75335	9.7 ± 1.5
	2	HEMC, HYDROXYMETHYLBILANE SYNTHASE	porphobilinogen deaminase activity, amino acid/cysteine biosynthesis, MEP pathway, defence responses	AT5G08280	4.3 ± 0.6
II	3	ERA-1	RNA-/GTP-binding, MEP pathway	AT5G66470	7.3 ± 0.6
	4	RBCL	PPP	ATCG00490	10.3 ± 1.2
III	5	RIBA2	Riboflavin biosynthesis, DHBPS activity	AT2G22450	118 ± 2.2
IV	6	DIHYDRODIPICOLINATE SYNTHASE 2 (DHDPS2)	diaminopimelate biosynthetic process, lysine biosynthetic process via diaminopimelate	AT2G45440	2.5 ± 0.4

3.7.2 CO-IP via Strep-affinity Purification from Chloroplast Extracts of Transgenic Plants

Another approach to find possible interactors was followed using the Strep-tactinII system. Therefore, the three *RIBA*-encoding sequences were cloned in frame with an HA-Strep tag in the *CaMV 35S*-driven pXCS-HA-Strep vector. Therefore, *RIBA1*, *RIBA2* and *RIBA3* cDNA sequences without stop codon were amplified with primer combinations CLP1/2, CLP 3/4 and CLP 5/6 (**Table S 3**), respectively, subcloned into pJet1.2 as described in chapter 2.7.9.1. Fragments were digested and subsequently ligated via their *EcoRI* and *XmaI* sites as described in chapters 2.7.9.2 and 2.7.9.3 into the pXCS-HA-Strep. RIBA1-pXCS-HA-Strep was transformed into heterozygous individuals of the *riba1* GABI T-DNA insertion line, RIBA2-pXCS-HA-Strep into the *riba2* T-DNA mutant line and RIBA3-pXCS-HA-Strep into the *riba3* T-DNA mutant line as described in 2.6.4. The T1 generation was selected as described in chapter 2.6.4.1.2. For the *riba1* GABI lines transformed with RIBA1-pXCS-HA-Strep the T1 progenies were examined via PCR for the existence of the T-DNA mutant allele in the respective progeny line as described in chapter 2.7.5.1.

T2 and and T3 progenies were used for chloroplast isolation as described in chapter 2.10.1.2 and stromal protein extracts were used for strepII affinity purification as described in chapter 2.18.1.2. As control, the same procedure was performed with plants expressing YCF54-HA-Strep (received from J. Herbst/A. Girke (Girke, 2015)) and *wt Col-0* extracts and further processed as described in chapters 2.18.1.2 and 2.18.1.3.

The results from the LC-MS analysis were arranged due to their "peptide-spectrum matches" (PSMs) value and categorised according to following criteria:

Set I: The protein is detected in all measured RIBA CO-IP fractions and in none of the measured control fractions.

Set II: The protein is detected in all measured RIBA CO-IP fractions and in none of the measured wt control fractions. It can also be detected in YCF54 control fractions, whereas their value of the summarised PSMs is always lower than of the RIBA CO-IP fractions.

Set III: The protein is detected in all measured RIBA CO-IP fractions and in none of the measured YCF54 control fractions. It can also be detected in wt control fractions, whereas their value of the summarised PSMs is always lower than of the RIBA CO-IP fractions.

Set IV: The protein is detected in all measured RIBA CO-IP fractions and in none of the YCF54 control fractions.

Results for RIBA1 are presented in **Table 41** for RIBA2 in **Table 42** and for RIBA3 in **Table 43**.

Table 41: **Putative RIBA1 interacting proteins.**
The proteins were purified by affinity chromatography of Strep tagged RIBA2 protein via Strep tactinII system, and subjected to LC-MS measurement. Incubation was done with chloroplast total or stromal extracts. Criteria for grouping of the proteins were described in the text above. Proteins that were detected in CO-IP experiments with other RIBA proteins are presented in bold letters.

Set	#	Protein	Role	AGI ID	Ø PSMs
III	1	BIOTIN CARBOXYL-CARRIER PROTEIN 1 (BCCP1)	Subunit of the acetyl-CoA carboxylase complex	AT5G16390	3.5 ±0.4
	2	BIOTIN CARBOXYL-CARRIER PROTEIN 2 (BCCP2)	Subunit of the acetyl-CoA carboxylase complex	AT5G15530	2.3 ±0.6
IV	3	FRUCTOSE-BISPHOSPHATE ALDOLASE 3 (FBA3)	Reversible reaction of fructose-1,6-bispohosphate to DHAP and G3P during glycolysis and Calvin cycle	AT2G01140	13 ±0.6
	4	**TRIOSE-PHOSPHATE/ PHOSPHATE TRANSLOCATOR (TPT1)**	**Transport of Triose-phosphates into cytosol for biosynthesis of sucrose, cysteine biosynthesis (IV in RIBA2)**	**AT5G46110**	**6.5 ±0.9**
	5	TRANSLOCON AT THE INNER ENVELOPE MEMBRANE OF CHLOROPLASTS 22-IV (TIC22-IV)	Guidance of preproteins from TOC through IMS to TIC	AT4G33350	1.8 ±0.6
?		**CP12 DOMAIN-CONTAINING PROTEIN 1 (CP12-1)**	**Involved in the formation of a supramolecular complex of GAPDH and PRK, negative regulator of reductive PPP**	**AT2G47400**	**4.8 ±0.4**

In the co-immunoprecipitation assays of RIBA1 and possible interacting proteins from the stroma extracts of 4-week-old heterozygous *riba1* GABI T-DNA insertion line plants, expressing RIBA1-pXCS-HA-Strep, no proteins met the criteria of sets I and II. BIOTIN CARBOXYL-CARRIER PROTEIN 1 and 2 (AT5G16390, AT5G15530) were detected and assigned to set III. These two proteins are isoforms of the biotin carboxylase-carrier subunit of the heteromeric acetyl-coenzyme A carboxylase (ACCase) catalysing the carboxylation of acetyl-CoA to malonyl-CoA (Li *et al.*, 2011), the substrate of the fatty acid synthase (FAS) (Brown *et al.*, 2010). The following two proteins were detected and assigned to set IV. 1.) FRUCTOSE-BISPHOSPHATE ALDOLASE 3 (FBA3, AT2G01140), which catalyses the reversible conversion of fructose 1,6-bisphosphate to dihydroxyacetone phosphate (DHAP) and glyceraldehyde 3-phosphate (G3P) and therefore, constitutes an important regulator of photosynthetic carbon flux (Uematsu *et al.*, 2012). 2.) TRANSLOCON AT THE INNER ENVELOPE MEMBRANE OF CHLOROPLASTS 22-IV (TIC22-IV, AT4G33350), which is an important component of the protein import machinery into the chloroplast (Rudolf *et al.*, 2013).

Table 42: **Putative RIBA2 interacting proteins.**
The proteins were purified by affinity chromatography of Strep tagged RIBA2 protein via Strep tactinII system, and subjected to LC-MS measurement. Incubation was done with chloroplast total or stromal extracts. Criteria for grouping of the proteins were described in the text above. Proteins that were detected in CO-IP experiments with other RIBA proteins are presented in bold letters.

Set	#	Protein	Role	AGI ID	Ø PSMs
I	1	L-Aspartase-like family protein	Adenylosuccinate lyase activity in purine metabolism	AT1G36280	2 ±0.5
II	2	Phosphoribosyltransferase family protein (PRS1)	ribose-phosphate diphosphokinase activity in purine metabolism	AT2G35390	8.5 ±1.2
	3	ALPHA-GLUCAN PHOSPHORYLASE 1 (PHS1)	Starch metabolism	AT3G29320	3.3 ±1
	4	GLYCERALDEHYDE-3-PHOSPHATE DEHYDROGENASE OF PLASTID 2 (GAPCP-2)	Glycolysis	AT1G16300	3.5 ±0.4
III	5	pfkB-like carbohydrate kinase family protein	Fructokinase activity (during glycolysis)	AT1G66430	1.3 ±0.4
IV	6	**TRIOSE-PHOSPHATE/ PHOSPHATE TRANSLOCATOR (TPT1)**	**Transport of Triose-phosphates into cytosol for biosynthesis of sucrose**	**AT5G46110**	**8.5 ±1.2**
	7	**Phosphoenolpyruvate carboxylase family protein**	**Functional annotation according to sequence homology as isocitrate lyase**	**AT1G21440**	**1.8 ±0.4**
	8	ABERRANT GROWTH AND DEATH 2 (AGD2)	L,L-diaminopimelate aminotransferase, lysine biosynthesis	AT4G33680	1.8 ±0.5
?		**CP12 DOMAIN-CONTAINING PROTEIN 1 (CP12-1)**	**Involved in the formation of a supramolecular complex of GAPDH and PRK, negative regulator of reductive PPP**	**AT2G47400**	**3.3 ±0.6**

In the co-immunoprecipitation of RIBA2 and possible interacting protein from stroma extracts of 4-week-old homozygous *riba2* SALK T-DNA insertion line plants expressing RIBA2-pXCS-HA-Strep one protein was detected and assigned to set I. Namely, the protein annotated as L-aspartase-like family protein (AT1G36280) containing a C-terminal adenylosuccinate lyase domain, which catalyses the conversion of phosphoribosylaminoimidazole succinocarboxamide (SAICAR) to aminoimidazole carboxamide ribonucleotide (AICAR). AICAR is the precursor of inosine mono phosphate (IMP) that, on the other hand, is an intermediate of the purine metabolism and hence important for GTP synthesis. Interestingly, the protein detected in set II is also a component of the purine metabolism pathway, located upstream of the formation of SAICAR. Namely, a protein annotated as phosphoribosyltransferase family protein (PRS1, AT2G35390), which catalyses the reversible formation of 5-phospho-ribosyl-α-1-diphosphate (PRPP) by the transfer of a diphosphoryl group from ATP to ribose-5-phosphate (Krath *et al.*, 1999). In set II, also the ALPHA-GLUCAN PHOSPHORYLASE 1 (PHS1, AT3G29320) was detected, an enzyme catalysing the phospholytic degradation of starch by the phosphorylation of the terminal glycosyl residue at the nonreducing end of glucan chains (Zeeman *et al.*, 2004, Smith *et al.*, 2005). The next protein on the list, also assigned to set II, was one of the chloroplastic isoforms of GLYCERALDEHYDE-3-PHOSPHATE DEHYDROGENASE OF PLASTID 2 (GAPCP-2, AT1G16300), which is the protein performing the conversion of G3P to glycerate 1,3-bisphosphate during glycolysis (Muñoz-Bertomeu *et al.*, 2009).

The only protein found in set III was the pfkB-like carbohydrate kinase family protein (AT1G66430) that is, based on its protein sequence, hypothesised to be able to catalyse the phosphorylation of fructose to fructose 6-phosphate (Plant Metabolic Network). ABERRANT GROWTH AND DEATH 2 (AGD2, AT4G33680), exhibiting LL-diaminopimelate aminotransferase activity during lysine biosynthesis (Hudson *et al.*, 2006), represented set IV.

Table 43: **Potential RIBA3 interacting proteins.**
The proteins were purified by affinity chromatography of Strep tagged RIBA3 protein via Strep tactinII system, and subjected to LC-MS measurement. Incubation was done with chloroplast total or stromal extracts. Criteria for grouping of the proteins were described in the text above. Proteins that were detected in CO-IP experiments with other RIBA proteins are presented in bold letters.

Set	#	Protein	Role	AGI ID	Ø PSMs
II	1	CYCLOPHILIN 38 (CYP38)	Peptidylprolyl cis/trans isomerase activity	AT3G01480	5.5 ±0.8
IV	2	**TRIOSE-PHOSPHATE/ PHOSPHATE TRANSLOCATOR (TPT1)**	**Transport of Triose-phosphates**	**AT5G46110**	**3.5 ±0.8**
	3	**Phosphoenolpyruvate carboxylase family protein**	**Isocitrate lyase, glucosinolate biosynthesis**	**AT1G21440**	**1.3 ±0.4**
?		**CP12 DOMAIN-CONTAINING PROTEIN 1 (CP12-1)**	**Involved in the formation of a supramolecular complex of GAPDH and PRK, negative regulator of reductive PPP**	**AT2G47400**	**4.3 ±0.5**

Proteins detected in the co-immunoprecipitation of RIBA3 and possible interacting proteins from stroma extracts of 4-week-old homozygous *riba3* SALK T-DNA insertion line plants expressing RIBA3-pXCS-HA-Strep are listed in **Table 43**. No protein was detected that meets the criteria of set I. CYCLOPHILIN 38 (CYP38, AT3G01480), which performs the enzymatic activity of a peptidylprolyl cis/trans isomerase (PPIase) and is hypothesised to be important for the biogenesis of photosystem II (Sirpiö *et al.*, 2008) met the criteria of set II.

The following proteins were found in more than one CO-IP experiments: 1.) TRIOSE-PHOSPHATE/ PHOSPHATE TRANSLOCATOR also called ACCLIMATION OF PHOTOSYNTHESIS TO THE ENVIRONMENT 2 (TPT1/APE2 AT5G46110) was found in set IV of all three RIBA proteins. It exports fixed carbon in form of G3P and 3-phosphoglycerate (3-PGA) from the chloroplast into the cytosol in strict 1:1 exchange with inorganic phosphate P_i (Flügge, 1999, Schneider *et al.*, 2002). 2.) The phosphoenolpyruvate carboxylase family protein (AT1G21440) was found in set IV of RIBA2 and RIBA3 and is hypothesised, according to sequence homology, to have isocitrate lyase activity during the glyoxylate cycle, which is located in glyoxysomes (Eprintsev *et al.*, 2009). The protein sequence on the other hand gives strong indications that this protein is imported to the chloroplast. 3.) CP12 DOMAIN-CONTAINING PROTEIN 1 (CP12-1, AT2G47400) is mentioned here, because, it was found in all three experiments, although it did not meet the criteria for set IV. It is a protein involved in the GAPDH and phosphoribulosekinase (PRK) complex formation, and hence, has an important role as a negative regulator of the Calvin-Benson cycle (Taiz *et al.*, 2015).

3.7.3 Bimolecular Fluorescence Complementation for Detection of Homo- and Heterodimerisation of RIBAs via DHBPS Domain

RIBA2 was introduced as a possible interacting protein of RIBA1 in the pull-down studies presented in **Table 40**. Homodimerization of bifunctional RIBA proteins has already been shown before in *Mycobacterium tuberculosis* (Singh *et al.*, 2013). Therefore, the purpose of this experiment was to explore 1.) possible homodimerisation of RIBA proteins as presented by Singh *et al.* (2013) and 2.) heterodimerisation between different plant RIBA isoforms as indicated in 3.7.1 for RIBA1 and RIBA2.designed bimolecular fluorescence complementation constructs, which contained the coding sequences of all three *Arabidopsis* RIBA isoforms as well as partial sequences of the functional domains of RIBA1, each fused to the C- and N-terminal part of YFP. Constructs that were used are described in **Table 44**. Inserts were amplified using primers stated in **Table 44** as described in chapter 2.7.5.2. For the design of the GCHII constructs, the sequence coding for the 5' terminal transit peptide had to be amplified separately and fused to the coding sequence of GCHII by overhang extension PCR as described in chapter 2.7.5.3. The inserts were subcloned in pJet1.2 as described in chapter 2.7.9.1 and cut with *Spe*I/*Sal*I. pSpyCE-35S and pSpyNE-35S were digested with *Spe*I/*Xho*I. The ligation was conducted as described in chapter 2.7.9.3. All possible N- and C-terminal YFP combinations were expressed in *N. benthamiana* via Agrobacteria mediated transient transformation of *N. benthamiana* leaves. The interaction of proteins or protein fragments fused to either terminal parts of YFP will become visible through spatial reconstitution of the functional YFP protein emitting fluorescence upon excitation. In this case through the simultaneous recording of chlorophyll autofluorescence and the possible overlay with the YFP signal emitted by interacting proteins, the subcellular localisation of the interaction between the two target proteins could be determined.

Table 44: **Constructs used for BIFC.**
The sequences of the primers indicated here are listed in **Table S 3**.

#	Designation	Insert	Vector	Primers
1	RIBA1-pSpyCE	RIBA1 full-length	pSpyCE	CLP22/23
2	RIBA1-pSpyNE		pSpyNE	
3	RIBA2-pSpyCE	RIBA2 full-length	pSpyCE	CLP24/25
4	RIBA2-pSpyNE		pSpyNE	
5	RIBA3-pSpyCE	RIBA3 full-length	pSpyCE	CLP26/27
6	RIBA3-pSpyNE		pSpyNE	
7	DHBPS-pSpyCE	RIBA1 DHBPS domain	pSpyCE	CLP22/28
8	DHBPS-pSpyNE		pSpyNE	
9	GCHII-pSpyCE	RIBA1 GCHII domain fused to transit peptide via overlap	pSpyCE	CLP22/29
10	GCHII-pSpyNE		pSpyNE	CLP30/23

The detected signals were classified into four categories, which are shown in **Figure 63**.

1.) globular structures within the chloroplasts, 2.) homogenous plastidic signal matching with chlorophyll autofluorescence (plastidic signal, PS), 3.) mixture of 1.) and 2.), as well as 4.) showing no signal (except chlorophyll autofluorescence).

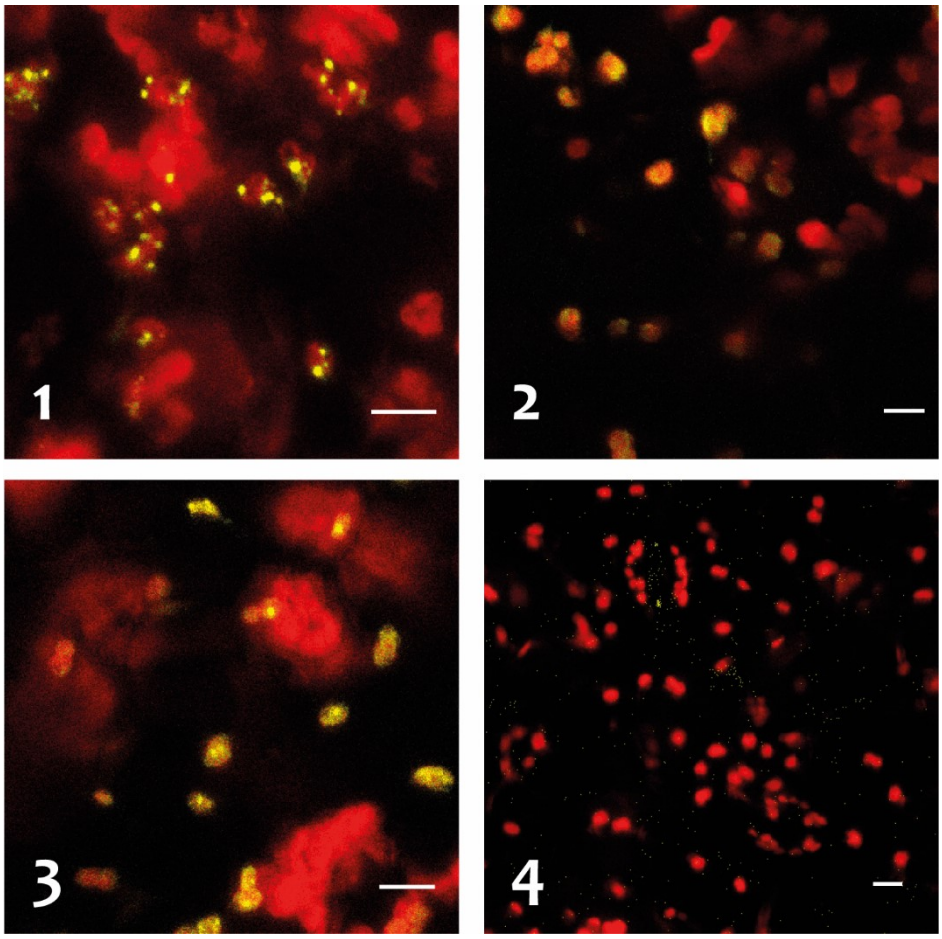

***Figure 63:* Categorisation of signals attained during BiFC study of RIBA proteins.**
Representative cLSM images as a merge of chlorophyll fluorescence (red) and YFP fluorescence following BiF complementation (yellow), depicting classification described in the text above. Scale bar represents 10 µm.

An overview of the results of the BiFC study is presented in **Figure 64**. All combinations of RIBA full-length constructs expressed with each other resulted in globular structures within the chloroplasts (cat. 1). The combination of two full-length RIBA2, each expressed with the two YFP halfs, generated only a faint fluorescence that could be interpreted as a weak plastidic signal (cat. 2). The combination of RIBA1 DHBPS fragment with itself and with the GCHII fragment resulted a plastidic signal (cat. 2). When the GCHII fragment was expressed with the two YFP parts, no YFP derived signal could be observed (cat. 4). When full-length sequences were combined with RIBA1 fragments, mixed signals (cat. 3) were detected in most cases, except when N-terminal YFP-RIBA1-GCHII was expressed in parallel with full-length RIBA2 or RIBA3. Thereby, only a very weak plastidic signal (cat. 2) was observed.

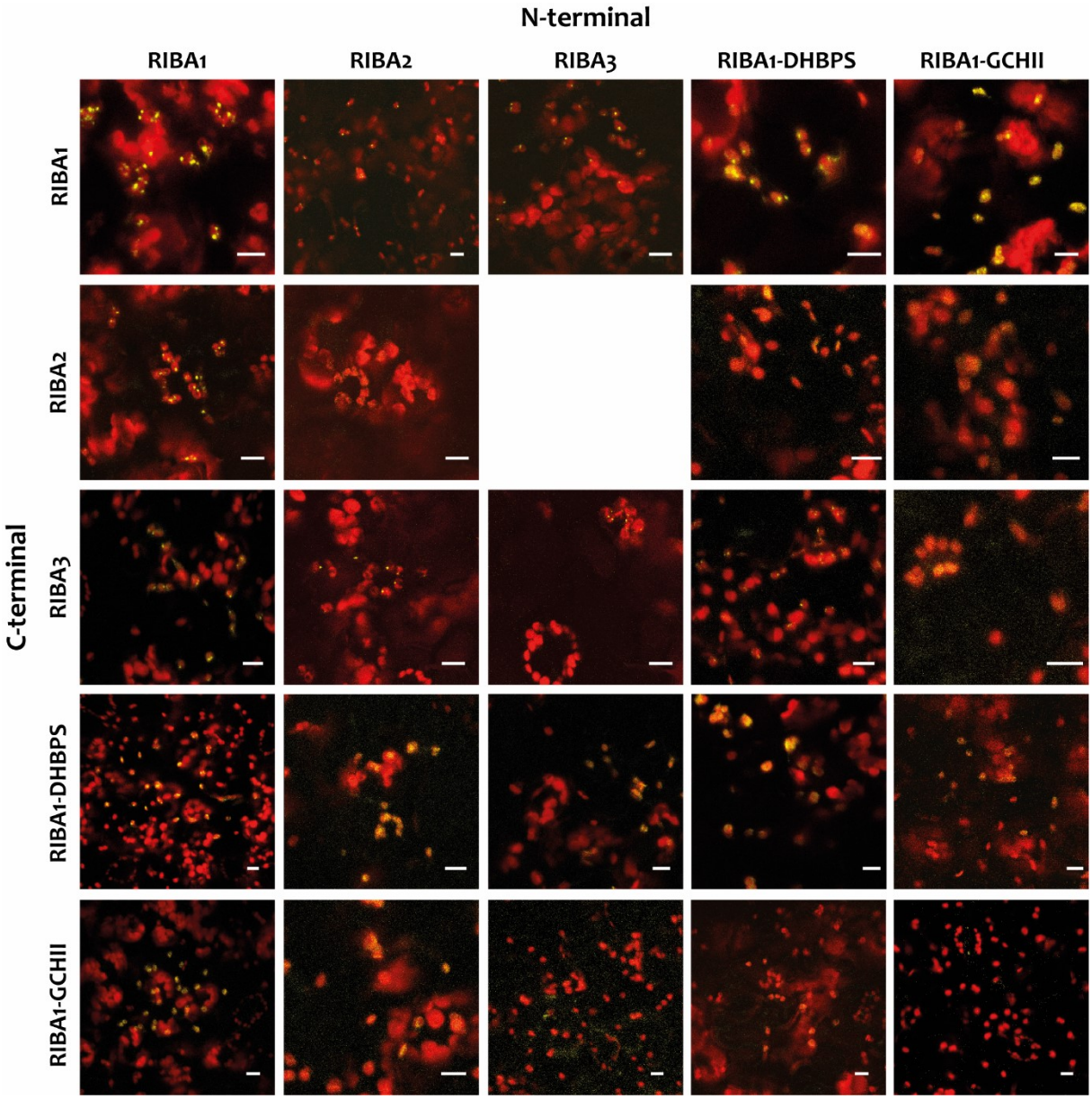

Figure 64: **Homo-and heterodimerisation study of RIBAs by BiFC.**
N. benthamiana leaves were co-infiltrated with full-length RIBAs and shortened RIBA1 fragments either fused to C' or N' terminal fragment of YFP. The RIBA1 fragments contained either only the DHBPS domain (RIBA1-DHBPS) or only the GCHII domain (RIBA1-GCHII) of RIBA1. Here, cLSM images as a merge of chlorophyll fluorescence (red) and YFP fluorescence following BiFC (yellow) are shown. Scale bar represents 10 µm.

When the globular structures were observed, it has to be taken into account that these structures might be artefacts due to the strong transient expression and a precipitation of the full-length proteins. Such aggregations could have led to an unspecific reconstitution of YFP. Therefore, the observations obtained with the combinations of merely full-length proteins were not taken into account and the observations of full-length proteins combined with RIBA1 fragments were handled with caution in the evaluation of the results that are summarised in **Table 45**.

Table 45: **Summary of the BiFC study for homo- and heterodimerisation behaviour of RIBA proteins.**

		N-terminal				
		RIBA1	**RIBA2**	**RIBA3**	**RIBA1-DHBPS**	**RIBA1-GCHII**
C-terminal	**RIBA1**	**?**	**?**	**?**	**possible interaction**	**possible interaction**
	RIBA2	**?**	**?**	**n/a**	**possible interaction**	**possible interaction**
	RIBA3	**?**	**?**	**?**	**possible interaction**	**possible interaction**
	RIBA1-DHBPS	**possible interaction**	**possible interaction**	**possible interaction**	**strong interaction**	**interaction**
	RIBA1-GCHII	**possible interaction**	**possible interaction**	**possible interaction**	**interaction**	**no interaction**

When, full-length fragments were combined with shortened RIBA1 fragments, a mixture of globular structures and plastidic signal was observed (cat.3). This observation suggests that parts of the full-length partners resided in soluble form and parts aggregated. In both conditions, they implemented the interaction with the soluble RIBA1 fragment and hence generated a "mixed" signal (cat.3). The results of the experiments with the shortened RIBA1 fragments support the following conclusions: 1.) A strong interaction was observed between RIBA1-DHBPS fragments. 2.) GCHII fragments did not interact with each other. 3.) DHBPS fragments combined with GCHII fragments seem to interact as well, but not as strongly as two DHBPS fragments. 4.) The combination of all full-length proteins with DHBPS or GCHII resulted a mixed signal (cat.3). The latter could be interpreted as an interaction, but must be seen cautiously due to above mentioned reasons and should be verified with the respective shortened fragments of RIBA2 and RIBA3.

4 Discussion

"What are called GMOs are done by changing the genes of the plant. […] And it's pretty incredible, because it reduce[s] the amount of pesticide[s] you need, raises productivity [and] can help with malnutrition by getting vitamin fortification." was stated by Bill Gates recently at the World Economic Forum in Davos when he was asked about his opinion on green biotechnology (Gates, 2016). Ariboflavinosis, the medical condition of riboflavin deficiency, concerns around 10 % of the population in developed and even approximately 40 % in undeveloped countries (Latham, 1997). Especially in countries where the diet is poor in milk and meat, riboflavin intake over vegetables is essential. Genetically modified plants can be a prospect to help with this problem. Hence, the importance of the elucidation of the flavin biosynthesis pathway in plants is important beyond the simple fact that it is essential for the survival and optimal growth of the plant itself.

The plant riboflavin biosynthesis was examined biochemically with recombinant enzymes, as well as *IN PLANTA* with transgenic lines lacking of RIBA gene family members. Additionally, *Arabidopsis* and tobacco mutants overexpressing RIBA1 were studied. Moreover, a metabolomics study and a screen for interacting proteins was conducted to gain deeper knowledge on the topic.

The discussion section will be divided according to the two main aims of this thesis, 1.) the characterisation of the RIBA isoforms in *Arabidopsis* thaliana and 2.) the characterisation of effects caused by deregulated flavin biosynthesis by using transgenic plants with increased or decreased RIBA1 contents, the dominant RIBA isoform. Finally, the two additional important aspects of my studies, namely metabolomic and interaction analyses, will be discussed in a third section.

4.1 Characterisation of RIBA Isoforms

The appearance of multiple members in the *RIBA* gene family is a phenomenon that can be traced back to the early bryophytes. In the *Physcomitrella patens* genome, two genes encoding for bifunctional RIBA proteins can be found, while e.g. the chlorophytes *Chlamydomonas reinhardii* and *Ostreococcus trauri* each possess only one gene (**Figure 21**). Already in *Selaginella moellendorfii,* a first, probably mono functional, RIBA3 (mutated DHBPS domain) is present. All angiosperms except the representative of the basal lineage *Amborella trichopoda* share the occurrence of at least three members of the *RIBA* gene family. The physiological role of the multiple members of this family has not been questioned up to date. In this thesis, one of the aims was the characterisation of all three RIBA isoforms, which existence is highly conserved among angiosperms.

4.1.1 Two Members of the *RIBA* Gene Family Have Lost Their Bifunctionality in Riboflavin Biosynthesis

It was demonstrated IN VITRO (**Figure 11**) and IN VIVO (**Figure 14**/**Figure 15**) that two of the three Arabidopsis RIBA isoforms, namely RIBA2 and RIBA3, have lost their bifunctional activity in the riboflavin biosynthesis pathway (Hiltunen et al., 2012). The measurements of enzyme kinetic capacities of the remaining enzyme functions revealed a major decline in the GCHII activity in RIBA3 compared to RIBA1, namely almost three times lower v_{max} and nearly three times higher K_m, indicating a better ability by RIBA1 to utilise GTP than RIBA3 (**Figure 12**). In contrast, it was shown that DHBPS activity in RIBA2 was not negatively influenced by the loss of the GCHII active domain (**Figure 13**). An organ specific expression profile (**Figure 25**) revealed that RIBA1 is the prevalent transcript in all tissues and that all three genes are transcribed in all tissues more or less at the same ratios. The GUS stains of RIBA1, RIBA2 and RIBA3 promoter activities suggest that while expression of RIBA1 was evenly strong in all tissues, RIBA2 and RIBA3 expression was generally weaker and especially weak in reproductive organs (**Figure 26**/**Figure 27).** Recently, Thieme et al. (2015) identified 2,006 mRNAs that were shown to be transported in the phloem of Arabidopsis plants, either from shoot to root or the opposite direction. The authors showed that among the annotated transcripts also *RIBA1* and *RIBA2* (as well as *LS*, *RS* and At*FMN*/*FHY*) are transported from shoot to root at full nutrition conditions. It is possible that RIBA1 and RIBA2 belong to a group of mobile RNAs that are allocated to different plant organs, depending on individual demand. In this case, higher demand for flavin biosynthesis could be caused by developmental or stress related processes.

4.1.2 Protein Properties of RIBA1 Missing in RIBA2 and RIBA3 Hint at a Divergence in Protein Function

In further experiments, it was demonstrated that FMN binds to RIBA1 approximately at a molar ratio of 1:1 (**Figure 16**). When FMN was added to the reaction, GCHII activity of RIBA1 was decreased (**Figure 17**), while riboflavin and FAD only had a minor effect at much higher concentrations that could be interpreted as unspecific (**Figure 18**). The type of inihibition was analysed in an enzyme kinetics assay with rising FMN concentrations (**Figure 19**). It was established that rising FMN concentrations caused the decrease of the maximal reaction rate (v_{max}), while the K_m values increased. This behaviour was interpreted as a so called mixed inhibition (Ochs, 2000) that is characterised by an inhibitor that binds to the enzyme causing a decrease in total enzyme activity (decrease of v_{max}). But instead of blocking the substrate binding site completely (as competitive inhibitors would do) the inhibitor evokes a conformational change that lowers the ability to utilise GTP (increasing K_m).

This is the first description of feedback regulation upon allosteric hindrance by flavins. It has been shown before that proteins of the riboflavin biosynthetic pathway bind riboflavin, e.g. lumazine synthase from *Schizosaccharomyces pombe* (Fischer *et al.*, 2002a, Gerhardt *et al.*, 2002), or riboflavin synthase that was shown to build a complex with riboflavin in yeast (Plaut *et al.*, 1970). There are, however, no reports about inhibition of enzyme activities on post-translational level upon flavin binding (Abbas & Sibirny, 2011). Otherwise, feedback inhibition is a usual mechanism in plants as seen e.g. for L-ascorbate on L-galactose dehydrogenase in spinach (Mieda *et al.*, 2004) and for lysine on dihydrodipicolinate synthase (Atkinson *et al.*, 2013). Since the actual FMN concentrations in plant cells are unknown so far, it only can be speculated whether concentrations of 0.9 µM FMN, causing a decrease of RIBA1 GCHII activity by 15 %, are reached within chloroplasts and hence how probable this feedback mechanism is *IN PLANTA*.

Reiland *et al.* (2009) identified RIBA1 as a phosphoprotein. They proposed three serine residues at the C-terminus as potential phosphorylation sites. The phosphorylation of RIBA1 could be verified *IN VITRO.* RIBA2 and RIBA3 were included in the analysis, but showed only a weak phosphorylation signal that was interpreted as a non-specific phosphorylation artifact under *IN VITRO* conditions (**Figure 20**). Such non-specific phosphorylation under *IN VITRO* conditions has been demonstrated before for recombinant proteins, in which phosphopeptides were either completely removed (Schramm *et al.*, 1994) or, as in the case of GENOMES UNCOUPLED 4 (GUN4) protein, mutated (A. Richter, unpublished). The physiological meaning of RIBA1 phosphorylation has to be assessed in future. Reversible phosphorylation of proteins is a ubiquitous post-translational modification (PTM), regulating protein functionality in plants by altering the folding of a protein upon the attachment or the removal of a phosphate group (Lehtimäki *et al.*, 2015, Silva-Sanchez *et al.*, 2015). Experiments assessing the physiological relevance of the RIBA1 phosphorylation will be highly interesting in future, due to this specific PTM's potential to influence on the whole flavin biosynthesis pathway through the regulation of the first enzyme. Due to the risk of the potentially harmful pyrimidine intermediates of the riboflavin pathway, the need for an element regulating the RIBA protein activity was previously debated by Frelin *et al.* (2015). Experiments exploring the consequences of phosphorylation or non-phosphorylation, would include recombinant RIBA1 proteins with modified phosphorylation sites. Such experiments could involve either a serine to alanine substitution to prevent the phosphorylation or a serine to aspartate substitution to mimic a constitutively phosphorylated state (Wittekind *et al.*, 1989, Willig *et al.*, 2011, Wang *et al.*, 2015). Furthermore, *IN PLANTA* complementation and localisation experiments by means of RIBA1 proteins with modified phosphorylation sites will give valuable information on the physiological significance of this PTM.

4.1.3 RIBA1 Depletion Has Severe Effects While RIBA2 and RIBA3 Can Be Abolished Without Visible Consequences

The identification of *riba2*, *riba3* and *riba2xriba3* knockout mutants (**Figure 52**/**Figure 53**) demonstrated that RIBA2, as well as RIBA3, can be abolished without any visible phenotypic consequences for *Arabidopsis* (**Figure 54**). In contrast, the examination of the siliques of heterozygous *riba1* mutant plants revealed that the *RIBA1* knockout causes embryo lethality in *Arabidopsis* (**Figure 29**/**Figure 30**). This observation, together with the knowledge that all three RIBA isoforms are targeted to the chloroplast (Hiltunen *et al.*, 2012) and are simultaneously expressed in all tissues (**Figure 25**), led to the hypothesis that RIBA2 and RIBA3 are not able to compensate for the loss of RIBA1.

Taken together, the results presented above might deliver an explanation why RIBA2 and RIBA3 cannot compensate the loss of RIBA1: 1.) the expression of RIBA2 and RIBA3 is much lower, especially in reproductive organs (**Figure 27**). 2.) RIBA3 shows three times decreased GCHII enzyme activity compared to RIBA1 (**Figure 12**). It is reasonable to say, that even if RIBA2 expression and activity would be sufficient for the substitution of the missing DHBPS activity of RIBA1, RIBA3 would not be able to compensate the loss of RIBA1 GCHII activity. It is also possible that for the *IN PLANTA* functionality of the riboflavin biosynthesis it is important that a bifunctional protein performs DHBPS and GCHII enzyme activities. In that case, monofunctional RIBA2 and RIBA3 might hinder each other sterically and hence might not be structurally able to perform both activities in parallel.

As long as the relevance of the phosphorylation of RIBA1 and the regulation of RIBA1 GCHI activity by FMN remain undeclared, both must be accounted as an additional reason for a missing complementation by RIBA2 and RIBA3.

Hence, the continuation of the complementation experiments that were started here (chapter 3.5.4) will be very important in future. It has to be contemplated that *RIBA1* expression by 35S::cAtRIBA1 did not evoke complementation of the *RIBA1* depletion in the *riba1* knockout to overcome embryo lethality. Western blot experiments showed that RIBA1 expression was initiated in plants carrying the 35S::cAtRIBA1 construct. The fact that the *Arabidopsis* line carrying the 35S::cAtRIBA1 construct showed an increase of total flavin amount by 18 % (**Table 33**) supports the assumption that the transgenic RIBA1 protein is fully functional. Hence, the missing complementation must result from misplaced expression at the critical time when complementation has to take place, namely during embryo development.

The time point of the maternal-to-zygotic transition has been evaluated before in tobacco. Zhao *et al.* (2011) demonstrated that independent zygotic gene expression is required for the onset of

embryogenesis. Pillot *et al.* (2010) blocked *RNA POLYMERASE II* expression in *Arabidopsis* zygotes and showed that this led to an arrest of embryo development in the preglobular stage. An analysis with the online tool Gene Expression Map of *Arabidopsis* Embryo Development showed that the *RIBA1* promoter is already highly active at the globular stage (**Figure 65**). Even though the *CaMV35S* promoter is generally considered as a constitutively active promoter, there have been contradicting reports in cotton (Sunilkumar *et al.*, 2002, Bakhsh *et al.*, 2009).

It is proposed that the *CaMV35S* promoter carried expression of *RIBA1* cDNA does not onset early enough to overcome the first stages of embryogenesis when riboflavin biosynthesis is needed. This hypothesis should be tested in future by comparing GUS staining of embryos from transgenic lines carrying the *RIBA1* and *CaMV35S* promoter constructs, described in chapter 3.4.2.

To overcome problems concerning suitable expression strength and time point, it was decided to use *RIBA1* promoter and UTR regions for the complementation constructs described in chapter 3.5.4. By this approach, purely the catalytic properties of RIBA2 and RIBA3 can be assessed and the question whether these isoforms are theoretically interchangeable can be answered.

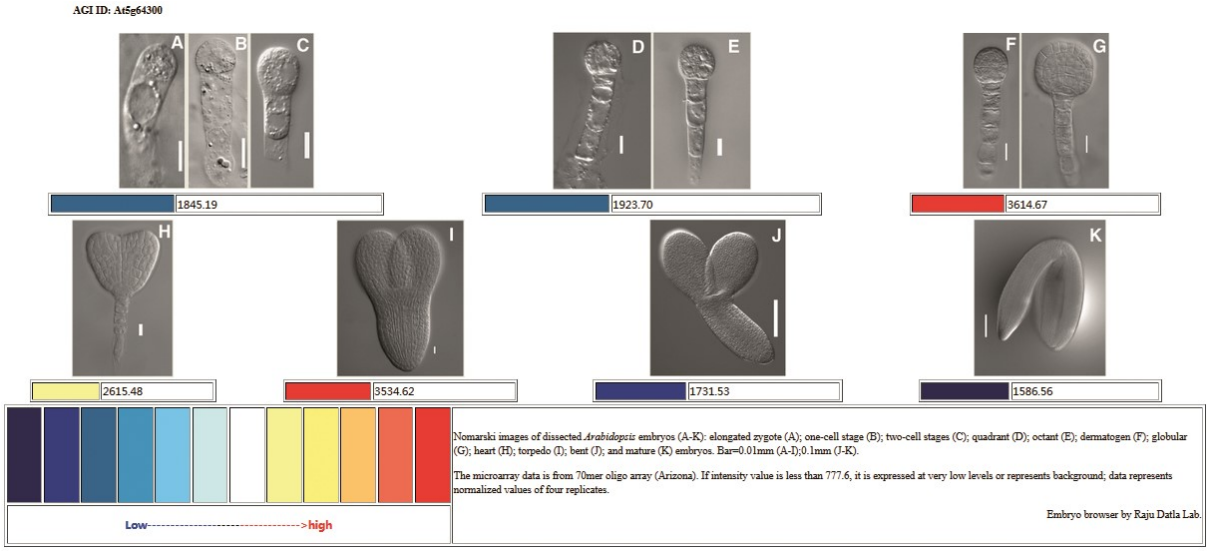

Figure 65: **Screenshot of the Gene Expression Map *Arabidopsis* Embryo Development result for *RIBA1*.**
The figure shows the results of a micro array analysis, assessing the expression strength of *Arabidopsis* genes during embryo development, in this case RIBA1 with the help of a heat map.

4.1.4 Monofunctional RIBA3 Exist Already in Lycophyta, While Monofunctional RIBA2 Exist Only in Brassicaceae

It was shown that monofunctional RIBA3 proteins already occurred before the evolution of spermatophytes (**Figure 21**), while monofunctional RIBA2 occur only in the Brassicaceae family. In fact, the monofunctionality of RIBA2 in the Brassicaceae clade is caused by a single deletion event (**Figure 22**/**Figure 23**).

Since *Arabidopsis* is able to compensate the loss of the GCHII activity by the second originally bifunctional RIBA isoform, it seems that it is not essential for the survival of the plant at the tested growth conditions. It is still possible that RIBA2 has a structural and/or regulatory function that might be important at natural growth conditions, with regular abiotic and biotic stress situations. A role as a scaffold protein would be imaginable to fine-tune RIBA1 activity and hence flavin biosynthesis. A similar hypothesis was reported by Brutinel *et al.* (2013) for a formerly bifunctional RIBA protein with only DHBPS activity in *Proteobacteria*.

The role of the monofunctional RIBA3 protein, however, remains questionable. It is possible that during the evolution of vascular plants, it has gained a function in a different metabolic pathway. Spoonamore, et al., 2006 have assessed similar questions in *Streptomyces coelicolor* where three open reading frames, encoding for GCHII proteins, were identified. They established that all three GCHII proteins produced slightly different molecules.

In plants, the fusion of the DHBPS and GCHII domains remains consitently and monofunctionalities (as demonstrated in **Figure 10**) are caused by exchanges of amino acid residues within the functional domains. The appearance of bifunctional and monofunctional RIBA isoforms in general is a phenomenon that can be traced back to the bacterial evolution (**Figure 24**). It could be demonstrated that bifunctional RibA proteins were the primordial form and that the monofunctional proteins appeared as the result of several gene fission events during the evolution of bacteria and fungi (Snel *et al.*, 2000). Knegt *et al.* (2008) as well as Herz *et al.* (2000) studied this phenomenon of the appearance of different kind of RibA forms in bacteria. They hypothesised that monofunctional forms have evolved because they constituted an advantage through a higher flexibility at unfavourable conditions. Moore (2004) elaborated this phenomenon in a review describing advantages of bifunctional proteins and the simultaneous occurrence of bi- und monofunctional proteins. Also here, regulatory and structural advantages are accentuated. It is stated that bifunctional proteins have evolved due to comparably limited proteome size in eukaryotes and the need for a dense connection of regulatory networks (Mattick & Gagen, 2001). It is considered that on the one hand bifunctional proteins, involved in major metabolic pathways, constitute an advantage due to coordinated expression and activity, but on the other hand the simultaneous existence of monofunctional proteins can in some situations ensure the adequate supply with both intermediates, as in the case of dihydrofolate reductase (Cella & Parisi, 1993).

Alternative roles of RIBA2 and RIBA3 were further assessed in *Arabidopsis* by metabolomic and interaction studies. The results are discussed in chapters 4.3 and 0.

4.2 Effects of a Deregulated Flavin Biosynthesis on Plants

4.2.1 Antisense and VIGS

Since *riba1* knockout mutants are not viable, different approaches were chosen to study the effects of *RIBA1* depletion. Firstly, transgenic Arabidopsis lines expressing antisense *RIBA1* mRNA were analysed. Their phenotype obtained by *RIBA1* depletion (**Figure 33**/**Figure 34**) was expectedly severe. Loss of almost one third of total flavin amount in the whole plant (**Table 33**) was accompanied by a bleaching phenotype (**Figure 32**), which spread continuously during leaf development and finally affected the entire plant leading to developmental arrest. Alternatively, RIBA1-VIGS experiments were performed to make use of a second *RIBA1* silencing approach. This second method was applied to differentiate better between primary and pleiotropic effects of silenced gene in plants. The data attained from the RIBA1-VIGS plants confirmed the observations which were obtained by the antisense *RIBA1* plants regarding the bleaching phenotype (**Figure 44**), altered RIBA protein content (**Figure 46**) and the flavin amounts (**Table 34**), as well as the expression pattern of the flavin biosynthesis genes (**Figure 45**/**Figure 47**).

While the bleaching phenotype of photoperiodically grown plants normally spread over the whole rosette of the plant and were followed by a subsequent arrest in development, these processes could be rescued by moving the plants under continuous light conditions (**Figure 41**). The continuous bleaching over the entire rosette could be stopped and young green leaves started to develop. This phenomenon hints at a special physiological reconstitution at continuous light conditions helping the plant to over-come the silencing of the *RIBA1* transcripts. Effects of continuous light conditions rescuing physiological defects have been reported before for circadian clock mutants (Michael *et al.*, 2008), the starch deficient mutant *phosphoglucomutase* (Caspar *et al.*, 1985, Smith & Stitt, 2007) and mutants with defects in chlorophyll biosynthesis, e.g. lacking GUN4 (Peter & Grimm, 2009). Interestingly, Maruta *et al.* (2012) reported that i.e. *RIBA1* transcript levels significantly increased in *wt Col-0* plants under continuous light conditions (Velez-Ramirez *et al.*, 2011). It is speculated that a boost of endogenous *RIBA1* expression in the antisense *RIBA1#2* plants under continuous light overcomes the antisense effect as seen by the recovered RIBA protein content (**Figure 42**) and flavin amounts (**Figure 43**). The reasons why riboflavin biosynthesis gene expression accelerates under continuous light conditions could be explained by a higher demand for flavins in continuous light-grown plants. It has been determined that plants under continuous light have to cope with oxidative stress. Hence, there is a demand for the antioxidant systems. Yabuta *et al.* (2007) demonstrated that plants adapted to continuous light contain significantly more L-ascorbate, whose synthesis on the other hand requires FAD.

Similar effects of flavin deficiency including the beaching phenotype have been described in *Arabidopsis* for the lumazine synthase mutant *cos1* (personal communication D. Xie) and the pyrimidine reductase mutant *photosensitive1* (*phs1*) (Ouyang *et al.*, 2010). Ouyang *et al.* (2010) delivered the sole detailed report about a flavin deficiency plant mutant up to date. The phenotype of the *phs1* mutant, which lacks the full-length PYRR protein (already described in chapter 1.3.4), significantly resembles that of the antisense *RIBA1#2* plants at normal and high light conditions. The bleaching phenotype was postulated to be the result of photooxidative stress due to loss of flavins that are needed by antioxidant systems. Ouyang and co-workers presented higher O_2^- contents, increased superoxide dismutase, dehydroascorbate reductase as well as GR activities at normal and high light conditions. They proposed that higher activity of the antioxidant system leads to consumption of FAD, which is not produced anymore, leading to the reduction of the FAD-dependent FNR activity so that electron flow through PSI is impaired leading to Mehler reaction and the generation of O_2^- at the acceptor side of PSI.

Even though a DAB staining of antisense *RIBA1#2* and RIBA1-VIGS plants, displaying the bleaching phenotype, did not reveal additional accumulation of H_2O_2 compared to wild type, as it was postulated before for flavin-deficient plants by Deng *et al.* (2011). However, it can be assumed that photo-oxidative stress is one main factor for the bleaching of the leaf tissue. The qPCR analysis of marker genes for photo-oxidative stress (**Figure 40**) *BAP1*, *ZAT12* and *GPX7* revealed that these transcripts were strongly up-regulated, indicating the activation of the antioxidant system. Interestingly, *FSD1*, encoding for a Fe-superoxide dismutase, was, in contrast to the assumption, strongly down-regulated. It seems that its expression is somehow hindered possibly as a consequence of the flavin deficiency. In flavin-deficient rats, inhibiting effects on Fe-superoxide dismutase activity have been reported before (Ashoori & Saedisomeolia, 2014). In fact, the lack of H_2O_2 accumulation in RIBA1 deficient tissues could perhaps be explained by a direct consequence of the up-regulated GPX7. GPX7 is known to catalyse the reduction of H_2O_2 to water (Chang *et al.*, 2009).

Transmission electron microscopy analysis of *rfd1* chloroplasts demonstrated that these mutants are characterised by barely structured and less electron-dense chloroplasts (Hedtke *et al.*, 2012). The pigment analysis of the white areas in antisense *RIBA1#2* leaves showed a 60-70 % decrease of all carotenoids (**Figure 31**), except antheraxanthin, which was almost 30 % increased, and zeaxanthin, which was increased above detection limit in the white areas. The accumulation of zeaxanthin may be a sign for photo-oxidative stress. Additionally, it must be kept in mind that the zeaxanthine epoxidase is flavin-dependent so that this effect can also be a consequence of an impaired zeaxanthine turnover.

These results led to the conclusion that flavin deficiency, caused by RIBA1 depletion, led on the one hand to an imbalance in the functionality of the mitochondrial (**Figure 40**) and photosynthetic electron transport chains, as already described by Ouyang *et al.* (2010). And, on the other hand promoted the generation of ROS, through a potential consequence of the loss of photo protective elements (carotenoids and xanthophylls) and antioxidant systems (ascorbate). The malfunctions of the electron transport chains and the lack of adequate amounts of antioxidants are likely the reasons for damage of the photosynthetic structures within the thylakoid membranes (Niyogi, 1999).

Mutants that are characterised by multi-coloured plant parts or completely white plants are called variegation and albino mutants, respectively. While albino plants are characterised by a complete loss of chlorophylls in vegetative parts causing lethality, the variegation mutants were originally defined by Kirk and Tilney-Bassett (1978) as "any plant that develops patches of different colors in its vegetative parts". The development of white and green parts within one leaf is probably the most common variegation phenotype. While the green parts contain normal chloroplasts, the white areas contain only abnormal plastids, deficient in chlorophyll and/or carotenoid pigments. The cells appear to be either photooxidised or blocked at different stages of chloroplast biogenesis (Yu *et al.*, 2007). The latter has been demonstrated by electron microscopy of the chloroplast ultrastructure showing vacuolation and a lack of thylakoid membrane organisation (Wetzel *et al.*, 1994).

The oldest (Rédei, 1967, Röbbelen, 1968) and one of the best characterised variegation mutant in *Arabidopsis* is the *immutans* mutant (Wetzel *et al.*, 1994, Wu *et al.*, 1999). IMMUTANS has been postulated to serve as the plastidial terminal oxidase, involved in the redox pathway that desaturates phytoene to ζ-carotene during carotenoid biosynthesis. IMMUTANS catalyses the oxidation of plastoquinol (PQH_2) to plastoquinone (PQ), which then in turn serves as electron acceptor for phytoene. Hence, IMMUTANS plays and important role both in carotenogenesis and redox state of the plastoquinone pool during chloroplast biogenesis (Foudree *et al.*, 2012). There are a lot of examples for variegated mutants which apart from *immutans* also lack enzymes involved in the carotenoid biosynthesis (Ruiz-Sola & Rodríguez-Concepción, 2012), e.g. phytoene desaturase (Qin *et al.*, 2007) or the ζ-carotene desaturase (Dong *et al.*, 2007). The *variegated 1* and *2* lack FtsH metalloprotease isoforms that have been shown to be important for the photosystem II repair and hence recovery and maintenance of the photosynthetic electron transport chain (Sakamoto *et al.*, 2003). *variegated 3* (Næsted *et al.*, 2004) as well as *gun1* (Koussevitzky *et al.*, 2007, Hu *et al.*, 2014) mutants have been demonstrated to be impaired in chloroplast development. Work on another bleached mutant revealed, it to be impaired in isoprenoid biosynthesis pathway a

metabolic routes connecting to carotenoid and chlorophyll biosynthesis, namely mutant lacking ispH (Hsieh & Goodman, 2005). ispH performs the last step of the plastid-localised non-mevalonate pathway. Several flavin-dependent enzymes are found to be involved in the isoprenoid biosynthesis pathway, like ISOPENTENYL DIPHOSPHATE ISOMERASE 1, which is FAD-dependent and catalyses the conversion of IPP to DMAPP (Phillips *et al.*, 2008). Moreover, flavoenzymes catalyse reactions within the carotenoid biosynthesis pathway, e.g. CAROTENE CIS TRANS ISOMERASE (CRTISO) (Yu *et al.*, 2011) and the zeaxanthine epoxidase that is known to be involved in the conversion of zeaxanthine to violaxanthine. For the zeaxanthine epoxidase, the contribution in carotenoid and ABA-biosynthesis, as well as the xanthophyll cycle (Schwarz *et al.*, 2015) has been postulated. Zeaxanthine epoxidase mutants are characterised by reduced ABA levels, accumulation of zeaxanthine and a phenotype accompanied by slightly yellow-brown leaves (Koornneef *et al.*, Duckham *et al.*, 1991).

Additionally to the initial statement, the role of impaired flavoenzyme function and activity involved in the carotenoid and isoprenoid biosynthesis should also be taken into account. Since isoprenoids are an important factor in providing intermediates for carotenoid and chlorophyll biosynthesis, inactivation of the precursor synthesis could be the primary defect in response to flavin deficiency.

4.2.2 RIBA1 Overexpressor Mutants

There is a big contrast in the effects observed by the reduction and the overexpression of RIBA1 in plants. While the former leads to the severe effects described before, the overexpression of At*RIBA1* in *A. thaliana* as well as *N. tabacum* does not have any visible effects. An average increase of total flavin amounts by 12 % in the tobacco overexpression line leaves (**Figure 51**) and by 18 % in *Arabidopsis* overexpression line plants (**Table 33**) could be measured. In both lines, the riboflavin and FMN contents were more elevated, namely riboflavin 28 % and 53 % and FMN 44 % and 29 % in tobacco and *Arabidopsis*, respectively, in comparison to wt plants. Since the relative proportions of riboflavin and FMN are less, compared to FAD, an increase does not affect the total flavin amount much. A strong increase in free FAD contents is not as probable anyhow due to its instability and tendency to convert back to FMN or riboflavin induced especially by light (Akimoto *et al.*, 2006).

The data demonstrates that the heterologous *Arabidopsis* RIBA1 is functional within the tobacco riboflavin pathway, which is not that surprising given its high degree of homology compared to the endogenous protein sequence. The obvious conclusion is that the high homology results in co-suppression of the endogenous tobacco RIBA transcripts by overexpression of the *Arabidopsis* transgene (**Figure 50**). Moreover, it was clearly shown that it was possible to stimulate the flavin biosynthetic machinery by the overexpression of RIBA1. This coincides with reports from *Pichia*

pastoris (Marx *et al.*, 2008), where riboflavin production could be enhanced through the overexpression of RIB1, the protein which performs GCHII activity in yeast. Hümbelin *et al.* (1999) reported before that the activity of RibBA is rate limiting in flavin biosynthesis in *B. subtilis*.

4.3 Metabolomes of RIBA

4.3.1 Metabolome of *riba1* Mutants Reveals Flavin Deficiency Effects

The reduction of flavin concentrations is prone to have widespread effects on the plant metabolism. Many changes, which were obtained by the metabolome analysis of primary metabolites, were detected in the tested plants (chapter 3.6.1). Here, these changes will be discussed, categorised into three subtopics.

Deregulations Within the Citric Acid Cycle Entail Consequences in Multiple Pathways

Within the citric acid cycle, two proteins are flavin-dependent. It is hypothesised that the flavin deficiency causes a deregulation of the metabolic flux through the citric acid cycle evoking many changes in the adjacent metabolic pathways. The FAD-dependent SUCCINATE DEHYDROGENASE 1 (SDH1) is one out of four subunits of complex II in the mitochondrial electron transport chain. Complex II is responsible for the oxidation of succinate to fumarate, which then in turn is converted via malate to oxalacetate, the precursor of asparate (Azevedo *et al.*, 2006). The impairment of the citric acid cycle at this step could lead to a reduction of aspartate content and hence entail the concerted reduction of homoserine and its derivate threonine. Araújo *et al.* (2011a) studied the effects of an impaired succinate dehydrogenase in tomato plants by expression of the antisense mRNA sequence of isoform 2 of the iron-sulfur binding protein (SDH2). Together with SDH1, SDH2 forms the peripheral unit of complex II and is therefore needed for the oxidation of succinate to fumarate. Araújo and co-workers demonstrated that the impairment of the SDH complex, indicated by significantly decreased succinate dehydrogenase activity entailing increased succinate contents, lead to a reduced rate of the citric acid cycle that was observable in strongly reduced levels of pyruvate, citrate and isocitrate. Like in the RIBA1 deficient plants, aspartate levels were significantly reduced in the antisense SDH2 plants compared to wild type.

Caused by the strongly reduced aspartate levels, the levels of the aspartate-derived amino acids homoserine and threonine were comparably low, while methionine and lysine were significantly increased. The accumulation of methionine can either be explained by the stimulation of the cystathionine γ-synthase (Kim *et al.*, 2002) or by the inhibition of the methionine degradation, which is catalysed by methionine adenosyltransferase. As a result of the latter, the plants might be suffering from a lack of s-adenosyl-methionine (SAM). One of the SAM-requiring enzymes is the

s-adenosylmethionine decarboxylase, which acts in the initiation of the spermidine synthesis by the spermidine synthase (Imai *et al.*, 2004). Reduced spermidine concentrations were determined in 6-week-old antisense *RIBA1#2* plants as well as in strong phenotypic RIBA1-VIGS plants. This could be a consequence of the SAM deficiency.

Further metabolites, which are connected to aspartate metabolism and should be mentioned, are β-alanine and nicotinic acid. β-alanine is synthesised either from aspartate or from uracil. Interestingly, β-alanine content was reduced as aspartate content, while uracil content was significantly increased in 6-week-old antisense *RIBA1#2* and RIBA1-VIGS plants. This shift might be another potential flavin deficiency effect caused by an impairment of the flavoenzyme dihydropyrimidine dehydrogenase, which performs the degradation of uracil to β-alanine (Zrenner *et al.*, 2009). Fujimoto *et al.* (1991) assessed the effect of riboflavin deficiency on dihydropyrimidine dihydrogen activity in rat liver. They demonstrated the decrease of dihydropyrimidine dihydrogen activity to approximately 25 % of control but no changes in uracil levels. The reduction of nicotinic acid could be caused by an impairment of the FAD-dependent aspartate oxidase, which performs the oxidation of aspartate to α-imminosuccinate (Noctor *et al.*, 2006, Macho *et al.*, 2012). β-nicotinate D-ribonucleotide, which is the common precursor of NAD and nicotinic acid (Katoh *et al.*, 2006) is processed from α-imminosuccinate.

The second flavin-dependent protein within the citric acid cycle is the dihydrolimoamide dehydrogenase subunit of the 2-oxoglutarate dehydrogenase (Millar *et al.*, 1999, Timm *et al.*, 2015) performing the oxidative decarboxylation of α-ketoglutarate to succinyl-CoA. The ornithine/arginine cycle derives directly from α-ketoglutarate and has the flavin-dependent glutamate synthase (GOGAT) at the first position catalysing the conversion of glutamine and α-ketoglutarate to glutamate (Temple *et al.*, 1998, Lea & Miflin, 2003, Linka & Weber, 2005). Within the ornithine/arginine cycle ornithine, spermidine and γ-aminobutyric acid (GABA) showed diverging behaviour. This behaviour of all three metabolites hints at a deregulation of this cycle due to flavin deficiency. It is likely that the possible impairment of the 2-oxoglutarate dehydrogenase leads to a redistribution of the products from the TCA cycle via the GABA-shunt to bypass 2-oxoglutarate dehydrogenase and to maintain succinate supply (Fait *et al.*, 2008). Araújo *et al.* (2012) tested the effects of an impaired 2-oxoglutarate dehydrogenase by an antisense approach in tomato. They measured an upregulation of the GABA shunt entailed by significantly increased GABA and significantly decreased ornithine levels. In the case of the flavin-deficient plants, the behaviour of three metabolites were striking, as spermidine and GABA were increased in 4-week-old antisense and weak phenotypic VIGS and decreased in the 6-week-old antisense and strong

phenotypic VIGS plants. The ornithine content, however, showed the opposite behaviour. Especially the GABA and ornithine levels in the 4-week-old antisense RIBA1#2 and weak phenotypic RIBA1-VIGS plants reflect the data gained by Araújo and co-workers (2012). It seems that also here at the early stage of RIBA1 reduction, the GABA shunt is activated, while later the effect inverts leading to less GABA and more ornithine.

Impairment of Flavin-dependent Amino Acid Catabolism

As stated before, many enzymes contributing to the amino acid catabolism are flavin-dependent. Therefore, special attention was paid on the evaluation of changes of metabolite contents connected to these reactions. Several metabolic changes recorded here can be attributed to the flavin deficiency of catabolic proteins.

The unusual accumulation of lysine is explained by the impaired lysine degradation through the FAD-dependent D-2-hydroxy acid dehydrogenase (Engqvist *et al.*, 2009, Araújo *et al.*, 2010). The accumulation of lysine is known to inhibit the aspartate kinase, performing the first step of the biosynthesis of aspartate-derived amino acids and hence contributing to the reduction of homoserine and threonine (Jander & Joshi, 2009) described before. Proline is another amino acid, whose increased contents in flavin-deficient plants can be interpreted as a consequence of an impaired flavoenzyme, namely proline dehydrogenase (PDH). This enzyme performs proline catabolism (Schertl *et al.*, 2014). Mani *et al.* (2002) evoked proline accumulation in *Arabidopsis* by reduction of PDH expression by the introduction of antisense *PDH*.

Isoleucine, as well as the aromatic amino acids tryptophan, phenylalanine and tyrosine were significantly increased in antisense *RIBA1#2* and RIBA1-VIGS plants. Evidence for the involvement of an electron transfer flavoprotein (ETF) in the catabolism of branched chain amino acids including isoleucine (Ishizaki *et al.*, 2006) and aromatic amino acids (Ishizaki *et al.*, 2005) has previously been presented. Ishizaki and co-workers presented elevated levels of aromatic amino acids as well as of the branched chain amino acids valine and isoleucine in the *Arabidopsis etf* mutants exposed to dark-induced starvation. Interestingly, chorismate synthase, the flavoenzyme catalysing the final step of the shikimate pathway (Tzin & Galili, 2010) and hence important for the synthesis of all three aromatic amino acids, is obviously not negatively affected by flavin deficiency.

Nitrogen Assimilation is Prioritised

Remarkably, the asparagine content was strongly increased, while the content of its precursor aspartate was strongly reduced. Due to its high N:C ratio, is asparagine an important nitrogen storage and transport molecule in plants (Lea *et al.*, 2007). Two enzymes involved in the nitrate assimilation are flavin-dependent, namely the before mentioned GOGAT and nitrate reductase (Lu

et al., 1994). The latter converts nitrate, which is absorbed from soil, to nitrite. Nitrite, however, is a highly reactive and potentially toxic molecule that has to be immediately reduced to ammonium by the nitrite reductase (Taiz *et al.*, 2015). The further processing of ammonium to amino acids requires the sequential action of glutamine synthase and GOGAT to produce glutamine and glutamate, respectively (Gaufichon *et al.*, 2013). Asparagine synthase transfers the amide nitrogen from glutamine to aspartate forming asparagine and glutamate (Taiz *et al.*, 2015). The reverse reaction performed by the asparaginase (Ivanov *et al.*, 2012) involves the degradation of asparagine to ammonium and aspartate.

The interpretation of this data has to be viewed with caution. As mentioned before the effect of flavin depletion affects many metabolic pathways at once. Stitt *et al.* (2010) stated before that technologies in which fluxes are only minimally changed should be used for metabolomics studies of mutations that involve major metabolic changes. Even though plants displaying different degrees of mutant phenotype were chosen in the experimental set-up at hand, the identification of primary and pleiotropic effects is very difficult. In future, an approach with inducible RIBA1 depletion systems, more closely covering the metabolic changes in closer timely manner are advisable. Nevertheless, the data obtained here, gives valuable information about the metabolic situation in flavin deficient plants.

4.3.2 Metabolome of Tobacco At*RIBA1* Overexpressors

For the analysis of metabolic effects of RIBA1 overexpression, two tobacco lines overexpressing AtRIBA1 were chosen. At the time when the metabolome was conducted, the co-suppressor line was not yet identified as such. For the metabolomics analysis non-phenotypic leaves of a plant, displaying a faint bleaching phenotype on older leaves were chosen, corresponding to leaf #5 from the leaf gradient analysis presented in chapter 3.5.2.6. According to the qPCR and flavin analysis conducted (**Figure 50**/**Figure 51**), the decrease of the endogenous *RIBA1* and *RIBA2* transcript levels (70 % and 40 %) did not affect the flavin quantities in the sampled leaves. Therefore, when comparing the two data sets, it must be kept in mind that these samples, which could be assumed to reflect the co-suppressor phenotype, were not derived from plant tissue with decreased flavin contents.

The metabolic pattern of the At*RIBA1* overexpression and the co-suppression line was more or less identical and can be described as a general down-regulation of the sugar metabolism and a strong shift towards citric acid cycle and amino acid biosynthesis. This behaviour can be described as a "high energy" metabolism and has normally two reasons. Scenario 1: the plant, which does not experience any additional stress is using the carbohydrates to produce amino acids for protein

production (growth), or scenario 2: the plant, which experiences stress due to energy shortage, shows low carbohydrate levels and degrades proteins in order to use the amino acids as alternative respiratory substrates (Araújo *et al.*, 2011b). In these samples, the exceptions from this low sugar - high amino acid - pattern are malonate, which is assumed to be a catabolism product of β-alanine (Hayaishi *et al.*, 1961, Stinson & Spencer, 1969). The accumulation of the sugar-derived L-ascorbate and dehydroascorbate, which belong to the glutathione ascorbate cycle, is probably an attempt induced to protect the plant from oxidative stress by detoxifying H_2O_2. This defence strategy is seemingly paralleled by the strong reduction of 3-caffeyl, cis- and trans-quinates, which are possibly serving as antioxidants (Hung *et al.*, 2006). The activation of the ascorbate-mediated antioxidant system might be a reaction to the approximately 60 % increased riboflavin content due to At*RIBA1* overexpression (**Figure 51**). As described before in chapter 1.4, at least the external application of riboflavin to plants evokes ROS production and hence the activation of the antioxidant system.

It can only be speculated which one of the above mentioned reasons for the high-energy metabolism implies here. The final interpretation would require further analyses regarding the physiological status of the overexpression plants, e.g. total protein content, dry weight, flowering behaviour and photosynthetic properties. A plant which experiences stress due to energy shortage (scenario 2) would probably display negatively affected physiological properties, whereas a plant from scenario 1 would display positively affected physiological properties. At least the outer view of the At*RIBA1* overexpression line did not reveal any phenotypic changes compared to *SNN* (**Figure 48**).

However, the similarity of the metabolomics pattern of the sampled At*RIBA1* overexpression line and the co-suppression line, in which the latter shows no changes in flavin contents (**Figure 51**), gives reason to ponder upon the data. It must be taken into account that it is possible that the metabolic changes recorded in the At*RIBA1* overexpression line are not due to changes in flavin contents but an unspecific reaction to the heterologous overexpression of transcripts. It would be advisable to repeat the metabolomics experiment with the *Arabidopsis* RIBA1 overexpression line, which was described in chapter 3.5.2.2. That way, a direct comparison to the data obtained with the antisense RIBA1#2 line would be possible.

4.3.3 Metabolome of *riba2* and *riba3* Mutants Reveal Some Metabolic Effects Common to the RIBA Gene Family

The metabolomics analysis of the *riba2*, *riba3* single and *riba2*x*riba3* double mutants was performed with the intention to get insights into the roles of RIBA2 and RIBA3 within the flavin biosynthesis pathway or alternatively into possible alternative roles of the enzymes in other metabolic

pathways. The results, however, turned out to be difficult to interpret concerning any alternative roles of the RIBA isoforms.

The fact that the flavin contents are not altered in the RIBA2 and RIBA3 mutants contradicts the assumption that these proteins are relevant for the flavin biosynthesis. However, it was expected that some regulatory effects might become visible in the metabolomics analysis, which do not become visible by modified flavin contents. Therefore, only metabolites which behave congruently in antisense *RIBA1#2* plants, as well as *riba2* and *riba3* mutants will be discussed.

Contents of trehalose, dehydroascorbate, threonine and β-alanine were reduced, while succinate, asparagine, methionine and phenylalanine amounts were accumulating in all compared samples. As discussed before, the described changes in succinate and β-alanine contents can be linked to possible flavin deficiency effects and suggest conserved roles of RIBA2 and RIBA3 within the flavin biosynthesis pathway. The similar pattern of altered contents of the aspartate-linked metabolites threonine, asparagine and methionine in the antisense *RIBA1#2* plants, as well as the *riba2* and *riba3* single mutant plants could also support the hypothesis that RIBA2 and RIBA3 are somehow involved in the flavin biosynthesis. In contrast, the aspartate content was reduced in the antisense *RIBA1#2* and higher in the *riba2* and *riba3* single mutant plants, which contradicts the proposition.

It shall be noted, that the sampling and measurements of the antisense *RIBA1#2* on the one hand and *riba2* and *riba3* single and double mutant datasets, on the other hand, were performed approximately 3 years apart and that the plants that were sampled were of different age and developmental status. The direct comparison of the datasets must thus be interpreted cautiously.

4.4 RIBA Interaction Study

The aim of the interaction study was to find evidence for a complex including several proteins involved in the riboflavin biosynthesis. The existence of a highly complicated structure consisting of a riboflavinsynthase trimer within an icosahedral lumazine synthase has been postulated in *B. subtilis* (Bacher *et al.*, 1980, Neuberger & Bacher, 1986, Haase *et al.*, 2014). Kis and Bacher (1995) demonstrated substrate channelling for the lumazine synthase/riboflavin synthase complex, which they proved to improve the overall catalytic rate of riboflavin synthesis. Icosahedral lumazine synthase complexes have been identified in spinach (Jordan *et al.*, 1999) and in *Arabidopsis* (Peltier *et al.*, 2006). Singh *et al.* (2013) have shown the dimerisation behaviour for bifunctional *M. tuberculosis* RIBA through the GCHII domain and the DHBPS activity to require the dimeric interface for its catalytic activity (Singh *et al.*, 2011). Richter *et al.* (1999) demonstrated that monofunctional *E. coli* DHBPS protein forms dimers, whereas no information about the organisation of monofunctional GCHII proteins is available.

Additionally, it was hoped that the identification of interacting proteins by pull-down or CO-IP experiments with RIBA2 and RIBA3 would give information about possible alternative physiological roles. The data was evaluated based on these premises.

4.4.1 Co-IP - Search for the Needle in a Hay Stack

A pulldown assay using recombinant RIBA1 protein was performed as a first experiment trying to find putative RIBA1 interacting proteins. Deeper screening of RIBA1, RIBA2 and RIBA3 interaction proteins was, however, performed by co-immunoprecipitations making use of *riba1*, *riba2* and *riba3* knockdown or knockout mutants expressing Strep-tagged RIBA1, RIBA2 or RIBA3 protein, respectively. According to the before mentioned premises, following conclusions were drawn: unfortunately, no other proteins involved in the flavin biosynthesis pathway could be detected. A possible homodimerisation could not be assessed with this approach, as bait and prey protein in that case were be identical. Heterodimerisation of RIBA1 and RIBA2 could be detected in the pull-down experiment with recombinant RIBA1 protein and the result was further assessed in a BiFC assay and will be discussed in chapter 4.4.2.

Otherwise, the Co-IP experiments resulted in proteins listed in **Table 41**, **Table 42** and **Table 43**. Interestingly, proteins involved in the fatty acid biosynthesis on the one hand and in carbon metabolism on the other hand (glycolysis, starch metabolism, pentose phosphate pathway) are highly represented. It is not likely that RIBA proteins are connected to all these pathways. However, a few proteins were found in the assays of more than one RIBA isoform, independently. These proteins seem to have a higher probability to interact with RIBA proteins, but should be verified in further experiments. These proteins were triose-5-phosphate/phosphate translocator (TPT1), phosphoenolpyruvate carboxylase family protein and CP12 domain containing protein 1. Two of these proteins are also involved in the primary carbon metabolic pathways. Consequently, they might be more abundant, but a connection to flavin biosynthesis is not excluded.

In fact, the pentose phosphate pathway is, as the first two proteins in **Table 42**, directly connected to purine metabolism. The proteins L-aspartase-like family protein and the phosphoribosyl-transferase family protein PRS1 perform steps in the purine metabolism and are thus connected to an important source of GTP. Interestingly, PRS1 can also catalyse the reversible formation of ribose-5-phosphate (Krath *et al.*, 1999) which can be converted to ribulose-5-phosphate, by the ribose-5-phosphate isomerase. The metabolic channelling of substrates or intermediates is a well-established phenomenon. It is known to regulate the competition of substrate between different pathways by achieving high local substrate concentrations (Winkel, 2004). It is possible that a

potentially high priority pathway like flavin biosynthesis establishes such direct connection through RIBA proteins to ensure the source of its substrates ribulose-5-phoshate and GTP.

All of these suggestions are very speculative and require further tests by yeast-two-hybrid or BiFC experiments.

4.4.2 BiFC Reveals Homo- and Heterodimerisation of RIBA Proteins Via The DHBPS Domain

The homo- and heterodimerisation of RIBA proteins was examined with full-length sequences as well as fragments of RIBA1, which contained either the DHBPS or the GCHII domain. The results included a mixture of purely chloroplast derived localisation signals, as well as signals that can be interpreted either as artificial aggregations or as subcompartmentalisation within the chloroplasts. Especially the expression of combinations of merely full-length proteins resulted in globular structures. Localisation data depicting substructures within the chloroplast were compared. A very similar pattern was documented before by Ampomah-Dwamena *et al.* (2015), demonstrating plastoglobuli localisation of PHYTOENE SYNTHASE 4 in apple and Vidi *et al.* (2007) showing the plastoglobular targeting of PLASTOGLOBULIN 34 (PGL34)-YFP fusion protein in tobacco leaves.

Work that was done in context with the localisation of RIBA proteins described in Hiltunen *et al.* (2012) revealed similar structures of GFP-tagged full-length RIBA proteins. The data presented there concerning the chloroplast spanning signal was attained by shortened RIBA fragments, which contained only the predicted transit peptide and short fragment of the N-terminus (Hiltunen *et al.*, 2012). Taken together with the results obtained by the BiFC experiments, this data suggests that there is a possibility that the globular structures observed are RIBA proteins associated with plastoglobuli. To date, no plastoglobuli specific targeting sequences have been identified. It has, however, been demonstrated that certain hydrophobic domains are required for the association to lipid bodies (Abell *et al.*, 2004). Vidi *et al.* (2007) reported that most of the PGL34 protein sequence was required for the correct targeting into the plastoglobuli and could show that shortened fragments, missing certain hydrophobic areas, were mistargeted to the stroma. In order to evaluate the likelihood of this hypothesis, a hydropathy analysis according to Kyte and Doolittle (1982) was performed for RIBA1 (**Figure 66**). This revealed a relatively low grand average of hydropathy (GRAVY) value of -0.257 for RIBA1 but proved the existence hydropathic areas within the full-length sequence, while the area used for the localisation study of RIBA1, here indicated as "RIBA1 N-terminus", is especially low in hydrophobic amino acids.

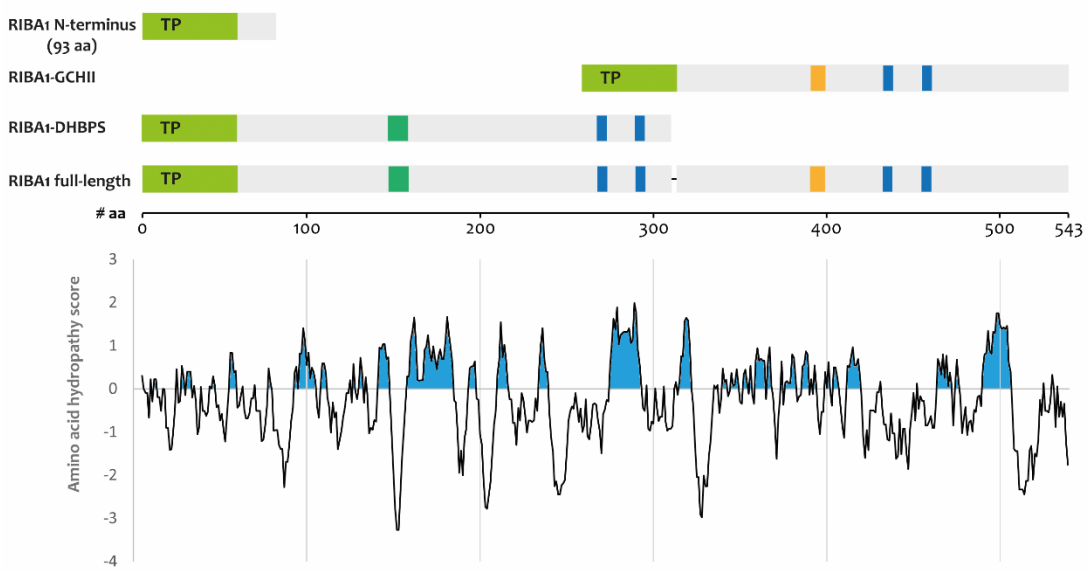

Figure 66: **Hydropathy analysis of RIBA1 protein sequence with protein fragments used for localisation studies of RIBA1 and BiFC indicated.**
The hydropathy analysis was performed according to Kyte and Doolittle (1982), wherein Amino acids are evaluated concerning their hydrophilicity/hydrophobicity and ranked according to their hydropathy score. Isoleucine with a hydropathy score of 4.5 is considered very hydrophobic while on the other side arginine with a hydropathy score of -4.5 as very hydrophilic.

Interestingly, Daniel Tomé has reported before (personal communication) that tagged lumazine synthase also forms globular structures (**Figure 67**). This hints at a general association of flavin biosynthesis proteins to plastoglobuli. It is possible that the plastoglobuli function as a scaffold to establish a spatial proximity of the proteins to each other and hence facilitate substrate channelling within the flavin biosynthesis pathway as discussed earlier in this chapter 0.

Figure 67: **Subcellular localisation of *Arabidopsis* lumazine synthase (COS1) c-terminally fused to GFP.**
Analysis was conveyed by confocal laser microscopy. D. Tomé and co-workers (personal communication) found that COS1-GFP localises to single globular features within the chloroplast in Arabidopsis protoplasts (adapted from Tomé et al., unpublished).

Vitamin biosynthesis within plastoglobuli has been demonstrated before by Vidi *et al.* (2006). They localised tocopherol biosynthesis within the plastoglobuli. The proteome data of plastoglobuli published by Ytterberg *et al.* (2006) is however somewhat contradictory to the hypothesis of flavin biosynthesis taking place in the plastoglobuli. None of the proteins mentioned in chapter 1.3.2 are listed there.

Despite the considerations concerning the inter plastid distribution of RIBA proteins, the BiFC data clearly states that in contrast to the homodimerisation data from *M. tuberculosis (Singh et al., 2011,*

Singh et al., 2013) Arabidopsis RIBA proteins dimerise through their DHBPS domain. Unfortunately, no evidence for the existence of a flavobiosynthesis complex could be gathered. The possibility of localisation at or in plastoglobuli, however, delivers a suggestion for a natural confinement in the proximity of such structures within the chloroplast stroma. The fact that flavins are in contrast to tocopherol rather hydrophilic makes this environment look unsuitable for flavin biosynthesis. However, the possibility of RIBAs and other proteins of flavin biosynthesis associating to plastoglobuli should be assessed in future research. This could be done by subcellular localisation study of GFP tagged RIBA proteins, co-expressed with a tagged plastoglobuli marker, e.g. PGL34-CFP.

4.5 Concluding Remarks and Future Perspectives

The aims of this thesis were on the one hand the characterisation of the RIBA isoforms in *Arabidopsis thaliana* as well as the characterisation of effects caused by deregulated flavin biosynthesis.

Based on this data, the physiological roles of RIBA2 and RIBA3, can only be contemplated. Further analyses will be necessary to identify the specific roles of RIBA2 and RIBA3. One approach to clarify whether RIBA2 and RIBA3 are involved in riboflavin biosynthesis would be to use the VIGS system to induce RIBA1 silencing (chapter 3.5.2.5) in the *riba2*x*riba3* double mutant described in chapter 3.5.3. Direct comparison with RIBA1-VIGS treated *wt Col-0* plants could give information whether the absence of RIBA2 and RIBA3 influences the RIBA1-VIGS effect.

All in all, this thesis delivers an important contribution to the clarification of the flavin biosynthesis pathway and a detailed description of the effects of a deregulated flavin biosynthesis pathway.

Finally, the first step towards the envisioned possibility to use biotechnologically modified plants to secure vitamin B_2 supply in the future was made. A good example for solving vitamin malnutrition through biotechnology of plants is the approach started by Beyer *et al.* (2002) who introduced different components of the β-carotene synthesis from *Narcissus pseudonarcissus* to rice in order to introduce provitamin A production in rice endosperm. The Golden Rice Project was initiated by an international composium to fight so called Vitamin A Deficiency-Related Disorders in developing countries where diet mainly consists of rice and other grain. This thesis has contributed to knowledge needed for comparable projects regarding plants with enhanced vitamin B_2 contents in the future.

References

Abbas, C.A. & Sibirny, A.A. (2011) Genetic Control of Biosynthesis and Transport of Riboflavin and Flavin Nucleotides and Construction of Robust Biotechnological Producers. *Microbiology and Molecular Biology Reviews*, **75**, 321-360.

Abell, B.M., Hahn, M., Holbrook, L.A. & Moloney, M.M. (2004) Membrane topology and sequence requirements for oil body targeting of oleosin. *Plant J*, **37**, 461-470.

Ahmad, M. & Cashmore, A.R. (1993) HY4 gene of A. thaliana encodes a protein with characteristics of a blue-light photoreceptor. *Nature*, **366**, 162-166.

Akimoto, M., Sato, Y., Okubo, T., Todo, H., Hasegawa, T. & Sugibayashi, K. (2006) Conversion of FAD to FMN and Riboflavin in Plasma: Effects of Measuring Method. *Biological and Pharmaceutical Bulletin*, **29**, 1779-1782.

Altschul, S.F., Madden, T.L., Schaffer, A.A., Zhang, J., Zhang, Z., Miller, W. & Lipman, D.J. (1997) Gapped BLAST and PSI-BLAST: a new generation of protein database search programs. *Nucleic Acids Res*, **25**, 3389-3402.

Altschul, S.F., Wootton, J.C., Gertz, E.M., Agarwala, R., Morgulis, A., Schaffer, A.A. & Yu, Y.K. (2005) Protein database searches using compositionally adjusted substitution matrices. *FEBS J*, **272**, 5101-5109.

Ampomah-Dwamena, C., Driedonks, N., Lewis, D., Shumskaya, M., Chen, X., Wurtzel, E.T., Espley, R.V. & Allan, A.C. (2015) The Phytoene synthase gene family of apple (Malus x domestica) and its role in controlling fruit carotenoid content. *BMC Plant Biology*, **15**, 1-14.

Araújo, W.L., Ishizaki, K., Nunes-Nesi, A., Larson, T.R., Tohge, T., Krahnert, I., Witt, S., Obata, T., Schauer, N., Graham, I.A., Leaver, C.J. & Fernie, A.R. (2010) Identification of the 2-Hydroxyglutarate and Isovaleryl-CoA Dehydrogenases as Alternative Electron Donors Linking Lysine Catabolism to the Electron Transport Chain of Arabidopsis Mitochondria. *Plant Cell*, **22**, 1549-1563.

Araújo, W.L., Nunes-Nesi, A., Osorio, S., Usadel, B., Fuentes, D., Nagy, R., Balbo, I., Lehmann, M., Studart-Witkowski, C., Tohge, T., Martinoia, E., Jordana, X., DaMatta, F.M. & Fernie, A.R. (2011a) Antisense Inhibition of the Iron-Sulphur Subunit of Succinate Dehydrogenase Enhances Photosynthesis and Growth in Tomato via an Organic Acid–Mediated Effect on Stomatal Aperture. *Plant Cell*, **23**, 600-627.

Araújo, W.L., Tohge, T., Ishizaki, K., Leaver, C.J. & Fernie, A.R. (2011b) Protein degradation - an alternative respiratory substrate for stressed plants. *Trends Plant Sci*, **16**, 489-498.

Araújo, W.L., Tohge, T., Osorio, S., Lohse, M., Balbo, I., Krahnert, I., Sienkiewicz-Porzucek, A., Usadel, B., Nunes-Nesi, A. & Fernie, A.R. (2012) Antisense Inhibition of the 2-Oxoglutarate Dehydrogenase Complex in Tomato Demonstrates Its Importance for Plant Respiration and during Leaf Senescence and Fruit Maturation. *Plant Cell*, **24**, 2328-2351.

Asai, S., Mase, K. & Yoshioka, H. (2010) A key enzyme for flavin synthesis is required for nitric oxide and reactive oxygen species production in disease resistance. *Plant J*, **62**, 911-924.

Ashoori, M. & Saedisomeolia, A. (2014) Riboflavin (vitamin B2) and oxidative stress: a review. *British Journal of Nutrition*, **111**, 1985-1991.

Atkinson, S.C., Dogovski, C., Downton, M.T., Czabotar, P.E., Dobson, R.C.J., Gerrard, J.A., Wagner, J. & Perugini, M.A. (2013) Structural, kinetic and computational investigation of Vitis vinifera DHDPS reveals new insight into the mechanism of lysine-mediated allosteric inhibition. *Plant molecular biology*, **81**, 431-446.

Azami-Sardooei, Z., França, S.C., De Vleesschauwer, D. & Höfte, M. (2010) Riboflavin induces resistance against Botrytis cinerea in bean, but not in tomato, by priming for a hydrogen peroxide-fueled resistance response. *Physiological and Molecular Plant Pathology*, **75**, 23-29.

Azevedo, R.A., Lancien, M. & Lea, P.J. (2006) The aspartic acid metabolic pathway, an exciting and essential pathway in plants. *Amino Acids*, **30**, 143-162.

Bacher, A., Baur, R., Eggers, U., Harders, H.D., Otto, M.K. & Schnepple, H. (1980) Riboflavin synthases of Bacillus subtilis. Purification and properties. *Journal of Biological Chemistry*, **255**, 632-637.

Bacher, A., Eberhardt, S., Eisenreich, W., Fischer, M., Herz, S., Illarionov, B., Kis, K. & Richter, G. (2001) Biosynthesis of riboflavin. *Vitam Horm*, **61**, 1-49.

Bakhsh, A., Rao, A.Q., Shahid, A.A., Husnain, T. & Riazuddin, S. (2009) CaMV 35S is a developmental promoter being temporal and spatial in expression pattern of insecticidal genes (Cry1ac & Cry2a) in cotton. *Research Journal of Cell and Molecular Biology*, **3**, 56-62.

Bandrin, S.V., Rabinovich, P.M. & Stepanov, A.I. (1983) [3 linkage groups of the genes of riboflavin biosynthesis in Escherichia coli]. *Genetika*, **19**, 1419-1425.

Barile, M., Giancaspero, T.A., Brizio, C., Panebianco, C., Indiveri, C., Galluccio, M., Vergani, L., Eberini, I. & Gianazza, E. (2013) Biosynthesis of flavin cofactors in man: implications in health and disease. *Curr Pharm Des*, **19**, 2649-2675.

Barion, S., Franchi, M., Gallori, E. & Di Giulio, M. (2007) The first lines of divergence in the Bacteria domain were the hyperthermophilic organisms, the Thermotogales and the Aquificales, and not the mesophilic Planctomycetales. *Biosystems*, **87**, 13-19.

Baruah, A., Šimková, K., Hincha, D.K., Apel, K. & Laloi, C. (2009) Modulation of 1O2-mediated retrograde signaling by the PLEIOTROPIC RESPONSE LOCUS 1 (PRL1) protein, a central integrator of stress and energy signaling. *The Plant Journal*, **60**, 22-32.

Barrero, J.M., Piqueras, P., González-Guzmán, M., Serrano, R., Rodríguez, P.L., Ponce, M.R. & Micol, J.L. (2005) A mutational analysis of the ABA1 gene of Arabidopsis thaliana highlights the involvement of ABA in vegetative development. *Journal of Experimental Botany*, **56**, 2071-2083.

Bauer, S., Kemter, K., Bacher, A., Huber, R., Fischer, M. & Steinbacher, S. (2003) Crystal structure of Schizosaccharomyces pombe riboflavin kinase reveals a novel ATP and riboflavin-binding fold. *J Mol Biol*, **326**, 1463-1473.

Becker, D., Kemper, E., Schell, J. & Masterson, R. (1992) New plant binary vectors with selectable markers located proximal to the left T-DNA border. *Plant Mol Biol*, **20**, 1195-1197.

Bellafiore, S., Barneche, F., Peltier, G. & Rochaix, J.-D. (2005) State transitions and light adaptation require chloroplast thylakoid protein kinase STN7. *Nature*, **433**, 892-895.

Beyer, P., Al-Babili, S., Ye, X., Lucca, P., Schaub, P., Welsch, R. & Potrykus, I. (2002) Golden Rice: Introducing the β-Carotene Biosynthesis Pathway into Rice Endosperm by Genetic Engineering to Defeat Vitamin A Deficiency. *The Journal of Nutrition*, **132**, 506S-510S.

Blazhenko, O.V. (2014) Glutathione deficiency leads to riboflavin oversynthesis in the yeast Pichia guilliermondii. *Curr Microbiol*, **69**, 10-18.

Blythe, A. (1879) The composition of cows milk in health and disease. *J. Chem. Soc. Lond*, **35**, 530.

Bocobza, S., Adato, A., Mandel, T., Shapira, M., Nudler, E. & Aharoni, A. (2007) Riboswitch-dependent gene regulation and its evolution in the plant kingdom. *Genes & development*, **21**, 2874-2879.

Bode, K., Hooks, M.A. & Couée, I. (1999) Identification, Separation, and Characterization of Acyl-Coenzyme A Dehydrogenases Involved in Mitochondrial β-Oxidation in Higher Plants. *Plant Physiology*, **119**, 1305-1314.

Borchardt, M. (2015) Identification and first anlyzes of T-DNA insertion mutants for all enzymatic steps of the riboflavin synthesis. In *Lebenswissenschaftliche Fakultät - Institut für Biologie*. Berlin: Humboldt Universität zu Berlin.

Boretsky, Y.R., Kapustyak, K.Y., Fayura, L.R., Stasyk, O.V., Stenchuk, M.M., Bobak, Y.P., Drobot, L.B. & Sibirny, A.A. (2005) Positive selection of mutants defective in transcriptional repression of riboflavin synthesis by iron in the flavinogenic yeast Pichia guilliermondii. *FEMS Yeast Res*, **5**, 829-837.

Boretsky, Y.R., Protchenko, O.V., Prokopiv, T.M., Mukalov, I.O., Fedorovych, D.V. & Sibirny, A.A. (2007) Mutations and environmental factors affecting regulation of riboflavin synthesis and iron assimilation also cause oxidative stress in the yeast Pichia guilliermondii. *J Basic Microbiol*, **47**, 371-377.

Boretsky, Y.R., Pynyaha, Y.V., Boretsky, V.Y., Fedorovych, D.V., Fayura, L.R., Protchenko, O., Philpott, C.C. & Sibirny, A.A. (2011) Identification of the genes affecting the regulation of riboflavin synthesis in the flavinogenic yeast Pichia guilliermondii using insertion mutagenesis. *FEMS Yeast Res*, **11**, 307-314.

Bradford, M.M. (1976) A rapid and sensitive method for the quantitation of microgram quantities of protein utilizing the principle of protein-dye binding. *Analytical Biochemistry*, **72**, 248-254.

Brochier, C. & Philippe, H. (2002) Phylogeny: a non-hyperthermophilic ancestor for bacteria. *Nature*, **417**, 244.

Brown, A., Slabas, A. & Rafferty, J. (2010) Fatty Acid Biosynthesis in Plants — Metabolic Pathways, Structure and Organization. In *Lipids in Photosynthesis* (Wada, H. and Murata, N. eds): Springer Netherlands, pp. 11-34.

Brutinel, E.D., Dean, A.M. & Gralnick, J.A. (2013) Description of a Riboflavin Biosynthetic Gene Variant Prevalent in the Phylum Proteobacteria. *Journal of bacteriology*, **195**, 5479-5486.

Brzezowski, P., Richter, A.S. & Grimm, B. (2015) Regulation and function of tetrapyrrole biosynthesis in plants and algae. *Biochimica et Biophysica Acta (BBA)-Bioenergetics*.

Büch, K., Stransky, H. & Hager, A. (1995) FAD is a further essential cofactor of the NAD(P)H and O2-dependent zeaxanthin-epoxidase. *FEBS Letters*, **376**, 45-48.

Caspar, T., Huber, S.C. & Somerville, C. (1985) Alterations in Growth, Photosynthesis, and Respiration in a Starchless Mutant of Arabidopsis thaliana (L.) Deficient in Chloroplast Phosphoglucomutase Activity. *Plant Physiology*, **79**, 11-17.

Cella, R. & Parisi, B. (1993) Dihydrofolate reductase and thymidylate synthase in plants: an open problem. *Physiologia Plantarum*, **88**, 509-521.

Chang, C.C.C., Ślesak, I., Jordá, L., Sotnikov, A., Melzer, M., Miszalski, Z., Mullineaux, P.M., Parker, J.E., Karpińska, B. & Karpiński, S. (2009) Arabidopsis Chloroplastic Glutathione Peroxidases Play a Role in Cross Talk between Photooxidative Stress and Immune Responses. *Plant Physiology*, **150**, 670-683.

Chatwell, L., Krojer, T., Fidler, A., Romisch, W., Eisenreich, W., Bacher, A., Huber, R. & Fischer, M. (2006) Biosynthesis of riboflavin: structure and properties of 2,5-diamino-6-ribosylamino-4(3H)-pyrimidinone 5'-phosphate reductase of Methanocaldococcus jannaschii. *J Mol Biol*, **359**, 1334-1351.

Christie, J.M., Salomon, M., Nozue, K., Wada, M. & Briggs, W.R. (1999) LOV (light, oxygen, or voltage) domains of the blue-light photoreceptor phototropin (nph1): Binding sites for the chromophore flavin mononucleotide. *Proceedings of the National Academy of Sciences of the United States of America*, **96**, 8779-8783.

Clough, S.J. & Bent, A.F. (1998) Floral dip: a simplified method forAgrobacterium-mediated transformation ofArabidopsis thaliana. *The Plant Journal*, **16**, 735-743.

Conrath, U., Beckers, G.J., Flors, V., García-Agustín, P., Jakab, G., Mauch, F., Newman, M.-A., Pieterse, C.M., Poinssot, B. & Pozo, M.J. (2006) Priming: getting ready for battle. *Molecular Plant-Microbe Interactions*, **19**, 1062-1071.

Consortium, T.U. (2015) UniProt: a hub for protein information. *Nucleic Acids Research*, **43**, D204-D212.

Coves, J., Niviere, V., Eschenbrenner, M. & Fontecave, M. (1993) NADPH-sulfite reductase from Escherichia coli. A flavin reductase participating in the generation of the free radical of ribonucleotide reductase. *J Biol Chem*, **268**, 18604-18609.

Czechowski, T., Bari, R.P., Stitt, M., Scheible, W.R. & Udvardi, M.K. (2004) Real-time RT-PCR profiling of over 1400 Arabidopsis transcription factors: unprecedented sensitivity reveals novel root- and shoot-specific genes. *Plant J*, **38**, 366-379.

Das, B.S., Das, D.B., Satpathy, R.N., Patnaik, J.K. & Bose, T.K. (1988) Riboflavin deficiency and severity of malaria. *European journal of clinical nutrition*, **42**, 277-283.

Daudi, A. & O'Brien, J.A. (2012) Detection of Hydrogen Peroxide by DAB Staining in Arabidopsis Leaves. Bio-protocol, pp. e263.

Davis, A., Hall, A., Millar, A., Darrah, C. & Davis, S. (2009) Protocol: Streamlined sub-protocols for floral-dip transformation and selection of transformants in Arabidopsis thaliana. *Plant Methods*, **5**, 3.

Deng, B., Deng, S., Sun, F., Zhang, S. & Dong, H. (2011) Down-regulation of free riboflavin content induces hydrogen peroxide and a pathogen defense in Arabidopsis. *Plant molecular biology*, **77**, 185-201.

Deng, B., Jin, X., Yang, Y., Lin, Z. & Zhang, Y. (2013) The regulatory role of riboflavin in the drought tolerance of tobacco plants depends on ROS production. *Plant Growth Regulation*, **72**, 269-277.

Dong, H. & Beer, S. (2000) Riboflavin induces disease resistance in plants by activating a novel signal transduction pathway. *Phytopathology*, **90**, 801-811.

Dong, H., Deng, Y., Mu, J., Lu, Q., Wang, Y., Xu, Y., Chu, C., Chong, K., Lu, C. & Zuo, J. (2007) The Arabidopsis Spontaneous Cell Death1 gene, encoding a [zeta]-carotene desaturase essential for carotenoid biosynthesis, is involved in chloroplast development, photoprotection and retrograde signalling. *Cell Res*, **17**, 458-470.

Duckham, S.C., Linforth, R.S.T. & Taylor, I.B. (1991) Abscisic-acid-deficient mutants at the aba gene locus of Arabidopsis thaliana are impaired in the epoxidation of zeaxanthin. *Plant, Cell & Environment*, **14**, 601-606.

Durek, P., Schmidt, R., Heazlewood, J.L., Jones, A., MacLean, D., Nagel, A., Kersten, B. & Schulze, W.X. (2010) PhosPhAt: the Arabidopsis thaliana phosphorylation site database. An update. *Nucleic Acids Research*, **38**, D828-D834.

Eberhardt, S., Richter, G., Gimbel, W., Werner, T. & Bacher, A. (1996) Cloning, sequencing, mapping and hyperexpression of the ribC gene coding for riboflavin synthase of Escherichia coli. *European Journal of Biochemistry*, **242**, 712-719.

Eichler, M., Lavi, R., Shainberg, A. & Lubart, R. (2005) Flavins are source of visible-light-induced free radical formation in cells. *Lasers in Surgery and Medicine*, **37**, 314-319.

Eichstädt, B. (2014) The Characterization of Tobacco AtRIBA1 Overexpressors. In *Mathematisch-Naturwissenschaftliche Fakultät 1 - Institut für Biologie*. Berlin: Humboldt Universität zu Berlin.

Elkind, Y., Edwards, R., Mavandad, M., Hedrick, S.A., Ribak, O., Dixon, R.A. & Lamb, C.J. (1990) Abnormal plant development and down-regulation of phenylpropanoid biosynthesis in transgenic tobacco containing a heterologous phenylalanine ammonia-lyase gene. *Proc Natl Acad Sci U S A*, **87**, 9057-9061.

Emanuelsson, O., Nielsen, H., Brunak, S. & von Heijne, G. (2000) Predicting subcellular localization of proteins based on their N-terminal amino acid sequence. *J Mol Biol*, **300**, 1005-1016.

Engqvist, M., Drincovich, M.F., Flügge, U.-I. & Maurino, V.G. (2009) Two d-2-Hydroxy-acid Dehydrogenases in Arabidopsis thaliana with Catalytic Capacities to Participate in the Last Reactions of the Methylglyoxal and β-Oxidation Pathways. *Journal of Biological Chemistry*, **284**, 25026-25037.

Eprintsev, A.T., Maslova, E.V., Fedorin, D.N. & Popov, V.N. (2009) Physicochemical and kinetic characteristics of isoforms of isocitrate lyase from corn. *Biochemistry (Moscow)*, **74**, 528-532.

Fait, A., Fromm, H., Walter, D., Galili, G. & Fernie, A.R. (2008) Highway or byway: the metabolic role of the GABA shunt in plants. *Trends Plant Sci*, **13**, 14-19.

Fernie, A.R., Trethewey, R.N., Krotzky, A.J. & Willmitzer, L. (2004) Metabolite profiling: from diagnostics to systems biology. *Nat Rev Mol Cell Biol*, **5**, 763-769.

Finn, R.D., Bateman, A., Clements, J., Coggill, P., Eberhardt, R.Y., Eddy, S.R., Heger, A., Hetherington, K., Holm, L., Mistry, J., Sonnhammer, E.L.L., Tate, J. & Punta, M. (2014) Pfam: the protein families database. *Nucleic Acids Research*, **42**, D222-D230.

Fischer, M. & Bacher, A. (2006) Biosynthesis of vitamin B2 in plants. *Physiologia Plantarum*, **126**, 304-318.

Fischer, M., Haase, I., Feicht, R., Richter, G., Gerhardt, S., Changeux, J.-P., Huber, R. & Bacher, A. (2002a) Biosynthesis of riboflavin. *European Journal of Biochemistry*, **269**, 519-526.

Fischer, M., Haase, I., Feicht, R., Schramek, N., Kohler, P., Schieberle, P. & Bacher, A. (2005) Evolution of vitamin B2 biosynthesis: riboflavin synthase of Arabidopsis thaliana and its inhibition by riboflavin. *Biol Chem*, **386**, 417-428.

Fischer, M., Romisch, W., Saller, S., Illarionov, B., Richter, G., Rohdich, F., Eisenreich, W. & Bacher, A. (2004) Evolution of vitamin B2 biosynthesis: structural and functional similarity between pyrimidine deaminases of eubacterial and plant origin. *J Biol Chem*, **279**, 36299-36308.

Fischer, M., Römisch, W., Schiffmann, S., Kelly, M., Oschkinat, H., Steinbacher, S., Huber, R., Eisenreich, W., Richter, G. & Bacher, A. (2002b) Biosynthesis of Riboflavin in Archaea Studies on the Mechanism of 3,4-Dihydroxy-2-butanone-4-phosphate Synthase of Methanococcus jannaschii. *Journal of Biological Chemistry*, **277**, 41410-41416.

Fitzpatrick, T.B., Basset, G.J.C., Borel, P., Carrari, F., DellaPenna, D., Fraser, P.D., Hellmann, H., Osorio, S., Rothan, C., Valpuesta, V., Caris-Veyrat, C. & Fernie, A.R. (2012) Vitamin Deficiencies in Humans: Can Plant Science Help? *Plant Cell*, **24**, 395-414.

Flügge, U.-I. (1999) Phosphate translocators in plastids. *Annual Review of Plant Biology*, **50**, 27-45.

Foor, F. & Brown, G.M. (1975) Purification and properties of guanosine triphosphate cyclohydrolase II from Escherichia coli. *Journal of Biological Chemistry*, **250**, 3545-3551.

Foudree, A., Putarjunan, A., Kambakam, S., Nolan, T., Fussell, J., Pogorelko, G. & Rodermel, S. (2012) The mechanism of variegation in immutans provides insight into chloroplast biogenesis. *Frontiers in Plant Science*, **3**.

Fox, K.M. & Karplus, P.A. (1994) Old yellow enzyme at 2 A resolution: overall structure, ligand binding, and comparison with related flavoproteins. *Structure*, **2**, 1089-1105.

Frago, S., Martinez-Julvez, M., Serrano, A. & Medina, M. (2008) Structural analysis of FAD synthetase from Corynebacterium ammoniagenes. *BMC Microbiol*, **8**, 160.

Frelin, O., Huang, L., Hasnain, G., Jeffryes, J.G., Ziemak, M.J., Rocca, J.R., Wang, B., Rice, J., Roje, S., Yurgel, S.N., Gregory, J.F., 3rd, Edison, A.S., Henry, C.S., de Crecy-Lagard, V. & Hanson, A.D. (2015) A

directed-overflow and damage-control N-glycosidase in riboflavin biosynthesis. *Biochem J*, **466**, 137-145.

Frost, C.J., Mescher, M.C., Carlson, J.E. & De Moraes, C.M. (2008) Plant Defense Priming against Herbivores: Getting Ready for a Different Battle. *Plant Physiology*, **146**, 818-824.

Fujimoto, S., Matsuda, K., Kikugawa, M., Kaneko, M. & Tamaki, N. (1991) Effect of vitamin B2 deficiency on rat liver dihydropyrimidine dehydrogenase activity. *Journal of nutritional science and vitaminology*, **37**, 89-98.

Gaber, A., Ogata, T., Maruta, T., Yoshimura, K., Tamoi, M. & Shigeoka, S. (2012) The involvement of Arabidopsis glutathione peroxidase 8 in the suppression of oxidative damage in the nucleus and cytosol. *Plant Cell Physiol*, **53**, 1596-1606.

Galluccio, M., Brizio, C., Torchetti, E.M., Ferranti, P., Gianazza, E., Indiveri, C. & Barile, M. (2007) Over-expression in Escherichia coli, purification and characterization of isoform 2 of human FAD synthetase. *Protein Expression and Purification*, **52**, 175-181.

Gasteiger, E., Hoogland, C., Gattiker, A., Duvaud, S.e., Wilkins, M.R., Appel, R.D. & Bairoch, A. (2005) *Protein identification and analysis tools on the ExPASy server*: Springer.

Gates, B. (2016) GMOs Will End Starvation in Africa(Blumenstein, R. ed. http://www.wsj.com/video/bill-gates-gmos-will-end-starvation-in-africa/3085A8D1-BB58-4CAA-9394-E567033434A4.html: The Wall Street Journal.

Gaufichon, L., Masclaux-Daubresse, C., Tcherkez, G., Reisdorf-Cren, M., Sakakibara, Y., Hase, T., ClÉMent, G., Avice, J.-C., Grandjean, O., Marmagne, A., Boutet-Mercey, S., Azzopardi, M., Soulay, F. & Suzuki, A. (2013) Arabidopsis thaliana ASN2 encoding asparagine synthetase is involved in the control of nitrogen assimilation and export during vegetative growth. *Plant, Cell & Environment*, **36**, 328-342.

Gelfand, M.S., Mironov, A.A., Jomantas, J., Kozlov, Y.I. & Perumov, D.A. (1999) A conserved RNA structure element involved in the regulation of bacterial riboflavin synthesis genes. *Trends in Genetics*, **15**, 439-442.

Gerhardt, S., Haase, I., Steinbacher, S., Kaiser, J.T., Cushman, M., Bacher, A., Huber, R. & Fischer, M. (2002) The Structural Basis of Riboflavin Binding to Schizosaccharomyces pombe 6,7-Dimethyl-8-ribityllumazine Synthase. *Journal of molecular biology*, **318**, 1317-1329.

Giancaspero, T.A., Colella, M., Brizio, C., Difonzo, G., Fiorino, G.M., Leone, P., Brandsch, R., Bonomi, F., Iametti, S. & Barile, M. (2015) Remaining challenges in cellular flavin cofactor homeostasis and flavoprotein biogenesis. *Frontiers in Chemistry*, **3**.

Giancaspero, T.A., Locato, V., de Pinto, M.C., De Gara, L. & Barile, M. (2009) The occurrence of riboflavin kinase and FAD synthetase ensures FAD synthesis in tobacco mitochondria and maintenance of cellular redox status. *FEBS J*, **276**, 219-231.

Girke, A. (2015) Untersuchungen über Konsequenzen einer deregulierten Chlorophyllsynthese und funktionelle Analyse des YCF54/LCAA-Proteins in Cyanobakterien und Pflanzen. In *Lebenswissenschaftliche Fakultät - Institut für Biologie*. Berlin: Humboldt Universität zu Berlin.

Goodstein, D.M., Shu, S., Howson, R., Neupane, R., Hayes, R.D., Fazo, J., Mitros, T., Dirks, W., Hellsten, U., Putnam, N. & Rokhsar, D.S. (2012) Phytozome: a comparative platform for green plant genomics. *Nucleic Acids Research*, **40**, D1178-D1186.

Griffin, M.D., Billakanti, J.M., Wason, A., Keller, S., Mertens, H.D., Atkinson, S.C., Dobson, R.C., Perugini, M.A., Gerrard, J.A. & Pearce, F.G. (2012) Characterisation of the first enzymes committed to lysine biosynthesis in Arabidopsis thaliana. *PLoS One*, **7**, e40318.

Grimm, B., Bull, A., Welinder, K., Gough, S. & Kannangara, C.G. (1989) Purification and partial amino acid sequence of the glutamate 1-semialdehyde aminotransferase of barley and Synechococcus. *Carlsberg Research Communications*, **54**, 67-79.

Gudipati, V., Koch, K., Lienhart, W.D. & Macheroux, P. (2014) The flavoproteome of the yeast Saccharomyces cerevisiae. *Biochim Biophys Acta*, **1844**, 535-544.

Haase, I., Gräwert, T., Illarionov, B., Bacher, A. & Fischer, M. (2014) Recent Advances in Riboflavin Biosynthesis. In *Flavins and Flavoproteins*: Springer, pp. 15-40.

Haase, I., Sarge, S., Illarionov, B., Laudert, D., Hohmann, H.-P., Bacher, A. & Fischer, M. (2013) Enzymes from the Haloacid Dehalogenase (HAD) Superfamily Catalyse the Elusive Dephosphorylation Step of Riboflavin Biosynthesis. *ChemBioChem*, **14**, 2272-2275.

Hare, P. & Staden, J.v. (1994) Cytokinin oxidase: biochemical features and physiological significance. *Physiologia Plantarum*, **91**, 128-136.

Hasnain, G., Frelin, O., Roje, S., Ellens, K.W., Ali, K., Guan, J.C., Garrett, T.J., de Crecy-Lagard, V., Gregory, J.F., 3rd, McCarty, D.R. & Hanson, A.D. (2013) Identification and characterization of the missing pyrimidine reductase in the plant riboflavin biosynthesis pathway. *Plant Physiol*, **161**, 48-56.

Hayaishi, O., Nishizuka, Y., Tatibana, M., Takeshita, M. & Kuno, S. (1961) Enzymatic studies on the metabolism of beta-alanine. *J Biol Chem*, **236**, 781-790.

Heazlewood, J.L., Durek, P., Hummel, J., Selbig, J., Weckwerth, W., Walther, D. & Schulze, W.X. (2008) PhosPhAt: a database of phosphorylation sites in Arabidopsis thaliana and a plant-specific phosphorylation site predictor. *Nucleic Acids Research*, **36**, D1015-D1021.

Hedtke, B., Alawady, A., Albacete, A., Kobayashi, K., Melzer, M., Roitsch, T., Masuda, T. & Grimm, B. (2012) Deficiency in riboflavin biosynthesis affects tetrapyrrole biosynthesis in etiolated Arabidopsis tissue. *Plant Mol Biol*, **78**, 77-93.

Hellens, R., Mullineaux, P. & Klee, H. (2000) Technical focus: a guide to Agrobacterium binary Ti vectors. *Trends Plant Sci*, **5**, 446-451.

Herguedas, B., Martinez-Julvez, M., Frago, S., Medina, M. & Hermoso, J.A. (2009) Crystallization and preliminary X-ray diffraction studies of FAD synthetase from Corynebacterium ammoniagenes. *Acta Crystallogr Sect F Struct Biol Cryst Commun*, **65**, 1285-1288.

Herz, S., Eberhardt, S. & Bacher, A. (2000) Biosynthesis of riboflavin in plants. The ribA gene of Arabidopsis thaliana specifies a bifunctional GTP cyclohydrolase II/3,4-dihydroxy-2-butanone 4-phosphate synthase. *Phytochemistry*, **53**, 723-731.

Hiltunen, H.-M., Illarionov, B., Hedtke, B., Fischer, M. & Grimm, B. (2012) Arabidopsis RIBA Proteins: Two out of Three Isoforms Have Lost Their Bifunctional Activity in Riboflavin Biosynthesis. *International Journal of Molecular Sciences*, **13**, 14086-14105.

Hitomi, K., DiTacchio, L., Arvai, A.S., Yamamoto, J., Kim, S.-T., Todo, T., Tainer, J.A., Iwai, S., Panda, S. & Getzoff, E.D. (2009) Functional motifs in the (6-4) photolyase crystal structure make a comparative framework for DNA repair photolyases and clock cryptochromes. *Proceedings of the National Academy of Sciences*, **106**, 6962-6967.

Hobbs, S.A., Warkentin, T. & DeLong, C.O. (1993) Transgene copy number can be positively or negatively associated with transgene expression. *Plant molecular biology*, **21**, 17-26.

Hossain, M.A. & Asada, K. (1985) Monodehydroascorbate reductase from cucumber is a flavin adenine dinucleotide enzyme. *Journal of Biological Chemistry*, **260**, 12920-12926.

Hsieh, M.-H. & Goodman, H.M. (2005) The Arabidopsis IspH Homolog Is Involved in the Plastid Nonmevalonate Pathway of Isoprenoid Biosynthesis. *Plant Physiology*, **138**, 641-653.

Hu, Z., Xu, F., Guan, L., Qian, P., Liu, Y., Zhang, H., Huang, Y. & Hou, S. (2014) The tetratricopeptide repeat-containing protein slow green1 is required for chloroplast development in Arabidopsis. *Journal of Experimental Botany*, **65**, 1111-1123.

Huala, E., Oeller, P.W., Liscum, E., Han, I.-S., Larsen, E. & Briggs, W.R. (1997) Arabidopsis NPH1: A Protein Kinase with a Putative Redox-Sensing Domain. *Science*, **278**, 2120-2123.

Huang, R., Choe, E. & Min, D. (2004) Kinetics for singlet oxygen formation by riboflavin photosensitization and the reaction between riboflavin and singlet oxygen. *Journal of food science*, **69**, C726-C732.

Huang, S. & Millar, A.H. (2013) Succinate dehydrogenase: the complex roles of a simple enzyme. *Current Opinion in Plant Biology*, **16**, 344-349.

Hudson, A.O., Singh, B.K., Leustek, T. & Gilvarg, C. (2006) An ll-Diaminopimelate Aminotransferase Defines a Novel Variant of the Lysine Biosynthesis Pathway in Plants. *Plant Physiology*, **140**, 292-301.

Hümbelin, M., Griesser, V., Keller, T., Schurter, W., Haiker, M., Hohmann, H., Ritz, H., Richter, G., Bacher, A. & Van Loon, A. (1999) GTP cyclohydrolase II and 3, 4-dihydroxy-2-butanone 4-phosphate synthase are rate-limiting enzymes in riboflavin synthesis of an industrial Bacillus subtilis strain used for riboflavin production. *Journal of Industrial Microbiology and Biotechnology*, **22**, 1-7.

Hung, T.M., Na, M., Thuong, P.T., Su, N.D., Sok, D., Song, K.S., Seong, Y.H. & Bae, K. (2006) Antioxidant activity of caffeoyl quinic acid derivatives from the roots of Dipsacus asper Wall. *J Ethnopharmacol*, **108**, 188-192.

Imai, A., Matsuyama, T., Hanzawa, Y., Akiyama, T., Tamaoki, M., Saji, H., Shirano, Y., Kato, T., Hayashi, H., Shibata, D., Tabata, S., Komeda, Y. & Takahashi, T. (2004) Spermidine Synthase Genes Are Essential for Survival of Arabidopsis. *Plant Physiology*, **135**, 1565-1573.

Ishizaki, K., Larson, T.R., Schauer, N., Fernie, A.R., Graham, I.A. & Leaver, C.J. (2005) The Critical Role of Arabidopsis Electron-Transfer Flavoprotein:Ubiquinone Oxidoreductase during Dark-Induced Starvation. *Plant Cell*, **17**, 2587-2600.

Ishizaki, K., Schauer, N., Larson, T.R., Graham, I.A., Fernie, A.R. & Leaver, C.J. (2006) The mitochondrial electron transfer flavoprotein complex is essential for survival of Arabidopsis in extended darkness. *The Plant Journal*, **47**, 751-760.

Ivanov, A., Kameka, A., Pajak, A., Bruneau, L., Beyaert, R., Hernández-Sebastià, C. & Marsolais, F. (2012) Arabidopsis mutants lacking asparaginases develop normally but exhibit enhanced root inhibition by exogenous asparagine. *Amino Acids*, **42**, 2307-2318.

Jander, G. & Joshi, V. (2009) Aspartate-Derived Amino Acid Biosynthesis in Arabidopsis thaliana. *The Arabidopsis Book*, e0121.

Jarillo, J.A., Capel, J., Tang, R.-H., Yang, H.-Q., Alonso, J.M., Ecker, J.R. & Cashmore, A.R. (2001) An Arabidopsis circadian clock component interacts with both CRY1 and phyB. *Nature*, **410**, 487-490.

Ji, H., Zhu, Y., Tian, S., Xu, M., Tian, Y., Li, L., Wang, H., Hu, L., Ji, Y., Ge, J., Wen, W. & Dong, H. (2014) Downregulation of leaf flavin content induces early flowering and photoperiod gene expression in Arabidopsis. *BMC Plant Biology*, **14**, 237.

Jordan, D.B., Bacot, K.O., Carlson, T.J., Kessel, M. & Viitanen, P.V. (1999) Plant riboflavin biosynthesis. Cloning, chloroplast localization, expression, purification, and partial characterization of spinach lumazine synthase. *J Biol Chem*, **274**, 22114-22121.

Kaiser, J., Schramek, N., Eberhardt, S., Puttmer, S., Schuster, M. & Bacher, A. (2002) Biosynthesis of vitamin B2. *Eur J Biochem*, **269**, 5264-5270.

Kanehisa, M. & Goto, S. (2000) KEGG: kyoto encyclopedia of genes and genomes. *Nucleic Acids Res*, **28**, 27-30.

Kanehisa, M., Goto, S., Sato, Y., Kawashima, M., Furumichi, M. & Tanabe, M. (2014) Data, information, knowledge and principle: back to metabolism in KEGG. *Nucleic Acids Res*, **42**, D199-205.

Karplus, P.A. & Daniels, M.J. (1991) Atomic structure of ferredoxin-NADP+ reductase: prototype for a structurally novel flavoenzyme family. *Science*, **251**, 60-66.

Karplus, P.A., Fox, K.M. & Massey, V. (1995) Flavoprotein structure and mechanism. 8. Structure-function relations for old yellow enzyme. *Faseb j*, **9**, 1518-1526.

Karthikeyan, S., Zhou, Q., Mseeh, F., Grishin, N.V., Osterman, A.L. & Zhang, H. (2003) Crystal structure of human riboflavin kinase reveals a beta barrel fold and a novel active site arch. *Structure*, **11**, 265-273.

Kato, T. & Park, E.Y. (2012) Riboflavin production by Ashbya gossypii. *Biotechnol Lett*, **34**, 611-618.

Katoh, A., Uenohara, K., Akita, M. & Hashimoto, T. (2006) Early Steps in the Biosynthesis of NAD in Arabidopsis Start with Aspartate and Occur in the Plastid. *Plant Physiology*, **141**, 851-857.

Kelly, M.J., Ball, L.J., Krieger, C., Yu, Y., Fischer, M., Schiffmann, S., Schmieder, P., Kühne, R., Bermel, W. & Bacher, A. (2001) The NMR structure of the 47-kDa dimeric enzyme 3, 4-dihydroxy-2-butanone-4-phosphate synthase and ligand binding studies reveal the location of the active site. *Proceedings of the National Academy of Sciences*, **98**, 13025-13030.

Kim, J., Lee, M., Chalam, R., Martin, M.N., Leustek, T. & Boerjan, W. (2002) Constitutive Overexpression of Cystathionine γ-Synthase in Arabidopsis Leads to Accumulation of Soluble Methionine andS-Methylmethionine. *Plant Physiology*, **128**, 95-107.

Kirk, J.T.O. & Tilney-Bassett, R.A.E. (1978) *The Plastids* 2nd edn. Amsterdam, the Netherlands: Elsevier/North Holland.

Kis, K. & Bacher, A. (1995) Substrate Channeling in the Lumazine Synthase/Riboflavin Synthase Complex of Bacillus subtilis. *Journal of Biological Chemistry*, **270**, 16788-16795.

Kis, K., Kugelbrey, K. & Bacher, A. (2001) Biosynthesis of Riboflavin. The Reaction Catalyzed by 6,7-Dimethyl-8-ribityllumazine Synthase Can Proceed without Enzymatic Catalysis under Physiological Conditions†. *The Journal of Organic Chemistry*, **66**, 2555-2559.

Knegt, F.H., Mello, L.V., Reis, F.C., Santos, M.T., Vicentini, R., Ferraz, L.F. & Ottoboni, L.M. (2008) ribB and ribBA genes from Acidithiobacillus ferrooxidans: expression levels under different growth conditions and phylogenetic analysis. *Res Microbiol*, **159**, 423-431.

Kohli, R.M. & Massey, V. (1998) The Oxidative Half-reaction of Old Yellow Enzyme: THE ROLE OF TYROSINE 196. *Journal of Biological Chemistry*, **273**, 32763-32770.

Koncz, C. & Schell, J. (1986) The promoter of TL-DNA gene 5 controls the tissue-specific expression of chimaeric genes carried by a novel type of Agrobacterium binary vector. *Molecular and General Genetics MGG*, **204**, 383-396.

Koornneef, M., Jorna, M.L., Brinkhorst-van der Swan, D.L.C. & Karssen, C.M. (1982) The isolation of abscisic acid (ABA) deficient mutants by selection of induced revertants in non-germinating gibberellin sensitive lines of Arabidopsis thaliana (L.) heynh. *Theoretical and Applied Genetics*, **61**, 385-393.

Koussevitzky, S., Nott, A., Mockler, T.C., Hong, F., Sachetto-Martins, G., Surpin, M., Lim, J., Mittler, R. & Chory, J. (2007) Signals from chloroplasts converge to regulate nuclear gene expression. *Science*, **316**, 715-719.

Krath, B.N., Eriksen, T.A., Poulsen, T.S. & Hove-Jensen, B. (1999) Cloning and sequencing of cDNAs specifying a novel class of phosphoribosyl diphosphate synthase in Arabidopsis thaliana1. *Biochimica et Biophysica Acta (BBA) - Protein Structure and Molecular Enzymology*, **1430**, 403-408.

Kritsky, M.S., Telegina, T.A., Vechtomova, Y.L., Kolesnikov, M.P., Lyudnikova, T.A. & Golub, O.A. (2010) Excited flavin and pterin coenzyme molecules in evolution. *Biochemistry (Moscow)*, **75**, 1200-1216.

Krupa, A., Sandhya, K., Srinivasan, N. & Jonnalagadda, S. (2003) A conserved domain in prokaryotic bifunctional FAD synthetases can potentially catalyze nucleotide transfer. *Trends Biochem Sci*, **28**, 9-12.

Kyte, J. & Doolittle, R.F. (1982) A simple method for displaying the hydropathic character of a protein. *Journal of molecular biology*, **157**, 105-132.

Laemmli, U.K. (1970) Cleavage of structural proteins during the assembly of the head of bacteriophage T4. *Nature*, **227**, 680-685.

Lamesch, P., Berardini, T.Z., Li, D., Swarbreck, D., Wilks, C., Sasidharan, R., Muller, R., Dreher, K., Alexander, D.L., Garcia-Hernandez, M., Karthikeyan, A.S., Lee, C.H., Nelson, W.D., Ploetz, L., Singh, S., Wensel, A. & Huala, E. (2012) The Arabidopsis Information Resource (TAIR): improved gene annotation and new tools. *Nucleic Acids Research*, **40**, D1202-D1210.

Lane, M. & Alfrey, C.P. (1965) The Anemia of Human Riboflavin Deficiency. *Blood*, **25**, 432-442.

Latham, M.C. (1997) *Human nutrition in the developing world*: Food & Agriculture Org.

Le Van, Q., Keller, P., Bown, D., Floss, H. & Bacher, A. (1985) Biosynthesis of riboflavin in Bacillus subtilis: origin of the four-carbon moiety. *Journal of bacteriology*, **162**, 1280-1284.

Lea, P.J. & Miflin, B.J. (2003) Glutamate synthase and the synthesis of glutamate in plants. *Plant Physiology and Biochemistry*, **41**, 555-564.

Lea, P.J., Sodek, L., Parry, M.A.J., Shewry, P.R. & Halford, N.G. (2007) Asparagine in plants. *Annals of Applied Biology*, **150**, 1-26.

Leferink, N.G., van den Berg, W.A. & van Berkel, W.J. (2008) l-Galactono-gamma-lactone dehydrogenase from Arabidopsis thaliana, a flavoprotein involved in vitamin C biosynthesis. *FEBS J*, **275**, 713-726.

Lehtimäki, N., Koskela, M.M. & Mulo, P. (2015) Post-translational modifications of chloroplast proteins: An emerging field. *Plant Physiol*.

Lermontova, I., Kruse, E., Mock, H.-P. & Grimm, B. (1997) Cloning and characterization of a plastidal and a mitochondrial isoform of tobacco protoporphyrinogen IX oxidase. *Proceedings of the National Academy of Sciences*, **94**, 8895-8900.

Leshner, R., HARTLAGE, P. & HAHN, D. (1981) Riboflavin deficiency-a reversible neurodegenerative disease. In *Annals of Neurology*: LIPPINCOTT-RAVEN PUBL 227 EAST WASHINGTON SQ, PHILADELPHIA, PA 19106, pp. 294-295.

Li, L., Hu, L., Han, L.-P., Ji, H., Zhu, Y., Wang, X., Ge, J., Xu, M., Shen, D. & Dong, H. (2014) Expression of turtle riboflavin-binding protein represses mitochondrial electron transport gene expression and promotes flowering in Arabidopsis. *BMC Plant Biology*, **14**, 381.

Li, W., Cowley, A., Uludag, M., Gur, T., McWilliam, H., Squizzato, S., Park, Y.M., Buso, N. & Lopez, R. (2015) The EMBL-EBI bioinformatics web and programmatic tools framework. *Nucleic Acids Research*, **43**, W580-584.

Li, X., Ilarslan, H., Brachova, L., Qian, H.-R., Li, L., Che, P., Wurtele, E.S. & Nikolau, B.J. (2011) Reverse-Genetic Analysis of the Two Biotin-Containing Subunit Genes of the Heteromeric Acetyl-Coenzyme A Carboxylase in Arabidopsis Indicates a Unidirectional Functional Redundancy. *Plant Physiology*, **155**, 293-314.

Liao, D.I., Calabrese, J.C., Wawrzak, Z., Viitanen, P.V. & Jordan, D.B. (2001) Crystal structure of 3,4-dihydroxy-2-butanone 4-phosphate synthase of riboflavin biosynthesis. *Structure*, **9**, 11-18.

Lienhart, W.D., Gudipati, V. & Macheroux, P. (2013) The human flavoproteome. *Arch Biochem Biophys*, **535**, 150-162.

Linka, M. & Weber, A.P.M. (2005) Shuffling ammonia between mitochondria and plastids during photorespiration. *Trends Plant Sci*, **10**, 461-465.

Lisec, J., Schauer, N., Kopka, J., Willmitzer, L. & Fernie, A.R. (2006) Gas chromatography mass spectrometry-based metabolite profiling in plants. *Nat. Protocols*, **1**, 387-396.

Liu, Y., Schiff, M., Marathe, R. & Dinesh-Kumar, S.P. (2002) Tobacco Rar1, EDS1 and NPR1/NIM1 like genes are required for N-mediated resistance to tobacco mosaic virus. *The Plant Journal*, **30**, 415-429.

Livak, K.J. & Schmittgen, T.D. (2001) Analysis of Relative Gene Expression Data Using Real-Time Quantitative PCR and the 2−ΔΔCT Method. *Methods*, **25**, 402-408.

Losi, A. (2004) The bacterial counterparts of plant phototropins. *Photochem Photobiol Sci*, **3**, 566-574.

Lu, G., Campbell, W.H., Schneider, G. & Lindqvist, Y. (1994) Crystal structure of the FAD-containing fragment of corn nitrate reductase at 2.5å resolution: relationship to other flavoprotein reductases. *Structure*, **2**, 809-821.

Lutziger, I. & Oliver, D.J. (2001) Characterization of Two cDNAs Encoding Mitochondrial Lipoamide Dehydrogenase from Arabidopsis. *Plant Physiology*, **127**, 615-623.

Macheroux, P., Kappes, B. & Ealick, S.E. (2011) Flavogenomics--a genomic and structural view of flavin-dependent proteins. *FEBS J*, **278**, 2625-2634.

Macho, A.P., Boutrot, F., Rathjen, J.P. & Zipfel, C. (2012) ASPARTATE OXIDASE Plays an Important Role in Arabidopsis Stomatal Immunity. *Plant Physiology*, **159**, 1845-1856.

Mack, C.P., Hultquist, D.E. & Shlafer, M. (1995) Myocardial flavin reductase and riboflavin: a potential role in decreasing reoxygenation injury. *Biochemical and Biophysical Research Communications*, **212**, 35-40.

Mack, M., van Loon, A.P. & Hohmann, H.-P. (1998) Regulation of Riboflavin Biosynthesis inBacillus subtilis Is Affected by the Activity of the Flavokinase/Flavin Adenine Dinucleotide Synthetase Encoded byribC. *Journal of bacteriology*, **180**, 950-955.

Mandal, M., Boese, B., Barrick, J.E., Winkler, W.C. & Breaker, R.R. (2003) Riboswitches Control Fundamental Biochemical Pathways in Bacillus subtilis and Other Bacteria. *Cell*, **113**, 577-586.

Mani, S., Van de Cotte, B., Van Montagu, M. & Verbruggen, N. (2002) Altered Levels of Proline Dehydrogenase Cause Hypersensitivity to Proline and Its Analogs in Arabidopsis. *Plant Physiology*, **128**, 73-83.

Mansoorabadi, S.O., Thibodeaux, C.J. & Liu, H.-w. (2007) The Diverse Roles of Flavin CoenzymesNature's Most Versatile Thespians. *The Journal of Organic Chemistry*, **72**, 6329-6342.

Maruta, T., Ichikawa, Y., Mieda, T., Takeda, T., Tamoi, M., Yabuta, Y., Ishikawa, T. & Shigeoka, S. (2010) The contribution of Arabidopsis homologs of L-gulono-1,4-lactone oxidase to the biosynthesis of ascorbic acid. *Biosci Biotechnol Biochem*, **74**, 1494-1497.

Maruta, T., Yoshimoto, T., Ito, D., Ogawa, T., Tamoi, M., Yoshimura, K. & Shigeoka, S. (2012) An Arabidopsis FAD Pyrophosphohydrolase, AtNUDX23, is Involved in Flavin Homeostasis. *Plant and Cell Physiology*, **53**, 1106-1116.

Marx, H., Mattanovich, D. & Sauer, M. (2008) Overexpression of the riboflavin biosynthetic pathway in Pichia pastoris. *Microb Cell Fact*, **7**, 1-11.

Massey, V. (1994) Activation of Molecular Oxygen by Flavins and Flavoproteins.

Massey, V., Strickland, S., Mayhew, S.G., Howell, L.G., Engel, P.C., Matthews, R.G., Schuman, M. & Sullivan, P.A. (1969) The production of superoxide anion radicals in the reaction of reduced flavins and flavoproteins with molecular oxygen. *Biochemical and Biophysical Research Communications*, **36**, 891-897.

Mattick, J.S. & Gagen, M.J. (2001) The Evolution of Controlled Multitasked Gene Networks: The Role of Introns and Other Noncoding RNAs in the Development of Complex Organisms. *Molecular Biology and Evolution*, **18**, 1611-1630.

McCormick, D.B., Oka, M., Bowers-Komro, D.M., Yamada, Y. & Hartman, H.A. (1997) Purification and properties of FAD synthetase from liver. *Methods Enzymol*, **280**, 407-413.

Mendel, G. (1866) Versuche über Pflanzenhybriden. *Verhandlungen des naturforschenden Vereines in Brunn 4: 3*, **44**.

Meyer, E.H., Tomaz, T., Carroll, A.J., Estavillo, G., Delannoy, E., Tanz, S.K., Small, I.D., Pogson, B.J. & Millar, A.H. (2009) Remodeled respiration in ndufs4 with low phosphorylation efficiency suppresses Arabidopsis germination and growth and alters control of metabolism at night. *Plant Physiol*, **151**, 603-619.

Michael, T.P., Breton, G., Hazen, S.P., Priest, H., Mockler, T.C., Kay, S.A. & Chory, J. (2008) A Morning-Specific Phytohormone Gene Expression Program underlying Rhythmic Plant Growth. *PLoS Biol*, **6**, e225.

Michaelis, L. & Menten, M.L. (1913) Die kinetik der invertinwirkung. *Biochem. z*, **49**, 352.

Mieda, T., Yabuta, Y., Rapolu, M., Motoki, T., Takeda, T., Yoshimura, K., Ishikawa, T. & Shigeoka, S. (2004) Feedback Inhibition of Spinach l-Galactose Dehydrogenase by l-Ascorbate. *Plant and Cell Physiology*, **45**, 1271-1279.

Millar, A.H., Hill, S.A. & Leaver, C.J. (1999) Plant mitochondrial 2-oxoglutarate dehydrogenase complex: purification and characterization in potato. *Biochem J*, **343 Pt 2**, 327-334.

Miller, E. & Nickoloff, J. (1995) Escherichia coli Electrotransformation. In *Electroporation Protocols for Microorganisms* (Nickoloff, J. ed: Humana Press, pp. 105-113.

Mironov, A.S., Gusarov, I., Rafikov, R., Lopez, L.E., Shatalin, K., Kreneva, R.A., Perumov, D.A. & Nudler, E. (2002) Sensing small molecules by nascent RNA: a mechanism to control transcription in bacteria. *Cell*, **111**, 747-756.

Mitsuda, H., Kawai, F., Suzuki, Y. & Yoshimoto, S. (1970a) Biogenesis of riboflavin in green leaves. VII. Isolation and characterization of spinach riboflavin synthetase. *J Vitaminol (Kyoto)*, **16**, 285-292.

Mitsuda, H., Tsuge, H., Tomozawa, Y. & Kawai, F. (1970b) Multiplicity of acid phosphatase catalyzing FMN hydrolysis in spinach leaves. *J Vitaminol (Kyoto)*, **16**, 52-57.

Moore, B. (2004) Bifunctional and moonlighting enzymes: lighting the way to regulatory control. *Trends Plant Sci*, **9**, 221-228.

Morgulis, A., Coulouris, G., Raytselis, Y., Madden, T.L., Agarwala, R. & Schaffer, A.A. (2008) Database indexing for production MegaBLAST searches. *Bioinformatics*, **24**, 1757-1764.

Müller, F. (1983) The flavin redox-system and its biological function. In *Radicals in Biochemistry*: Springer Berlin Heidelberg, pp. 71-107.

Mullineaux, P., Ball, L., Escobar, C., Karpinska, B., Creissen, G. & Karpinski, S. (2000) Are diverse signalling pathways integrated in the regulation of arabidopsis antioxidant defence gene expression in response to excess excitation energy? *Philos Trans R Soc Lond B Biol Sci*, **355**, 1531-1540.

Mullis, K., Faloona, F., Scharf, S., Saiki, R., Horn, G. & Erlich, H. (1986) Specific enzymatic amplification of DNA in vitro: the polymerase chain reaction. *Cold Spring Harb Symp Quant Biol*, **51 Pt 1**, 263-273.

Muñoz-Bertomeu, J., Cascales-Miñana, B., Mulet, J.M., Baroja-Fernández, E., Pozueta-Romero, J., Kuhn, J.M., Segura, J. & Ros, R. (2009) Plastidial Glyceraldehyde-3-Phosphate Dehydrogenase Deficiency Leads to Altered Root Development and Affects the Sugar and Amino Acid Balance in Arabidopsis. *Plant Physiology*, **151**, 541-558.

Næsted, H., Holm, A., Jenkins, T., Nielsen, H.B., Harris, C.A., Beale, M.H., Andersen, M., Mant, A., Scheller, H., Camara, B., Mattsson, O. & Mundy, J. (2004) Arabidopsis VARIEGATED 3 encodes a chloroplast-targeted, zinc-finger protein required for chloroplast and palisade cell development. *Journal of Cell Science*, **117**, 4807-4818.

Nakayama, M., Akashi, T. & Hase, T. (2000) Plant sulfite reductase: molecular structure, catalytic function and interaction with ferredoxin. *Journal of Inorganic Biochemistry*, **82**, 27-32.

Narita, S., Tanaka, R., Ito, T., Okada, K., Taketani, S. & Inokuchi, H. (1996) Molecular cloning and characterization of a cDNA that encodes protoporphyrinogen oxidase of Arabidopsis thaliana. *Gene*, **182**, 169-175.

Neuberger, G. & Bacher, A. (1986) Biosynthesis of riboflavin. Enzymatic formation of 6, 7-dimethyl-8-ribityllumazine by heavy riboflavin synthase from Bacillus subtilis. *Biochemical and Biophysical Research Communications*, **139**, 1111-1116.

Nguyen, K.V. & Burrows, C.J. (2012) Whence Flavins? Redox-Active Ribonucleotides Link Metabolism and Genome Repair to the RNA World. *Accounts of Chemical Research*, **45**, 2151-2159.

Niyogi, K.K. (1999) PHOTOPROTECTION REVISITED: Genetic and Molecular Approaches. *Annual Review of Plant Physiology and Plant Molecular Biology*, **50**, 333-359.

Noctor, G., Arisi, A.-C.M., Jouanin, L., Kunert, K.J., Rennenberg, H. & Foyer, C.H. (1998) Glutathione: biosynthesis, metabolism and relationship to stress tolerance explored in transformed plants. *Journal of Experimental Botany*, **49**, 623-647.

Noctor, G., Queval, G. & Gakière, B. (2006) NAD(P) synthesis and pyridine nucleotide cycling in plants and their potential importance in stress conditions. *Journal of Experimental Botany*, **57**, 1603-1620.

Ochs, R.S. (2000) Understanding enzyme inhibition. *Journal of Chemical Education*, **77**, 1453.

Ogawa, T., Yoshimura, K., Miyake, H., Ishikawa, K., Ito, D., Tanabe, N. & Shigeoka, S. (2008) Molecular Characterization of Organelle-Type Nudix Hydrolases in Arabidopsis. *Plant Physiology*, **148**, 1412-1424.

Onate-Sanchez, L. & Vicente-Carbajosa, J. (2008) DNA-free RNA isolation protocols for Arabidopsis thaliana, including seeds and siliques. *BMC Research Notes*, **1**, 93.

op den Camp, R.G., Przybyla, D., Ochsenbein, C., Laloi, C., Kim, C., Danon, A., Wagner, D., Hideg, E., Gobel, C., Feussner, I., Nater, M. & Apel, K. (2003) Rapid induction of distinct stress responses after the release of singlet oxygen in Arabidopsis. *Plant Cell*, **15**, 2320-2332.

Ouyang, M., Ma, J., Zou, M., Guo, J., Wang, L., Lu, C. & Zhang, L. (2010) The photosensitive phs1 mutant is impaired in the riboflavin biogenesis pathway. *J Plant Physiol*, **167**, 1466-1476.

Peltier, J.-B., Cai, Y., Sun, Q., Zabrouskov, V., Giacomelli, L., Rudella, A., Ytterberg, A.J., Rutschow, H. & van Wijk, K.J. (2006) The Oligomeric Stromal Proteome of Arabidopsis thaliana Chloroplasts. *Molecular & Cellular Proteomics*, **5**, 114-133.

Peter, E. & Grimm, B. (2009) GUN4 Is Required for Posttranslational Control of Plant Tetrapyrrole Biosynthesis. *Molecular Plant*, **2**, 1198-1210.

Phillips, M.A., D'Auria, J.C., Gershenzon, J. & Pichersky, E. (2008) The Arabidopsis thaliana Type I Isopentenyl Diphosphate Isomerases Are Targeted to Multiple Subcellular Compartments and Have Overlapping Functions in Isoprenoid Biosynthesis. *Plant Cell*, **20**, 677-696.

Pillot, M., Baroux, C., Vazquez, M.A., Autran, D., Leblanc, O., Vielle-Calzada, J.P., Grossniklaus, U. & Grimanelli, D. (2010) Embryo and Endosperm Inherit Distinct Chromatin and Transcriptional States from the Female Gametes in Arabidopsis. *Plant Cell*, **22**, 307-320.

Plaut, G.W., Beach, R.L. & Aogaichi, T. (1970) Studies on the mechanism of elimination of protons from the methyl groups of 6,7-dimethyl-8-ribityllumazine by riboflavin synthetase. *Biochemistry*, **9**, 771-785.

Popp, A., Lotze-Campen, H. & Bodirsky, B. (2010) Food consumption, diet shifts and associated non-CO2 greenhouse gases from agricultural production. *Global Environmental Change*, **20**, 451-462.

Porra, R.J., Thompson, W.A. & Kriedemann, P.E. (1989) Determination of accurate extinction coefficients and simultaneous equations for assaying chlorophylls a and b extracted with four different solvents:

verification of the concentration of chlorophyll standards by atomic absorption spectroscopy. *Biochimica et Biophysica Acta (BBA) - Bioenergetics*, **975**, 384-394.

Powers, H.J. (2003) Riboflavin (vitamin B-2) and health. *The American journal of clinical nutrition*, **77**, 1352-1360.

Pulido, P., Spinola, M.C., Kirchsteiger, K., Guinea, M., Pascual, M.B., Sahrawy, M., Sandalio, L.M., Dietz, K.J., Gonzalez, M. & Cejudo, F.J. (2010) Functional analysis of the pathways for 2-Cys peroxiredoxin reduction in Arabidopsis thaliana chloroplasts. *J Exp Bot*, **61**, 4043-4054.

Qin, G., Gu, H., Ma, L., Peng, Y., Deng, X.W., Chen, Z. & Qu, L.-J. (2007) Disruption of phytoene desaturase gene results in albino and dwarf phenotypes in Arabidopsis by impairing chlorophyll, carotenoid, and gibberellin biosynthesis. *Cell Res*, **17**, 471-482.

Rawat, R., Sandoval, F.J., Wei, Z., Winkler, R. & Roje, S. (2011) An FMN hydrolase of the haloacid dehalogenase superfamily is active in plant chloroplasts. *J Biol Chem*, **286**, 42091-42098.

Rédei, G.P. (1967) Biochemical Aspects of a Genetically Determined Variegation in Arabidopsis. *Genetics*, **56**, 431-443.

Reiland, S., Messerli, G., Baerenfaller, K., Gerrits, B., Endler, A., Grossmann, J., Gruissem, W. & Baginsky, S. (2009) Large-scale Arabidopsis phosphoproteome profiling reveals novel chloroplast kinase substrates and phosphorylation networks. *Plant Physiol*, **150**, 889-903.

Ren, J., Kotaka, M., Lockyer, M., Lamb, H.K., Hawkins, A.R. & Stammers, D.K. (2005) GTP Cyclohydrolase II Structure and Mechanism. *Journal of Biological Chemistry*, **280**, 36912-36919.

Rice, P., Longden, I. & Bleasby, A. (2000) EMBOSS: the European Molecular Biology Open Software Suite. *Trends Genet*, **16**, 276-277.

Richter, G., Kelly, M., Krieger, C., Yu, Y., Bermel, W., Karlsson, G., Bacher, A. & Oschkinat, H. (1999) NMR studies on the 46-kDa dimeric protein, 3,4-dihydroxy-2-butanone 4-phosphate synthase, using 2H, 13C, and 15N-labelling. *European Journal of Biochemistry*, **261**, 57-65.

Richter, G., Ritz, H., Katzenmeier, G., Volk, R., Kohnle, A., Lottspeich, F., Allendorf, D. & Bacher, A. (1993) Biosynthesis of riboflavin: cloning, sequencing, mapping, and expression of the gene coding for GTP cyclohydrolase II in Escherichia coli. *J Bacteriol*, **175**, 4045-4051.

Richter, G., Volk, R., Krieger, C., Lahm, H.W., Rothlisberger, U. & Bacher, A. (1992) Biosynthesis of riboflavin: cloning, sequencing, and expression of the gene coding for 3,4-dihydroxy-2-butanone 4-phosphate synthase of Escherichia coli. *J Bacteriol*, **174**, 4050-4056.

Ritz, H., Schramek, N., Bracher, A., Herz, S., Eisenreich, W., Richter, G. & Bacher, A. (2001) Biosynthesis of riboflavin: studies on the mechanism of GTP cyclohydrolase II. *J Biol Chem*, **276**, 22273-22277.

Rivlin, R.S. (1973) Riboflavin and cancer: a review. *Cancer Res*, **33**, 1977-1986.

Rizhsky, L., Davletova, S., Liang, H. & Mittler, R. (2004) The zinc finger protein Zat12 is required for cytosolic ascorbate peroxidase 1 expression during oxidative stress in Arabidopsis. *J Biol Chem*, **279**, 11736-11743.

Röbbelen, G. (1968) Genbedingte rotlicht-empfindlichkeit der chloroplastendifferenzierung bei Arabidopsis. *Planta*, **80**, 237-254.

Rodríguez-Celma, J., Lattanzio, G., Grusak, M.A., Abadía, A., Abadía, J. & Lopez-Millan, A.-F. (2011) Root responses of Medicago truncatula plants grown in two different iron deficiency conditions: changes in root protein profile and riboflavin biosynthesis. *Journal of proteome research*, **10**, 2590-2601.

Rodriguez-Celma, J., Vazquez-Reina, S., Orduna, J., Abadia, A., Abadia, J., Alvarez-Fernandez, A. & Lopez-Millan, A.F. (2011) Characterization of flavins in roots of Fe-deficient strategy I plants, with a focus on Medicago truncatula. *Plant Cell Physiol*, **52**, 2173-2189.

Rudolf, M., Machettira, A.B., Groß, L.E., Weber, K.L., Bolte, K., Bionda, T., Sommer, M.S., Maier, U.G., Weber, A.P.M., Schleiff, E. & Tripp, J. (2013) In Vivo Function of Tic22, a Protein Import Component of the Intermembrane Space of Chloroplasts. *Molecular Plant*, **6**, 817-829.

Ruiz-Sola, M.Á. & Rodríguez-Concepción, M. (2012) Carotenoid Biosynthesis in Arabidopsis: A Colorful Pathway. *The Arabidopsis Book / American Society of Plant Biologists*, **10**, e0158.

Sabar, M., De Paepe, R. & de Kouchkovsky, Y. (2000) Complex I Impairment, Respiratory Compensations, and Photosynthetic Decrease in Nuclear and Mitochondrial Male Sterile Mutants of Nicotiana sylvestris. *Plant Physiology*, **124**, 1239-1250.

Sakamoto, W., Zaltsman, A., Adam, Z. & Takahashi, Y. (2003) Coordinated Regulation and Complex Formation of YELLOW VARIEGATED1 and YELLOW VARIEGATED2, Chloroplastic FtsH Metalloproteases Involved in the Repair Cycle of Photosystem II in Arabidopsis Thylakoid Membranes. *Plant Cell*, **15**, 2843-2855.

Sambrook, J. & Russell, D.W. (2001) *Molecular cloning : a laboratory manual* 3rd edn. Cold Spring Harbor, N.Y.: Cold Spring Harbor Laboratory Press.

Sancar, A. (2003) Structure and Function of DNA Photolyase and Cryptochrome Blue-Light Photoreceptors. *Chemical Reviews*, **103**, 2203-2238.

Sandoval, F.J. & Roje, S. (2005) An FMN hydrolase is fused to a riboflavin kinase homolog in plants. *J Biol Chem*, **280**, 38337-38345.

Sandoval, F.J., Zhang, Y. & Roje, S. (2008) Flavin nucleotide metabolism in plants: monofunctional enzymes synthesize fad in plastids. *J Biol Chem*, **283**, 30890-30900.

Sanger, F., Nicklen, S. & Coulson, A.R. (1977) DNA sequencing with chain-terminating inhibitors. *Proceedings of the National Academy of Sciences*, **74**, 5463-5467.

Santos, M.A., Jimenez, A. & Revuelta, J.L. (2000) Molecular characterization of FMN1, the structural gene for the monofunctional flavokinase of Saccharomyces cerevisiae. *J Biol Chem*, **275**, 28618-28624.

Schertl, P., Cabassa, C., Saadallah, K., Bordenave, M., Savouré, A. & Braun, H.-P. (2014) Biochemical characterization of proline dehydrogenase in Arabidopsis mitochondria. *FEBS Journal*, **281**, 2794-2804.

Schlicke, H., Hartwig, A.S., Firtzlaff, V., Richter, A.S., Glässer, C., Maier, K., Finkemeier, I. & Grimm, B. (2014) Induced Deactivation of Genes Encoding Chlorophyll Biosynthesis Enzymes Disentangles Tetrapyrrole-Mediated Retrograde Signaling. *Molecular Plant*, **7**, 1211-1227.

Schlosser, T., Schmidt, G. & Stahmann, K.P. (2001) Transcriptional regulation of 3,4-dihydroxy-2-butanone 4-phosphate synthase. *Microbiology*, **147**, 3377-3386.

Schlosser, T., Wiesenburg, A., Gatgens, C., Funke, A., Viets, U., Vijayalakshmi, S., Nieland, S. & Stahmann, K.P. (2007) Growth stress triggers riboflavin overproduction in Ashbya gossypii. *Appl Microbiol Biotechnol*, **76**, 569-578.

Schneider, A., Häusler, R.E., Kolukisaoglu, Ü., Kunze, R., Van Der Graaff, E., Schwacke, R., Catoni, E., Desimone, M. & Flügge, U.I. (2002) An Arabidopsis thaliana knock-out mutant of the chloroplast triose phosphate/phosphate translocator is severely compromised only when starch synthesis, but not starch mobilisation is abolished. *The Plant Journal*, **32**, 685-699.

Schramm, K., Niehof, M., Radziwill, G., Rommel, C. & Moelling, K. (1994) Phosphorylation of c-Raf-1 by Protein Kinase A Interferes with Activation. *Biochemical and Biophysical Research Communications*, **201**, 740-747.

Schwarz, N., Armbruster, U., Iven, T., Brückle, L., Melzer, M., Feussner, I. & Jahns, P. (2015) Tissue-Specific Accumulation and Regulation of Zeaxanthin Epoxidase in Arabidopsis Reflect the Multiple Functions of the Enzyme in Plastids. *Plant and Cell Physiology*, **56**, 346-357.

Seo, M., Koiwai, H., Akaba, S., Komano, T., Oritani, T., Kamiya, Y. & Koshiba, T. (2000) Abscisic aldehyde oxidase in leaves of Arabidopsis thaliana. *The Plant Journal*, **23**, 481-488.

Sievers, F., Wilm, A., Dineen, D., Gibson, T.J., Karplus, K., Li, W., Lopez, R., McWilliam, H., Remmert, M., Söding, J., Thompson, J.D. & Higgins, D.G. (2011) Fast, scalable generation of high-quality protein multiple sequence alignments using Clustal Omega. In *Molecular Systems Biology*, pp. 539.

Silva-Sanchez, C., Li, H. & Chen, S. (2015) Recent advances and challenges in plant phosphoproteomics. *Proteomics*, **15**, 1127-1141.

Singh, M., Kumar, P. & Karthikeyan, S. (2011) Structural basis for pH dependent monomer–dimer transition of 3,4-dihydroxy 2-butanone-4-phosphate synthase domain from Mycobacterium tuberculosis. *Journal of Structural Biology*, **174**, 374-384.

Singh, M., Kumar, P., Yadav, S., Gautam, R., Sharma, N. & Karthikeyan, S. (2013) The crystal structure reveals the molecular mechanism of bifunctional 3,4-dihydroxy-2-butanone 4-phosphate synthase/GTP cyclohydrolase II (Rv1415) from Mycobacterium tuberculosis. *Acta Crystallogr D Biol Crystallogr*, **69**, 1633-1644.

Sirpiö, S., Khrouchtchova, A., Allahverdiyeva, Y., Hansson, M., Fristedt, R., Vener, A.V., Scheller, H.V., Jensen, P.E., Haldrup, A. & Aro, E.-M. (2008) AtCYP38 ensures early biogenesis, correct assembly and sustenance of photosystem II. *The Plant Journal*, **55**, 639-651.

Smedts, H.P.M., Rakhshandehroo, M., Verkleij-Hagoort, A.C., Vries, J.H.M., Ottenkamp, J., Steegers, E.A.P. & Steegers-Theunissen, R.P.M. (2008) Maternal intake of fat, riboflavin and nicotinamide and the risk of having offspring with congenital heart defects. *European Journal of Nutrition*, **47**, 357-365.

Smith, A.M. & Stitt, M. (2007) Coordination of carbon supply and plant growth. *Plant, Cell & Environment*, **30**, 1126-1149.

Smith, A.M., Zeeman, S.C. & Smith, S.M. (2005) STARCH DEGRADATION. *Annual Review of Plant Biology*, **56**, 73-98.

Snel, B., Bork, P. & Huynen, M. (2000) Genome evolution. Gene fusion versus gene fission. *Trends Genet*, **16**, 9-11.

Soole, K. & Menz, R.I. (1995) Functional molecular aspects of the NADH dehydrogenases of plant mitochondria. *Journal of Bioenergetics and Biomembranes*, **27**, 397-406.

Steinbacher, S., Schiffmann, S., Richter, G., Huber, R., Bacher, A. & Fischer, M. (2003) Structure of 3, 4-Dihydroxy-2-butanone 4-Phosphate Synthase from Methanococcus jannaschii in Complex with Divalent Metal Ions and the Substrate Ribulose 5-Phosphate IMPLICATIONS FOR THE CATALYTIC MECHANISM. *Journal of Biological Chemistry*, **278**, 42256-42265.

Sterner, R.T. & Price, W.R. (1973) Restricted riboflavin: within-subject behavioral effects in humans. *The American journal of clinical nutrition*, **26**, 150-160.

Stinson, R.A. & Spencer, M.S. (1969) Beta alanine aminotransferase (s) from a plant source. *Biochem Biophys Res Commun*, **34**, 120-127.

Stitt, M., Sulpice, R. & Keurentjes, J. (2010) Metabolic Networks: How to Identify Key Components in the Regulation of Metabolism and Growth. *Plant Physiology*, **152**, 428-444.

Sudarsan, N., Barrick, J.E. & Breaker, R.R. (2003) Metabolite-binding RNA domains are present in the genes of eukaryotes. *Rna*, **9**, 644-647.

Sunilkumar, G., Mohr, L., Lopata-Finch, E., Emani, C. & Rathore, K.S. (2002) Developmental and tissue-specific expression of CaMV 35S promoter in cotton as revealed by GFP. *Plant molecular biology*, **50**, 463-479.

Susin, S., Abian, J., Sanchez-Baeza, F., Peleato, M.L., Abadia, A., Gelpi, E. & Abadia, J. (1993) Riboflavin 3'-and 5'-sulfate, two novel flavins accumulating in the roots of iron-deficient sugar beet (Beta vulgaris). *Journal of Biological Chemistry*, **268**, 20958-20965.

Suwastika, I.N., Denawa, M., Yomogihara, S., Im, C.H., Bang, W.Y., Ohniwa, R.L., Bahk, J.D., Takeyasu, K. & Shiina, T. (2014) Evidence for lateral gene transfer (LGT) in the evolution of eubacteria-derived small GTPases in plant organelles. *Front Plant Sci*, **5**, 678.

Shevchuk, N.A., Bryksin, A.V., Nusinovich, Y.A., Cabello, F.C., Sutherland, M. & Ladisch, S. (2004) Construction of long DNA molecules using long PCR-based fusion of several fragments simultaneously. *Nucleic Acids Research*, **32**, e19.

Taheri, P. & Tarighi, S. (2010) Riboflavin induces resistance in rice against Rhizoctonia solani via jasmonate-mediated priming of phenylpropanoid pathway. *Journal of Plant Physiology*, **167**, 201-208.

Taiz, L., Zeiger, E., Moller, I.M. & Mirphy, A. (2015) *Plant physiology and development* Sixth edition. edn. Sunderland, Massachusetts: Sinauer Associates.

Temple, S.J., Vance, C.P. & Stephen Gantt, J. (1998) Glutamate synthase and nitrogen assimilation. *Trends Plant Sci*, **3**, 51-56.

Timm, S., Wittmiß, M., Gamlien, S., Ewald, R., Florian, A., Frank, M., Wirtz, M., Hell, R., Fernie, A.R. & Bauwe, H. (2015) Mitochondrial Dihydrolipoyl Dehydrogenase Activity Shapes Photosynthesis and Photorespiration of Arabidopsis thaliana. *Plant Cell*.

Torchetti, E.M., Brizio, C., Colella, M., Galluccio, M., Giancaspero, T.A., Indiveri, C., Roberti, M. & Barile, M. (2010) Mitochondrial localization of human FAD synthetase isoform 1. *Mitochondrion*, **10**, 263-273.

Tzin, V. & Galili, G. (2010) The Biosynthetic Pathways for Shikimate and Aromatic Amino Acids in Arabidopsis thaliana. *The Arabidopsis Book / American Society of Plant Biologists*, **8**, e0132.

Thieme, C.J., Rojas-Triana, M., Stecyk, E., Schudoma, C., Zhang, W., Yang, L., Miñambres, M., Walther, D., Schulze, W.X., Paz-Ares, J., Scheible, W.-R. & Kragler, F. (2015) Endogenous Arabidopsis messenger RNAs transported to distant tissues. *Nature Plants*, **1**, 15025.

Uematsu, K., Suzuki, N., Iwamae, T., Inui, M. & Yukawa, H. (2012) Increased fructose 1,6-bisphosphate aldolase in plastids enhances growth and photosynthesis of tobacco plants. *Journal of Experimental Botany*, **63**, 3001-3009.

Velásquez, A.C., Chakravarthy, S. & Martin, G.B. (2009) Virus-induced Gene Silencing (VIGS) in Nicotiana benthamiana and Tomato. *Journal of Visualized Experiments : JoVE*, 1292.

Velez-Ramirez, A.I., van Ieperen, W., Vreugdenhil, D. & Millenaar, F.F. (2011) Plants under continuous light. *Trends Plant Sci*, **16**, 310-318.

Vidi, P.-A., Kanwischer, M., Baginsky, S., Austin, J.R., Csucs, G., Dörmann, P., Kessler, F. & Bréhélin, C. (2006) Tocopherol Cyclase (VTE1) Localization and Vitamin E Accumulation in Chloroplast Plastoglobule Lipoprotein Particles. *Journal of Biological Chemistry*, **281**, 11225-11234.

Vidi, P.-A., Kessler, F. & Bréhélin, C. (2007) Plastoglobules: a new address for targeting recombinant proteins in the chloroplast. *BMC Biotechnol*, **7**, 1-12.

Voet, D. & Voet, J.G. (1990) *Biochemistry* New York u.a.: Wiley.

Voinnet, O., Rivas, S., Mestre, P. & Baulcombe, D. (2003) An enhanced transient expression system in plants based on suppression of gene silencing by the p19 protein of tomato bushy stunt virus. *Plant J*, **33**, 949-956.

Volk, R. & Bacher, A. (1990) Studies on the 4-carbon precursor in the biosynthesis of riboflavin. Purification and properties of L-3,4-dihydroxy-2-butanone-4-phosphate synthase. *Journal of Biological Chemistry*, **265**, 19479-19485.

Volk, R. & Bacher, A. (1991) Biosynthesis of riboflavin. Studies on the mechanism of L-3,4-dihydroxy-2-butanone 4-phosphate synthase. *Journal of Biological Chemistry*, **266**, 20610-20618.

Vorwieger, A., Gryczka, C., Czihal, A., Douchkov, D., Tiedemann, J., Mock, H.P., Jakoby, M., Weisshaar, B., Saalbach, I. & Baumlein, H. (2007) Iron assimilation and transcription factor controlled synthesis of riboflavin in plants. *Planta*, **226**, 147-158.

Wachter, A., Tunc-Ozdemir, M., Grove, B.C., Green, P.J., Shintani, D.K. & Breaker, R.R. (2007) Riboswitch control of gene expression in plants by splicing and alternative 3′ end processing of mRNAs. *Plant Cell*, **19**, 3437-3450.

Waldron, C., Murphy, E.B., Roberts, J.L., Gustafson, G.D., Armour, S.L. & Malcolm, S.K. (1985) Resistance to hygromycin B. *Plant molecular biology*, **5**, 103-108.

Walsh, C. (1980) Flavin coenzymes: at the crossroads of biological redox chemistry. *Accounts of Chemical Research*, **13**, 148-155.

Walter, M., Chaban, C., Schütze, K., Batistic, O., Weckermann, K., Näke, C., Blazevic, D., Grefen, C., Schumacher, K. & Oecking, C. (2004) Visualization of protein interactions in living plant cells using bimolecular fluorescence complementation. *The Plant Journal*, **40**, 428-438.

Wallace, A., Frolich, E.F. & ElGazzar, A. (1967) Root excretions in iron-deficient tobacco plants and possible effects on iron nutrition: California Univ., Los Angeles (USA). Lab. of Nuclear Medicine and Radiation Biology.

Wang, Q., Barshop, William D., Bian, M., Vashisht, Ajay A., He, R., Yu, X., Liu, B., Nguyen, P., Liu, X., Zhao, X., Wohlschlegel, James A. & Lin, C. (2015) The Blue Light-Dependent Phosphorylation of the CCE Domain Determines the Photosensitivity of Arabidopsis CRY2. *Molecular Plant*, **8**, 631-643.

Wang, W., Kim, R., Yokota, H. & Kim, S.H. (2005) Crystal structure of flavin binding to FAD synthetase of Thermotoga maritima. *Proteins*, **58**, 246-248.

Warburg, O. & Christian, W. (1932) Ein zweites sauerstoffübertragendes Ferment und sein Absorptionsspektrum. *Naturwissenschaften*, **20**, 688-688.

Wegrzyn, J.L., Lee, J.M., Tearse, B.R. & Neale, D.B. (2008) TreeGenes: A Forest Tree Genome Database. *International Journal of Plant Genomics*, **2008**.

Wetzel, C.M., Jiang, C.-Z., Meehan, L.J., Voytas, D.F. & Rodermel, S.R. (1994) Nuclear—organelle interactions: the immutans variegation mutant of Arabidopsis is plastid autonomous and impaired in carotenoid biosynthesis. *The Plant Journal*, **6**, 161-175.

White, J., Chang, S.Y., Bibb, M.J. & Bibb, M.J. (1990) A cassette containing the bar gene of Streptomyces hygroscopicus: a selectable marker for plant transformation. *Nucleic Acids Research*, **18**, 1062.

Willig, A., Shapiguzov, A., Goldschmidt-Clermont, M. & Rochaix, J.-D. (2011) The Phosphorylation Status of the Chloroplast Protein Kinase STN7 of Arabidopsis Affects Its Turnover. *Plant Physiology*, **157**, 2102-2107.

Winkel, B.S.J. (2004) METABOLIC CHANNELING IN PLANTS. *Annual Review of Plant Biology*, **55**, 85-107.

Winkler, W., Nahvi, A. & Breaker, R.R. (2002) Thiamine derivatives bind messenger RNAs directly to regulate bacterial gene expression. *Nature*, **419**, 952-956.

Witte, C.-P., Noël, L.D., Gielbert, J., Parker, J.E. & Romeis, T. (2004) Rapid one-step protein purification from plant material using the eight-amino acid StrepII epitope. *Plant molecular biology*, **55**, 135-147.

Wittekind, M., Reizer, J., Deutscher, J., Saier, M.H. & Klevit, R.E. (1989) Common structural changes accompany the functional inactivation of HPr by seryl phosphorylation or by serine to aspartate substitution. *Biochemistry*, **28**, 9908-9912.

Wittrahm, R. (2014) Genetic and biochemical characterization of the RIBA protein family in Arabidopsis. In *Lebenswissenschaftliche Fakultät - Institut für Biologie*. Berlin: Humboldt Universität zu Berlin.

Wu, D., Wright, D.A., Wetzel, C., Voytas, D.F. & Rodermel, S. (1999) The IMMUTANS Variegation Locus of Arabidopsis Defines a Mitochondrial Alternative Oxidase Homolog That Functions during Early Chloroplast Biogenesis. *Plant Cell*, **11**, 43-55.

Wu, M., Repetto, B., Glerum, D.M. & Tzagoloff, A. (1995) Cloning and characterization of FAD1, the structural gene for flavin adenine dinucleotide synthetase of Saccharomyces cerevisiae. *Mol Cell Biol*, **15**, 264-271.

Xiang, D., Venglat, P., Tibiche, C., Yang, H., Risseeuw, E., Cao, Y., Babic, V., Cloutier, M., Keller, W., Wang, E., Selvaraj, G. & Datla, R. (2011) Genome-Wide Analysis Reveals Gene Expression and Metabolic Network Dynamics during Embryo Development in Arabidopsis. *Plant Physiology*, **156**, 346-356.

Xiao, S., Dai, L., Liu, F., Wang, Z., Peng, W. & Xie, D. (2004) COS1: an Arabidopsis coronatine insensitive1 suppressor essential for regulation of jasmonate-mediated plant defense and senescence. *Plant Cell*, **16**, 1132-1142.

Yabuta, Y., Mieda, T., Rapolu, M., Nakamura, A., Motoki, T., Maruta, T., Yoshimura, K., Ishikawa, T. & Shigeoka, S. (2007) Light regulation of ascorbate biosynthesis is dependent on the photosynthetic electron transport chain but independent of sugars in Arabidopsis. *Journal of Experimental Botany*, **58**, 2661-2671.

Yadav, S. & Karthikeyan, S. (2015) Structural and biochemical characterization of GTP cyclohydrolase II from Helicobacter pylori reveals its redox dependent catalytic activity. *Journal of Structural Biology*, **192**, 100-115.

Yan, J., Zhang, C., Gu, M., Bai, Z., Zhang, W., Qi, T., Cheng, Z., Peng, W., Luo, H., Nan, F., Wang, Z. & Xie, D. (2009) The Arabidopsis CORONATINE INSENSITIVE1 Protein Is a Jasmonate Receptor. *Plant Cell*, **21**, 2220-2236.

Yarmolinsky, D., Brychkova, G., Fluhr, R. & Sagi, M. (2013) Sulfite reductase protects plants against sulfite toxicity. *Plant Physiol*, **161**, 725-743.

Yruela, I., Arilla-Luna, S., Medina, M. & Contreras-Moreira, B. (2010) Evolutionary divergence of chloroplast FAD synthetase proteins. *BMC Evol Biol*, **10**, 311.

Ytterberg, A.J., Peltier, J.-B. & van Wijk, K.J. (2006) Protein Profiling of Plastoglobules in Chloroplasts and Chromoplasts. A Surprising Site for Differential Accumulation of Metabolic Enzymes. *Plant Physiology*, **140**, 984-997.

Yu, F.E.I., Fu, A., Aluru, M., Park, S., Xu, Y., Liu, H., Liu, X., Foudree, A., Nambogga, M. & Rodermel, S. (2007) Variegation mutants and mechanisms of chloroplast biogenesis. *Plant, Cell & Environment*, **30**, 350-365.

Yu, Q., Ghisla, S., Hirschberg, J., Mann, V. & Beyer, P. (2011) Plant Carotene Cis-Trans Isomerase CRTISO: A NEW MEMBER OF THE FADRED-DEPENDENT FLAVOPROTEINS CATALYZING NON-REDOX REACTIONS. *Journal of Biological Chemistry*, **286**, 8666-8676.

Yu, X., Liu, H., Klejnot, J. & Lin, C. (2010) The Cryptochrome Blue Light Receptors. *The Arabidopsis Book / American Society of Plant Biologists*, **8**, e0135.

Zeeman, S.C., Thorneycroft, D., Schupp, N., Chapple, A., Weck, M., Dunstan, H., Haldimann, P., Bechtold, N., Smith, A.M. & Smith, S.M. (2004) Plastidial alpha-glucan phosphorylase is not required for starch degradation in Arabidopsis leaves but has a role in the tolerance of abiotic stress. *Plant Physiol*, **135**, 849-858.

Zrenner, R., Riegler, H., Marquard, C.R., Lange, P.R., Geserick, C., Bartosz, C.E., Chen, C.T. & Slocum, R.D. (2009) A functional analysis of the pyrimidine catabolic pathway in Arabidopsis. *The New Phytologist*, **183**, 117-132.

Zhang, S., Yang, X., Sun, M., Sun, F., Deng, S. & Dong, H. (2009) Riboflavin-induced Priming for Pathogen Defense in Arabidopsis thaliana. *Journal of Integrative Plant Biology*, **51**, 167-174.

Zhang, Z., Schwartz, S., Wagner, L. & Miller, W. (2000) A greedy algorithm for aligning DNA sequences. *J Comput Biol*, **7**, 203-214.

Zhao, J., Xin, H., Qu, L., Ning, J., Peng, X., Yan, T., Ma, L., Li, S. & Sun, M.-X. (2011) Dynamic changes of transcript profiles after fertilization are associated with de novo transcription and maternal elimination in tobacco zygote, and mark the onset of the maternal-to-zygotic transition. *The Plant Journal*, **65**, 131-145.

Appendix

Table S 1: List of genotyping and sequencing primers used in experiments.

#	Designation	Sequence (5‘ → 3‘)	Info
P1	pJet1.2 fw	CGACTCACTATAGGGAGAGCGGC	Standard sequencing and colony PCR primers
P2	pJet1.2 rev	AAGAACATCGATTTTCCATGGCAG	
P3	SeqNOS	TACATGCTTAACGTAATTCAACAG	
P4	pROK_LB_4	CTGGCGTAATAGCGAAGAGG	
P5	pET22b_fw	ACCCCTCAAGACCCGTTTAG	
P6	pET22b_rev	GGTGATGTCGGCGATATAGG	
P7	35S_fw	ATCCTTCGCAAGACCCTTCC	
P8	M13_rev	TTCACACAGGAAACAGCTATGAC	
P9	RibA1_down_fw2	GACTCTGAGCCATAAACTCC	Genotyping of *riba1*
P10	RibA1_wt_Hanna_fw	GTTGGTTTGAAGGGATATGG	
P11	Rib3_checkR	TCATGGCTGCAACTCTTACG	
P12	Rib3fw	CATTACGTCGATGATGGATTCTGCTTTA	
P13	RibA1_R65_wt_fw	TGAAGCTGATGACAAATAATCCCGC	
P14	RibA1_fardown2_rev	GATTGAGCCACTGCGGAAGAAATC	
P15	SALK_445_fw	TGATGATGGTTCCATGGCTA	
P16	GabiLB	CCCATTTGGACGTGAATGTAGACAC	
P17	067_check2_fw	GAGACGTGAGGGATGGTGAT	
P18	RTrib1_rev	AAATTAGTGGAACGTGCTTCTGCG	
P19	R21_fw	CCATTTGGAACGAGCTTGGTG	Genotyping of *riba2*
P20	R21_rev	CTAAACCGGCCAACACAGTC	
P21	R98_fw	CATTACGTCGATGATGGATTCTGC	Genotyping of *riba3*
P22	R98_rev	CGTAAGAGTTGCAGCCATGATC	

***Table S 2*: List of qPCR primer pairs (QPP). If not stated otherwise were designed by myself with Pearlprimer software.**

#	Target Gene	Designation	Sequence (5'→3')
QPP1	RIBA1	qRT_At5g64300_fw2/rev2	TTGTTACTTCTTGTTGTCGGG/ TGATGATCCACATTCCACAC
		*1 qRT_At5g64300_fw5/rev5	AGTATGTTGGTTTGAAGGGATATGG/ TTCGTGATAAGACTCAATAGAGGGA
QPP2	RIBA2	qRT_At2g22450_fw2/rev2	GGTTCCACTCATTACTACTCCT/ AAACTAAGTCACTCAAGAAGCC
QPP3	RIBA3	qRT_At5g59750_fw1/rev1	AGACTAATGACGAATAACCCTG/ ATATCTTCTGTTCTCCTTGGTG
QPP4	PYRD	qRT_At4g20960_fw1/rev1	CTCAGGTATTCTATGTCTGTCAATGG/ TATCCACCACTATCCGAAGCC
QPP5	PYRR	qRT_At3g47390_fw1/rev1	CTGCTATATCATCCAGTGTCATCCA/ TGCTTGTGTCATCTCTACCATCC
QPP6	Lumazine synthase (LS)	qRT_At2g44050_fw1/rev1	GCAATAAGGGAGCTGAAACTG/ CCAAATGGGACAACATCAAGAG
QPP7	Riboflavin synthase (RS)	qRT_At2g20650_fw1/rev1	TTGATTTGATGGGACTTGGGA/ GCACCATTACGAAGAAACAGAG
QPP8	FMN/FHy	qRT_At4g21470_fw2/rev2	CCGCTAACTTGTCAACAAAGGA/ CCTGCCCAACCAAAGTACAC
QPP9	RIBF1	qRT_At5g23330_fw2/rev2	AAGTCTCATCCACACGAGTCC/ GCTCTGTTACATACCTCACATCTC
QPP10	RIBF2	qRT_At5g08340_fw2/rev2	CAGAACCCAAGATATGCCAAGTG/ CCAACTAGAAGCAAACATGCCT
QPP11	SAND (At2g28390)	*2 SAND fw/rev	AACTCTATGCAGCATTTGATCCACT/ TGATTGCATATCTTTATCGCCATC
QPP12	BAP1 (At3g61190)	*3 qRT_BAP1_fw/rev	GTGGGATCGTCAATCTTTCG/ GGCCACCGTATCCATCAATC
QPP13	FSD1 (At4G25100)	*4 qRT_FSD1_fw/rev	TCCAGAACCGAAGACCAGAT/ AGAACTCACTGTCACTGAAGTC
QPP14	GPX7 (AT4G31870)	*5 qRT_GPX7_fw/rev	GCTGGTGGTTTCCTTGGTGAT/ CTCTCGACAACTTTGCCCTTTTT
QPP15	ZAT1 (At5g59820)	*3 qRT_ZAT1_fw/rev	TGCGAGTCACAAGAAGCCTA/ GTGTCCTCCCAAAGCTTGTC
QPP16	METC1 (At3g03070)	*6 qRT_At3g03070_fw/rev	AAAGCCCTAATCCGATCTCAGA/ GGTGTCTCCTTCACAAGCAACA
QPP17	METC3 (At2g02050)	*6 qRT_At2g02050_fw/rev	GCACTTGGATCTAGAGATATGT/ CGTTTCCTTGTAGTTTATTCTG
QPP18	METC11 (At2g19680)	*6 qRT_At2g19680_fw/rev	CATCAAAATTGGTTCAACTTCA/ CTTTCCTAAATGTTTCGTAGCG
QPP19	METC13 (At1g51650)	*6 qRT_At1g51650_fw/rev	TGCCACTGTTGAGAAGTGCCAA/ TGTGAAGGTGAATCCTCTGCCG
QPP20	PPOXI (HEMG1)	*7 qRT_At4g01690_fw/rev	CCTCTTTCTGAATCTGCTGCAA/ CTGCTGCAACTGGTGGGTAA
QPP21	PPOXII (HEMG2)	*7 qRT_At5g14220_fw/rev	AGCCAAAGCTTCCACTGACG/ CAACAGTCGCTGAAGGTCAGAA
QPP22	TUA (At5g19780)	*8 RT_TUA_fw2/rev2	TGGTTCTGGATTGGGTTCTC/ ACAGCATGAAATGGATACGG

*1 for detection of RIBA1 mRNA originating from overexpression by 35S::cAtRIBA1 construct, *2According to Czechowski *et al.* (2004), *3 According to Baruah *et al.* (2009), *4 A. Richter/Pearl primer software, *5 According to Gaber *et al.* (2012), *6 According to Li *et al.* (2014), *7 designed by D. Hackenberg, *8 designed by B. Hedtke.

Table S 3: **List of cloning primers (CLP) utilised in the experiments.**

#	Designation	Sequence (5'→3')	Experiment	Ref.
CLP1	AtRibA1_pXCS-Strep_fw	CGGAATTCAAATTTTTGATTTTGCGATAAGGG	Strep HA tagged RIBA expression in plants	2.9.8
CLP2	AtRibA1_pXCS-Strep_rev	ATCCCGGGGGACTCAGATTCAGA		
CLP3	AtRibA2_ pXCS-Strep_fw	CGGAATTCAGCACACCAAAAAATATCACCGG		
CLP4	AtRibA2_pXCS-Strep_rev	ATCCCGGGAGGAGTAGTAATGAGTGG		
CLP5	AtRibA3_ pXCS-Strep_fw	CGGAATTCAACCTTAAAAATATGTCTGAAATTT		
CLP6	AtRibA3_ pXCS-Strep_rev	ATCCCGGGAGCTAATGGCTGATC		
CLP7	RibA2_PsiI_fw	AATTATAACAGTCGACGGGCCCG	Complementation of *E.coli* Mutants	3.2.2
CLP8	RibA2_PsiI_rev	GCTTATAATACCTCGCGAATGCATCT		
CLP9	AtRIBA1_fw	ACCCGGGACAATGTCTTCCATCAATTTATCC	Complementation of *riba1*	3.5.4
CLP10	AtRIBA1_rev	ACCCGGGTCAGGACTCAGATTCAGACTCAATC		
CLP11	AtRibA1genomisch_SmaI_fw	GTCCCGGGCCGGAGAGATCTCGATC		
CLP12	AtRibA1genomisch_PmlI_rev2	ATCACGTGGGAGTGTTTTTGCTTT		
CLP13	AtRibA1_Prom_XbaI_fw2	CGTCTAGAGTGTGAAGCTGAAAGTGAA		
CLP14	AtRibA1_Prom_OL_A2_rev	GACGCCATTTTCTATATCCGTAGACGAA		
CLP15	AtRibA2_OL_A1Prom_fw2	GATATAGAAAATGGCGTCGCTTACTCTCC		
CLP16	AtRibA2_OL_A1'_rev2	GTTTTTAAGCTTAAGGAGTAGTAATGAGTGGAA		
CLP17	AtRibA1_3'UTR_OL_A2_fw2	TACTCCTTAAGCTTAAAAACCAGGACGAAC		
CLP18	AtRibA1_Prom_OL_A3_rev2	AATCCATCATTTTCTATATCCGTAGACGAA		
CLP19	AtRibA3_OL_A1Prom_fw2	GATATAGAAAATGATGGATTCTGCTTTATATCATC		
CLP20	AtRibA3_OL_A13'_rev2	GTTTTTAAGCTCAAGCTAATGGCTGATCG		
CLP21	AtRibA1_3'UTR_OL_A3_fw2	ATTAGCTTGAGCTTAAAAACCAGGACGAAC		
CLP22	RibA1_BiFC_fw	CGACTAGTATGTCTTCCATCAATTTATCCT	BiFC	3.7.3
CLP23	RibA1_BiFC_rev2	ATGTCGACGGACTCAGATTCAGA		
CLP24	RibA2_BiFC_fw	CGACTAGTATGGCGTCGCTTACTC		
CLP25	RibA2_BiFC_rev2	CTGTCGACAGGAGTAGTAATGAGTGGA		
CLP26	RibA3_BiFC_fw	CGACTAGTATGATGGATTCTGCTTTATATCA		
CLP27	RibA3_BiFC_rev2	CTGTCGACAGCTAATGGCTGATC		
CLP28	RibA1_BiFC_DHBPS_rev	ATGTCGACTCTCTTTCTTCTATACCTGATC		
CLP29	RibA1_BiFC_TP_OL_GCHII_rev	TAATTTATCCTTAACTTTTCCAGTATTGGTT		
CLP30	RibA1_BiFC_GCHII_OL_TP_fw	AAGTTAAGGATAAATTAGTGGAACGTGC		
CLP31	RibA1.1_ GUS_fw	AGTCGACGTGTGAAGCTGAAAGTG	GUS Promoter analysis	3.4.2
CLP32	RibA1_GUS_rev	TACATGTTTTCTATATCCGTAGACGAAATTAAG		
CLP33	RibA2_GUS_fw	AAAGCTTGCAATGGAGTGCATGATCTCTATTG		
CLP34	RibA2_GUS_rev	TCCATGGTTTCACCGGAGTTTTGAAGAG		
CLP35	RibA3.1_GUS_fw	AAAGCTTCTGAACACAAAACCCACC		
CLP36	RibA3_GUS_rev	TCCATGGTTCGACGTAATGAAACATATATC		
CLP37	RibA1_VIGS_fw3	TAGTCGACCTGTTTTAGCTGGACTGG	VIGS	3.5.2.5
CLP38	RibA1_VIGS_rev3	CCGTTACCTTAGGACTCAGATTCAGACTC		

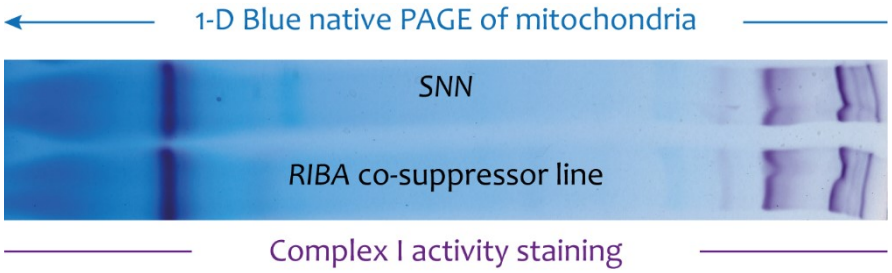

Figure S 1: **Complex I activity staining of the 1-D Blue native PAGE of mitochondria isolated from *SNN* and *RIBA1* co-suppressor tobacco line.**
For the isolation of the mitochondria (2.10.2) severely bleached leaf areas of the RIBA1 co-suppressor plant were chosen. Blue native PAGE was performed as described in chapter 2.10.3 and in-gel Complex I activity assay as described in chapter 2.10.3.1.

Data S 1: **Sequences of synthetic genes At*RIBA1-3*.**
Nucleotide sequences were modified in avoidance of rare codons known to hinder expression in *E. coli* and by introduction of restriction sites for cloning (italics). N-terminally a sixfold His motif and an enterokinase cleavage site were added (underlined).

At*RIBA1*_artificial sequence:

*CATATG*CATCATCACCACCATCATGGCGATGACGACGATAAGGGTTTCTCTTCTATCCCTGAGGCAATTGAAGATATCCGCCAAGGTA
AACTTGTGGTGGTTGTGGATGATGAAGATCGTGAAAATGAAGGTGATTTGGTGATGGCTGCTCAGTTAGCAACACCTGAAGCTATG
GCTTTTATTGTGCGTCATGGTACCGGCATCGTTTGTGTGAGCATGAAAGAAGATGATCTCGAGCGTTTGCACCTTCCTCTCATGGTGA
ATCAGAAGGAAAACGAAGAGAAGCTCTCTACTGCATTTACAGTGACTGTGGATGCAAAACATGGTACAACAACGGGTGTATCAGCT
CGTGACCGCGCAACAACCATCTTGTCTCTTGCATCACGTGATTCAAAGCCTGAGGATTTCAATCGTCCAGGTCATATCTTCCCACTTA
AGTACCGCGAAGGTGGTGTTCTGAAACGTGCTGGCCACACTGAAGCATCTGTAGATCTCACTGTTTTAGCTGGCCTGGACCCTGTTGG
TGTACTTTGTGAAATTGTTGATGACGATGGTTCTATGGCTCGTTTACCAAAACTTCGTGAATTTGCCGCAGAGAACAACCTGAAAGTT
GTTTCGATCGCAGATTTGATCCGCTATCGCCGTAAGCGCGATAAACTAGTGGAACGTGCTTCTGCAGCTCGGATCCCAACAATGTGG
GGCCCTTTCACTGCTTACTGCTATCGATCCATCTTAGACGGCATCGAGCACATTGCAATGGTTAAGGGTGAGATTGGTGACGGTCAA
GACATTCTCGTACGCGTTCATTCTGAATGTCTCACAGGTGACATCTTTGGCTCTGCACGTTGTGATTGCGGCAACCAGCTGGCACTCTC
GATGCAACAGATCGAGGCTACCGGTCGCGGTGTGCTGGTTTACCTCCGTGGTCATGAAGGTCGCGGTATCGGTTTAGGTCACAAGCT
CCGCGCTTACAATCTGCAAGATGCTGGTCGTGACACGGTTGAAGCTAATGAGGAATTAGGTCTTCCTGTTGATTCTCGTGAGTATGGT
ATTGGTGCACAGATCATTCGCGATTTAGGTGTTCGCACAATGAAGCTGATGACAAATAATCCCGCAAAGTATGTTGGTTTAAAGGGC
TATGGCTTAGCCATTGTTGGTCGCGTCCCTCTCTTGAGTCTTATCACGAAGGAGAATAAGCGCTATCTGGAGACAAAGCGTACCAAG
ATGGGTCACATGTATGGCTTGAAGTTCAAAGGTGATGTTGTGGAGAAGATTGAGTCTGAATCTGAGTCCT*AAGCTT*

At*RIBA2*_artifical sequence:

*CATATG*CATCATCACCACCATCATGGCGATGACGACGATAAGGGTTTTGCGTCTATTCCTCAAGCTATTGAAGATATTCGTCATGGCA
AGATGGTAGTTGTTGTAGATGATGAAGATCGTGAAAACGAAGGTGATTTGATCATGGCGGCATCTTTGGCCACACCTGAAGCTATGG
CTTTTGTTGTAAAGCATGGCACCGGTATCGTGTGTGTGAGCATGAAAGGCGAAGACTTGGAGCGCTTAGAGCTCCCTTTAATGGTAA
CGCGTAAGGATAACGAGGAAAAACTCCGTACGGCCTTCACGGTTTCAGTGGACGCAAAAAAGGGTACATCCACAGGTGTCTCAGCT
CGTGATCGCGCGCAAACAATCTTAACCCTTGCATCAAAAGATTCGAAACCTGAAGATTTCAATCGTCCTGGTCATATTTTTCCTTTGC
GCTACCGTGAAGGTGGTGTTCTTAAACGCGCAGGTCATACAGAAGCCTCTGTTGACTTGACTGTGTTGGCCGGTTTAGAACCAGTAT
CTGTTTTATGTGAGATTGTAGATGATGATGGTTCAATGGCTCGCTTACCACGCCTCCGTCAATTCGCTCAAGAGAACAACTTGAAATT
AATTTCAATCGCTGATTTAATCCGGTACCGTCGCAAACGCGAGCGTCTGGTTGAGTTTACCGCGGTTGCGCCTATCCCGACAATGTGG
GGACCATTCAAAGCACATTGCTTTAAGTCATTACTTGATGGTGTTGAGCACATTGCAATGGTCAAGGGTGAAATCGGTGATGGCAAG
GATATTCTCGTGCGTGTACACGCGGAGTGTATCACAGATGATATCTTCGGTAATAGCTCTGGTGGCAAACAGTTAGCAATTGCAATG
CGCCTGATTGAAGAGAATGGTCGCGGTGTTTTTGTCTACTTACGTGGTCCTGAAAGTAAAGGCATCGATCTCAGCCACAAGCCTCGT
ACTTACAACACGAATTCAGATCAAGCCGAGGGTGTTTCATTTCCCGTTGCTTCACGTGAATACGGCATTGGTGCACAAATTCTCCGTG
ATCTTGGTGTTCGCGAGATGAAGGTGATGACGAATAATCCAGCACATTACGTAGGTCTTAAAGGCTATGGTTTATCAATTTCTGGTA
AGGTTCCACTCATTACTACTCCTT*AAGCTT*

At*RIBA2*_artifical sequence:

CATATGCATCATCACCACCATCATGGCGATGACGACGATAAGGGTTATTCCTCTATTGAACTTGCTCTTCAAGCTCTCCGCAAAGGTA
AGTTTGTGATCGTTGTCGACGATGAAACCGGTGATGTTGAAGGCAATCTGATCATGGCTGCAACTCTTACGAGTCCAAAAGACATCG
CTTTTCTGATTAAGAATGGTTCAGGTATTGTCTCAGTTGGTATGAAGAAAGAAAACCTTGAACGCTTAAGCCTTACACTTATGTCACC
TGAAATGGAAGACGAAGATTCCTCTGCTCCAACTTTCACCATCACTGTGGATGCAAAATCTGGCACATCAACTGGCGTATCAGCTTC
AGACCGCGCGATGACGGTTCTTGCACTTTCGTCTCTCGATGCTAAACCAGATGATTTCCGCCGTCCTGGTCATGTATTCCCTCTCAAGT
ATCGTGATGGTGGCGTTTTACGTCGCGCTGGTCACACCGAGGCTTCAGTGGATCTCATGATCTTGGCTGGTTTACGTCCCCTCTCTGTT
CTTTCAGCTATTCTTGATCAAGAAGATGGTTCTATGGCTTCACTGCCGTATATGAAAAAGCTAGCTACGGAACATGATATCCCCATTG
TATCGTTGACTGATTTAATCCGCTATCGTCGCAAGCGTGATAAACTTGTTGAGCGCATCACAGTGTCGCGATTGCCTACCAAATGGGG
TCTTTTCCAGGCTTATTGTTATCGTTCGAAACTCGATGGTACCGAAAATATCGCCCTCGTTAAGGGTAACGTTGGTAATGGTGAGGAC
ATTCTGGTGCGTGTACATTCAGAGTGCTTGACAGGCGACATTTTTGGCTCAGCACGTTGTGACTGTGGCAACCAATTGGACTTAGCCA
TGGAGTTAATCGAGAAAGAGGGCCGCGGTGTTGTTGTGTATCTCCGTGGCCACGAAGGCCGTGGCATTGGCCTAGGTCACAAACTTC
GCGCTTATAACCTGCAGGACGAAGGTCACGACACTGTTCAGGCCAATGTTGAACTTGGCCTCTCCATCGATTCACGTGAATACGGTA
TCGGTGCTCAGATGCTCCGCGACATTGGTGTGCGTACGATGCGCCTAATGACGAATAACCCTGCCAAATTCACTGGTCTGAAAGGCT
ACGGTCTCGCTGTAGTTGGCCGTGTGCCGGTGGTGACACCAATCACCAAGGAGAACCGTCGCTATATGGAGACCAAACGCAAGAAG
ATGGGTCACATTTATATCTCTGATAACAACGATCAGCCATTAGCATAAGCTT

Eidesstattliche Erklärung

Hiermit erkläre ich an Eides statt, dass ich die vorliegende Doktorarbeit selbständig und ohne unerlaubte fremde Hilfe verfasst und keine anderen als die angegebenen Quellen und Hilfsmittel nach §7, Absatz 3 der Promotionsordnung vom 06. Juli 2009 der Mathematisch-Naturwissenschaftlichen Fakultät I der Humboldt-Universität zu Berlin verwendet habe. Weiterhin versichere ich, dass die vorliegende Dissertationsschrift keiner anderen Prüfungsbehörde im In- oder Ausland in dieser oder ähnlicher Form vorgelegt wurde.

Berlin, 17.04.2016

Hanna-Maija Hiltunen